Radiolabeling of defined polymer architectures with fluorine-18 and iodine-131 for *ex vivo* and *in vivo* evaluation: Visualization of structure-property relationships

Dissertation
zur Erlangung des Grades
„Doktor der Naturwissenschaften“
im Promotionsfach Chemie

am Fachbereich Chemie, Pharmazie und Geowissenschaften
der Johannes Gutenberg-Universität Mainz

Dorothea Moderegger
geb. in Göttingen

Mainz 2012

Abstract

Nuclear medicine imaging techniques such as PET are of increasing relevance in pharmaceutical research being valuable (pre)clinical tools to non-invasively assess drug performance *in vivo.* Therapeutic drugs, e.g. chemotherapeutics, often suffer from a poor balance between their efficacy and toxicity. Here, polymer based drug delivery systems can modulate the pharmacokinetics of low M_w therapeutics (prolonging blood circulation time, reducing toxic side effects, increasing target site accumulation) and therefore leading to a more efficient therapy. In this regard, poly-*N*-(2-hydroxypropyl)-methacrylamide (HPMA) constitutes a promising biocompatible polymer. Towards the further development of these structures, non-invasive PET imaging allows insight into structure-property relationships *in vivo*. This performant tool can guide design optimization towards more effective drug delivery. Hence, versatile radiolabeling strategies need to be developed and establishing ^{18}F- as well as ^{131}I-labeling of diverse HPMA architectures forms the basis for short- as well as long-term *in vivo* evaluations.

By means of the prosthetic group [^{18}F]FETos, ^{18}F-labeling of distinct HPMA polymer architectures (homopolymers, amphiphilic copolymers as well as block copolymers) was successfully accomplished enabling their systematic evaluation in tumor bearing rats. These investigations revealed pronounced differences depending on individual polymer characteristics (molecular weight, amphiphilicity due to incorporated hydrophobic laurylmethacrylate (LMA) segments, architecture) as well as on the studied tumor model. Polymers showed higher uptake for up to 4 h p.i. into Walker 256 tumors *vs.* AT1 tumors (correlating to a higher cellular uptake *in vitro*). Highest tumor concentrations were found for amphiphilic HPMA-*ran*-LMA copolymers in comparison to homopolymers and block copolymers. Notably, the random LMA copolymer P4* (M_w=55 kDa, 25% LMA) exhibited most promising *in vivo* behavior such as highest blood retention as well as tumor uptake. Further studies concentrated on the influence of PEGylation ('stealth effect') in terms of improving drug delivery properties of defined polymeric micelles. Here, [^{18}F]fluoroethylation of distinct PEGylated block copolymers (0%, 1%, 5%, 7%, 11% of incorporated PEG_{2kDa}) enabled to systematically study the impact of PEG incorporation ratio and respective architecture on the *in vivo* performance. Most strikingly, higher PEG content caused prolonged blood circulation as well as a linear increase in tumor uptake (Walker 256 carcinoma).

Due to the structural diversity of potential polymeric carrier systems, further versatile ^{18}F-labeling strategies are needed. Therefore, a prosthetic ^{18}F-labeling approach based on the Cu(I)-catalyzed click reaction was established for HPMA-based polymers, providing incorporation of fluorine-18 under mild conditions and in high yields. On this basis, a preliminary µPET study of a HPMA-based polymer – radiolabeled *via* the prosthetic group [^{18}F]F-PEG_3-N_3 – was successfully accomplished.

By revealing early pharmacokinetics, ^{18}F-labeling enables to time-efficiently assess the potential of HPMA polymers for efficient drug delivery. Yet, investigating the long-term fate is essential, especially regarding prolonged circulation properties and passive tumor accumulation (EPR effect). Therefore, radiolabeling of diverse HPMA copolymers with the longer-lived isotope iodine-131 was accomplished enabling *in vivo* evaluation of copolymer P4* over several days. In this study, tumor retention of ^{131}I-P4* could be demonstrated at least over 48h with concurrent blood clearance thereby confirming promising tumor targeting properties of amphiphilic HPMA copolymer systems based on the EPR effect.

Kurzzusammenfassung

Bildgebende Verfahren der Nuklearmedizin wie die PET haben in der pharmazeutischen Forschung zur nicht-invasiven Abschätzung von Arzneiwirkungen vermehrt an Relevanz gewonnen. (Chemo-)Therapeutika weisen oft eine schlechte Bilanz von Nutzen und Toxizität auf. An diesem Punkt können Transportsysteme auf Polymerbasis die Pharmakokinetik niedermolekularer Therapeutika (Verlängerung der Blutzirkulation, Verringerung von Nebenwirkungen, erhöhte Anreicherung im Zielgewebe) verändern, wodurch eine effizientere Therapie erreicht werden kann. Für Anwendungen im Bereich des Wirkstofftransports stellt Hydroxypropylmethacrylamid (HPMA) ein vielversprechendes Polymersystem dar. Zur Optimierung solcher Systeme ermöglicht die Bildgebung mittels PET hier einen Einblick in Struktur-Wirkungsbeziehungen, wodurch die Entwicklung effizienter Transportsysteme erleichtert wird. Hierfür bedarf es der Entwicklung vielseitiger Radiomarkierungsstrategien und Etablierung von ^{18}F- und ^{131}I-Markierungen unterschiedlichster HPMA Architekturen. Dies schafft die Grundlage zur Durchführung von Kurz- und Langzeit *in vivo* Evaluierungen.

Mittels der prosthetischen Gruppe [^{18}F]FETos gelang eine erfolgreiche ^{18}F-Markierung verschiedener HPMA Architekturen (Homopolymere, amphiphile Copolymere sowie Blockcopolymere), was ihre systematische Evaluierung in tumor-tragenden Ratten ermöglichte. Diese Untersuchungen zeigten deutliche Unterschiede in Abhängigkeit individueller Polymercharakteristika (M_w, Amphiphilie und Architektur durch Einbau hydrophober Laurylmethacrylat-(LMA) Segmente) sowie des untersuchten Tumormodells. Entgegen dem AT1 Tumormodell zeigten die Polymere in Walker 256 Tumoren eine höhere Anreicherung (in Übereinstimmung mit erhöhter Zellaufnahme *in vitro*). Höchste Tumoranreicherung wiesen verglichen mit Homo- und Blockcopolymer Systemen die statistischen LMA-Copolymere auf. Insbesondere Copolymer P4* (M_w=55 kDa, 25% LMA) zeigte aussichtsreiche *in vivo* Charakteristika, u.a. die höchste Blutretention sowie Tumoraufnahme. Weitere Studien konzentrierten sich auf die Untersuchung des Einflusses einer PEGylierung (‚Stealth Effekt') hinsichtlich der Verbesserung der Wirkstofftransporteigenschaften definierter Polymermizellen. Durch [^{18}F]Fluorethylierung verschieden PEGylierter Blockcopolymere (0%, 1%, 5%, 7%, 11% an eingebautem PEG_{2kDa}) konnte systematisch der Einfluss des PEG Einbauverhältnisses hinsichtlich *in vivo* Eigenschaften untersucht werden. Hier zeigte sich, dass ein höherer PEG-Einbau zu verlängerter Blutzirkulation sowie linearem Anstieg der Tumoraufnahme (Walker 256 Karzinom) führte.

Die strukturelle Vielfalt an Trägersystemen erfordert differenzierte ^{18}F-Markierungsstrategien. Dahingehend konnte ein weiterer prosthetischer ^{18}F-Markierungsansatz basierend auf der Cu(I)-katalysierten Click-Reaktion für HPMA basierte Polymere etabliert werden, was die Einführung von ^{18}F unter milden Bedingungen und in hohen Ausbeuten ermöglichte. Auf dieser Basis konnte erfolgreich eine µPET Studie eines über [^{18}F]F-PEG_3-N_3 markierten Polymers durchgeführt werden.

Durch das Aufzeigen initialer Pharmakokinetiken ermöglicht es die ^{18}F-Markierung, das Potential von HPMA Polymeren hinsichtlich effektiven Wirkstofftransportes zeiteffizient abschätzen zu können. Dennoch ist die Untersuchung der Langzeitverteilung der Trägerstrukturen essentiell, insbesondere bezüglich verlängerter Zirkulationseigenschaften und passiver Tumoranreicherung (EPR-Effekt). Daher wurden Radiomarkierungen verschiedener HPMA Polymere mit dem längerlebigen Isotop ^{131}I durchgeführt, wodurch eine Evaluierung von P4* über mehrere Tage ermöglicht wurde. In dieser Studie konnte eine Tumorretention von ^{131}I-P4* über 48 h bei gleichzeitiger Blutclearance gezeigt werden, was die vielversprechenden Eigenschaften amphiphiler HPMA Copolymere hinsichtlich EPR-basierter Tumoranreicherung bestätigte.

Contents

1 Introduction

Current (chemo)therapeutic drugs often suffer from a narrow therapeutic index, which is defined as the ratio of the toxic dose to the therapeutic dose of a drug. Improving this poor balance between efficacy and toxicity is a major objective in modern drug development. One particular direction consists in searching for innovative drug delivery concepts for therapeutic areas such as cancer, inflammatory and infective diseases.

The vast majority of systemically applied pharmaceuticals in clinical routine are substances of low molecular weight (typically below 500 g/mol) which distribute evenly within the body by diffusion and exhibit a short retention in the blood stream due to rapid clearance. Only a comparably small portion of the administered drug is effectively able to act on the target site. To achieve a therapeutic concentration, large quantities of the drug in many cases are administered leading to adverse effects accompanying therapy. Consequently, enormous effort towards improved drug delivery has been carried out over the past decades leading to a new field of medical and scientific research termed “nanomedicine” using nanoscale carriers that selectively deliver bioactive substances to diseased sites.

1.1 Nanomedicine

The field of nanomedicine uses nano-sized tools for the diagnosis, prevention and treatment of a disease to gain increased understanding of the complex underlying patho-physiology of disease with the ultimate goal of improving quality-of-life [1]. This definition encompasses a large number of drug delivery systems, among them liposomes, polymers, micelles and antibodies being clinically relevant examples of nanomedicines (Figure 1) [2].

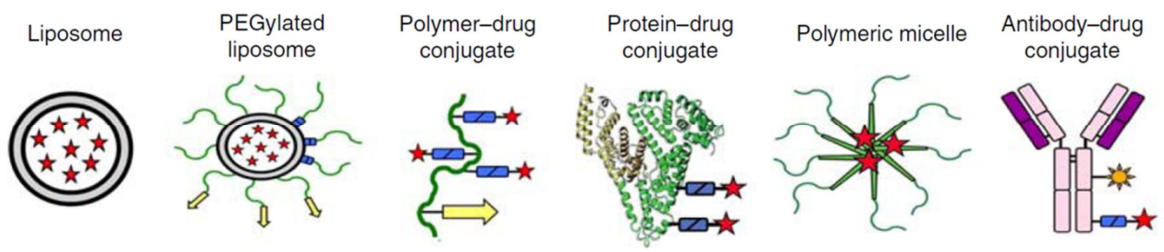

Figure 1: Examples of clinically relevant nanomedicines (adapted from[2]).

1.1.1 Biological rationale using nanomedicines

Nanosized drug delivery systems are being designed in order to improve the therapeutic index of systemically applied pharmaceutics. Also, (chemo)therapeutic drugs should be delivered more selectively in order to improve the drug concentration at the target site. The approach of incorporating low molecular weight drugs into macromolecular devices – either by encapsulation or covalent attachment – can help to overcome the limitations of conventional medicines. Being often hydrophobic, the incorporation into nanosized delivery systems may enhance the solubility as well as stability of hydrophobic drugs *in vivo* and a therapeutic concentration can be maintained over a longer period of time. In case of proteins, polymer conjugation such as PEGylation [3] can increase the half-life by reducing kidney clearance or providing protection against degrading enzymes. Furthermore, the modular design of nanomedical platforms allows incorporating multiple functions in one system. Imaging and targeting moieties can be integrated as well. This multifunctionality of nanosized devices allows making use of two general concepts – "active" and/or "passive" targeting – in order to guide drugs more precisely to pathological sites.

The concept of "passive targeting", which is utilized by most of the systems (particularly liposomes, polymers and micelles) is based on the inherent tendency of macromolecules to accumulate in tumor tissue. Compared to healthy tissue, tumors are characterized by an impaired lymphatic drainage and a fast and defective formation of new blood vessels (angiogenesis), leading to an increased permeability of blood vessels in cancer tissue. While low molecular drugs can diffuse evenly into normal and tumor tissue through the endothelium, the passage through the capillary walls for macromolecules is disabled in healthy tissue. In solid tumors however, macromolecules can extravasate through the leaky vasculature and are retained due to the dysfunctional lymphatic drainage. The resulting passive accumulation observed for macromolecular systems exceeding about 20 kDa due to the pathophysiology of tumor tissue, has been termed "enhanced permeability and retention (EPR) effect" [4] which is depicted in Figure 2.

The concept of "active targeting" addressing receptors aims to enhance the efficacy of the pharmaceutical entity by improved recognition and uptake by the target cell. The concept of drug targeting goes back to Paul Ehrlichs' envisioned 'magic bullet' almost a century ago, and today, promising nanomedical antibody-drug conjugates for receptor-mediated targeting are currently evaluated in clinical trials [5].

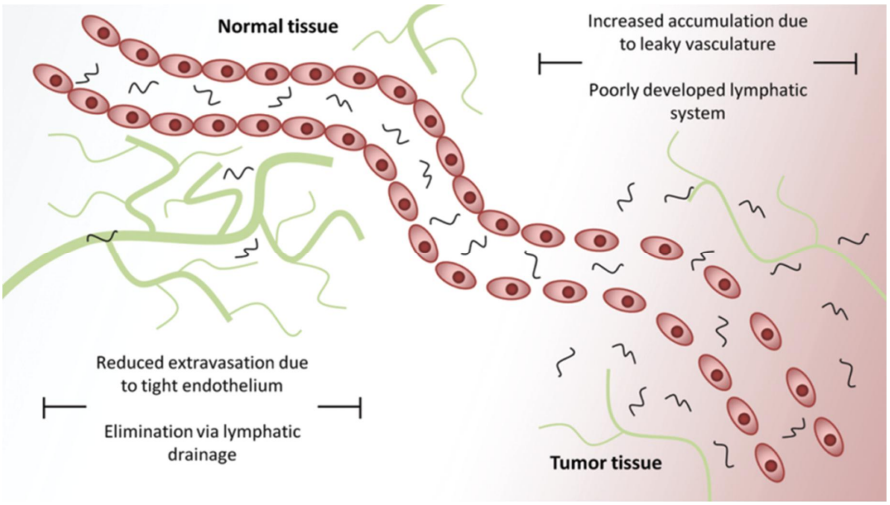

Figure 2: Schematic representation of passive drug targeting to tumors by means of the EPR effect [6].

Depending on the route of administration, nanomedical formulations need to circumvent various and complex patho-physiological and biological barriers [7] to reach the target site, underlining the importance of a careful, pharmacokinetically-guided design of carrier systems. For systemic administration, knowledge about the distribution within the whole organism and the routes of elimination is indispensable. To reach the cell, epithelial barriers need to be overcome, which might be facilitated due to the leakier vasculature of tumor tissue. Nevertheless, this EPR-mediated effect does not count for every cancer type, considering the significant differences in the degree of vascularization and vascular permeability which becomes manifest in the immense heterogeneity of cancer [8]. In addition, the 'leaks' resulting from hypervascularization are dynamic which complicates to determine an optimal size range or limit for macromolecules able to extravasate. With maturation of vessels, the gaps between endothelial cells were shown to narrow and in the case of a liposome based carrier system, a higher uptake was observed for smaller tumors [9]. The extent of passive targeting achieved is for the most part determined by initial blood clearance with a short plasma half-life – due to renal/hepatic clearance or *via* uptake in the reticuloendothelial system (RES) – limiting the portion that actually reaches the tumor. Overall most effective tumor localization has been achieved using systems with a high early phase plasma concentration combined with a longer plasma residence time [10-12]. Therefore many approaches to enhance the plasma half-life have been carried out aiming to decrease protein binding to avoid unspecific uptake by the cells of the mononuclear phagocyte system (RES) or to simply enlarge and to stabilize the particle to diminish rapid clearance. These 'stealth approaches' often include PEGylation, a derivatization of the surface using polyethylene glycol (PEG) chains [13].

Depending on the target within the body also the distribution within the cells of a tissue and ways into the cell by means of different mechanisms of cellular uptake to reach sub-cellular levels have to be considered. Many approaches towards cytosolic macromolecular delivery have been carried out exploiting the heterogeneity of internalizations pathways (receptor-mediated endocytosis, adsorptive endocytosis and fluid-phase endocytosis) accessible for macromolecular drug delivery systems [14].

1.1.2 Polymer Therapeutics

The 'first generation' nanomedicines were designed on the basis of a rational pharmakokinetically driven design and deep knowledge of the characteristics influencing the behavior *in vivo* lead to more than forty 'first generation' nanomedicines that have entered routine clinical use up to now [1]. Along with liposomes, nanoparticles and antibody conjugates, polymer-based drug delivery systems have proven to be amongst the most successful nanomedicines. The concept of using a synthetic polymer backbone as a platform to deliver drugs was first proposed by H. Ringsdorf in the 1970s [15]. His original model of a pharmacologically active polymer combines the relevant qualities for drug delivery (Fig. 3): A device for controlling physico-chemical properties of the macromolecule (electric charge, solubility) – this can be either an attached molecule or the polymeric backbone itself –, a drug linked to the polymer chain and a targeting moiety guiding the conjugate to the the desired site of action.

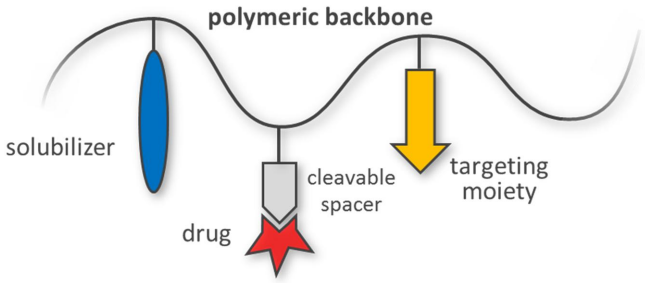

Figure 3: Model of a pharmacologically active polymer as envisioned by H. Ringsdorf.

The possibility to functionally design and tailor synthetic polymers in terms of molecular weight, architecture and size for medical purposes has resulted in a huge class of polymer based drug delivery systems termed polymer therapeutics [16, 17]. The encompassed subclasses of polymer therapeutics are polymeric drugs (polymers with inherent activity), polymer-protein conjugates, polyplexes, polymer-drug conjugates and polymeric micelles as schematically drafted in Figure 4.

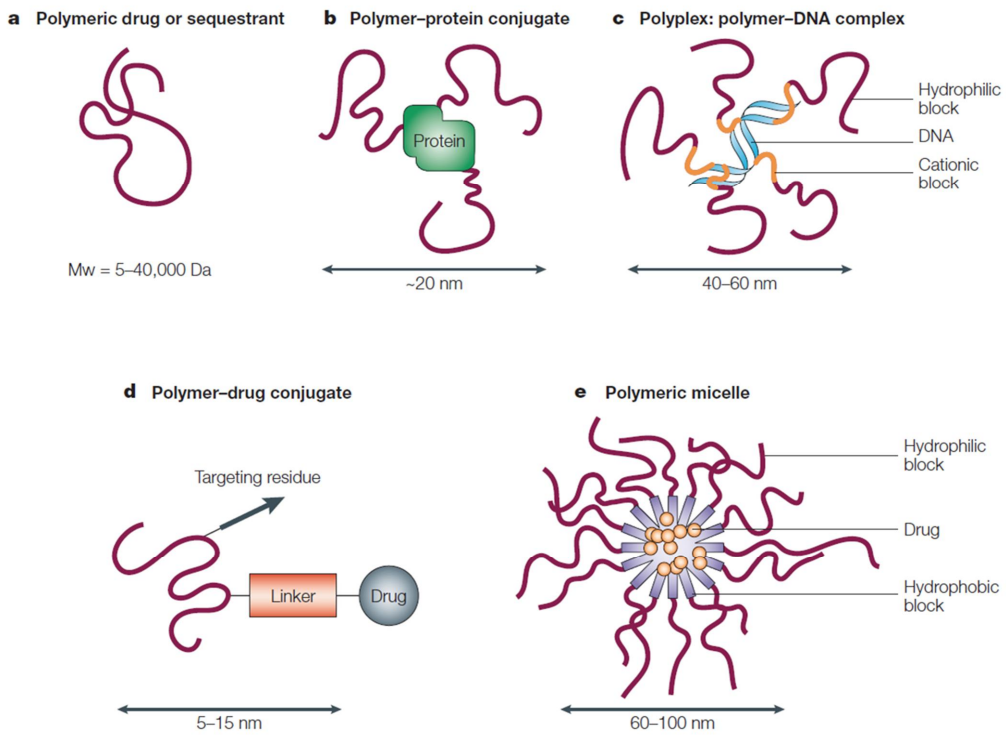

Figure 4: The class of polymer therapeutics comprising five groups of polymer-based drugs [16].

To be effective as transport vehicle, the polymer system has to meet the demands of being water soluble, non-immunogenic, non-toxic and should provide the possibility to achieve high drug payloads. Poly-*N*-(2-hydroxypropyl)methacrylamide (pHPMA), polyethylene glycol (PEG) and polyglutamic acid (PG) mainly fulfill these requirements and are up to now the clinically most relevant polymeric backbones [18-20].

1.1.2.1 HPMA-based polymer therapeutics

In comparison to PEG, which offers only two groups for functionalization, pHPMA has arouse as promising versatile polymeric backbone. First explored as potential plasma expander in the 1970s [21] it has been intensively studied for nanomedical drug delivery purposes resulting in the first synthetic polymer-based drug conjugate to enter clinical trial in 1994. PK1 consisted of the chemotherapeutic drug doxorubicin being covalently bound to a HPMA copolymer by a peptidyl linker (Fig. 5). This conjugate has displayed greatly reduced toxicity compared to unbound doxorubicin in chemotherapy refractory patients [22] and up to now six HPMA anticancer conjugates have progressed to clinical trials using doxorubicin, paclitaxel, camptothecin and platinates as therapeutic agents [23].

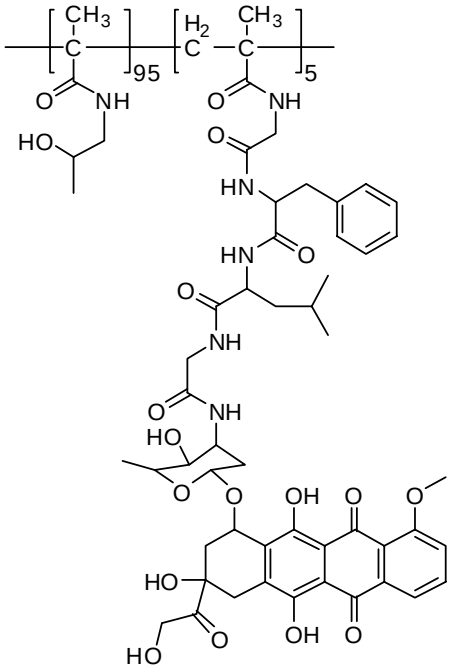

Figure 5: Structure of the HPMA copolymer doxorubicin PK1.

HPMA is not inherently biodegradable, bearing the risk of potential accumulation of polymer chains in healthy tissues. For clinical application using high doses of administration, most HPMA copolymers were thus designed with molecular weights < 40000 g/mol to ensure elimination by glomerular filtration based on the limit for glomerular excretion found for HPMA-based polymers of about 45 kDa [24].

The HPMA conjugates that entered clinical testing were synthesized mostly *via* free radical polymerization (PM) technique [25] using HPMA and methacryloylated peptidyl-nitrophenylester as comonomers. This route appeared to be rather difficult concerning clinical demands such as careful characterization, reproducibility, purification and precision. Free radical polymerization leads to a relatively broad molecular weight distribution and undefined end groups being unfavorable concerning the above mentioned criteria. A measure of the size heterogeneity of a polymer is the polydispersity index (PDI), i.e. the quotient of the weight average molecular weight (M_w) divided by the number average molecular weight (M_n) in a given polymer portion. For monodisperse polymers such as proteins, the PDI equals 1.0, while for artificial polymers higher values – typically about 2 – are reached, representing a higher degree of polydispersity. Often, further fractionation methods were applied for large scale batches to achieve lower final molecular weight distributions for clinical testings [18]. Other synthetic routes, e.g. the use of drug-bearing comonomers for direct binding to pHPMA were explored but few attempts translated controlled radical polymerization techniques into synthesis of HPMA conjugates.

Controlled radical polymerization techniques such as nitroxide-mediated polymerization (NMP) [26], atom transfer radical polymerization (ATRP) [27] and reversible addition fragmentation chain transfer (RAFT) polymerization [28] are promising techniques for the controlled synthesis of polymers regarding medical applications. This is due to the underlying mechanism allowing higher controllability. All controlled radical PMs are based on a rapid dynamic equilibration between a small amount of growing free radicals and a large majority of the dormant chains. In case of the RAFT-PM, which is amongst one of the most versatile methods, the PM process is controlled by a RAFT agent, mostly a thiocarbonylthio compound. Hereby, polymer intermediates are obtained, which are endfunctionalized with thiocarbonylthio groups and radical termination reactions are significantly suppressed. Consequently, copolymers of complex architectures and very narrow polydispersities can be obtained. Controlled radical PM techniques such as ATRP require transition metals such as copper as catalysts which is not required in the case of the RAFT-PM. Considering the inherent toxicity of copper it renders the RAFT-PM technique worthwhile for the preparation of polymer based transport vehicles.

Combining RAFT polymerization technique with reactive ester chemistry using functional reactive ester monomers [29], high variability can be achieved in terms of introducing functionality to a precisely characterizable reactive ester precursor polymer. This approach has been successfully applied for the synthesis of multifunctional HPMA-based polymers [30-32]. In a simplified form, the synthetic pathway underlying this concept is depicted in Figure 6. Here, starting from a reactive ester monomer (pentafluorophenyl methacrylate, PFPMA), a PFPMA-homopolymer is synthesized *via* RAFT-PM which can be subsequently derivatized using primary amines by polymeranalogous reaction. Besides the incorporation of 2-hydroxypropylamine yielding HPMA polymers, this synthetic route further enables the convenient introduction of various functionalities and with respect to medical applications, primary amines of targeting vectors, therapeutics or labeling probes for *in vivo* and *in vitro* evaluations can be easily inserted.

Despite the synthetic progress, HPMA conjugates are multicomponent systems and each conjugate represents a novel chemical entity which implicates the necessity to understand the *in vivo* behavior and metabolic fate of the construct for the clinical application.

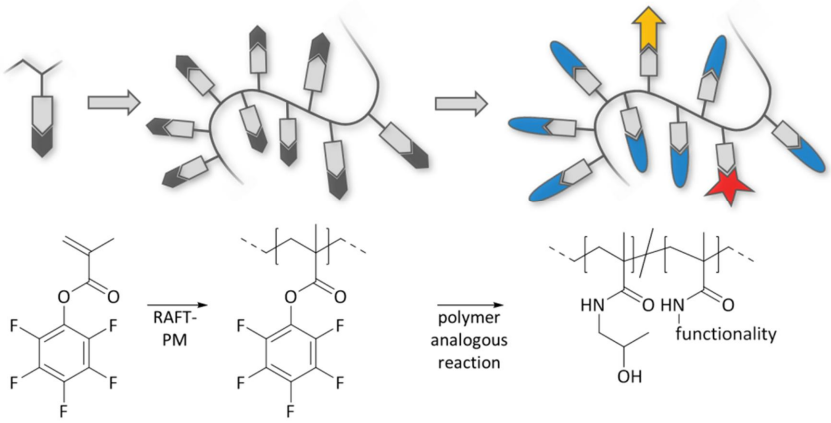

Figure 6: Schematic synthesis of functional HPMA polymers using RAFT polymerization technique and reactive ester approach.

1.2 Imaging of nanomedicines

The vast majority of nanomedical formulations so far designed failed pre-clinical or clinical testing. With the diversity of polymer based carrier architectures, quantitative correlation of *in vivo* data of the drug delivery system's performance is needed. Notably, detailed information on blood kinetics, clearance mechanism, clearance rate as well as target accumulation of the carrier (and of the loaded drug as well) are crucial regarding clinical implementation. An essential feature which guided the successful translations was the use of various reporter probes which were integrated in the devices to visualize the *in vivo* fate in a non-invasive manner [1, 18, 33, 34]. Hence, the effectiveness of the administered nanomedicine as well as disease progression and therapeutic response could be observed. Having accurate diagnostics to identify disease-specific nanoprobes for the patients' needs helps to progress towards personalized medicine. Imaging approaches have been essentially to select promising candidates at an early stage in the clinical development process [35]. Furthermore, by imaging *in vivo* pharmacokinetics, the influence of specific characteristics such as charge, hydrophilic-lipophilic balance or flexibility affecting the performance *in vivo* of carrier systems can be studied, which is essential to optimize and further functionalize carrier systems to guide the way to new generation nanomedicines.

Various imaging techniques have been translated into nanomedicines including ultrasound, bioluminescence, fluorescence imaging, magnetic resonance spectroscopy (MRS), magnetic resonance imaging (MRI), single photon emission computed tomography (SPECT) and positron emission tomography (PET) [36, 37]. Besides using reporter probes for validation of carrier systems,

more and more nanomedicine formulations are being designed where diagnostic and therapeutic agents are combined within a single formulation. With regard to the possibilities notably synthetic polymer based carrier systems offer in terms of functionalization, the translation of this approach has led to a new field in nanomedical research termed 'nanotheranostics' [38, 39], covering systems and strategies in which disease diagnosis and therapy are combined. This offers great potential for early detection, accurate diagnosis and personalized therapy especially for cancer diseases. Table 1 highlights the particular characteristics, benefits and limitations that all molecular imaging techniques do exhibit together.

Table 1: Advantages and limitations of molecular imaging modalities (adapted from [35, 37]).

imaging modality	advantages	limitations
ultrasound	• clinical translation • high spatial and temporal resolution • low costs	• microbubbles as contrast agents • operator dependency • targeted imaging limited
fluorescence	• easy labeling • variety of fluorescent molecules and detection wavelengths • good spatial resolution • no ionizing radiation	• limited clinical translation • potential incompatibility and toxicity • limited wavelength range • limited tissue penetration
SPECT	• clinical translation • highly sensitive	• requires use of ionizing radiation • limited spatial resolution
PET	• clinical translation • highly sensitive • functional imaging • quantification possible	• limited spatial resolution • relevant radionuclides often have relatively short half-lives
MRI	• clinical translation • high spatial resolution • signal enhancement by incorporation of contrast agents into nanodevices • no ionizing radiation	• low sensitivity • real-time imaging is difficult • potential toxicity • imaging time
CT	• clinical translation • depicts anatomical features precisely	• radiation • concentrations of contrast agents • definitive diagnosis is still difficult by CT alone • poor soft-tissue contrast

Imaging technologies such as CT, MRI and ultrasound are primarily morphological/anatomical imaging techniques with high spatial resolution. In contrast, molecular imaging modalities such as PET and SPECT offer the potential to detect diseased sites even before morphological abnormalities become apparent by detecting molecular and cellular changes of diseases. With the development of multimodality molecular imaging devices (PET/CT, PET/MRI [40]), which combine the strengths of both morphological and molecular imaging, detection of pathophysiological changes in early disease phases at high structural resolution becomes possible. The value for translation molecular imaging

techniques into nanomedical science for basic research and clinical application will be highlighted below.

1.2.1 Radionuclide-based molecular imaging in nanomedicine

The recognized value of radionuclide-based molecular imaging goes back to the tracer concept, envisioned by the Hungarian George de Hevesy (1885-1966) who was awarded the Nobel prize in 1943 *"for his work on the use of isotopes as tracers in the study of chemical processes"* [41]. With respect to biological questions *in vivo*, molecules of interest can be traced by using only nominal amounts of an incorporated reporter probe at the picomolar level, given that the number of nuclides directly correlates to the applied activity ($A=\lambda \cdot N$). Hence, for example in the case of 500 MBq fluorine-18, only an amount of about 50 pmol of the nuclide is administered, providing the basis to monitor uninfluenced biochemical processes *in vivo.* On this basis, radionuclide-based molecular imaging techniques have also been of particular interest in nanomedical scientific research as they are highly sensitive and exhibiting unlimited tissue penetration.

Whereas for small molecules, structure-activity relationships as well as *in vivo* proof-of-principle studies are widely established and mandantory to date, the translation into nanomedical science is by far not trivial. Hence, numerous scientific research has been carried out using radioactive reporter probes for potential nanomedical formulations in order to gain insight into structure-activity relationships and pharmacokinetics of the nanosized devices *in vivo*. Several examples of using radionuclide-based imaging of polymeric nanomedicines are noteworthy, highlighting the use of these techniques for assessing their suitability *in vivo* and to identify structure-property relationships. For example, poly(amido amine) (PAMAM) dendrimers were labeled with indium-111 and yttrium-88 to follow targeted delivery in a mouse tumor model. In this study, the labeling moiety itself was shown to alter significantly the biodistribution. Here, PAMAM dendrimers that have been saturated with non-radioactive isotopes of the radionuclide after labeling showed reversed biodistribution compared to the non-saturated dendrimers [42]. Furthermore, the PET nuclide copper-64 was introduced into starlike polymer nanostructures enabling *in vivo* PET imaging. These studies revealed a strong impact of polymer architecture on the *in vivo* behavior when comparing the nanosized starlike polymers to their linear-arm polymer precursors of much smaller size. Although both small and nanosized structures exhibited PEG chain segments in order to avoid rapid *in vivo* clearance, only the nanoscale star polymers showed highly enhanced circulation, even elevated with increasing PEG chain lenghts [43].

Besides these examples – showing the need and profit of non-invasive imaging of potential drug delivery systems – molecular imaging techniques further were of high significance in the

development of HPMA-based drug delivery systems. During the development process of pHPMA drug conjugates for cancer therapy, various imaging techniques guided the way towards preclinical and clinical testing, successfully resulting in six HPMA conjugates that entered clinical trials among them two drug conjugates developed for gamma camera imaging [22, 44].

Most of the *in vivo* studies of HPMA-based systems in animal models as well in patients have been carried out so far using (non-radioactive) MRI contrast agents or radionuclides for γ-Ray scintigraphy or SPECT [45-47]. The former mentioned MRI imaging technique does not allow for quantification and high doses of potentially toxic contrast agents are needed which likely alter the overall carrier structure. For this purpose, iodine-131 as well as technetium-99m was used to allow both scintigraphic imaging and quantification of HPMA-based polymers. Studies on structure-property relationships using HPMA copolymers of different charge were included, and significantly higher retention of the neutral polymers concerning most organs were observed [48]. Functionalization using chemotherapeutic drugs (doxorubicin, gemcitabine) resulted in significantly higher uptake in the spleen as well as the kidney compared to a drug-free control copolymer [49] and higher renal concentrations have been also observed for a biotinylated HPMA copolymer, which in this case was assigned to biotin transporters present in the kidneys [50].

The outlined studies illustrate the importance of a careful *in vivo* evaluation, whenever modifications of the nanosized carrier systems are conducted either by incorporation of targeting moieties, (chemotherapeutic)drugs or even imaging probes as all modifications might influence the performance *in vivo* leading to new chemical entities. Despite the great potential the molecular imaging technique PET is offering (cf. Table 1) this technique has so far been rather neglected in the development process of nanomedicines, especially in the case of the carrier system pHPMA.

1.2.2 Positron emission tomography

Positron emission tomography is a noninvasive imaging technique providing the possibility to quantitatively study physiology *in vivo* [51]. PET is clinically employed to detect various diseases due to pathophysiological changes in diseased tissue, rather than morphological changes, using nanomolar amounts of tracer. Performed in the intact organism with sufficient spatial and temporal resolution for studying biological processes *in vivo*, PET is as well at the forefront of exploratory clinical trials in the field of monitoring drug action thus improving the overall drug development process [35].

PET imaging is enabled by introducing positron emitting radionuclides into pharmacologically active molecules. Suitable radionuclides are neutron deficient nuclei which stabilize *via* positron decay.

During the process of decay, a proton of the nucleus converts into a neutron, thereby emitting a positron (β^+) as well as a neutrino (ν_e) thus maintaining parity of charge and spin (cf. fig 7).

a) $${}^{A}_{Z}X_{N} \longrightarrow {}^{A}_{Z-1}Y_{N+1} + \beta^+ + \nu_e$$

b) $${}^{1}_{1}p_{0} \longrightarrow {}^{1}_{0}n_{1} + \beta^+ + \nu_e$$

Figure 7: Equations of the positron decays: a) Nuclide scale, b) Nucleon scale.

The emitted positron has a continuous spectrum of kinetic energy. It travels for a short distance of about E_{max} ~ 0.5 - 2.4 mm in the surrounding body tissue thereby dispensing its kinetic energy by means of elastic collisions. This process can be detected due to the following annihilation, when the thermalized antimatter positron recombines with its counterpart, the electron. The energy of this annihilation process of $E = 2 \cdot m_e$ is released in the form of two gamma ray photons of 511 keV each, which veer away from the position of annihilation at an angle of 180° (cf. Fig 8).

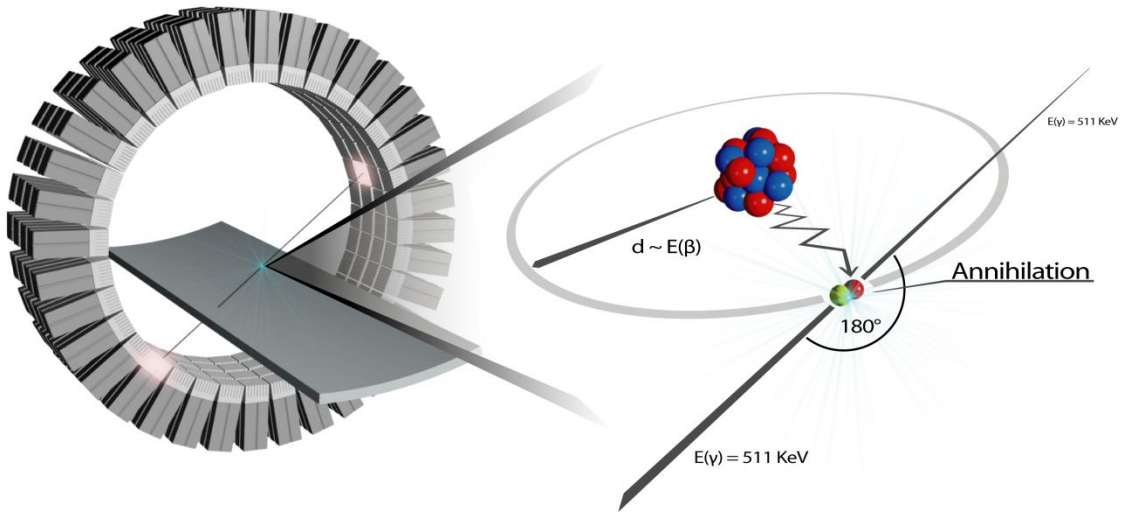

Figure 8: Schematic illustration of the principle behind PET showing the emission of the positron and the annihilation reaction creating two photons of 511 keV.

Whenever two of these gamma ray photons that have traveled out through the body along a 'line of coincidence' are registered by detectors located on opposite sides of the detector ring simultaneously, these events of coincidence are processed and the detection of millions of these coincident events provide the approximate location of the probe. Considering that the registered events only trace back to the location of annihilation rather than the point of initial positron emission (decay of the nuclide), the resolution of the PET images in part depends of the beta energy of the

used positron emitter leading to better resolved images using positron emitter of low beta energy. The high sensitivity of PET systems enables to record rapid acquisition sequences (in the range of seconds) allowing for kinetic studies of tracer distribution over time in regions of interest (e.g. organs, tumor tissue). Coincidence protocols and adsorption (transmission) measurements finally yield quantitative distribution data in terms of A/cm^3 and physiological outputs such as mol/cm^3·min (because activity A parallels the mole number of the labeled compound). Table 2 summarizes the nuclear characteristics of selected PET nuclides suitable for molecular imaging of nanosized drug delivery systems by means of positron emission tomography.

Table 2: Nuclear characteristics of PET radionuclides

nuclide	$t_{1/2}$	decay (%)	β_{max} energy (keV)	production
^{68}Ga	67.7 min	β^+ (89) EC (11)	1899	^{68}Ge /^{68}Ga generator
^{18}F	109.7 min	β^+ (96.7) EC (0.1)	635	^{18}O (p, n) ^{18}F
^{44}Sc	4.0 h	β^+ (100)	1474	^{44}Ti/^{44}Sc generator
^{64}Cu	12.7 h	β^+ (17) EC (44)	653	^{64}Ni (p, n) ^{64}Cu
^{90}Nb	14.6 h	β^+ (53) EC (47)	1500	^{90}Zr (p, n) ^{90}Nb
^{86}Y	14.7 h	β^+ (33) EC (66)	3141	^{86}Sr (p, n) ^{86}Y
^{76}Br	16.2 h	β^+ (55) EC (45)	3941	^{76}Se (p, n) ^{76}Br
^{89}Zr	3.3 d	β^+ (23) EC (77)	901	^{89}Y (p, n) ^{89}Zr
^{124}I	4.2 d	β^+ (23) EC (77)	2138	^{124}Te (p, n) ^{124}I ^{124}Te (d, 2n) ^{124}I

PET is extensively applied due to its value in locating cancerous diseases, imaging myocardial perfusion, detecting coronary heart diseases, in characterizing early stage neurological disorders (e.g. Alzheimer and Parkinson disease) as well as identifying abnormal neurotransmitter activities or cerebral tumors [52, 53]. To benefit from this technique, positron emitting nuclei as listed above need to be incorporated selectively into target molecules.

In case of translating PET imaging into nanomedicines, certain factors have to be considered. First, the PET nuclides need to be incorporated into the nanoparticle, either by labeling the particle itself

(on the surface or in the core) or by labeling the payload encapsulated inside the carrier. Therefore the structure of the carrier system and the radiolabeling strategy need to be designed to get a robust, stable radiolabel for *in vivo* applications. On the other hand, the choice of the appropriate radionuclide is among the most important aspect for the design and application and the half-life of the positron emitter needs to be attuned to the timeframe to be studied *in vivo* and should reflect binding kinetics of the probe and target as well as the pharmacokinetics of the carrier system *in vivo*.

1.3 Radiolabeling strategies for PET imaging

The chemistry to incorporate positron emitters into molecules designed as novel or clinically used PET tracers can be divided into two general types depending on the characteristics of the nuclide: covalent and ionic.

In covalent chemistry, the nuclide is incorporated either *via* displacement or addition reactions. Covalent incorporation of PET nuclides in most cases does not significantly alter the structure but the chemical procedures are often lengthy, tedious and providing low yields. Representative PET nuclides incorporated using covalent attachment chemistry are nonmetals such as ^{18}F, ^{11}C, ^{76}Br and ^{124}I. Metal radioisotopes including ^{68}Ga, ^{44}Sc, ^{64}Cu, ^{90}Nb, ^{86}Y and ^{89}Zr require chelates for being connected to tracers and complexation of metal-based PET nuclides is often achieved in high yields. For stable complexation, high affinity chelating agents based on polyamino carboxylic acids e.g. diethylene triamine pentaacetic acid (DTPA), 1,4,7,10-tetraazacyclododecane-N,N'',N''',N''''-tetraacetic acid (DOTA) or 1,4,7-triazacyclododecane-N,N'',N'''-tetraacetic acid (NOTA) provide kinetic and thermodynamic stability in terms of metal-based radiolabeling. Due to its high stability of its complexes with many M^{2+} and M^{3+}-ions, DOTA is the most commonly applied chelate. Despite the favorable complex chemistry regarding radiolabeling and the convenient accessibility of relevant metal radionuclides from radionuclide generators, chemical properties may be altered due to the prerequisite of a rather large chelating group.

1.3.1 Radiolabeling strategies for ^{18}F-radiolabeling

Being an almost ideal radionuclide within the spectrum of available positron emitters, fluorine-18 is the most often used radionuclide for diagnostic PET imaging. The low kinetic energy of the positron emitted during positron decay (β^+_{max} = 635 keV, cf. Table 2) and a less than 0.3 mm path in soft tissues prior to annihilation produces high spatial image resolution which can be down to 1 mm using dedicated small-animal PET scanners [54]. Furthermore, its physical half-life of 110 minutes is

sufficient long enough to allow more complex radiosynthesis, longer *in vivo* investigation and also to distribute the isotope after cyclotron production to clinical PET centers without cyclotron or radiopharmaceutical production facilities. Fluorine-18 can either be obtained as gaseous electrophilic [^{18}F]F_2 which mostly is cyclotron produced *via* the ^{20}Ne(d,α)^{18}F reaction. Given that elemental fluorine has to be added to the target gas to inhibit target wall adsorption, only low molar activities are obtained when using electrophilic [^{18}F]F_2 for radiolabeling. Hence, nucleophilic [^{18}F]fluoride is used most commonly for radiofluorination approaches. It can be produced in high molar radioactivity (no carrier added) at cyclotrons *via* proton irradiation of ^{18}O-enrichted water (^{18}O(p,n)^{18}F reaction) [55]. To covalently introduce [^{18}F]fluoride into target molecules for subsequent PET studies, different approaches can be applied. Those can be roughly classified in direct ^{18}F-labeling approaches and indirect radiofluorination approaches based on multistage reactions *via* ^{18}F-fluorinated synthons (prosthetic groups) .

1.3.1.1 Direct ^{18}F-labeling methods using [^{18}F]fluoride

To introduce [^{18}F]F^- *via* nucleophilic substitution, the nucleophilicity of the fluoride anion needs to be strongly increased. After production, fluoride is obtained as an aqueous solution and is strongly hydrated due to its high charge density. Fluoride is easily protonated and formed hydrogen fluoride withdraws [^{18}F]F^- for subsequent radiolabeling. Radiofluorination demands aprotic but polar conditions and removal of bulk [^{18}O]water and solubilization in an organic solvent is indispensable. With the use of anion exchange resins and azeotropic distillation with acetonitrile hydration of the anion can be lowered. Using soft cations (Cs^+, Rb^+) to generate weak ion pairs and/or phase transfer catalysts, the [^{18}F]fluoride is further activated providing almost 'naked' [^{18}F]fluoride of high nucleophilicity. Often, a system consisting of the aminopolyether Kryptofix 2.2.2 and potassium carbonate is used and radiolabeling is performed in dipolar aprotic solvents such as acetonitrile (MeCN), dimethyl sulfoxide (DMSO) or dimethylformamide (DMF). Exhibiting good thermal stability, ionic liquids have also been investigated as solvents for radiofluorination and ^{18}F-radiolabeling can be achieved yet in the presence of water [56]. Nucleophilic radiofluorination of aliphatic compounds proceed *via* a S_N2 mechanism and halogens or sulphonic acid ester groups (mesylate, tosylate and triflate) are introduced as leaving groups in the precursor molecules. Direct nucleophilic [^{18}F]fluorinations are being of particular interest for introducing fluorine-18 in small bifunctional alkyl [^{18}F]fluorides for prosthetic labeling approaches (see below). An example of use regarding nucleophilic fluorinations is the synthesis of the radiopharmaceutical 2-deoxy-2-[^{18}F]fluoro-D-glucose ([^{18}F]FDG) [57], which is by far the most relevant clinical PET tracer in terms of assessing glucose metabolism in the heart, lungs, the brain and most importantly in cancerous disease. The synthesis of [^{18}F]FDG *via* nucleophilic substitution of protected mannose triflate precursor is depicted in Figure 9.

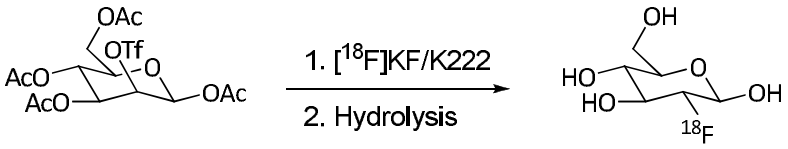

Figure 9: Synthesis of [^{18}F]FDG via nucleophilic n.c.a. [^{18}F]fluorination [57].

Due to the metabolic stability of the ^{18}F-aryl bond, nucleophilic aromatic ^{18}F-fluorination is often applied to introduce ^{18}F into radiopharmaceuticals bearing aromatic systems. For nucleophilic aromatic substitution, the aryl ring needs to be activated and hence has to be derivatized with a good leaving group in o- or p-position to at least one electron withdrawing substituent and typically employed leaving groups are halogens, $-NO_2$ or $-Me_3N^+$. Nucleophilic aromatic substitution reactions require quite harsh reaction conditions which also counts for introducing fluorine-18 into heteroarenes, especially pyridines – however, [^{18}F]2-fluoropyridines can be achieved in almost quantitative yields applying nucleophilic aromatic substitution [58]. A newer and highly useful approach for the synthesis of [^{18}F]fluoroaromatic compounds is the use of substituted diaryliodonium salts [59,60] which, upon nucleophilic attack of [^{18}F]fluoride, yield the substituted arenes and corresponding iodoarenes. With this approach, even unactivated or electron-rich [^{18}F]fluoroaromatic compounds become accessible [61].

1.3.1.2 Radiofluorination using [^{18}F]fluorinated synthons

The direct single-step introduction of [^{18}F]fluorine into target molecules is often difficult and sometimes impossible mostly due to the harsh reaction conditions direct radiofluorination requires. Especially when it comes to electron-rich arenes, complex and/or sensitive molecules exhibiting a variety of reactive functional groups (e.g. macromolecules and peptides) this approach often proves to be inappropriate. Therefore, alternative labeling strategies – especially for more complex molecules, including nanosized drug delivery systems – have to be developed to selectively incorporate fluorine-18 in order to enable subsequent *in vivo* evaluation by means of PET.

Indirect labeling approaches are based on [^{18}F]fluorinated reactive species (labeling synthons or prosthetic groups) in which [^{18}F]F^- is initially introduced by using the harsh conditions of direct fluorinations, and are coupled to the target molecule in a second step applying distinct reaction conditions. Many aliphatic as well as aromatic prosthetic groups have been developed for indirect fluorine-18 labeling so far and have been successfully applied for introducing [^{18}F]fluorine into various nanosized structures [62, 63].

An important class of labeling agents are the functionalized straight chain aliphatic [^{18}F]fluorides, which are obtained from α,ω-bifunctional agents upon reaction with [^{18}F]F^- (cf. Fig. 10). Among the

aliphatic labeling synthons, the most widely used are those of a short alkyl chain, especially [^{18}F]fluoromethyl bromide and 2-[^{18}F]fluoroethyl-1-tosylate ([^{18}F]FETos) [64].

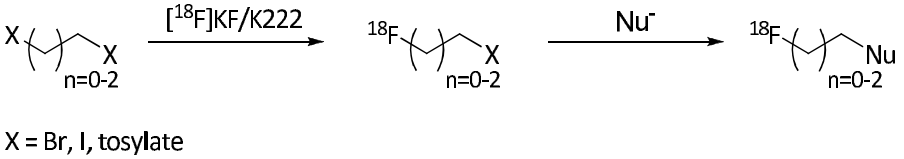

Figure 10: Prostetic fluorine-18 labeling approach using [^{18}F]fluoroaliphatic synthons.

[^{18}F]Fluoralkyl synthons can be coupled with nucleophilic substrates containing phenol, amide, thiophenol and amine functional groups. In terms of radiofluorination, the incorporation of these rather small groups has been proven to be most suitable for a large array of biorelevant molecules – e.g. neurotransmitter analogues of dopamine, serotonin, cocaine as well as benzodiazepines and amino acids [65, 66] – considering that alterations of the structure may considerably influence their properties *in vivo*. Using small labeling synthons to introduce fluorine-18 into macromolecular carrier systems appears to be highly rational in terms of studying structure-property relationships *in vivo* by means of PET.

Beside ^{18}F-fluoralkylation, important prosthetic groups to be mentioned are based on ^{18}F-fluoracylation [67] and ^{18}F-fluoramidation [68] reactions which have been widely used for the labeling of peptides and proteins under mild conditions using thiol, amino or hydroxyl functions for coupling [69].

The increased stability of the ^{18}F-aryl linkage has been taken advantage of in a variety of labeling synthons based on [^{18}F]fluorbenzenes which are prepared *via* nucleophilic aromatic substitution of a good leaving group at the aromatic ring of the precursor molecule. Many aryl-based prosthetic groups have been developed, among them 4-[^{18}F]fluorobenzaldehyde, *N*-succinimidyl 4-[^{18}F]-fluorobenzoate (^{18}F-SFB), 4-[^{18}F]-fluorobenzylamine as well as [^{18}F]*N*-(4-fluorobenzyl)-2-bromoacetamide [70]. The aryl-based labeling synthon ^{18}F-SFB was recently used to attach [^{18}F]fluorine to amino-functionalized diamond nanoparticles (NH_2-DNPs), holding great promise as platforms for biomedical applications in order to study the influence of nanoparticle size and formulation on the *in vivo* biodistribution by means of PET [62].

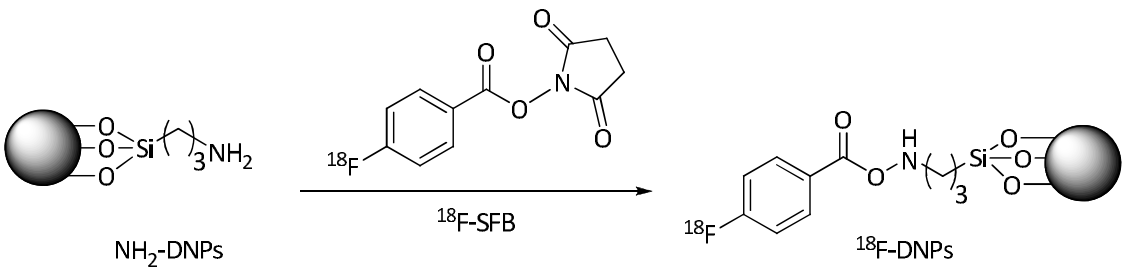

Figure 11: Radiolabeling of amino-functionalized diamond nanoparticles using the aryl-based prosthetic labeling synthon ^{18}F-SFB (adapted from [62]).

A promising new approach for labeling target molecules by means of prosthetic ^{18}F-labeling is based on the Huisgen Cu(I) catalyzed 1,3 dipolar cycloaddition between azides and alkynes forming 1,2,3-triazoles. Among a range of highly efficient reactions, termed as 'click reactions' [71], the mentioned Cu(I) catalyzed cycloaddition has arouse strong scientific interest, ideally fulfilling the criteria of providing high yields, wideness in scope, stereospecificity and simple purification. Being highly efficient, the click reaction proceeds under very mild reaction conditions such as aqueous solutions and at ambient temperatures, without the need to apply any protection group chemistry, and is at the same time highly selective. These features are remarkably beneficial for radiopharmaceutical applications [72], notably for radiolabeling of sensitive or complex molecules such as proteins and nanosized carrier systems and the click labeling approach was first applied to fluorine-18 for the radiolabeling of *N*-(3-azidopropionyl) peptides [73] (cf. Figure 12).

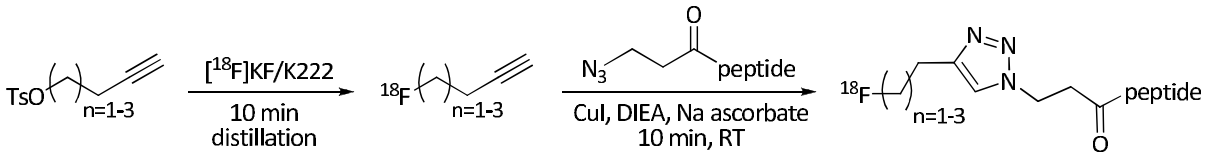

Figure 12: [^{18}F]fluorination via "click chemistry" [73].

To achieve stereospecificity as well as to shorten reaction times, the Huisgen 1,3 dipolar cycloaddition requires catalysis *via* a copper(I) species, which can be either provided by directly adding a Cu(I) salt or by generating an active Cu(I) species *in situ* e.g. by reduction of a Cu(II) salt or oxidation of metallic Cu(0). Usually, Cu(II)sulfate and sodium ascorbate are used for generating Cu(I) *in situ*, as originally published by Sharpless [74], but the use of Cu(I) iodide in combination with a nitrogen base was shown to result in drastically improved radiochemical yields within short reaction times. Furthermore, the junction formed *via* this cycloaddition, i. e. the triazole ring, has been proven to be very stable under physiological conditions. Thus making use of this approach for *in vivo* imaging applications seems highly attractive [75].

Owing to its ease, the click reaction has also entered the field of macromolecular chemistry for the prosthetic ^{18}F-labeling of nanoparticles. In these studies, a trimodal nanoparticle – a dextranated core-shell nanoparticle [cross-linked iron oxide (CLIO)] – was radiofluorinated *via* click approach and multimodality fusion image of PET, MRI and fluorescence-mediated tomography showed a vascular half-life of nearly 6 hours in mice as well as subsequent internalization into macrophages of liver, spleen and phagocytic cells [63, 76].

1.3.2 Radioiodination for long term studies

To date, fluorine-18 has proven to be the ideal radioisotope for non-invasive scientific and clinical molecular imaging and offers great potential for its use in the field of nanomedicines. Despite the favorable characteristics for high resolution PET imaging, the time-frame for fluorine-18 based imaging is limited to about three half-lives of the nuclide, allowing for *in vivo* studies of up to six hours revealing initial pharmacokinetics and drug action.

Though radioisotopes of a shorter half-life limit synthesis procedures as well as the time frame for biological studies, longer lived isotopes are needed in order to investigate the long-term fate of the administered radiopharmaceutical. This might be of particular interest for the development of new chemical entities such as nanosized drug delivery systems in order to assess the long-term outcome of the carrier system. In terms of non-biodegradable nanomedicines, knowledge about both the location and the amount of the carrier system left in the organism might be crucial for developing therapeutic nanocarrier based innovations. Here, longer-lived radioisotopes of iodine are valuable in this purpose with the most prominent ones being the PET isotope iodine-124 ($t_{1/2}$ = 4.2 d) and the γ-emitting isotopes iodine-123 ($t_{1/2}$ = 13.2 h), iodine-125 ($t_{1/2}$ = 59.4 d) as well as iodine-131 ($t_{1/2}$ = 8.02 d) [77].

Analogous to fluorine, radioiodine can be introduced into molecules using electrophilic or nucleophilic substitution reactions. However, iodine is more easily oxidized to an electrophilic species than fluorine and electrophilic radioiodination reactions are preferred. Convenient radiolabeling approaches generate electrophilic iodine from Na[I*]I *in situ* using oxidants such as peracetic acid, chloramine-T, *N*-chlorosuccinimide (NCS) or 1,3,4,6-Tetrachloro-3α,6α-diphenylglycoluril (Iodogen) [78] (cf. Figure 13).

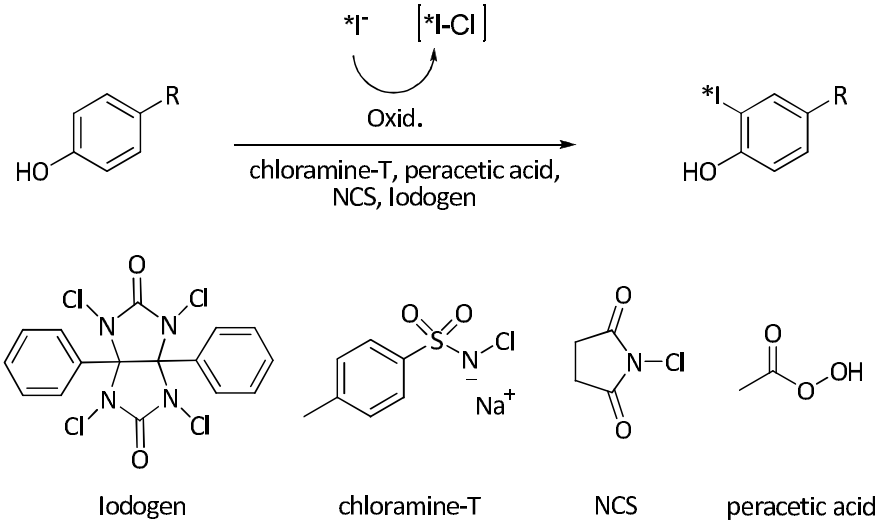

Figure 13: Direct radioiodination via electrophilic aromatic substitution and oxidants used for in situ oxidation.

Introducing radioiodine into aromatic systems is favored due to the higher stability of the aromatic C-I bond, but loss of iodine *in vivo* can still be observed, as often seen for iodinated proteins, where iodine is attached *via* tyrosine residues at the *ortho*-position to the hydroxyl function [79,80]. Higher *in vivo* stability is achieved when using destannylation of trialkyltin-precursors, allowing radioiodination of deactivated aromatic compounds. Owing to the inherent toxicity of alkyltin moieties, careful purification as well as saturation of product has to be carried out making this promising approach challenging for complex molecules such as nanosized drug carrier systems.

1.4 References

[1] Duncan, R; Gaspar, R. Nanomedicine(s) under the Microscope. *Mol Pharm* 2011; 8 (6); 2101-2141.

[2] Lammers, T; Hennink, WE; Storm, G. Tumour-targeted nanomedicines: principles and practice. *Br J Cancer* 2008; 99 (3); 392-397.

[3] Pasut, G; Veronese, FM. PEG conjugates in clinical development or use as anticancer agents: An overview. *Adv Drug Deliver Rev* 2009; 61 (13); 1177-1188.

[4] Maeda, H; Wu, J; Sawa, T; Matsumura, Y; Hori, K. Tumor vascular permeability and the EPR effect in macromolecular therapeutics: a review. *J Control Release* 2000; 65 (1-2); 271-284.

[5] Nelson, AL; Dhimolea, E; Reichert, JM. Development trends for human monoclonal antibody therapeutics. *Nat Rev Drug Discov* 2010; 9 (10); 767-774.

[6] Larson, N; Ghandehari, H. Polymeric Conjugates for Drug Delivery. *Chem Mater* 2012; 24 (5); 840-853.

[7] Sugano, K; Kansy, M; Artursson, P; Avdeef, A; Bendels, S; Di, L; Ecker, GF; Faller, B; Fischer, H; Gerebtzoff, G; Lennernaes, H; Senner, F. Coexistence of passive and carrier-mediated processes in drug transport. *Nat Rev Drug Discov* 2010; 9 (8); 597-614.

[8] Hanahan, D; Weinberg, RA. Hallmarks of Cancer: The Next Generation. *Cell* 2011; 144 (5); 646-674.

[9] Harrington, KJ; Mohammadtaghi, S; Uster, PS; Glass, D; Peters, AM; Vile, RG; Stewart, JS. Effective targeting of solid tumors in patients with locally advanced cancers by radiolabeled pegylated liposomes. *Clin Cancer Res* 2001; 7 (2); 243-254.

[10] Noguchi, Y; Wu, J; Duncan, R; Strohalm, J; Ulbrich, K; Akaike, T; Maeda, H. Early phase tumor accumulation of macromolecules: a great difference in clearance rate between tumor and normal tissues. *Jpn J Cancer Res* 1998; 89 (3); 307-314.

[11] Seymour, LW; Miyamoto, Y; Maeda, H; Brereton, M; Strohalm, J; Ulbrich, K; Duncan, R. Influence of molecular weight on passive tumour accumulation of a soluble macromolecular drug carrier. *Eur J Cancer* 1995; 31 (5); 766-770.

[12] Papahadjopoulos, D; Allen, TM; Gabizon, A; Mayhew, E; Matthay, K; Huang, SK; Lee, KD; Woodle, MC; Lasic, DD; Redemann, C. Sterically stabilized liposomes: improvements in pharmacokinetics and antitumor therapeutic efficacy. *Proc Natl Acad Sci U.S.A* 1991; 88 (24); 11460-11464.

[13] Greenwald, RB; Choe, YH; McGuire, J; Conover, CD. Effective drug delivery by PEGylated drug conjugates. *Adv Drug Deliver Rev* 2003; 55 (2); 217-250.

[14] Rajendran, L; Knölker, H; Simons, K. Subcellular targeting strategies for drug design and delivery. *Nat Rev Drug Discov* 2010; 9 (1); 29-42.

[15] Ringsdorf, H. Structure and properties of pharmacologically active polymers. *Journal of Polymer Science: Polymer Symposia* 1975; 51 (1); 135-153.

[16] Duncan, R. The dawning era of polymer therapeutics. *Nat Rev Drug Discov* 2003; 2 (5); 347-360.

[17] Veronese, FM; Schiavon, O; Pasut, G; Mendichi, R; Andersson, L; Tsirk, A; Ford, J; Wu, G; Kneller, S; Davies, J; Duncan, R. PEG–Doxorubicin Conjugates: Influence of Polymer Structure on Drug Release, in Vitro Cytotoxicity, Biodistribution, and Antitumor Activity. *Bioconjug Chem* 2005; 16 (4); 775-784.

[18] Duncan, R. Development of HPMA copolymer-anticancer conjugates: Clinical experience and lessons learnt. *Adv Drug Deliver Rev* 2009; 61 (13); 1131-1148.

[19] Matsumura, Y; Kataoka, K. Preclinical and clinical studies of anticancer agent-incorporating polymer micelles. *Cancer Science* 2009; 100 (4); 572-579.

[20] Singer, JW; Shaffer, S; Baker, B; Bernareggi, A; Stromatt, S; Nienstedt, D; Besman, M. Paclitaxel poliglumex (XYOTAX; CT-2103): an intracellularly targeted taxane. *Anticancer Drugs* 2005; 16 (3); 243-254.

[21] Sprincl, L; Kopeček, J. New types of synthetic infusion solutions. III. Elimination and retention of poly-[*N*-(2-hydroxypropyl)methacrylamide] in a test organism. *J Biomed Mater Res* 1976; 10 (6); 953-963.

[22] Vasey, PA; Kaye, SB; Morrison, R; Twelves, C; Wilson, P; Duncan, R; Thomson, AH; Murray, LS; Hilditch, TE; Murray, T; Burtles, S; Fraier, D; Frigerio, E; Cassidy, J. Phase I Clinical and Pharmacokinetic Study of PK1 [*N*-(2-Hydroxypropyl)methacrylamide Copolymer Doxorubicin]: First Member of a New Class of Chemotherapeutic Agents–Drug-Polymer Conjugates. *Clin Cancer Res* 1999; 5 (1); 83-94.

[23] Duncan, R; Vicent, MJ. Do HPMA copolymer conjugates have a future as clinically useful nanomedicines? A critical overview of current status and future opportunities. *Adv Drug Deliver Rev* 2010; 62 (2); 272-282.

[24] Seymour, LW; Kopeček, J. Effect of molecular weight of *N*-(2-hydroxypropyl)methacrylamide copolymers on body distribution and rate of excretion after subcutaneous, intraperitoneal, and intravenous administration to rats. *J Biomed Mater Res* 1987; 21 (11); 1341-1358.

[25] Kopeček, J; Bažilová, H. Poly[*N*-(2-hydroxypropyl)methacrylamide]—I. Radical polymerization and copolymerization. *Eur Polym J* 1973; 9 (1); 7-14.

[26] Hawker, CJ; Bosman, AW; Harth, E. New Polymer Synthesis by Nitroxide Mediated Living Radical Polymerizations. *Chem Rev* 2001; 101 (12); 3661-3688.

[27] Matyjaszewski, K; Xia, J. Atom Transfer Radical Polymerization. *Chem Rev* 2001; 101 (9); 2921-2990.

[28] Moad, G; Rizzardo, E; Thang, SH. Living Radical Polymerization by the RAFT Process. *Aust J Chem* 2005; 58; 379-410.

[29] Eberhardt, M; Theato, P. Synthesis of pentafluorophenyl(meth)acrylate polymers: New precursor polymers for the synthesis of multifunctional materials. *Eur Polym J* 2005; 41 (7); 1569-1575.

[30] Barz, M; Tarantola, M; Fischer, K; Schmidt, M; Luxenhofer, R; Janshoff, A; Theato, P; Zentel, R. From Defined Reactive Diblock Copolymers to Functional HPMA-Based Self-Assembled Nanoaggregates. *Biomacromolecules* 2008; 9 (11); 3114-3118.

[31] Barz, M; Luxenhofer, R; Zentel, R; Kabanov, AV. The uptake of *N*-(2-hydroxypropyl)-methacrylamide based homo, random and block copolymers by human multi-drug resistant breast adenocarcinoma cells. *Biomaterials* 2009; 30 (29); 5682-5690.

[32] Hemmelmann, M; Knoth, C; Schmitt, U; Allmeroth, M; Moderegger, D; Barz, M; Koynov, K; Hiemke, C; Rösch, F; Zentel, R. HPMA Based Amphiphilic Copolymers Mediate Central Nervous Effects of Domperidone. *Macromol Rapid Commun* 2011; 32 (9-10); 712-717.

[33] Janib, SM; Moses, AS; MacKay, JA. Imaging and drug delivery using theranostic nanoparticles. *Adv Drug Deliver Rev* 2010; 62 (11); 1052-1063.

[34] Mérian, J; Gravier, J; Navarro, F; Texier, I. Fluorescent Nanoprobes Dedicated to in Vivo Imaging: From Preclinical Validations to Clinical Translation. *Molecules* 2012; 17 (5); 5564-5591.

[35] Willmann, JK; van Bruggen, N; Dinkelborg, LM; Gambhir, SS. Molecular imaging in drug development. *Nat Rev Drug Discov* 2008; 7 (7); 591-607.

[36] Liu, Y; Welch, MJ. Nanoparticles Labeled with Positron Emitting Nuclides: Advantages, Methods, and Applications. *Bioconjug Chem* 2012; 120206095602009.

[37] Cabral, H; Nishiyama, N; Kataoka, K. Supramolecular Nanodevices: From Design Validation to Theranostic Nanomedicine. *Acc Chem Res* 2011; 44 (10); 999-1008.

[38] Barreto, JA; O'Malley, W; Kubeil, M; Graham, B; Stephan, H; Spiccia, L. Nanomaterials: Applications in Cancer Imaging and Therapy. *Adv Mater* 2011; 23 (12); H18.

[39] Lammers, T; Aime, S; Hennink, WE; Storm, G; Kiessling, F. Theranostic Nanomedicine. *Acc Chem Res* 2011; 44 (10); 1029-1038.

[40] Schober, O; Rahbar, K; Riemann, B. Multimodality molecular imaging-from target description to clinical studies. *Eur J Nucl Med Mol Imaging* 2009; 36 (2); 302-314.

[41] "The Nobel Prize in Chemistry 1943". Nobelprize.org. http://www.nobelprize.org/nobel_prizes/chemistry/laureates/1943/.

[42] Kobayashi, H; Wu, C; Kim, MK; Paik, CH; Carrasquillo, JA; Brechbiel, MW. Evaluation of the in vivo biodistribution of indium-111 and yttrium-88 labeled dendrimer-1B4M-DTPA and its conjugation with anti-Tac monoclonal antibody. *Bioconjug Chem*; 10 (1); 103-111.

[43] Fukukawa, K; Rossin, R; Hagooly, A; Pressly, ED; Hunt, JN; Messmore, BW; Wooley, KL; Welch, MJ; Hawker, CJ. Synthesis and Characterization of Core-Shell Star Copolymers for In Vivo PET Imaging Applications. *Biomacromolecules* 2008; 9 (4); 1329-1339.

[44] Julyan, PJ; Seymour, LW; Ferry, DR; Daryani, S; Boivin, CM; Doran, J; David, M; Anderson, D; Christodoulou, C; Young, AM; Hesslewood, S; Kerr, DJ. Preliminary clinical study of the distribution of HPMA copolymers bearing doxorubicin and galactosamine. *J Control Release* 1999; 57 (3); 281-290.

[45] Wang, Y; Ye, F; Jeong, E; Sun, Y; Parker, DL; Lu, Z. Noninvasive visualization of pharmacokinetics, biodistribution and tumor targeting of poly[*N*-(2-hydroxypropyl)methacrylamide] in mice using contrast enhanced MRI. *Pharm Res* 2007; 24 (6); 1208-1216.

[46] Lu, Z; Ye, F; Vaidya, A. Polymer platforms for drug delivery and biomedical imaging. *J Control Release* 2007; 122 (3); 269-277.

[47] Lu, Z. Molecular imaging of HPMA copolymers: Visualizing drug delivery in cell, mouse and man. *Adv Drug Deliver Rev* 2010; 62 (2); 246-257.

[48] Lammers, T; Kühnlein, R; Kissel, M; Šubr, V; Etrych, T; Pola, R; Pechar, M; Ulbrich, K; Storm, G; Huber, P; Peschke, P. Effect of physicochemical modification on the biodistribution and tumor accumulation of HPMA copolymers. *J Control Release* 2005; 110 (1); 103-118.

[49] Lammers, T; Subr, V; Ulbrich, K; Peschke, P; Huber, PE; Hennink, WE; Storm, G. Simultaneous delivery of doxorubicin and gemcitabine to tumors in vivo using prototypic polymeric drug carriers. *Biomaterials* 2009; 30 (20); 3466-3475.

[50] Kissel, M; Peschke, P; Šubr, V; Ulbrich, K; Strunz, A; Kühnlein, R; Debus, J; Friedrich, E. Detection and cellular localisation of the synthetic soluble macromolecular drug carrier pHPMA. *Eur J Nucl Med Mol Imaging* 2002; 29 (8); 1055-1062.

[51] Phelps, ME. Positron emission tomography provides molecular imaging of biological processes. *PNAS* 2000; 97 (16); 9226-9233.

[52] Czernin, J; Phelps, ME. Positron emission tomography scanning: current and future applications. *Annu Rev Med* 2002; 53; 89-112.

[53] Hammoud, DA; Hoffman, JM; Pomper, MG. Molecular Neuroimaging: From Conventional to Emerging Techniques. *Radiology* 2007; 245 (1); 21-42.

[54] Levin, CS; Hoffman, EJ. Calculation of positron range and its effect on the fundamental limit of positron emission tomography system spatial resolution. *Phys Med Biol* 1999; 44 (3); 781-799.

[55] Coenen, HH; Elsinga, PH; Iwata, R; Kilbourn, MR; Pillai, MRA; Rajan, MGR; Wagner, HN; Zaknun, JJ. Fluorine-18 radiopharmaceuticals beyond [^{18}F]FDG for use in oncology and neurosciences. *Nucl Med Biol* 2010; 37 (7); 727-740.

[56] Kim, DW; Choe, YS; Chi, DY. A new nucleophilic fluorine-18 labeling method for aliphatic mesylates: reaction in ionic liquids shows tolerance for water. *Nucl Med Biol* 2003; 30 (4); 345-350.

[57] Hamacher, K; Coenen, HH; Stöcklin, G. Efficient Stereospecific Synthesis of No-Carrier-Added 2-[^{18}F]-Fluoro-2-Deoxy-D-Glucose Using Aminopolyether Supported Nucleophilic Substitution. *J Nucl Med* 1986; 27 (2); 235-238.

[58] Dolci, L; Dolle, F; Jubeau, S; Vaufrey, F; Crouzel, C. 2-[^{18}F]fluoropyridines by no-carrier-added nucleophilic aromatic substitution with [^{18}F]FK-K222—a comparative study. *J Labelled Cpd Radiopharm* 1999; 42 (10); 975-985.

[59] Pike, VW; Aigbirhio, FI. Reactions of cyclotron-produced [^{18}F]fluoride with diaryliodonium salts? A novel single-step route to no-carrier-added [^{18}]fluoroarenes. *J Chem Soc, Chem Commun* 1995 (21); 2215.

[60] Pike, VW; Butt, F; Shah, A; Widdowson, DA. Facile synthesis of substituted diaryliodonium tosylates by treatment of aryltributylstannanes with Koser's reagent. *J Chem Soc, Perkin Trans 1* 1999 (3); 245-248.

[61] Ross, TL; Ermert, J; Hocke, C; Coenen, HH. Nucleophilic ^{18}F-Fluorination of Heteroaromatic Iodonium Salts with No-Carrier-Added [^{18}F]Fluoride. *J Am Chem Soc* 2007; 129 (25); 8018-8025.

[62] Rojas, S; Gispert, JD; Martín, R; Abad, S; Menchón, C; Pareto, D; Víctor, VM; Álvaro, M; García, H; Herance, JR. Biodistribution of Amino-Functionalized Diamond Nanoparticles. *In Vivo* Studies Based on ^{18}F Radionuclide Emission. *ACS Nano* 2011; 5 (7); 5552-5559.

[63] Devaraj, NK; Keliher, EJ; Thurber, GM; Nahrendorf, M; Weissleder, R. ^{18}F Labeled Nanoparticles for *in Vivo* PET-CT Imaging. *Bioconjug Chem* 2009; 20 (2); 397-401.

[64] Zhang, M; Suzuki, K. [^{18}F]Fluoroalkyl agents: synthesis, reactivity and application for development of PET ligands in molecular imaging. *Curr Top Med Chem* 2007; 7 (18); 1817-1828.

[65] Coenen, HH. Fluorine-18 Labeling Methods: Features and Possibilities of Basic Reactions. In *PET Chemistry*. *The Driving Force in Molecular Imaging*, *Ernst Schering Foundation Symposium Proceedings*; Schubiger PA, Lehmann L, Friebe M, Eds.; Springer Heidelberg, 2007; 64; 15-50.

[66] Ross, TL; Wester, HJ. 42 ^{18}F: Labeling Chemistry and Labeled Compounds. In *Handbook of Nuclear Chemistry*; Vértes A, Nagy S, Klencár Z, Lovas R, Rösch F, Eds.; Springer Heidelberg, 2011; 4; 2021-2071.

[67] Block, D; Coenen, HH; Stöcklin, G. N.C.A. ^{18}F-fluoroacylation via fluorocarboxylic acid esters. *J Labelled Cpd Radiopharm* 1988; 25 (2); 185-200.

[68] Jelinski, M; Hamacher, K; Coenen, HH. C-Terminal ^{18}F-fluoroethylamidation exemplified on [Gly-OH^{9}] oxytocin. *J Labelled Cpd Radiopharm* 2002; 45 (3); 217-229.

[69] Kilbourn, MR; Dence, CS; Welch, MJ; Mathias, CJ. Fluorine-18 labeling of proteins. *J Nucl Med* 1987; 28 (4); 462-470.

[70] Wuest, F. Fluorine-18 Labeling of Small Molecules: The Use of ^{18}F-Labeled Aryl Fluorides Derived from No-Carrier-Added ^{18}Fluoride as Labeling Precursors. In *PET Chemistry*. *The Driving Force in Molecular Imaging*, *Ernst Schering Foundation Symposium Proceedings*; Schubiger PA, Lehmann L, Friebe M, Eds.; Springer Heidelberg, 2007; 64; 51-78.

[71] Kolb, HC; Finn, MG; Sharpless, BK. Click Chemistry: Diverse Chemical Function from a Few Good Reactions. *Angew Chem Int Ed* 2001; 40 (11); 2004-2021.

[72] Glaser, M; Robins, EG. 'Click labelling' in PET radiochemistry. *J Labelled Cpd Radiopharm* 2009; 52 (10); 407-414.

[73] Marik, J; Sutcliffe-Goulden, JL. Click for PET: rapid preparation of [^{18}F]fluoropeptides using Cu^{I} catalyzed 1,3-dipolar cycloaddition. *Tetrahedron Lett* 2006; 47 (37); 6681-6684.

[74] Rostovtsev, VV; Green, LG; Fokin, VV; Sharpless, BK. A Stepwise Huisgen Cycloaddition Process: Copper(I)-Catalyzed Regioselective "Ligation" of Azides and Terminal Alkynes. *Angew Chem Int Ed* 2002; 41 (14); 2596-2599.

[75] Ross, TL. The Click Chemistry Approach Applied to Fluorine-18. *CRP* 2010; 3 (3); 202-223.

[76] Nahrendorf, M; Keliher, EJ; Marinelli, B; Waterman, P; Feruglio, PF; Fexon, L; Pivovarov, M; Swirski, FK; Pittet, MJ; Vinegoni, C; Weissleder, R. Hybrid PET-optical imaging using targeted probes. *Proc Natl Acad Sci U.S.A* 2010; 107 (17); 7910-7915.

[77] Adam, MJ; Wilbur, DS. Radiohalogens for imaging and therapy. *Chem Soc Rev* 2005; 34 (2); 153-163.

[78] Eisenhut, M; Mier, W. 44 Radioiodination Chemistry and Radioiodinated Compounds. In *Handbook of Nuclear Chemistry*; Vértes A, Nagy S, Klencár Z, Lovas R, Rösch F, Eds.; Springer Heidelberg, 2011; 4; 2121-2141.

[79] Garg, S; Garg, PK; Zalutsky, MR. N-succinimidyl 5-(trialkylstannyl)-3-pyridinecarboxylates: a new class of reagents for protein radioiodination. *Bioconjug. Chem* 1991; 2 (1); 50-56.

[80] Zalutsky, MR; Narula, AS. A method for the radiohalogenation of proteins resulting in decreased thyroid uptake of radioiodine. *Int J Rad Appl Instrum A* 1987; 38 (12); 1051-1055.

[81] Allmeroth, M; Moderegger, D; Biesalski, B; Koynov, K; Rösch, F; Thews, O; Zentel, R. Modifying the Body Distribution of HPMA-Based Copolymers by Molecular Weight and Aggregate Formation. *Biomacromolecules* 2011; 12 (7); 2841-2849.

2 Objectives and outline

With the potential to improve the effectiveness of (chemo)therapeutic drugs, the development of efficient drug delivery systems has propelled into the focus of both material and medical science. Notably, polymer based carrier systems stand out due to the feasible combination of pharmacological functionalities as well as versatility of architectures that may be achieved. In particular, poly-*N*-(2-hydroxypropyl)methacrylamide (HPMA) is a promising biocompatible polymeric backbone and sophisticated synthesis towards well-defined polymer architectures and comfortable introduction of various functions substantiates the development of HPMA-based carriers for improved drug delivery. In this regard, profound knowledge of the carrier systems' fate *in vivo* is needed, since careful physico-chemical characterizations as well as evaluations *in vitro* are often incapable in predicting the performance in the living organism. Here, radiolabeling in combination with non-invasive monitoring by means of quantitative PET imaging constitutes a valuable tool providing insight in pharmacokinetics of the delivery system *in vivo* and contributing to guide design optimization in the direction of efficient drug delivery.

In order to accomplish *in vivo* evaluations, sophisticated radiolabeling strategies are required and need to be developed being adaptable to architecturally diverse polymeric systems.

Therefore, a major part of this work concentrated on establishing versatile and efficient labeling strategies for site-specific incorporation of the positron emitter fluorine-18 into varying polymer structures. For this purpose, ^{18}F-labeling approaches with secondary labeling precursors are chosen. The synthon [^{18}F]FETos allows for site-specific radiofluorination at phenolic groups and the applicability of [^{18}F]fluoroethylation regarding different polymer architectures should be studied in order to optimize radiolabeling parameters toward individual polymer architectures. Concurrently, radio-analytical as well as separation methodologies are needed meeting the demands of diverse macromolecular systems. On this basis, purification of the radiolabeled polymers for *in vivo* evaluations as well as investigations on the labeling stability *in vitro* and subsequently *ex vivo* need to be accomplished.

Referring to the variety of potential drug delivery systems, the development of further versatile ^{18}F-labeling strategies is essential. In this regard, using the Huisgen azide-alkyne cycloaddition ('click reaction') constitutes a promising approach for mild and efficient radiofluorination using alkyne- or azide-functionalized labeling synthons. Hence, implementation of a prosthetic ^{18}F-labeling approach to HPMA polymers based on the click reaction using the labeling synthon [^{18}F]F-PEG$_3$-N$_3$ was a further

goal of this work. Subsequent to optimization of labeling parameters, radio-analytics and purification, automated production of this labeling synthon should be accomplished for time-efficient and reliable preparation of [^{18}F]F-PEG$_3$-N$_3$. Following optimized synthon preparation, ^{18}F-labeling of alkyne-functionalized HPMA-based polymers *via* this 'click-labeling' approach should be studied regarding optimization of labeling parameters, purification as well as labeling stability. On this basis, the appropriateness of this approach for *in vivo* evaluation of potential HPMA-based carrier systems needs to be estimated by subsequently conducting small animal µPET imaging.

Based on its half-life, ^{18}F-labeling ($t_{1/2}$ = 110 min) enables assessing the suitability of carrier systems for drug delivery applications by means of initial pharmacokinetics investigated up to several hours. In order to evaluate HPMA-based polymer architectures in the long-term, especially regarding EPR-mediated passive tumor retention, radiolabeling using longer-lived isotopes needs to be applied. Therefore, ^{131}I-labeling ($t_{1/2}$ = 8 d) of HPMA-based polymers should be accomplished in order to investigate pharmacokinetics and tumor retention over several days. By applying direct radiolabeling *via* electrophilic aromatic substitution, I-131 can be incorporated at the same functional group (tyramine) used for [^{18}F]fluoroethylation and hence this labeling approach does not demand for structural modification of the polymeric systems. Labeling parameters – such as type and amount of *in situ* oxidant as well as solvent – need to be investigated in order to promote efficient radioiodination of architecturally diverse polymers. Furthermore, appropriate radio-analytical and purification methods as well as stability studies of the labeled polymers should be realized.

With these versatile labeling approaches established (^{18}F as well as ^{131}I), a major rationale of the present work consists in implementing these labeling techniques on diverse HPMA-based polymer architectures in order to investigate the influence of individual physico-chemical polymer parameters on the pharmacokinetics *in vivo* and *ex vivo*. Notably, systematic biological evaluation should allow to study the significance of polymer architecture regarding organ distribution, clearance pathways, blood retention as well as tumor uptake. Here, ^{18}F-labeling can be applied to identify the short-term disposition, thereby time-efficiently hinting at the suitability of a particular carrier architecture regarding effective drug delivery. ^{131}I-labeling of HPMA-based polymer architectures and subsequent evaluation by means of *ex vivo* organ distribution over several days may complement the obtained short-term pharmacokinetics, especially regarding long-term blood retention and EPR-mediated tumor accumulation.

Individual polymer characteristics, such as molecular weight, size, amphiphilicity (hydrophobic laurylmethacrylate (LMA) incorporation) and architecture (amphiphilic LMA-random or LMA-block copolymers exhibiting different superstructure formation in hydrophilic media) may highly determine

the *in vivo* fate regarding clearance pathways and tumor uptake. Hence, investigation of these distinct parameters using ^{18}F-radiolabeling of diverse HPMA-based polymer structures (cf. Figure 1) – varying in the aforementioned characteristics – and subsequent evaluation *in vivo* identifies qualities which favorably alter the pharmacokinetics concerning effective drug delivery. In this regard, specific focus within this work is laid on amphiphilic blockcopolymeric systems which constitute attractive drug delivery systems due to the more defined micellar structures formed in hydrophilic media in which hydrophobic (chemo)therapeutics can be incorporated. Considering the impact of surface characteristics on the *in vivo* performance, further studies should concentrate on investigating whether and to what extent surface properties – i.e. degree of PEGylation – impart favorable pharmacokinetics towards efficient drug delivery.

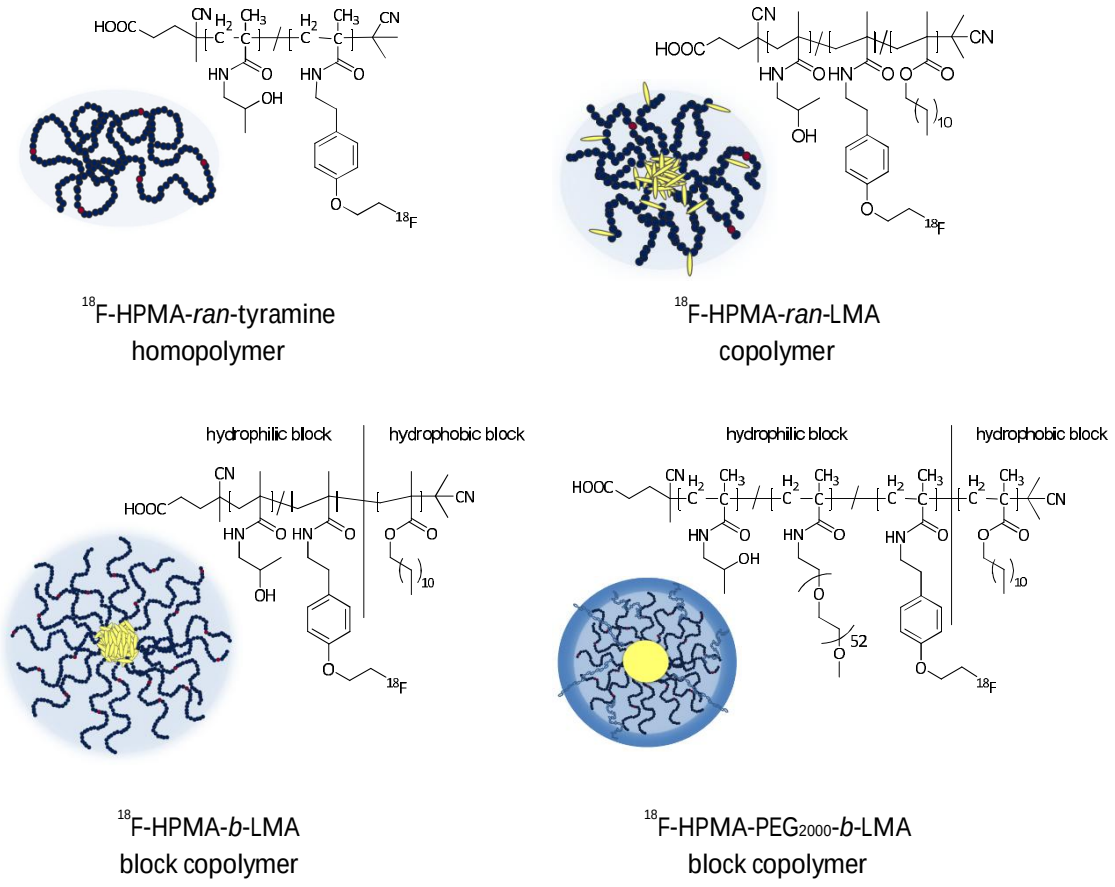

Figure 1: Structures of different HPMA-based polymeric systems to be evaluated in vivo by means of [^{18}F]fluoroethylation radiolabeling.

With respect to tumor retention, not only specific polymer characteristics need to be taken into account. Here, *in vivo* evaluation in the animal model of the rat using different tumor models ought to be considered enabling to identify time-dependent as well as regional intratumoral disparities in

polymer disposition due to individual tumor specific characteristics such as cellular uptake or vascular permeability.

Within the scope of the present thesis, the above outlined aspects have been worked on in terms of individual projects, which were summarized in the form of manuscripts. Together with additional findings complementing the obtained results, these manuscripts are presented separately in section 3.

3 Manuscrips and supplementary results

This work ist based on the following manuscrips:

(I) M. Herth, M. Barz, D. Moderegger, M. Allmeroth, M. Jahn, O. Thews, R. Zentel, F. Rösch: *Radioactive labeling of defined HPMA-based polymeric structures using [^{18}F]FETos for in vivo imaging by Positron Emission Tomography (PET).* Biomacromolecules (2009); 10 (7); 1697-1703 (doi: 10.1021/bm8014736).

(II) M. Allmeroth, D. Moderegger, B. Biesalski, K. Koynov, F. Rösch, O. Thews, R. Zentel: *Modifying the Body Distribution of HPMA-Based Copolymers by Molecular Weight and Aggregate Formation.* Biomacromolecules (2011); 12 (7); 2841-2849 (doi: 10.1021/bm2005774).

(III) M. Allmeroth, Dorothea Moderegger, B. Biesalski, D. Gündel, K. Koynov, H.-G. Buchholz, F. Rösch, R. Zentel, O. Thews: *Structure and size of HPMA-based polymers decide on tumor accumulation but the tumor model makes a difference: A quantitative in vivo PET study*. Angewandte Chemie, in preparation.
Supplementary results: Influence of hydrophobic LMA incorporation of HPMA-based random copolymers on the behavior *in vivo*

(IV) D. Moderegger, M. Allmeroth, R. Zentel, O. Thews, F. Rösch: *Comparative study on short and long-term distribution of HPMA-ran-LMA copolymers in vivo by means of ^{18}F and ^{131}I-labeling revealing tumor retention over time*, Macromolecular Rapid Communication, in preparation.

(V) M. Allmeroth, D. Moderegger, D. Gündel, H.-G. Buchholz, K. Koynov, F. Rösch, O. Thews, R. Zentel: *PEGylation of HPMA-based block copolymers enhances tumor accumulation in vivo: A quantitative study using radiolabeling and Positron Emission Tomography*, Journal of Controlled Release, in preparation.

(VI) D. Moderegger, M. Allmeroth, H. Schieferstein, H.-G. Buchholz, O. Thews, R. Zentel, F. Rösch: *Fluorine-18 labeling approach for HPMA-based polymers via click chemistry,* in preparation.

3.1 Radioactive labeling of defined HPMA-based polymeric structures using [^{18}F]FETos for *in vivo* imaging by Positron Emission Tomography (PET)

Radioactive labeling of defined HPMA-based polymeric structures using [^{18}F]FETos for *in vivo* imaging by Positron Emission Tomography (PET)

Matthias M. Herth[1#], Matthias Barz[2#],Dorothea Moderegger[1], Mareli Allmeroth[2], Markus Jahn[1], Oliver Thews[3], Rudolf Zentel[2*], Frank Rösch[1*]

[#] both authors are equally contributed

[1] Institute of Nuclear Chemistry, Johannes Gutenberg-University Mainz, Fritz-Strassmann-Weg 2, 55128 Mainz, Germany

[2] Institute of Organic Chemistry, Johannes Gutenberg-University Mainz, Duesbergweg 10-14, 55099 Mainz, Germany

[3] Institute of Pathophysiology, Johannes Gutenberg-University Mainz, Duesbergweg 6, 55128 Mainz, Germany

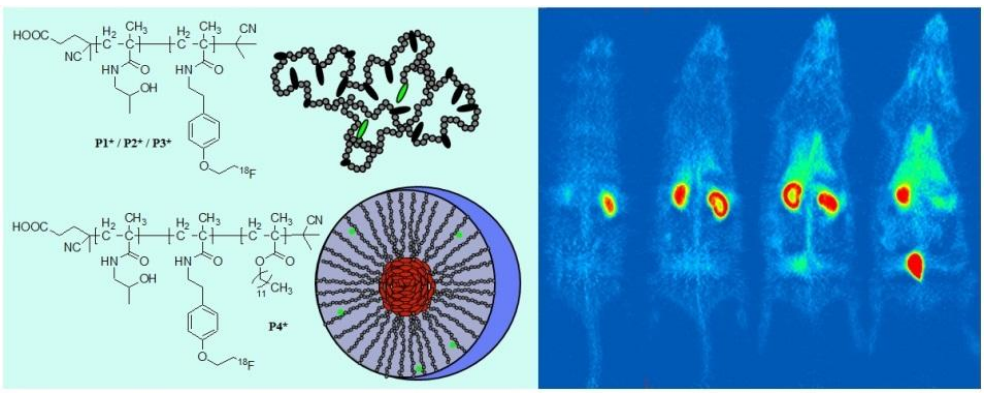

Abstract

During the last decades polymer-based nanomedicine has turned out to be a promising tool in modern pharmaceutics. The following article describes the synthesis of well-defined random and block copolymers by RAFT polymerization with potential medical application. The polymers have been labeled with the positron-emitting nuclide fluorine-18. The polymeric structures are based on the biocompatible *N*-(2-hydroxypropyl)-methacrylamide (HPMA). To achieve these structures, functional reactive ester polymers with a molecular weight within the range of 25000-110000 g/mol were aminolyzed by 2-hydroxypropylamine and tyramine (3%) to form ^{18}F-labelable HPMA-polymer precursors. The labeling procedure of the phenolic tyramine moieties *via* the secondary labeling synthon 2-[^{18}F]fluoroethyl-1-tosylate ([^{18}F]FETos) provided radiochemical fluoroalkylation yields of ~80% for block copolymers and >50% for random polymer architectures within a synthesis time of 10 min and a reaction temperature of 120 °C. Total synthesis time including synthon synthesis, ^{18}F-labeling, and final purification *via* size exclusion chromatography took less than 90 min and yielded stable ^{18}F-labeled HPMA-structures in isotonic buffer solution. Any decomposition could be detected within 2 h. To determine the *in vivo* fate of ^{18}F-labeled HPMA-polymers, preliminary small animal Positron Emission Tomography (PET) experiments were performed in healthy rats, demonstrating the renal clearance of low molecular weight polymers. Futhermore, low metabolism rates could be detected in urine as well as in the blood. Thus, we expect this new strategy for radioactive labeling of polymers as a promising approach for *in vivo* PET studies.

Keywords: HPMA-polymers, RAFT polymerization, ^{18}F-labeling, *in vivo* imaging of polymers, PET

Introduction

Polymer-based therapeutics are of increasing interest in the development of nanomedical tools for medical diagnosis and treatment [1-3]. For example, micelles [4-11] and polymer drug conjugates [12-15], containing various functionalities among a single molecule, have been applied to drug delivery applications. In this respect, polymers can interact with different biological targets selectively, carrying drugs or fulfilling biological tasks.

Functionalities can be introduced in a polymeric system either by polymerizing a mixture of monomers leading to random copolymers or by synthesizing reactive polymer structures that can be transferred into functional structures by a polymer analogous reaction afterward. The reactive ester approach offers two major advantages: On one hand only homopolymers have to be synthesized

which can be precisely characterized; on the other hand copolymerization parameters can be disregarded. Copolymers based on N-(2-hydroxypropyl)-methacrylamide (HPMA) and active ester methacrylates have been applied to various medical *in vivo* applications [1, 4, 16, 17].

However, to optimize medical application detailed knowledge about the biodistribution of polymers in the living organism is necessary. It provides insights in pharmacokinetics of the medical substance or metabolism pathways within the target tissue or other organs. The nonspecific interaction between proteins and polymer surfaces determines the *in vivo* fate of drug carriers [18-20].Therefore, particle-sizes, compositions, physical properties, and surface chemistry influences the behavior of nanomaterials *in vivo* [21].

To understand and finally fine-tune these parameters for *in vivo* therapies or diagnostics, appropriate imaging strategies are needed. In this respect, non-invasive, quantitative, and repetitive whole body molecular imaging techniques such as positron emission tomography (PET) and single photon emission computed tomography (SPECT) using adequate radiolabeled derivatives would provide a significant advance in the understanding of mentioned interactions. Compared with other imaging methods, PET and SPECT bear the advantages of high sensitivity (the level of detection approaches 10^{-12} M of tracer) and isotropism (i.e., ability to detect organ accumulation accurately, regardless of tissue depth, whereas fluorescence emission is limited by a low penetration depth) which provide reliability for *in vivo* quantitative imaging analysis. For macromolecules, most frequently used radioactive nuclides for *in vivo* imaging are chelated metals, such as ^{111}In or ^{99m}Tc for SPECT and ^{64}Cu for PET [22-24]. Nevertheless, PET offers the more precise and detailed imaging technique due to higher spatial and temporal resolution as well as quantification [25].

Recent research has demonstrated the use of chelators (e.g., DOTA derivatives) for the attachment of metallic PET radionuclides [24]. This strategy may have a major drawback. Typically, the chelating agent itself is rather large, bulky and charged and as a result may strongly influence the particle structure and consequently its biological behavior. This work introduces a new approach for ^{18}F-labeling polymers with a rather small synthon 2-[^{18}F]fluoroethyl-1-tosylate ([^{18}F]FETos) that should not influence the structural properties of the self-assembled nanoobject itself.

The imaging time frame of polymer-based therapeutics differs regarding their biological targeting. Due to this fact, long-term and short-term imaging is needed. An example for long-time imaging is passive polymer accumulation in tumor tissue. In contrast, there is a need for short-term in blood pool imaging. All these mentioned applications are of major interest in clinical research, for example, in tumor diagnostics [25] and therapy [3], in certain heart dysfunctions [26, 27], or tissue perfusion

[28]. In this context, ^{18}F-labeled HPMA polymers should allow precise imaging of short-term pharmacokinetics of nanostructures.

Materials and Methods

Materials

All chemicals were reagent grade and obtained from Aldrich. The chemicals were used without further purification unless otherwise indicated. Dioxane used in the synthesis was freshly destilled from a sodium/potassium mixture. 2,2'-Azobis(isobutyronitrile) (AIBN) was recrystallized from diethyl ether and stored at -7 °C. Lauryl methacrylate was distilled and kept at -7 °C.

Characterization

^{1}H, ^{13}C, and ^{19}F-NMR spectra were obtained at 300 or 400 MHz using a FT-spectrometer from Bruker and analyzed using the ACDLabs 6.0 software. The polymers were dried at 40 °C overnight under vacuum and afterward submitted to gel permeation chromatography (GPC). GPC was performed in tetrahydrofurane (THF) as solvent and with the following parts: pump PU 1580, auto sampler AS 1555, UV-detector UV 1575, RI-detector RI 1530 from Jasco, and miniDAWN Tristar light scattering detector from Wyatt. Columns were used from MZ-Analysentechnik: MZ-Gel SDplus 10^2 Å, MZ-Gel SDplus 10^4 Å, and MZ-Gel SDplus 10^6 Å. The elution diagrams were analyzed using the ASTRA 4.73.04 software from Wyatt Technology. Calibration was done using polystyrene standards. The flow rate was 1 mL/min at a temperature of 25 °C. Radio-TLCs (thin layer chromatography) were analyzed *via* an Instant Imager (Canberra Packard). HPLC was performed with a Sykam S 1100 pump and a Knauer UV-detector (K-2501), whereas SEC was performed with a waters pump (1500 Series), a Waters UV-detector (2487 λ Absorbence Detector), and a Berthold LB 509 radiodetector. μPET studies were performed with a Siemens MicroPET Focus 120 camera.

Animals

Male Wistar rats (150-300 g) housed in the animal care facility of the University of Mainz were used in this study. All experiments had previously been approved by the regional animal ethics committee and were conducted in accordance with the German Law for Animal Protection.

Synthesis of 4-Cyano-4-((thiobenzoyl)sulfanyl)pentanoic Acid

The 4-cyano-4-((thiobenzoyl) sulfanyl)pentanoic acid was used as the chain transfer agent (CTA) and synthesized according to the literature [29].

Synthesis of Pentafluorophenyl Methacrylate (PFMA)

Pentafluorophenyl methacrylate (PFMA) was prepared according to the literature [30].

General Synthesis of the Macro-Chain Transfer Agents (CTA)

The macro CTA was prepared according to the literature [31]. RAFT polymerizations of PFMA using 4-cyano-4-((thiobenzoyl) sulfanyl)pentanoic acid were performed in a Schlenk tube. The reaction vessel was loaded with 2,2'-azobisisobutyronitrile (AIBN), 4-cyano-4-((thiobenzoyl)sulfanyl)pentanoic acid (CTA) (molar ratio of AIBN/CTA = 1:8), and 15 g of PFMA in 20 mL of dioxane. Following three freeze-vaccum-thaw cycles, the tube was immersed in an oil bath at 70 °C. Afterward the polymer poly(PFMA) was three times precipitated into hexane, isolated by centrifugation, and dried for 12 hours at 30 °C under vacuum. In the end, a slightly red powder was obtained. Yield: 59%. ^{1}H-NMR ($CDCl_3$) δ [ppm] 1.6-2.2 (br), 0.9-1.5 (br). ^{19}F-NMR ($CDCl_3$) δ [ppm] -165.0 (br), -159.7 (br), -153.1 (br).

General Synthesis of Block Copolymers

The block copolymer was prepared according to the literature [32].

Removal of Dithioester End Groups

The dithiobenzoate end group was removed according to the procedure reported by Perrier et al. [33]. Typically, 200 mg of polymer (M_n = 25.000 g/mol) and 40 mg AIBN (20 times higher than copolymer, mol/mol) were dissolved in 3 mL of anhydrous dioxane/DMSO (4:1). The solution was heated at 80 °C for 2 h. Finally the copolymer was precipitated three times in 100 mL of diethyl ether and collected by centrifugation. In the case of the block copolymer, the crude product was first precipitated in EtOH two times and finally one time in diethyl ether. The copolymer was dried under vacuum for a period of 24 h (yield: 92%). The absence of the dithiobenzoate end group was confirmed by UV-vis spectroscopy.

Polymer Analogous Reactions of Homopolymers

In a typical reaction, 300 mg PPFMA without ditihioester end group was dissolved in 4 mL abs. dioxane and 1 mL of abs. dimethylsulfoxide (DMSO). A colorless solution was obtained. Afterward,

8 mg tyramine and 20 mg triethylamine were added. The mixture was kept at 25 °C for 4 h, and finally, 200 mg hydroxypropylamine and 200 mg triethylamine were added. The reaction was allowed to proceed under the above-mentioned conditions overnight. The solution was concentrated in vacuum and introduced to a column filtration using Sephadex LH-20 in dioxane and precipitated in diethyl ether, removed by centrifugation, and dried under vacuum at 30 °C for 14 h. Yield: 85%. ^{1}H-NMR (DMSO-d_6) δ [ppm] 6.6-7.2 (br), 4.5-4.8 (br), 3.4-3.9 (br), 2.6-3.0 (br), 0.9-1.3 (br).

Polymer Analogous Reactions of Block Copolymers

In a typical reaction, 300 mg poly(PFMA)-*block*-poly(lauryl methacrylate) was dissolved in 4 mL of abs. dioxane and 1 mL of abs. dimethylsulfoxide (DMSO). A colorless solution was obtained. Afterward, 8 mg tyramine and 20 mg triethylamine were added. The mixture was kept at 25 °C for 4 h. In the end, 200 mg hydroxypropylamine and 200 mg triethylamine were added. The reaction was allowed to run under the above-mentioned conditions overnight. The solution was concentrated in vacuum, introduced to a column filtration using Sephadex LH-20 in dioxane and precipitated in diethyl ether, removed by centrifugation and dried under vacuum at 30 °C for 14 h. Yield: 82%. ^{1}H-NMR (DMSO-d_6): δ [ppm]) 6.6-7.2 (br), 4.5-4.8 (br), 3.4-3.9 (br), 2.6-3.0 (br), 0.9-1.5 (br), 0.8-0.9 (br t).

Synthesis of 2-[^{18}F]Fluoroethyl-1-tosylate [^{18}F]FETos

To a dried Kryptofix2.2.2./[^{18}F]fluoride complex, 4 mg ethyleneglycol-1,2-ditosylate in 1 mL of acetonitrile was added and heated under stirring in a sealed vial for 3 min. Purification of the crude product was accomplished using HPLC (Lichrosphere RP18-EC5, 250×10 mm, acetonitrile/water 50:50, flow rate: 5 mL/min, R_f: 8 min). After diluting the HPLC fraction containing the [^{18}F]FETos with water (HPLC fraction/water 1:4), the product was loaded on a C18-Sepac cartridge, dried under a nitrogen stream, and eluted with 1.2 mL of DMSO. The whole preparation time was about 40 min and the overall radiochemical yield was between 60 and 80% [34].

Radioactive Labeling of Polymers Using [^{18}F]FETos

In a typical reaction, 3 mg of polymer was dissolved in 1 mL DMSO. A clear solution with a concentration of 3 mg/mL was obtained. To this solution, 1 µL of 5 N sodium hydroxide solution and [^{18}F]FETos solution were added. The clear solution was kept at temperatures from 80-150 °C for 20 min. For kinetic measurements, samples were taken from the solution every 5 min. The decay-corrected radiochemical yield (RCY) was checked by TLC (Merck 60 F_{254}) and SEC (HiTrap Desalting

Column, Sephadex G-25 Superfine, column volume 5 mL; flow rate: 1 mL PBS-buffer solution) leading to comparable results.

Stability

In a typical test, labeled polymers were reinjected into a SEC column (HiTrap Desalting Column, Sephadex G-25 Superfine, column volume 5 mL; flow rate: 1 mL PBS-buffer solution) and checked for impurities.

In Vitro Binding of Polymers to Human Serum Albumine

Solutions with a concentration of 40 mg/mL of human serum albumine (HSA; S1), 1 mg/mL of polymer P2 (S2) as well as a mixture of 0.2 mg P2 and 40 mg HSA in 1 mL of S3 were prepared. A TLC in MeOH/H_2O (4:1) using RP-18$F_{(254s)}$ TLC plates was performed by spotting the prepared isotonic solutions. R_f values (S1, 0.8; S2, 0; S3, 0.8 and 0).

Ex Vivo Metabolism Studies ^{18}F-Labeled Particles

Male Wistar rats were anaesthetized with pentobarbital (40 mg/kg, i.p., Narcoren, Merial, Hallbergmoos, Germany) and a catheter was inserted into the left jugular vein for radiotracer application, a second catheter was inserted into the left carotic artery and a tube was placed in the trachea. The radiotracer was injected i.v. at a dose of ~10 MBq of the labeled ^{18}F-polymer. At 5, 10, 20, 30 and 60 min post-injection, blood samples were collected and analyzed. Whole blood was centrifuged at 7500 rpm for 5 min at 4 °C to separate plasma and blood cells. Plasma and blood cell fractions were obtained and radioactivity was measured with an automatic γ-counter (2470 Wizard^2; Perkin-Elmer). The percentage of radioactivity bound to plasma and blood cells was calculated thereafter. In addition, at 60 min p.i. samples of the urine were obtained from puncture of the animal's bladder. For metabolic studies the blood plasma and urine fractions were analyzed *via* reverse phase thin layer chromatography applying the same conditions described in section 2.14.

Initial *In Vivo* PET Studies of ^{18}F-Labeled HPMA-Polymers

Positron emission tomography scans were performed with a Siemens/Concorde Microsystems microPET Focus 120 small animal PET (μPET) scanner. Animals were anaesthetized with pentobarbital (40 mg/kg, i.p., Narcoren, Merial, Hallbergmoos, Germany) and a catheter was inserted into the left jugular vein for radiotracer application and a tube was placed in the trachea. During PET measurements the animals were placed in supine position and breathed room air spontaneously through a tracheal tube. Listmode acquisition was started with the tracer injection of 15-25 MBq

(specific activity: 1.5 to 2.5 x 10^{-3} GBq/μmol). The ^{18}F-labeled tracers were applied *via* i.v. injection into the jugular vein catheter. The tracer distribution was followed for up to 4 h after injection. Thereafter, a whole body scan of the rat was performed.

Results and Discussion

The synthesis and ^{18}F-labeling of functional HPMA-copolymers and block copolymers is based on precisely characterized active ester polymers [30], which can be easily modified using primary amines. The synthetic route to functional block copolymers based on the clinically approved *N*-(2-hydroxypropyl) methacrylamide (HPMA) was recently described by Barz et al. [32]. Random and block copolymers based on HPMA with phenolic hydroxyl groups in the polymer backbone (scheme 1) were synthesized using the active ester approach. The reactive ester homopolymers and block copolymers have been synthesized by the RAFT polymerization method [29] leading to well-defined polymers with narrow molecular weight distributions. In general, the obtained polymers exhibit a polydispersity index (PDI) of 1.2-1.3 (Table 1) and have been characterized by NMR and GPC (Figure 1). The reactive polymers have been transferred to HPMA-based polymeric structures as previously reported [32].

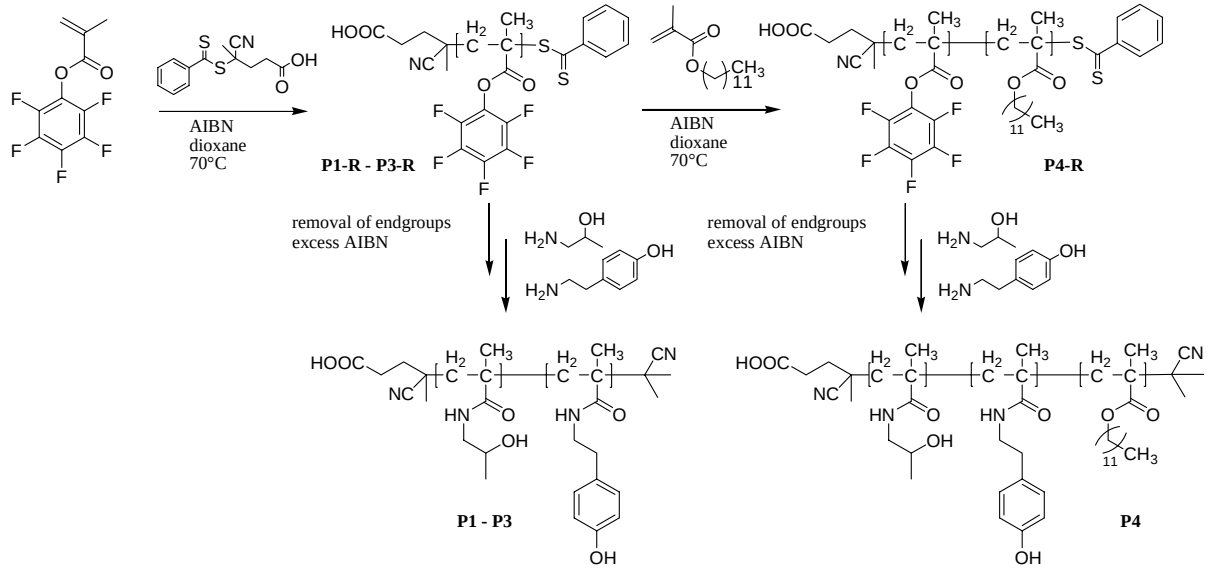

Scheme 1: Synthetic Pathway to Functional Precursor Polymers via RAFT Polymerization

Table 1: Synthesized reactive and functional polymers as precursors for radioactive labeling

polymer	block ratio	ratio of tyramin units at the polymer %	M_n (number average of molecular weight)	M_w (weight average of molecular weight)	PDI
P1-R	-	-	21090[b]	25090[b]	1.19[b]
P2-R	-	-	50260[b]	60840[b]	1.21[b]
P3-R	-	-	103900[b]	134100[b]	1.29[b]
P4-R	87:13[a]	-	22680[b]	27920[b]	1.25[b]
P1	-	3[a]	10980[c]	13050[c]	1.19
P2	-	3[a]	26140[c]	31640[c]	1.21
P3	-	3[a]	54030[c]	69730[c]	1.29
P4	87:13[a]	3[a]	12570[c]	15880[c]	1.25

[a] As determined by ^{1}H-NMR spectroscopy after aminolysis with hydroxypropylamine yielding P1 to P4. [b] As determined by GPC in THF as solvent for the activated ester polymers P1-R to P4-R. The value for P1 and P2 is recalculated from the molecular structure. [c] Calculated from the block ratio obtained by ^{1}H-NMR spectroscopy and GPC data of P1-R to P4-R.

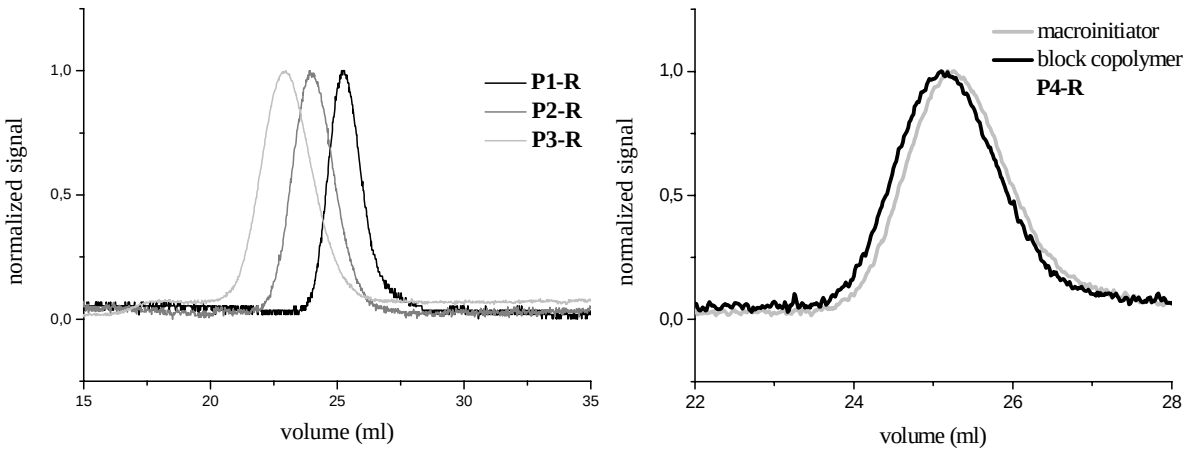

Figure 1: GPC elugram of reactive homopolymers P1-R, P2-R and P3-R (a) and GPC elugram of the macro initiator and final block copolymer P4-R (b).

To achieve regio-selective introduction of an ^{18}F-label, the reactive polymers have been reacted with 2-hydroxy-1-aminopropane and besides with a rather small amount (3%) of tyramine (4-(2-aminoethyl) phenol) to the hydrophilic block to minimize the influence on the polymer´s structure. For ^{18}F-labeling purposes, the phenolic tyramine moieties were first deprotonated using a

smaller amount of base compared to the introduced phenolic hydroxy groups and subsequently labeled using [^{18}F]FETos (Scheme 2).

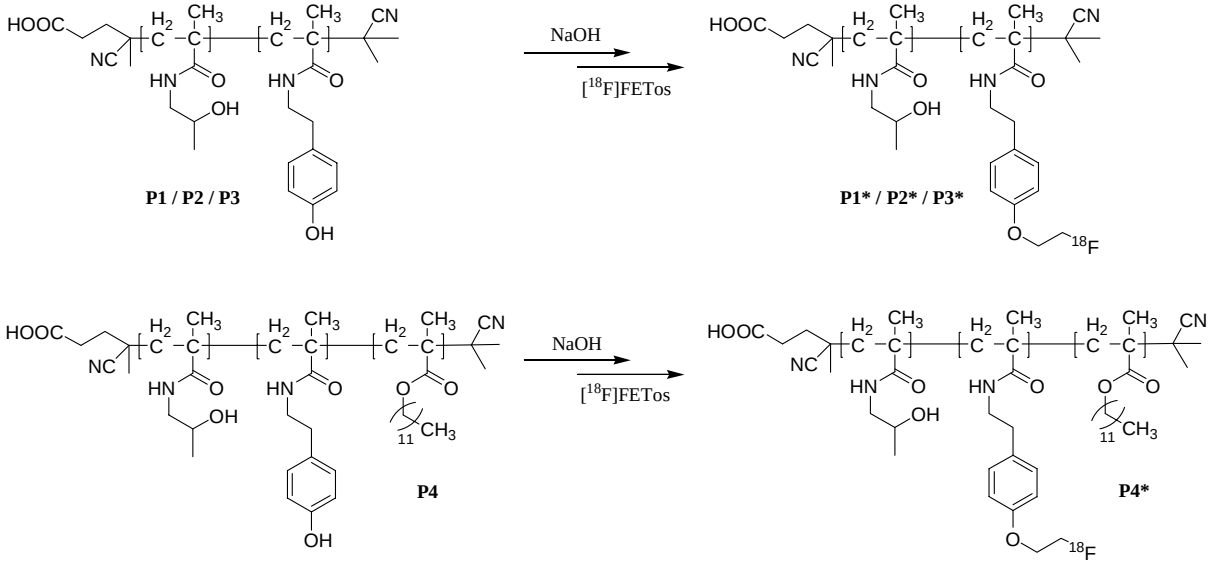

Scheme 2: Radioactive labeling of polymers using [^{18}F]FETos.

The radioactive labeling kinetics for 4 different polymers (P1-P4) have been evaluated and optimized. A clear dependence of the molecular weight on the decay-corrected radiochemical yield (RCY) at constant temperature could be observed. Higher molecular weight of the polymer led to minor RCY (Figure 2). This expected effect could be explained by the decrease in the surface-volume ratio. Less phenolic moieties should therefore be able to better interact with [^{18}F]FETos. This effect is obvious at all temperatures.

Five different temperatures from 60 up to 150 °C were studied and resulted in the expected tendency of increasing RCY with rising temperature until a maximum yield at ~120 °C reached. At all temperatures, the polymer itself is stable and does not decompose. The results are plotted in figure 3. The optimal RCY could be obtained at 120 °C in a reaction time of 10 min. However, even at 60 °C a suitable RCY of ~20% was observed after 15-20 min. This offers the possibility of labeling at ambient temperatures which is a necessary for incorporating temperature sensitive molecules into the polymer. The impact of sample mass of the polymer samples turned out to be rather small due to the fact that the amount of labeling agent [^{18}F]FETos is 10^4 to 10^7 times lower compared to the amount of polymer used. This leads to quasi-first order reaction kinetics, explaining the results. Purification was carried out by size exclusion chromatography (SEC) workup in PBS-buffer leading to a pure, labeled polymer and took ~10 min.

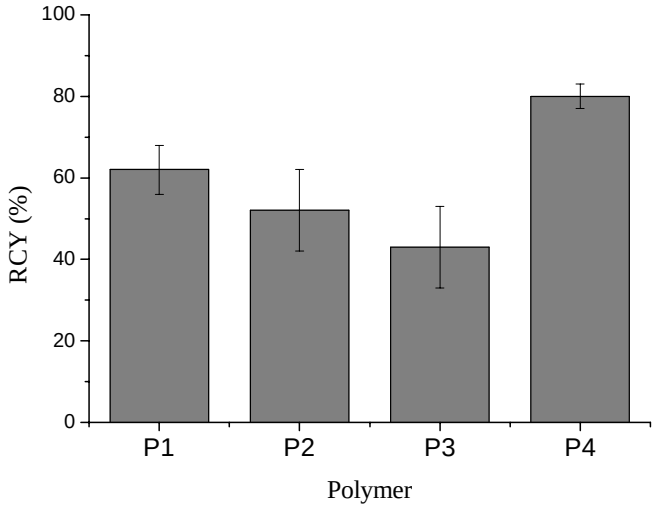

Figure 2: Corrected radiochemical labeling yields (RCY) of the random copolymers P1, P2, and P3 and the block copolymer P4 after 20 min at 100 °C using 3 mg of each precursor polymer.

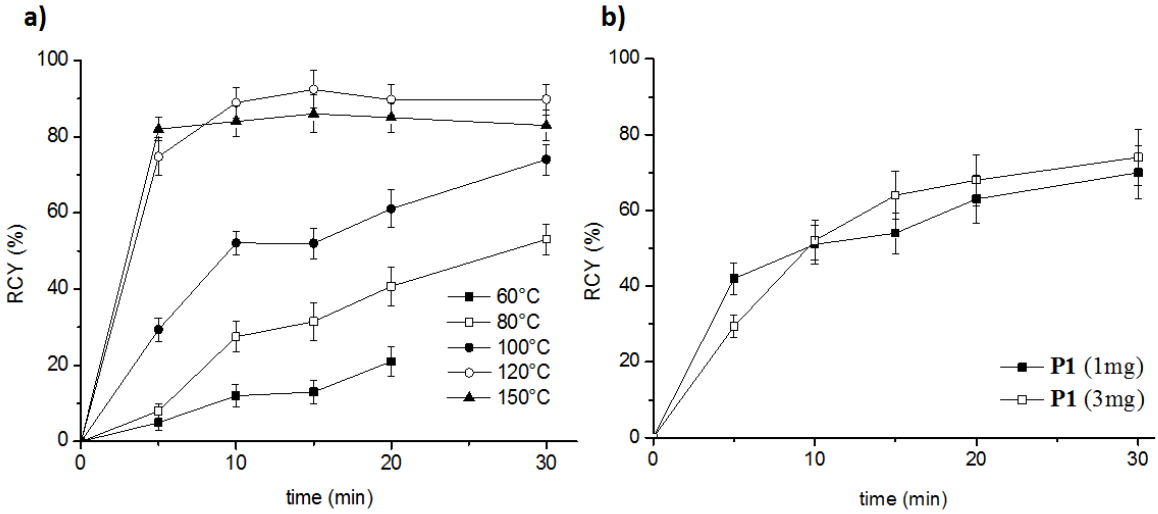

Figure 3: Corrected radiochemical labeling yields (RCY) of P1 depending on temperature (a) and amount of precursor at 100 °C (b).

The highest RCYs of 50% for random and ~80% for block copolymers have been obtained for the block copolymer P4. An explanation can be micellization in polar DMSO. Tyramine units are trapped in the hydrophilic part of the superstructure. Therefore, the local concentration of phenolic hydroxyl groups is higher compared to the random coil structures. This may result in high labeling yields. The specific radioactivity (A_s) of the polymers was found to be 30 MBq/$g_{polymer}$.

The stability of the polymer was tested 2 h after initial purification and no decomposition occurred (see Figure 4).

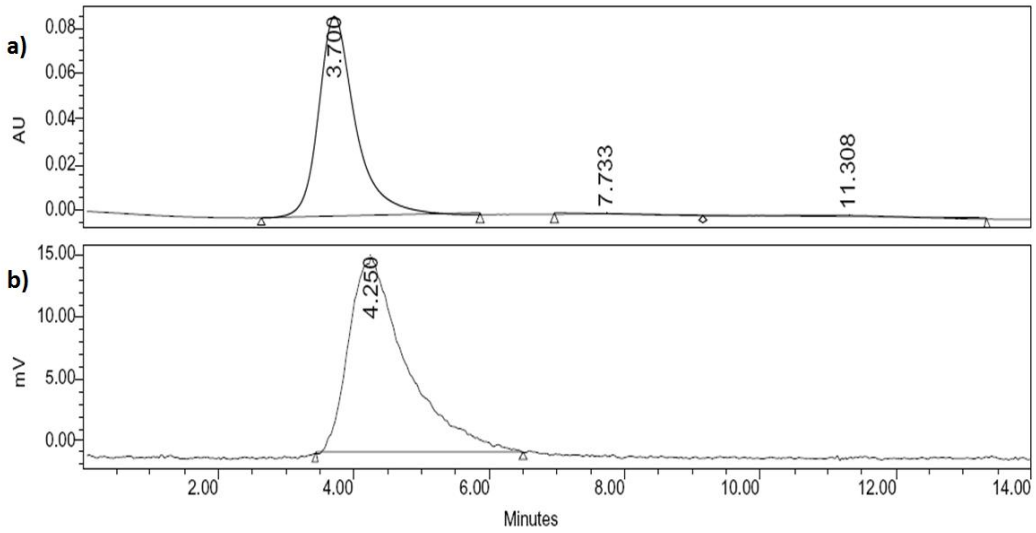

Figure 4: SEC elugram of the ^{18}F-labeled polymer P2 proofing stability 2 h after the initial purification in isotonic solution indicating any low molecular weight contamination due to decomposition: UV detector (a) and gamma counter (b).*

These promising results enabled initial PET experiments to determine the *in vivo* fate of these polymers in healthy rats. PET scans with polymer P2* were performed. As expected for slightly negative charged low molecular weight HPMA-based polymers [35], a strong accumulation was observed in the kidneys and in the bladder. Figure 5 shows a representative whole body *µ*PET image of the ^{18}F-labeled polymer P2*.

A metabolism study demonstrated the *in vivo* stability of the labeled HPMA-particles. Only a maximum content of ~20% radioactive metabolites could be detected in the blood. Interestingly, this amount does not change during 1 h of investigation hinting on a stable ^{18}F-labeled polymer after initial metabolism. *In vitro*, the labeled polymer was not bound to human serum albumine (Figure 6a), indicating that the synthesized polymer does not show physical interaction with proteins. However, *in vivo* analysis of the metabolism showed that approximately 20-30% of the radioactivity was found bound to plasma proteins (Figure 6b, "radioactivity bound to metabolites"), indicating that the polymer undergoes some kind of metabolism and the ^{18}F-label may detach from the polymer. A more detailed study has to be carried out to investigate the stability of the O-fluoro-ethyl label and the influence of structural diverse polymers on *in vivo* metabolism.

The accumulation of radioactivity in the kidneys and the bladder in the PET study can be explained by the renal clearance of the ^{18}F-labeled HPMA-polymers. A metabolism study of the urine demonstrated only the existence of ^{18}F-labeled macromolecules within the bladder indicating the polymer per se is not metabolized in the organism.

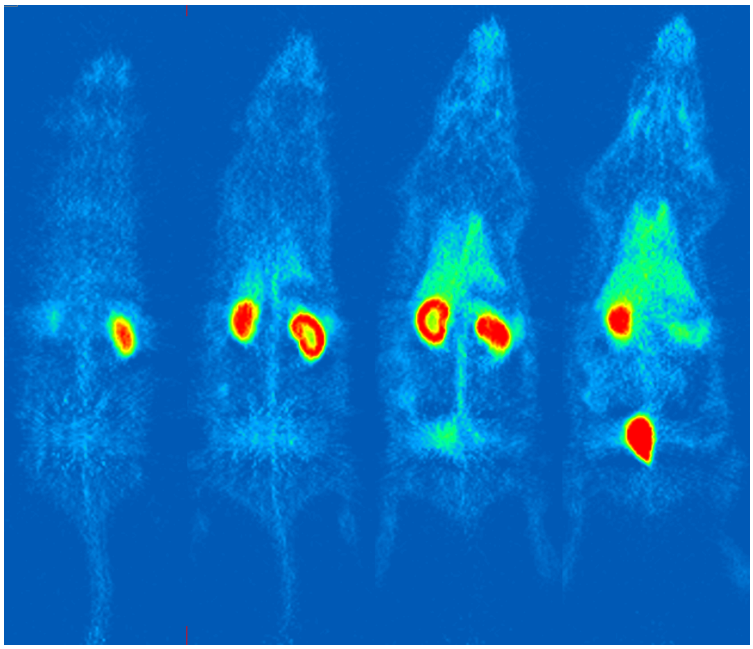

Figure 5: A representative whole body µPET summed image 140 - 150 min p.i. of the ^{18}F-labeled polymer P2 proofing the renal clearance. The most prominent accumulation is seen in the kidneys and the bladder.*

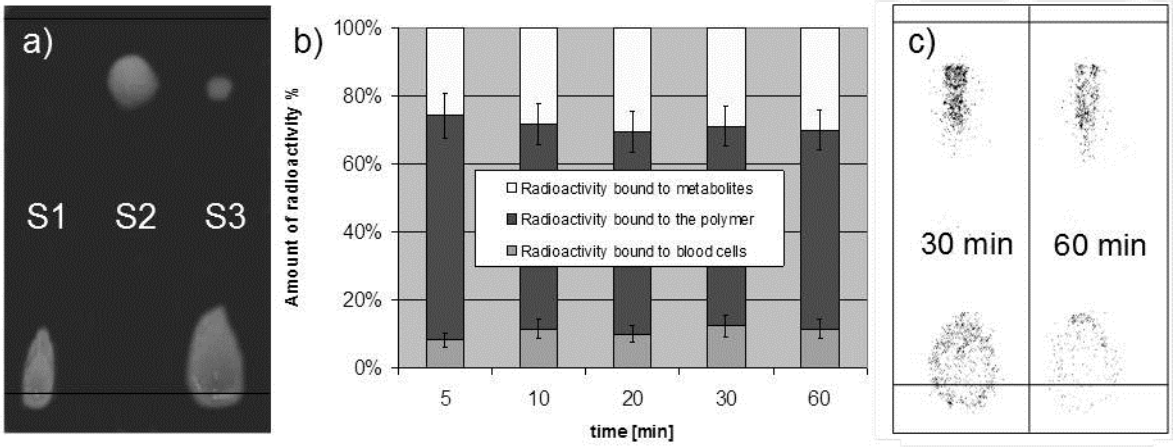

Figure 6: Metabolic analyses of ^{18}F-labeled HPMA. (a) RP-TLC in MeOH/H_2O (4:1) of isotonic solutions: 40 mg/mL of human serum albumine (HSA; S1), 1 mg/mL of polymer P2 (S2), as well as a mixture of 0.2 mg P2 and 40 mg HSA in 1 mL of S3. Staining was performed using Seebach Reagent. (b) Distribution of radioactivity among blood cells, proteins, and free polymer ^{18}F-labeled P2 in plasma water from 5 to 60 min p.i. determined by radio RP-TLC and automatic γ-counter. (c) Comparison of metabolism of polymer ^{18}F-labeled P2* in blood 30 and 60 min p.i. monitored by radio RP-TLC in MeOH/H_2O (4:1), ensuring a small amount of metabolite.*

Altogether, total ^{18}F-fluorination including [^{18}F]FETos synthesis, polymer labeling and polymer purification *via* SEC took no longer than 90 min and resulted in an ^{18}F-labeled polymer which can now be used for PET imaging over a period from 5-10 h. This time scale appears reasonable to study the particle distribution and accumulation regarding short-term pharmacokinetics.

Conclusion

A new versatile ^{18}F-labeling strategy for polymeric particles has been introduced. Defined and functional HPMA-based random and block copolymers have been synthesized by RAFT polymerization and labeled in high RCY of >50% using [^{18}F]FETos in a reaction time of ~ 10 min. Overall synthesis, including [^{18}F]FETos synthesis, polymer labeling, and polymer purification *via* SEC, was carried out in less than 90 min. The labeled polymer showed no decomposition. First metabolism and *μ*PET experiments showed promising results concerning the *in vivo* behavior of the ^{18}F-labeled polymer P2*. The accumulation of radioactivity in kidneys and bladder is due to the renal clearance of the intact compound. Slight metabolism was observed in the blood. However, after initial metabolism, no further degradation could be detected.

In summary, a new method to label polymer precursors by ^{18}F-fluorine has been carried out enabling biological evaluation of polymeric systems *in vivo via μ*PET in the close future. This approach will provide the possibility of precise *in vivo* imaging of polymeric nanoparticles over a period of 5-10 h. Furthermore, this approach may lead to a detailed understanding in which way alterations in physical properties of the nanostructures such as size, surface chemistry or core material will influence the fate of nanoparticles in living systems.

Acknowledgment

The authors wish to thank Sabine Höhnemann and Vasko Kramer for the synthesis of [^{18}F]FETos as well as Nicole Bausbacher and Hans-Georg Buchholz for assistance during PET measurements. We also want to thank Prof. Dr. Helmut Ringsdorf for excellent and fruitful discussion. Financial support by Friedrich-Naumann-Stiftung, the European Network of Excellence (EMIL), and Polymat Graduate School of Excellence is gratefully acknowledged.

References and Notes

[1] Jemal, A.; Murray, T.; Ward, E.; Samuels, A.; Tiwari, R. C.; Ghafoor, A.; Feuer, E. J.; and Thun, M. J. Cancer statistics, *CA Cancer J. Clin.* 2005, *55*, 10.

[2] Thompson, J. F.; Scolyer, R. A.; and Kefford, R. F. *Lancet* 2005, *365*, 687.

[3] Duncan, R. *Nat. Rev. Cancer* 2006, *6* (9), 688.

[4] Ringsdorf, H. *J. Polym. Sci,. Polym. Symp*. 1975, *51*, 135.

[5] Adams, M. L.; Lavasanifar, A.; Kwon, G. S. *J. Pharm. Sci.* 2003, *92*, 1343.

[6] Bae, Y.; Fukushima, S.; Harada, A.; Kataoka, K. *Angew. Chem., Int. Ed.* 2003, *42*, 4640.

[7] Kakizawa, Y.; Harada, A.; Kataoka, K. *Biomacromolecules* 2001, *2*, 491.

[8] Kim, S. Y.; Shin, I. L. G.; Lee, Y. M.; Cho, C. S.; Sung, Y. K. *J. Controlled Release* 1998, *51*, 13.

[9] Kwon, G.; Naito, M.; Yokoyama, M.; Okano, T.; Sakurai, Y.; Kataoka, K. *Langmuir* 1993, 9*,* 945.

[10] Nasongkla, N.; Bey, E.; Ren, J.; Ai, H.; Khemtong, C.; Guthi, J. S.; Chin, S. F.; Sherry, A. D.; Boothman, D. A.; Gao, J. *Nano Lett.* 2006, *6*, 2427.

[11] Torchilin, V. P. *Pharm. Res.* 2007, *24*, 1.

[12] Hongrapipat, J.; Kope Ková, P.; Prakongpan, S.; Kopecek, J. *Int. J. Pharm.* 2008, *351*, 259.

[13] Mitra, A.; Nan, A.; Papadimitriou, J. C.; Ghandehari, H.; Line, B. R. *Nucl. Med. Biol.* 2006, *33*, 43.

[14] Satchi-Fainaro, R.; Puder, M.; Davies, J. W.; Tran, H.T.; Samson, D. A.; Greene, A. K.; Corfas, G.; Folkman, J. *Nat. Med.* 2004, *10*, 225

[15] Vicent, M. J.; Greco, F.; Nicholson, R. I.; Paul, A.; Griffiths, P. C.; Duncan, R. *Angew. Chem., Int. Ed.* 2005, *44*, 2.

[16] Duncan, R. *PSTT* 1999, *2*, 441.

[17] Konak, C.; Matyjaszewski, K.; Kopeckova, P.; Kopecek, J. *Polymer* 2002, *43*, 3735.

[18] Ayhan, H.; Tuncel, A.; Bor, N.; Piskin, E. *J. Biomater. Sci., Polym. Ed*. 1995, *7*, 329.

[19] Norde, W.; Lyklema, J. *J Biomater Sci Polym Ed*. 1991, 2, 183.

[20] Schwendener, R.A.; Lagocki, P.A.; Rahman, Y.E. *Biochim. Biophys. Acta* 1984, *772*, 93.

[21] Krenning, E. P.; Kwekkeboom, D. J.; Valkema, R.; Pauwels, S.; Kvols, L. K.; De Jong, M. *Ann. N.Y. Acad. Sci.* 2004, *1014*, 234.

[22] Harrington, K.J.; Rowlinson-Busza, G.; Syrigos, K. N.; Uster, P.S.; Abra, R. M.; Stewart, J.S.W. *Br. J. Cancer* 2000, *83*, 232.

[23] Wunderlich, G.; Grüning, T.; Paulke, B. R.; Lieske, A.; Kotzerke, J. *Nucl. Med. Biol.* 2003, *31*, 87.

[24] Nahrendorf, M.; Zhang, H.; Hembrador, S.; Panizzi, P.; Sosnovik, D. E.; Aikawa, E.; Libby, P.; Swirski, F. K.; Weissleder, R. *Circulation* 2008, *117*, 379.

[25] Wolf, G. L. *Targeted Delivery of Imaging Agents;* CRC Ress: Boca Raton, FL, 1995; Vol. 3.

[26] Stein, P. D. *Curr. Opin. Pulm. Med.* 1999, *2*, 295.

[27] Rubin, G. D. *J. Thorac. Imaging* 1997, *12*, 128-149.

[28] Mathias, C. J.; Green, M. A. *Appl. Radiat. Isot.* 2008, *66*, 1910-1912.

[29] Moad, G.; Rizzardo, E.; Tang, S. H. *Polymer* 2008, *49*, 1079-1131.

[30] Eberhardt, M.; Mruk, R.; Zentel, R; Theato, P. *Eur. Polym. J.* 2005, *41*, 1569.

[31] Eberhardt, M.; Theato, P. *Macromol. Rapid. Commun*. 2005, *26*, 1488.

[32] Barz, M.; Tarantola, M.; Fischer, K.; Schmidt, M.; Luxenhofer, R.; Janshoff, A.; Theato, P.; Zentel, R. *Biomacromolecules* 2008, *9*, 3114.

[33] Perrier, S.; Takolpuckdee, P.; Mars, C. A. *Macromolecules* 2005, *38*, 2033.

[34] Bauman, A.; Piel, M.; Schirrmacher, R.; Rösch, F. *Tetrahedron Lett.* 2003, *44*, 9165.

[35] Kissel, M.; Peschke, P.; Subr, V.; Ulbrich, K.; Schumacher, J.; Debus, J.; Friedrich, E. *PDA J. Pharm. Sci. Technol.* 2001, *55*, 191.

3.2 Modifying the body distribution of HPMA-based copolymers by molecular weight and aggregate formation

Modifying the body distribution of HPMA-based copolymers by molecular weight and aggregate formation

Mareli Allmeroth[1,§], Dorothea Moderegger[1,*], Barbara Biesalski[¢], Kaloian Koynov[†], Frank Rösch[*], Oliver Thews[‡] and Rudolf Zentel[§]

[1] both authors contributed equally

[§] Institute of Organic Chemistry, Johannes Gutenberg University, Duesbergweg 10-14, 55099 Mainz, Germany

* Institute of Nuclear Chemistry, Johannes Gutenberg University, Fritz-Strassmann-Weg 2, 55128 Mainz, Germany

[¢] Institute of Physiology and Pathophysiology, University Medicine Mainz, Duesbergweg 6, 55128 Mainz, Germany

[†] Max-Planck-Institute for Polymer Research, Ackermannweg 10, 55128 Mainz, Germany

[‡] Institute of Physiology, University Halle, Magdeburger Str. 6, 06097 Halle (Saale), Germany

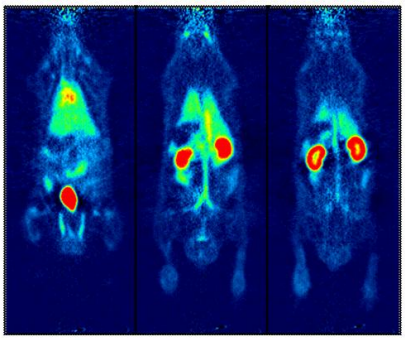

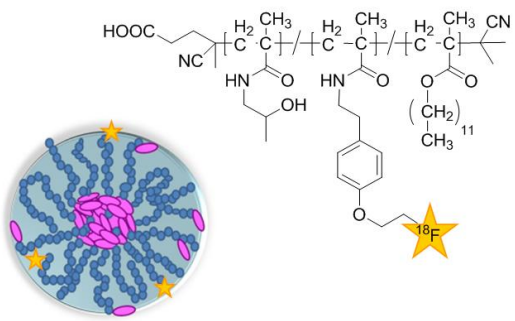

Abstract

There is a recognized need to create well defined polymer probes for *in vivo* and clinical positron emission tomography (PET) imaging to guide the development of new generation polymer therapeutics. Using the RAFT polymerization technique in combination with the reactive ester approach, here we have synthesized well-defined and narrowly distributed *N*-(2-hydroxypropyl)methacrylamide homopolymers (pHPMA) (P1* and P2*) and random HPMA copolymers consisting of hydrophilic HPMA and hydrophobic lauryl methacrylate comonomers (P3* and P4*). The polymers had molecular weights below (P1* and P3*) and above the renal threshold (P2* and P4*). Whereas the homopolymers dissolve in isotonic solution as individual coils, the random copolymers form larger aggregates above their critical micelle concentration (around 40 nm) as determined by Fluorescence Correlation Spectroscopy. Structure-property relationships of the pharmacokinetics and biodistribution of the different polymer architectures were monitored in the living organism following radiolabeling with the positron emitter ^{18}F *via* fluoroethylation within a few hours. *Ex vivo* organ biodistribution and *in vivo* μPET imaging studies in male Copenhagen rats revealed that both size and the nature of the aggregate formation (hydrophobically modified copolymers) played a major role in blood clearance and biodistribution, especially concerning liver and kidney accumulation. The high molecular weight random copolymer P4* (hydrophobically modified) in particular combines low liver uptake with enhanced blood circulation properties, showing the potential of hydrophobic interactions – as seen for the represented model system – that are valuable for future drug carrier design.

Keywords: HPMA, RAFT polymerization, Structure-property relationships, Drug delivery, Fluorine-18 labeling, PET

Introduction

"Polymer therapeutics" – a term describing polymeric drugs, polymer-drug conjugates, polymer-protein conjugates, polymeric micelles and polyplexes – became an emerging field of interest in both chemical and medical sciences over the last four decades [1]. Their diversity regarding loading capacity with multiple pharmaceutics, reduction of usually occurring toxic side effects as well as an inherent tendency to accumulate in tumor tissue due to the EPR (Enhanced Permeability and Retention)-effect [2, 3], constitutes them as an attractive tool for clinical applications. Based on the first concept of Ringsdorf in the 1970's [4] concerning a macromolecular-based drug delivery vehicle for active and passive targeting for improving the therapeutic action, fundamental research in this

discipline has evolved. Intensive studies on polymer-drug conjugates [5-9], micelle forming polymers [10-13] or newly established polymer-enzyme combination therapy [14-16] have been carried out, demonstrating the great potential of the route pursued. Altogether only poly(ethylene glycol) (PEG), poly-*N*-(2-hydroxypropyl)methacrylamide) (HPMA) copolymers, dextran derivatives as well as polyglutamic acid based drug conjugates have progressed into clinical trials, six among them being HPMA anticancer conjugates [1, 9, 17].

Regarding the clinical application of polymer based therapeutics, there is a need for appropriate preclinical screening methodologies to select a suitable therapy for the individual patient [18, 19]. In this respect introducing small radioactive probes into the polymeric system and using nuclear medicine imaging techniques such as positron emission tomography (PET), pharmacokinetics and distribution of the polymer therapeutic can be easily monitored. Depending on the biological time-frame to be monitored, PET-nuclide and labeling strategy need to be adjusted. Based on the short-lived positron emitter fluorine-18 ($t_{1/2}$ = 110 min), we have recently developed PET based HPMA copolymers for short-term *in vivo* visualization, thereby being time-efficient and enabling minimal radiation exposure concerning a clinical application [20]. In contrast, also new labeling approaches for HPMA-based polymers using PET-nuclides of longer half-lives, e.g. $^{72/74}$As ($t_{1/2}(^{72}As)$ = 26 h), $t_{1/2}(^{74}As)$ = 17.8 d) were established, offering the possibility for long-term PET-imaging with time-frames of weeks to months [21].

By introducing fluorine-18 as PET nuclide, initial excretion pathways and organ uptake can be identified and measured quantitatively. Due to its excellent physical and nuclear characteristics, fluorine-18 is considered the ideal radioisotope for PET imaging probes, providing visualization of high spatial resolution and because of its size not influencing the polymeric structure. In contrast to radionuclides for SPECT (Single Photon Emission Computed Tomography) (e.g. ^{123}I, ^{131}I and ^{99m}Tc) – so far used to image HPMA-based polymers [22, 23] – fluorine-18 as short-lived isotope combines the requirements for fast and detailed screening of potential drug carrier systems giving insight into individual early phase accumulations and clearance mechanisms.

Regarding the therapeutic effects of a polymer based drug carrier system its backbone plays a crucial role. Essential requirements are mainly either biodegradability or biocompatibility with final excretion properties. Being water soluble, non-toxic and non-immunogenic, poly-*N*-(2-hydroxypropyl)methacrylamide), has evolved as promising biocompatible artificial polymer, already intensively studied *in vitro* and *in vivo* [9, 24-26]. Compared to PEG it possesses the advantage of multifunctionality whereas PEG only has two functional end groups. That enables covalent

conjugation of a higher drug payload, attachment of recognition units for receptor-mediated targeting or combination therapy [15].

When being developed as a polymer therapeutic, it is important that a polymer should be as well-defined as possible [27]. The first HPMA-based polymers were, however, originally made by free radical polymerization [28-31] and required lengthy as well as laborious fractionation processes to reduce their polydispersity [32]. With the introduction of living radical polymerization techniques, well-defined polymer structures became available, either by ATRP or by RAFT techniques [33-36]. Especially in combination with the reactive ester approach [12, 20, 37], RAFT offers an elegant access to different polymer architectures and various functional groups, e.g. imaging moieties or therapeutics can be attached. By applying this route, HPMA random as well as block copolymers of specific composition can be easily prepared, exhibiting the tendency to aggregate in solution due to hydrophobic laurylmethacrylate side chains [12].

To be effective as an antitumor agent, a polymer drug conjugate must be able to localize to the tumor tissue by the EPR effect [2, 38] (resulting from leaky tumor blood vessels and a lack of lymphatic drainage) and prevent the drug from localizing to normal tissues that are potential sites of toxicity. Furthermore long circulation properties in the blood pool might be beneficial for a controlled and continuous drug release.

Lammers et al. [39] applied radiolabeling with SPECT isotope iodine-131 to investigate the influence of the incorporation of various functional groups into HPMA (copolymers) on the body distribution and accumulation in the tumor. This work included polymer therapeutics like PK1 polymers but focused on functional groups which interact by H-bonding or ionic charges like carboxylate, amine groups or peptides. The authors found that the copolymer units mostly reduced the circulation time in the body but did not change the relative accumulation in different tissues as well as the tumor. Classical polymeric therapeutics like PK1 or PK2 [40, 41] often carry hydrophobic pharmaceutics. Based on these characteristics they are – in a physico-chemical sense – hydrophobically modified copolymers. This underlines the importance to focus also on the aspect of intra- and intermolecular aggregate formation due to hydrophobic interactions in model systems. In this respect, the synthesis of HPMA-based hydrophilic/ hydrophobic copolymers and their aggregate formation makes model systems available in which it is easy to vary the size and the hydrophilic/hydrophobic balance. Experiments with cell cultures already demonstrated the tremendous influence of the variation of these segments on the cellular uptake of HPMA-based polymers [12] and recent studies underline their potential to transport pharmaceutics across the blood-brain-barrier [42].

Consequently, the aim of the present study focused on the determination of correlations between size and aggregate formation due to hydrophobic interactions and resulting biological properties (body and organ distribution) of well-defined HPMA-based polymers in living animals.

Applying fast and versatile radiolabeling techniques for noninvasive high resolution PET imaging helps to understand how the *in vivo* fate of a polymer model system can be affected by structural modification thus speeding up the time consuming evaluation process necessary for the design of potential drug carrier candidates.

Materials and Methods

Materials

All solvents were of analytical grade, as obtained by Sigma Aldrich and Acros Organics. Dioxane was distilled over a sodium/potassium composition. Lauryl methacrylate was distilled to remove the stabilizer and stored at -18 °C. 2,2'-Azo-bis-(isobutyronitrile) (AIBN) was recrystallized from diethyl ether and stored at -18 °C as well.

Characterization

^{1}H-NMR spectra were obtained by a Bruker AC 300 spectrometer at 300 MHz, ^{19}F-NMR analysis was carried out with a Bruker DRX-400 at 400 MHz. All measurements were accomplished at room temperature and spectroscopic data were analyzed using ACDLabs 9.0 1D NMR Manager. The synthesized polymers were dried at 40 °C under vacuum over night, followed by Gel Permeation Chromatography (GPC). GPC was performed in tetrahydrofuran (THF) as solvent, using following equipment: pump PU 1580, autosampler AS 1555, UV detector UV 1575 and RI detector RI 1530 from Jasco as well as a miniDAWN Tristar light scattering detector from Wyatt. Columns were used from MZ Analysentechnik, 300x8.0 mm: MZ-Gel SDplus 106 Å 5 µm, MZ-Gel SDplus 104 Å 5 µm and MZ-Gel SDplus 102 Å 5 µm. GPC data were evaluated by using the software PSS WinGPC Unity from Polymer Standard Service Mainz. The flow rate was set to 1 mL/min with a temperature of 25 °C.

For synthesis of 2-[^{18}F]fluoroethyl-1-tosylate ([^{18}F]FETos), a Sykam S 1100 pump and a Knauer UV-detector (K-2501) HPLC system were used. Size Exclusion Chromatography (SEC) of ^{18}F-labeled polymers was performed using HiTrap™ Desalting Column, Sephadex G-25 Superfine and a waters pump (1500 series), a Waters UV-detector (2487 λ absorbance detector) and a Berthold LB 509 radiodetector.

In *ex vivo* studies, fluorine-18 activities were determined using a Perkin Elmer 2470 Wizard^2 γ–counter.

Synthesis of the polymers

The polymers P1* to P4* were prepared in analogy to reference [12, 20]. The details are added as supplementary information.

Characterization of the polymers

The amphiphilic character of the hydrophobically modified HPMA copolymers (P3* and P4*) was characterized by a “du Noüy” ring tensiometer used to determine the cmc (critical micelle concentration) in isotonic sodium chloride solution. The protocol can be found as supplementary data.

The hydrodynamic radii of the polymeric systems were determined by Fluorescence Correlation Spectroscopy (FCS) using a commercial FCS setup. This method proves the aggregate formation of the copolymers. The details can be found in the supplementary information.

Radiolabeling and purification for *ex vivo* and *in vivo* experiments

Synthesis of [^{18}F]FETos, labeling of polymers P1* - P4* as well as purification of labeled polymers for *ex vivo* and *in vivo* experiments was accomplished according to literature [20].

For metabolic studies, blood samples were taken 140 min p.i., centrifuged and blood plasma was analyzed using SEC. Details are provided as supplementary information.

Animal experiments

Tumor and animal model

Tumor experiments were performed with the subline AT1 R-3327 Dunning prostate carcinoma of the rat. Tumors were used when they reached a volume of 1 to 2 mL approximately 10 to 14 days after tumor cell injection. At this time point tumors were in the exponential growing phase and did not show signs of necrosis (confirmed by histology; data not shown). All experiments had previously been approved by the regional animal ethics committee and were conducted in accordance with the German Law for Animal Protection and the UKCCCR Guidelines [43]. Details are provided as supplementary information.

Biodistribution measurements

In order to assess the distribution of the radiolabeled polymers in different organs of the animals, the polymer (concentration of 1 mg in 1 mL sodium chloride solution) was injected i.v. in anaesthetized tumor-bearing rats *via* the tail vein with a mean activity of 18.7 ± 5.8 MBq. After 120 or 240 min, the animals were sacrificed and different organ (kidney, liver, lung, spleen, heart, skeletal muscle, small intestine, testis, blood) and tumor samples were taken. The tissue samples were weighed and minced. Finally, the ^{18}F-activity in the organs was measured in a γ-counter.

Small animal PET studies

In addition the uptake of the different polymers in tumors and organs was imaged using PET. Details of the imaging procedure are described as supplementary information.

Results and Discussion

Synthetic concept of HPMA-based homo- and random copolymers

To study the *in vivo* behavior of different polymeric architectures in dependence of their molecular weight and the effect of aggregate formation due to the presence of hydrophobic segments, diverse HPMA-based polymeric systems were synthesized applying the RAFT polymerization technique [33, 34, 44]. Barz et al. already found that especially the aggregate formation significantly influences the cellular entry into MCF7/ADR cells *in vitro* [12]. Here we aimed to gain more knowledge about structure-property relationships not only on the cellular level but in the living organism. First results emphasized a successful radioactive labeling of such polymers [20]. For further systematic studies, a series of HPMA homopolymers and HPMA-*ran*-LMA copolymers were prepared, with molecular weights chosen to be below and above the renal threshold (limit of renal clearance of HPMA copolymers M_w < 40000 g/mol [45]). The incorporation of the hydrophobic lauryl methacrylate constitutes the basis for aggregate formation. Due to differences in size and aggregate formation we expected different pharmacological behavior in terms of organ accumulation, circulation time as well as excretion characteristics. The synthetic route to these polymers (P1*-P4*) is depicted in scheme 1.

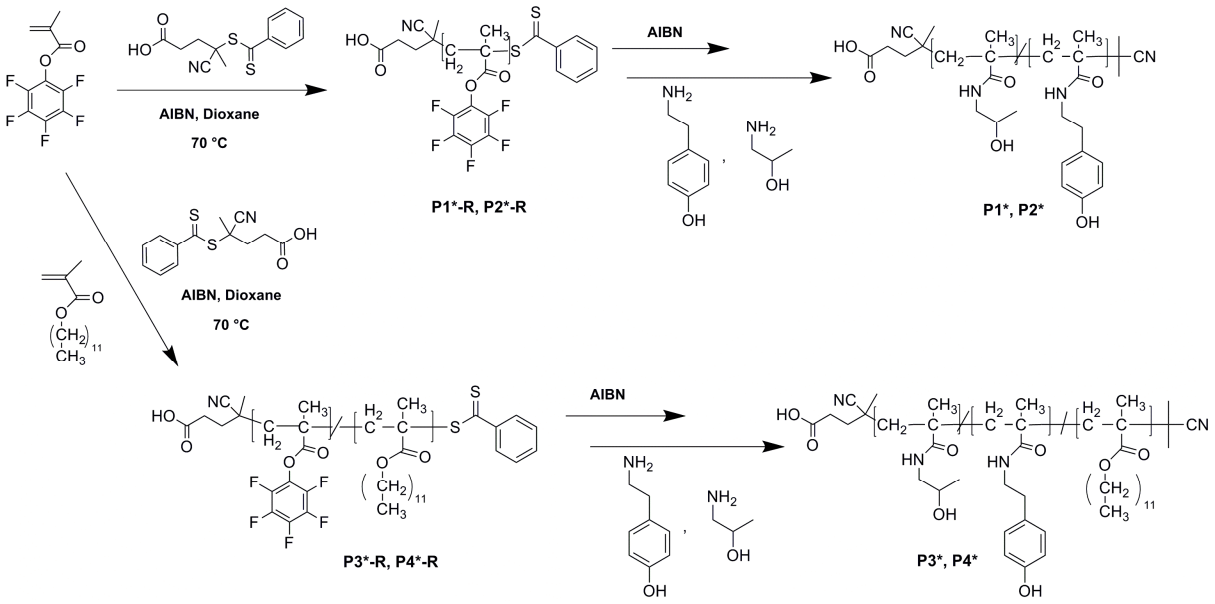

Scheme 1: Reaction scheme of polymeric precursor systems based on the reactive ester approach and their polymer-analogous conversion for further radioactive labeling

Starting with the pentafluorophenyl methacrylate monomer, the precursor homopolymers P1*-R and P2*-R were synthesized and by simultaneous addition of lauryl methacrylate, the statistical copolymers P3*-R and P4*-R. The polymerization was achieved according to literature [12, 46, 47]. These reactive polymers can afterwards be converted to HPMA-based polymers by a clean conversion. A main advantage of this synthetic route to HPMA-*ran*-LMA copolymers lies in the random copolymerization of two methacrylate-based monomers (both esters). Due to the comparable copolymerization parameters, a random, non-blocky integration of both monomers is reasonable (copolymerization parameters were determined with r_1 and r_2 both < 1). This provides an important advantage compared to the copolymerization of amides with esters [48]. In addition the primarily formed reactive polymers P1*-R to P4*-R are well soluble and do not form aggregates as all monomer units are hydrophobic. The dithioester endgroup was cleaved by an excess of 2,2'-azo-bis-(isobutyronitrile), a method first presented by Perrier et al. [49], possessing the benefit of avoiding side reactions during the post-polymerization step. The polymeric precursors were functionalized by aminolysis *via* tyramine groups, necessary for further radioactive labeling. The incorporation efficiency was calculated to be 2 - 4% for each polymer chain. 2-Hydroxypropylamine was finally added, resulting in the polymeric structures P1*-P4*. Full conversion of the reactive ester side groups could be proven by means of ^{19}F-NMR spectroscopy, demonstrating complete disappearance of the ^{19}F-signals at the polymeric backbone.

Molecular weights and incorporation ratios of polymeric architectures

Overall, four different polymeric systems were synthesized (all hydrophilic polymers P1* and P2* for reference and hydrophilic/ hydrophobic copolymers P3* and P4*), each architecture exhibiting a low and high molecular weight sample. Characterization of the precursor structures P1*-R - P4*-R was carried out using gel permeation chromatography. The results are summarized in table 1. As indicated, well-defined polymeric systems with relatively narrow molecular weight distribution have been achieved by the RAFT polymerization process [PDI= 1.26-1.49].

Table 1: Analytical data of reactive ester homopolymers (P1-R, P2*-R) and random copolymers (P3*-R, P4*-R) as well as the final polymeric structures P1*-P4* (see Scheme 1)*

nomenclature	polymeric structure	monomer ratio	M_n in g/mol	M_w in g/mol	PDI[b]
P1*-R	homopolymer	100%[a]	18000[b]	23000[b]	1.29
P2*-R	homopolymer	100%[a]	87000[b]	130000[b]	1.49
P3*-R	random copolymer	80:20[a]	17000[b]	21000[b]	1.26
P4*-R	random copolymer	80:20[a]	57000[b]	80000[b]	1.41
P1*	homopolymer	100%[c]	9000[d]	12000[d]	1.29
P2*	homopolymer	100%[c]	52000[d]	77000[d]	1.49
P3*	random copolymer	82:18[c]	11000[d]	14000[d]	1.26
P4*	random copolymer	75:25[c]	39000[d]	55000[d]	1.41

[a] Calculated monomer ratio. [b] Determination by GPC in THF as solvent. [c] Monomer ratio determined by ^{1}H-NMR spectroscopy after polymer-analogous reaction with 2-hydroxypropylamine (P1*-P4*). [d] Calculated from the molecular weights of the reactive ester polymers P1*-R to P4*-R as determined by GPC in THF as solvent.

Aggregation parameter

The major distinction between homo- and copolymers relies in the formation of micelle-like structures due to the incorporation of hydrophobic groups, in our case lauryl methacrylate. To determine the concentration-dependant aggregation behavior of the copolymers P3* and P4*, the critical micelle concentration (cmc) was determined by surface tension measurements with a "du Noüy" ring tensiometer. Stock solutions of 0.1 mg/mL in 0.9% NaCl solution were prepared and the measurement was performed at 37 °C to mimic *in vivo* conditions. For the low molecular weight copolymer P3* a cmc value of 4.6 x 10^{-3} mg/mL was obtained. Copolymer P4* exhibited a lower cmc of 1.6 x 10^{-3} mg/mL which is reasonable due to the increased LMA ratio. Based on these data it can be assumed that the polymeric aggregates are also present in the bloodstream of the rat (blood volume of the rat ~16 mL [50], corresponding to a concentration of 6.3 x 10^{-2} mg/mL polymer in the blood after intravenous injection of 1 mL of a 1 mg/mL isotonic solution). Even after renal clearance

of more than 50% of the polymer injected, the micellar-like structure should be retained. The cmc-values are additionally summarized in table 2.

Table 2: Critical micelle concentration of random copolymers (P3, P4*) in isotonic NaCl solution at 37°C*

nomenclature	polymeric structure	cmc in mg/mL[a]	cmc in mol/L
P3*	random copolymer	4.6×10^{-3}	4.2×10^{-7}
P4*	random copolymer	1.6×10^{-3}	4.2×10^{-8}

[a] As determined by surface tension *vs*. concentration applying the ring method of the "du Noüy" ring tensiometer.

To facilitate size determination of the aggregates formed from the amphiphilic copolymers in water, we additionally attached fluorescent Oregon Green 488 cadaverine onto the polymer chains. Fluorescence Correlation Spectroscopy was used to determine the diffusion constants of the individual polymer chains as well as of the aggregates and hence their hydrodynamic radii. The homopolymer P1* exhibited a hydrodynamic radius of 1.1 nm and the higher molecular weight polymer P2* a size of 3 nm (NaCl solution). Both values are a bit smaller than expected (for P4* in methanol, as non aggregating solvent, we observed a hydrodynamic radius of 6 nm) and are just taken as proof for the existence of individual random coils. The random copolymers P3* and P4* showed a different behavior and a superstructure formation. Copolymer P3* possessed a hydrodynamic radius of 33 nm and the random copolymer P4* an R_h of ~40 nm. Both values are much too large for individual chains, but also for classical micelles in which the size should not be much larger than two times the size of the individual chain. These data are consistent with earlier observations from our group [12]. They may be explained by the formation of "compound micelles" [51]. Also Haag and coworkers reported the formation of unexpectedly large supramolecular assemblies for nonionic dendritic amphiphiles being composed of hydrophilic polyglycerol dendrons and hydrophobic C11 or C16 alkyl chains [52]. The formation of more complex hydrophobic/hydrophilic superstructures can be the reason for the hydrodynamic radii of the random copolymer superstructures. A collection of the sizes for polymers P1*-P4* is given in table 3.

Table 3: Size of homopolymers (P1, P2*) and random copolymers (P3*, P4*) in isotonic NaCl solution by FCS at RT*

nomenclature	concentration in mg/mL	R_h in nm	**Δ** R_h in nm
P1*	0.1 mg	1.1	+/- 0.1
P2*	0.1 mg	3.0	+/- 0.2
P3*	0.1 mg	33.4	+/- 1.7
P4*	0.1 mg	39.9	+/- 2.2

Radioactive labeling with [^{18}F]fluorine

To study the behavior of the different polymeric architectures *in vivo*, the positron emitter fluorine-18 ($t_{1/2}$= 109.7 min) was introduced for both *ex vivo* organ distribution measurements as well as µPET imaging *via* a prosthetic labeling procedure using [^{18}F]FETos. Compared to γ-imaging using SPECT nuclides (e.g. ^{99m}Tc or ^{123}I), PET provides images of much higher spatial resolution due to the nuclear characteristics of fluorine-18. For labeling purposes the polymeric backbone had been derivatized with 2 - 4% of tyramine groups (these groups were present during the experiments described above), thus offering a reactive site for the regio-selective incorporation of the [^{18}F]fluoroethyl moiety [20]. The applied indirect labeling method is shown in scheme 2. In a first step fluorine-18 is incorporated *via* nucleophilic substitution yielding [^{18}F]FETos and subsequently transferred to a solution of the tyramine derivatized polymer which is deprotonated using a small amount of base.

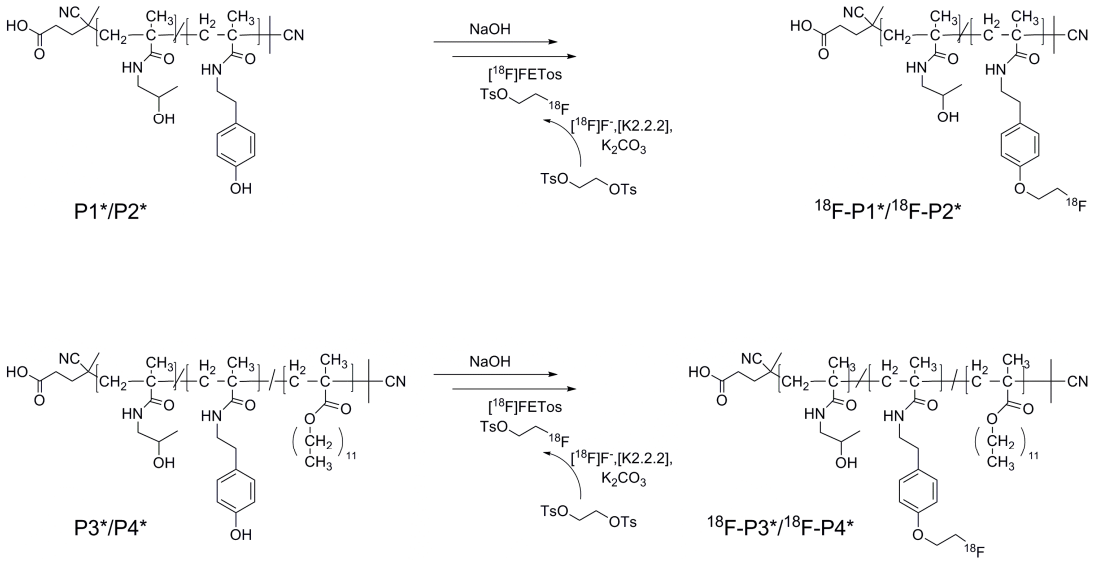

Scheme 2: Radioactive labeling of homopolymers (P1, P2*) and random copolymers (P3*, P4*) via prosthetic labeling procedure using [^{18}F]FETos*

Decay-corrected radiochemical yields (RCY) were determined by SEC and are summarized in table 4. RCYs were found to be dependent on the molecular weight and the lauryl methacrylate ratio at constant temperature. RCYs for the low molecular weight HPMA-based polymers were higher compared to the high molecular weight counterpart. We assume that this is the result of the lower accessibility of phenolic groups in the interior of the polymer coils. Likewise minor RCYs were observed for the lauryl methacrylate derivatives under the same conditions probably due to the formation of hydrophobic pockets leading to less accessible tyramine moieties.

Table 4: Decay-corrected radiochemical labeling yields of homopolymers (^{18}F-P1, ^{18}F-P2*) and random copolymers (^{18}F-P3*, ^{18}F-P4*) after 15 min at 120 °C using 3 mg ofeach polymer precursor in DMSO*

nomenclature	polymeric structure	monomer ratio[a]	M_w in g/mol[a]	RCY in %
^{18}F-P1*	homopolymer	100%	12.000	37± 6
^{18}F-P2*	homopolymer	100%	77.000	24 ±2
^{18}F-P3*	random copolymer	82:18	14.000	26 ±1
^{18}F-P4*	random copolymer	75:25	55.000	10 ±2

[a] cf. Table 1.

For biological experiments, the radiolabeled polymer systems were freed from low molecular weight by-products using SEC leading to a pure, ^{18}F-labeled polymer solution ready for *ex vivo* and *in vivo* experiments in an overall synthesis of less than 90 min beginning at the start of [^{18}F]FETos synthesis.

Altogether we were able to successfully apply the [^{18}F]fluoroethylation labeling method to a new series of HPMA homopolymers and HPMA-*ran*-LMA copolymers using optimized labeling conditions thus enabling *in vivo* imaging of different polymeric architectures.

Biodistribution studies

Fig. 1A shows the impact of the molecular weight of the HPMA-homopolymers ^{18}F-P1* and ^{18}F-P2* on the biodistribution in different tissues *ex vivo*. The smaller polymer (^{18}F-P1*, 12 kDa) showed highest concentrations in the kidneys (15.2 $\pm$ 3.1 % ID/g tissue) and the liver (1.6 $\pm$ 0.1 %ID/g tissue) 2 h after i.v. injection. These results correlate to already published data on the molecular weight dependence of HPMA copolymers [45], ensuring that the non-biodegradable HPMA-based polymer is cleared from the blood stream by renal filtration if the molecular weight is low enough. In other organs only marginal accumulation of the polymer was found.

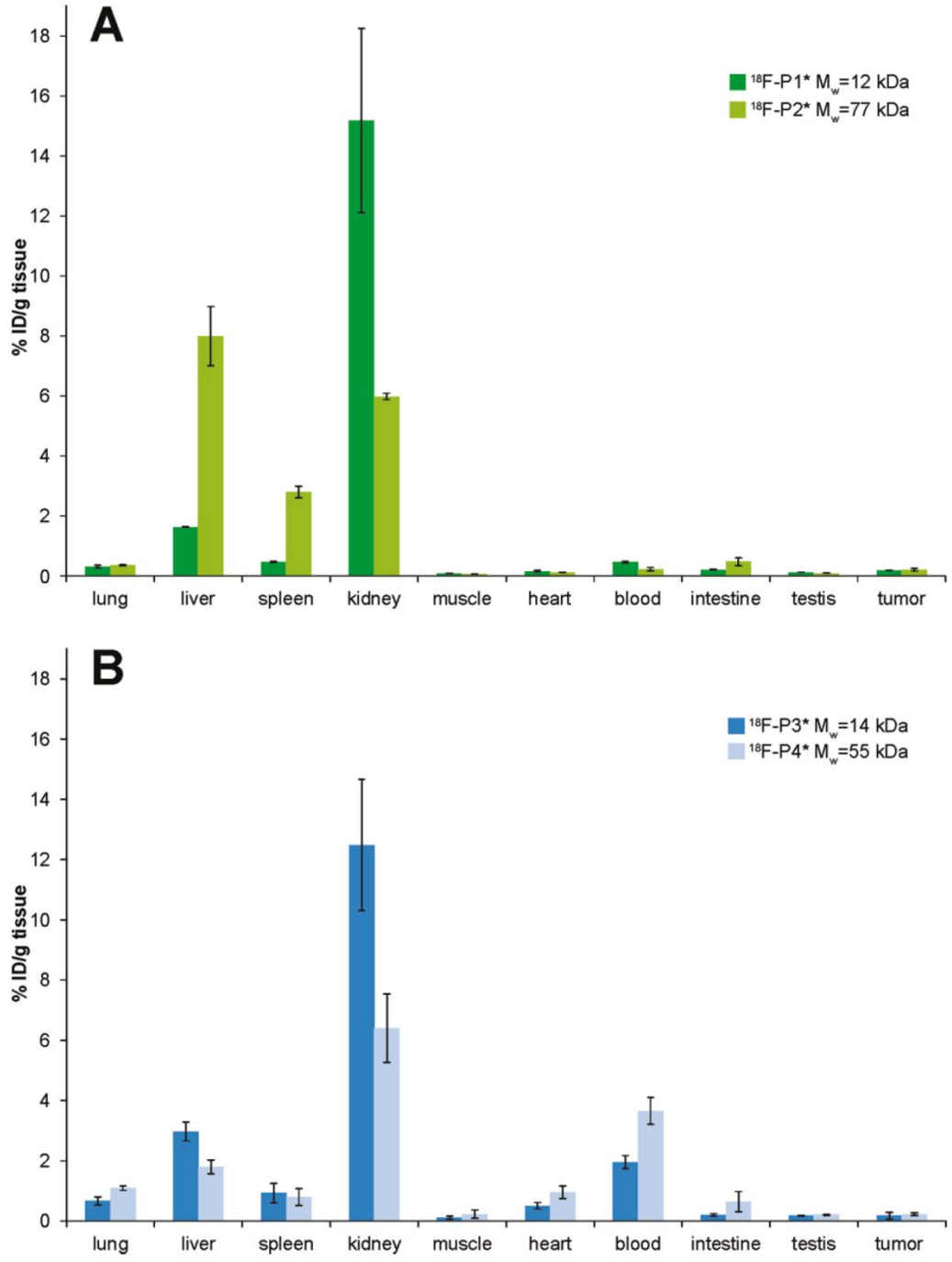

Figure 1: Influence of low and high molecular weight HPMA-based homopolymers and random HPMA-LMA copolymers on their biodistribution in male Copenhagen rats bearing AT1 R3327 Dunning prostate carcinoma 2 h post i.v. injection. (A) Recovered dose of injected ^{18}F-P1 (M_w = 12 kDa) versus ^{18}F-P2* (M_w = 77 kDa) in %ID/g tissue in organs of interest. (B) Recovered dose of molecular weight average 14 kDa (^{18}F- P3*) and 55 kDa (^{18}F- P4*) HPMA ran-LMA copolymers (n=3).*

In contrast, the high molecular weight homopolymer ^{18}F-P2* (77 kDa) was found less pronounced in the kidneys (6.0 ± 0.1 %ID/g tissue, Fig. 1A) whereas in the liver the concentration was 4-times higher (8.0 ± 1.0 %ID/g tissue) as compared to the ^{18}F-P1* polymer. In addition, the accumulation in the spleen was also much higher (2.8 ± 0.2 %ID/g tissue). These results indicate that the majority of i.v. injected radiolabeled high molecular weight polymer ^{18}F-P2* cannot be filtered by the renal system and is presumably taken up by the macrophages of the MPS (mononuclear phagocyte system) [53] or is excreted by the liver and bile. This indicates that the molecular weight is an important factor for the route of elimination of well-defined polymeric architectures, as already demonstrated for ^{125}I-labeled HPMA copolymers by Seymour et al. [45]. In comparison, the differences between the two polymers in other organs are marginal. In summary, most of the data received by the presented biodistribution study on HPMA-based homopolymers are comparable to the results of Lammers et al. who could demonstrate that different radioiodinated molecular weight poly(HPMA) showed significant disparities in body distribution [39]. Nevertheless the polymers differed slightly in molecular weight and the incorporation of the labeling group may also influence the *in vivo* behavior. By applying [^{18}F]fluoroethylation labeling, accumulation tendencies consistent with the above mentioned results could be obtained, accomplished in a shorter time span and enabling the benefit of non-invasive high resolution PET imaging – both favorable for patient selection concerning clinical therapies in the future [19].

Similar experiments were performed with the well-defined HPMA-*ran*-LMA copolymers ^{18}F-P3* and ^{18}F-P4* which differed in molecular weight (14 kDa *vs*. 55 kDa). These substances are different from the so far studied HPMA-based copolymer systems for drug delivery [13, 17, 54] because the copolymerization of two methacrylate-based monomers (pentafluorophenyl- and lauryl methacrylate) allows the preparation of randomly distributed copolymers. The incorporation efficiency of the hydrophobic fatty acid segment was calculated to be 18% for the low molecular weight copolymer ^{18}F-P3* and 25% for the high molecular weight copolymer ^{18}F-P4*, respectively. When the body distribution of these probes was studied (Fig. 1B) the low molecular weight polymer ^{18}F-P3* was preferentially localized in kidney (12.6 ± 1.7 %ID/g tissue), liver (3.0 ± 0.4 %ID/g tissue) and blood (2.0 ± 0.3 %ID/g tissue). In contrast, the high molecular weight polymer ^{18}F-P4* showed higher levels in the blood (3.7 ± 0.5 %ID/g tissue) and levels were lower in kidney (6.4 ± 1.2 %ID/g tissue) and liver (1.8 ± 0.3 %ID/g tissue). Both polymers were also found at low concentration in other organs such as lung, spleen and heart (Fig. 1B).

When comparing the corresponding polymers of the different types (homopolymer *vs*. copolymer) of the approximately same sizes (^{18}F-P1* *vs.* ^{18}F-P3* and ^{18}F-P2* *vs*. ^{18}F-P4*) several pronounced

differences can be seen. The most striking difference between the homo- and the copolymers is, that independently from the molecular weight, the HPMA-*ran*-LMA copolymer stays longer in the blood compartment. The small homopolymer was excreted rapidly by the kidneys and the large one by the liver, both leading to a negligible polymer concentration in the blood. The copolymers were excreted in the same principal manner, however, much slower leading to marked sustained blood concentration. With an assumed blood volume of the rat of 16 mL 50 the %ID/g blood values found for the copolymers translate into values of about 30% (^{18}F-P3*) and 60% (^{18}F-P4*) of the injected dose being still present in the blood compartment 2 h p.i., illustrating significant retention of the copolymeric systems in the blood stream. Especially the uptake of the larger copolymer ^{18}F-P4* by the liver was much lower than for the comparable homopolymer (as indicated by a 4-times lower accumulation in the liver, illustrated in Fig. 2). Since the blood within the liver has not been washed out completely before taking the tissue samples, the measured signal might be slightly influenced by the tracer concentration in the blood. The question of specific liver uptake could be addressed in further experiments by using tracers with longer-lived isotopes for measuring late-stage accumulation after complete blood clearance.

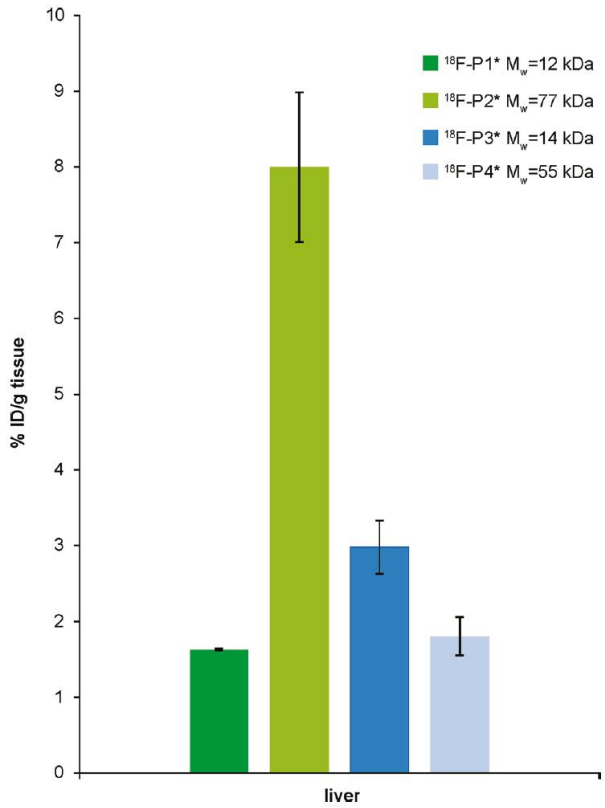

Figure 2: Liver uptake of ^{18}F-P1 - ^{18}F-P4* in dependency of their molecular weight and polymer architecture 2 h p.i. expressed as %ID/g tissue.*

In addition, the accumulation in the spleen (e.g. by uptake in macrophages) was less pronounced in the case of the copolymer ^{18}F-P4*. These results are indicating that the incorporation of the hydrophobic lauryl methacrylate segment holds a considerable impact on the biodistribution and especially on recognition mechanisms of the reticuloendothelial system (RES). By avoiding an increased uptake of the polymers by the cells of the MPS or by minimizing the renal filtration processes, the presence in the blood stream can be significantly enhanced. The feature of a high long-lasting blood concentration is of high importance as a long-term uptake into a tumor or other organs of interest depends mainly on the plasma concentration of the drug.

Furthermore it was tested whether ^{18}F-labeling of polymers cannot only be used for body distribution studies *ex vivo* but also for imaging and quantification of the compound's uptake into tumors. For this purpose, tumor-bearing rats (AT1) were used, the tumor cell line was implanted subcutaneously on the hind food dorsum. The polymer was taken up into the tumor tissue, however, only to a very low amount. Despite the considerably higher concentration found for the copolymer systems in the blood pool 2 h p.i., no significant differences in tumor uptake was observed for all polymers tested. In fact, the concentration in tumor tissue was only marginally higher than in the reference tissue (testis) in the field of view. Lammers et al. [39] reported for the same tumor model a much higher tumor uptake for large polymers (molecular weight 65 kDa) over a period of 168 h. Since in the present study only an observation period of 2 hours was used (due to the short half-life of ^{18}F) the results are not directly comparable. Besides, the fact that during 168 h AT1 tumors are markedly growing which leads to a visual overestimation of polymer uptake in the images, the elimination (renal or liver/bile) of the polymer used by Lammers et al. seems to be much lower resulting in a longer persistance of the polymer in the circulation. However, the uptake in the lung described by Lammers et al. [39] was not seen with any of the polymers in the present study (Fig. 1) and cannot be explained at present.

Ex vivo blood analysis

Using radiolabeling to trace polymeric architectures *in vivo*, metabolic stability of the radiolabel should be high. Loss of the radiolabel from the polymer due to radiolysis or enzymatic dehalogenation might lead to false estimation of accumulation patterns or to undesirable accumulation in sensitive tissues, as in the case of iodine which accumulates in the thyroid [39, 55], limiting diagnostic imaging e.g. with high gamma energy emitting ^{131}I. To study whether low molecular weight radioactive byproducts are present in the blood, blood samples were taken 140 min p.i. and blood plasma was analyzed using SEC. As shown in Figure 3 for random copolymer ^{18}F-P4* the SEC chromatogram comprised only one radioactive fraction of high molecular weight,

indicating that the radioactivity remains associated with the polymers over a time period of more than 2 h.

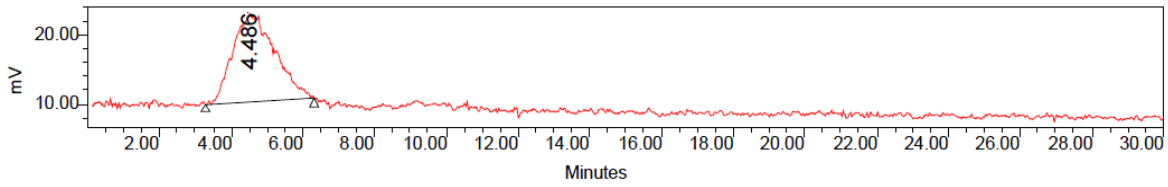

Figure 3: Sephadex G-25 chromatography of a blood plasma sample taken 140 min p.i. of the random copolymer ^{18}F-P4 showing only one radioactive fraction of high molecular weight.*

µPET imaging

In addition to the biodistribution, differences in the pharmacokinetics of the various polymeric structures were visualized using µPET as non-invasive method with high spatial resolution. Therefore dynamic PET images were obtained over 120 min after i.v. injection of the labeled polymers.

Representative whole body µPET images of both radiolabeled homopolymer systems of low and high molecular weight are shown in Fig. 4. µPET images of low molecular weight homopolymer ^{18}F-P1* (12 kDa) reveals that after 2 h almost the entire radioactivity localizes in kidneys and bladder (Fig. 4A) whereas accumulation in other organs was barely visible. In correspondence with the biodistribution data obtained (Fig. 1A), µPET imaging of homopolymer ^{18}F-P1* precisely identifies a renal clearance as expected for a hydrophilic polymeric system of 12 kDa being below the renal threshold for HPMA copolymers (M_w < 40 kDa) [45].

In contrast, whole-body µPET images of the high molecular weight homopolymer ^{18}F-P2* (77 kDa) demonstrate enrichment predominant in liver and spleen (Fig. 4B), thereby again reflecting the findings of the biodistribution experiments. Despite the high molecular weight of 77 kDa (above the renal excretion threshold), small amounts of radioactivity can still be found in the kidneys but excretion *via* the bladder was extremely slow. The µPET images obtained for ^{18}F-P1* and ^{18}F-P2* are demonstrated below.

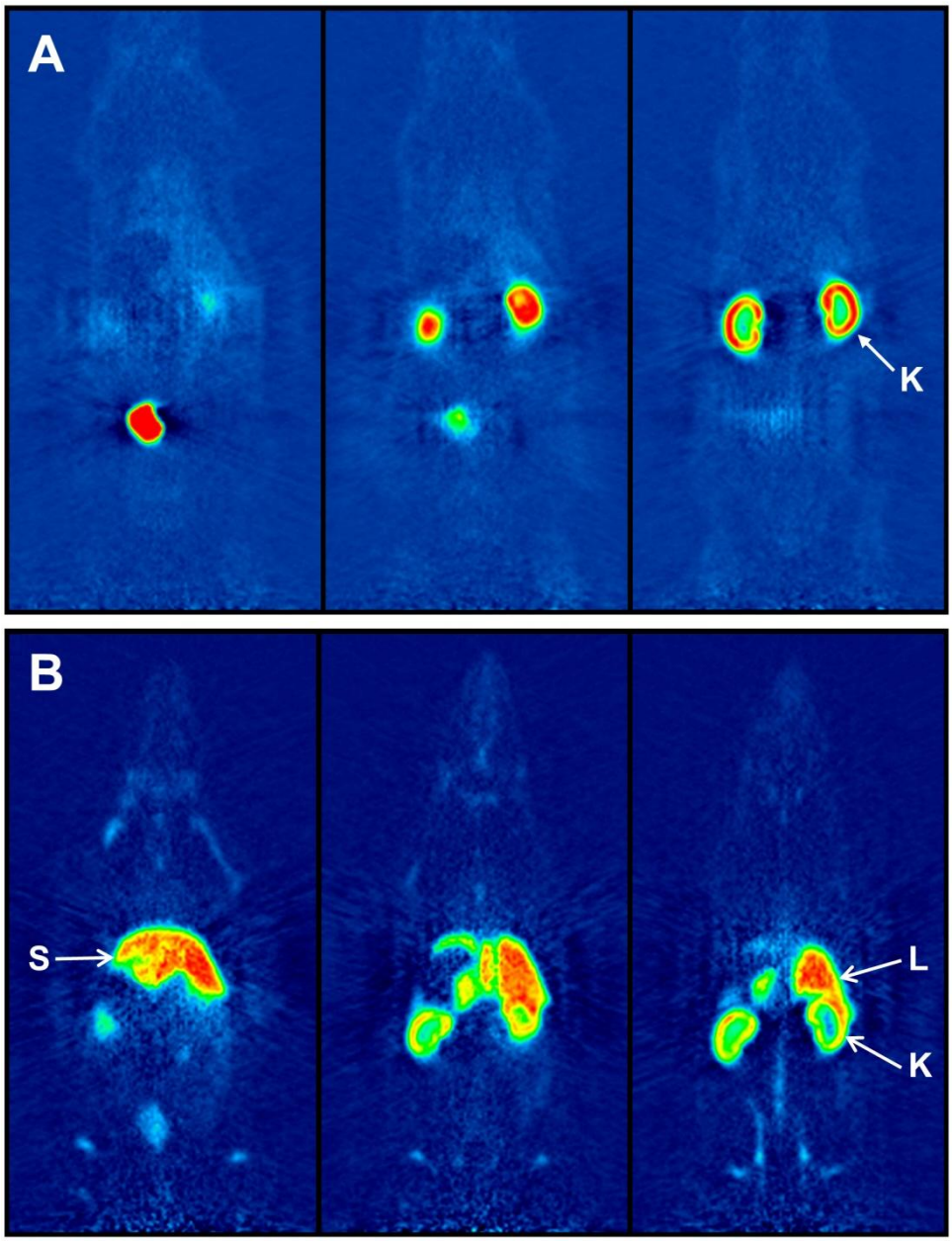

Figure 4: µPET imaging of ^{18}F-labeled homopolymers. Representative coronar µPET summed images in different depths 120-135 min after i.v. injection. (A) M_w= 12 kDa homopolymer ^{18}F-P1 showing kidney elimination (K). (B) M_w = 77 kDa homopolymer ^{18}F-P2* indicating accumulation in liver (L), spleen (S) and kidneys (K).*

In contrast, imaging the distribution pattern of the large HPMA-*ran*-LMA copolymer ^{18}F-P4* *in vivo*, it clearly shows a reduced liver uptake (which is in good correspondence to the biodistribution experiments) (Fig. 5) as compared to the large homopolymer (Fig. 4B). Elimination of ^{18}F-P4* *via* the kidneys is comparable to the high molecular weight homopolymer ^{18}F-P2*. In contrast to the homopolymer, the retention of the copolymer in the circulation (blood compartment) 2 h post injection is much higher (Fig. 5, heart, aorta), already indicated by the biodistribution measurements.

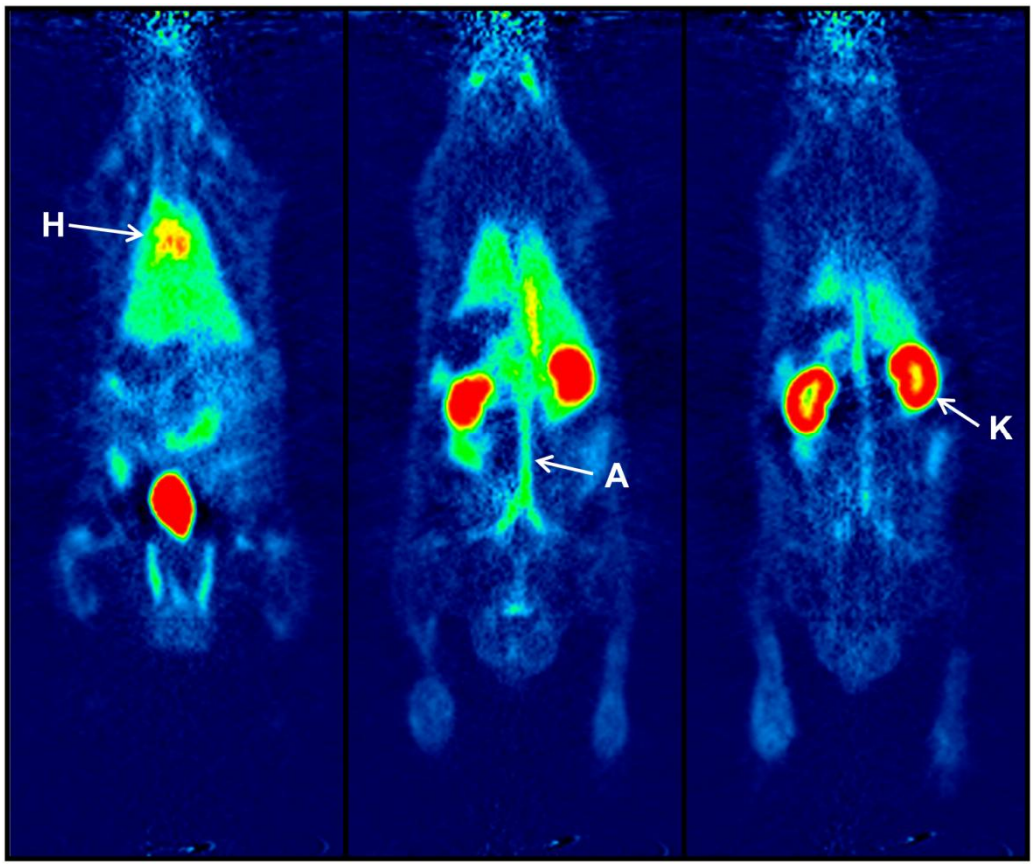

Figure 5: Representative coronar µPET images of HPMA-ran-LMA copolymer ^{18}F-P4 (55 kDa) 2 h after i.v. injection. The images show accumulation in kidneys (K) and bladder as well as remaining activity in the blood (heart (H); aorta (A)).*

Conclusion

In this study we could demonstrate that the introduction of a radioactive probe allows systematic insights into the correlation between chemical structure and biodistribution of HPMA-based polymers of different M_w. In our case we compared homopolymers *vs*. random copolymers exhibiting lauryl methacrylate as hydrophobic segment. As stability of the polymers could be ensured, the results emphasize the special benefit of introducing a radioactive label, in particular when applying positron emission tomography, PET. It enables a precise tracing of the different polymer architectures in the organism and thereby gaining detailed knowledge about structure-property relationships of the polymers influencing their early-phase organ accumulation.

The differing structures (P1* and P2* homopolymers *vs*. P3* and P4* random copolymers) had a major impact on the biodistribution pattern in the living organism. Our results differ from the results of Lammers [39] by the fact that the relative ratio of the accumulation in different tissue depends

strongly on aggregate formation or not. Especially the retention of the high M_w homopolymer and random copolymer is quite different. Despite a large superstructure formation of the HPMA-*ran*-LMA copolymers, renal clearance could still be proven and liver accumulation was comparably low. Furthermore the random copolymer P4* exhibited increased enrichment in the blood stream (nearly 60% after 2 h p.i.), underlining its feasibility as model system for the design of amphiphilic transport vehicles for therapeutics *in vivo*. These results emphasize the significance of both (1) a good characterization of the polymers and their aggregates and (2) the use of *in vivo* pharmacokinetics – as it is available by PET – to evaluate the potential of biocompatible polymers as potential drug carriers.

Acknowledgement

The authors would like to thank Nicole Bausbacher, Bengü Yilmaz and Hans-Georg Buchholz for their support during animal studies and following interpretation. Furthermore we gratefully acknowledge Dr. Clemens K. Weiss and Elke Muth for their assistance during cmc determination measurements. We also want to thank the Max-Planck Graduate Center (MPGC, M. Allmeroth) as well as the Graduate School Materials Science in Mainz (Excellence Initiative, DFG/GSC 266, D. Moderegger) for financial support. In addition the authors are very thankful for financial support of the DFG (Rösch: RO 985/30-1; Thews: TH 482/4-1, Zentel: ZE 230/21-1) and SAMT Initiative Mainz. We also thank Prof. Helmut Ringsdorf, Prof. Dr. Ruth Duncan and Dr. Matthias Barz for stimulating discussions.

References

[1] Duncan, R. *Nat Rev Drug Discovery* 2003, *2*, 347-360.

[2] Matsumura, Y.; Maeda, H. *Jpn. J. Cancer Res*. 1986, *46*, 6387-6392.

[3] Maeda, H.; Bharate, G. Y.; Daruwalla, J. *Eur. J. Pharm. Biopharm.* 2009, *71*, 409-419.

[4] Ringsdorf, H. *J. Polym. Sci. Polym. Symp.* 1975, *51*, 135-153.

[5] Obereigner, B.; Burešová, M.; Vrána, A.; Kopeček, J. *J. Polym. Sci. Polym. Symp.* 1979, *66*, 41-52.

[6] Solovsky, M. V.; Ulbrich, K.; Kopecek, J. *Biomaterials* 1983, *4*, 44-48.

[7] Duncan, R.; Seymour, L. W.; O'Hare, K. B.; Flanagan, P. A.; Wedge, S.; Hume, I. C.; Ulbrich, K.; Strohalm, J.; Subr, V.; Spreafico, F.; Grandi, M.; Ripamonti, M.; Farao, M.; Suarato, A. *J. Controlled Release* 1992, *19*, 331-346.

[8] Kopecek, J.; Kopecková, P.; Minko, T.; Lu, Z.-R. *Eur. J. Pharm. Biopharm.* 2000, *50*, 61-81.

[9] Duncan, R. *Adv. Drug Delivery Rev.* 2009, *61*, 1131-1148.

[10] Kataoka, K.; Harada, A.; Nagasaki, Y. *Adv. Drug Delivery Rev.* 2001, *47*, 113-131.

[11] Gaucher, G.; Dufresne, M.-H.; Sant, V. P.; Kang, N.; Maysinger, D.; Leroux, J.-C. *J. Controlled Release* 2005, *109*, 169-188.

[12] Barz, M.; Luxenhofer, R.; Zentel, R.; Kabanov, A. V. *Biomaterials* 2009, *30*, 5682-5690.

[13] Talelli, M.; Rijcken, C. J. F.; van Nostrum, C. F.; Storm, G.; Hennink, W. E. *Adv. Drug Delivery Rev.* 2010, *62*, 231-239.

[14] Duncan, R.; Gac-Breton, S.; Keane, R.; Musila, R.; Sat, Y. N.; Satchi, R.; Searle, F. *J. Controlled Release* 2001, *74*, 135-146.

[15] Vicent, M. J.; Greco, F.; Nicholson, R. I.; Paul, A.; Griffiths, P. C.; Duncan, R. *Angew. Chem., Int. Ed.* 2005, *44*, 4061-4066.

[16] Greco, F.; Vicent, M. J. *Adv. Drug Delivery Rev.* 2009, *61*, 1203-1213.

[17] Duncan, R.; Vicent, M. J. *Adv. Drug Delivery Rev.* 2010, *62*, 272-282.

[18] Lammers, T.; Subr, V.; Ulbrich, K.; Hennink, W. E.; Storm, G.; Kiessling, F. *Nano Today* 2010, *5*, 197-212.

[19] Lammers, T.; Kiessling, F.; Hennink, W. E.; Storm, G. *Mol. Pharmaceutics* 2010, *7*, 1899-1912.

[20] Herth, M. M.; Barz, M.; Moderegger, D.; Allmeroth, M.; Jahn, M.; Thews, O.; Zentel, R.; Rösch, F. *Biomacromolecules* 2009, 10, 1697-1703.

[21] Herth, M. M.; Barz, M.; Jahn, M.; Zentel, R.; Rösch, F. *Bioorg. Med. Chem. Lett.* 2010, *20*, 5454-5458.

[22] Pimm, M. V.; Perkins, A. C.; Strohalm, J.; Ulbrich, K.; Duncan, R. *J. Drug Targeting* 1996, *3*, 375-383.

[23] Mitra, A.; Nan, A.; Ghandehari, H.; McNeil, E.; Mulholland, J.; Line, B. *Pharm. Res.* 2004, *21*, 1153-1159.

[24] Šprincl, L.; Exner, J.; Štěrba, O.; Kopeček, J. *J. Biomed. Mat. Res.* 1976, *10*, 953-963.

[25] Minko, T.; Kopecková, P.; Pozharov, V.; Kopecek, J. *J. Controlled Release* 1998, *54*, 223-233.

[26] Kopecek, J.; Kopecková, P. *Adv. Drug Delivery Rev.* 2010, *62*, 122-149.

[27] Barz, M.; Luxenhofer, R.; Zentel, R.; Vicent, M. *J. Polym. Chem.* 2011, DOI: 10.1039/C0PY00406E.

[28] Kopecek, J. *Polim. Med.* 1977, *7*, 191-221.

[29] Kopecek, J.; Bazilová, H. *Eur. Polym. J.* 1973, *9*, 7-14.

[30] Rathi, R. C.; Kopečková, P.; Říhová, B.; Kopeček, J. *J. Polym. Sci., Part A: Polym. Chem.* 1991, *29*, 1895-1902.

[31] Ulbrich, K.; Subr, V.; Strohalm, J.; Plocová, D.; Jelínková, M.; Ríhová, B. *J. Controlled Release* 2000, *64*, 63-79.

[32] Seymour, L. W.; Duncan, R.; Strohalm, J.; Kopeček, J. *J. Biomed. Mat. Res.* 1987, *21*, 1341-1358.

[33] Chiefari, J.; Chong,Y. K.; Ercole, F.; Krstina, J.; Jeffery, J.; Le, T.; Mayadunne, R.; Meijs, G.; Moad, C.; Moad, G.; Rizzardo,E.; Thang, S. H. *Macromolecules* 1998, *31*, 5559-5562.

[34] Moad, G.; Rizzardo, E.; Thang, S. H. *Aust. J. Chem.* 2005, *58*, 379-410.

[35] Matyjaszewski, K.; Xia, J. *Chem. Rev.* 2001, *101*, 2921-2990.

[36] Scales, C. W.; Vasilieva, Y. A.; Convertine, A. J.; Lowe, A. B.; McCormick, C. L. *Biomacromolecules* 2005, *6*, 1846-1850.

[37] Gauthier, M. A.; Gibson, M. I.; Klok, H.-A. *Angew. Chem., Int. Ed*. 2009, *48*, 48-58.

[38] Maeda, H.; Wu, J.; Sawa, T.; Matsumura, Y.; Hori, K. *J. Controlled Release* 2000, *65*, 271-284.

[39] Lammers, T.; Kühnlein, R.; Kissel, M.; Subr, V.; Etrych, T.; Pola, R.; Pechar, M.; Ulbrich, K.; Storm, G.; Huber, P.; Peschke, P. *J. Controlled Release* 2005, *110*, 103-118.

[40] Julyan, P. J.; Seymour, L. W.; Ferry, D. R.; Daryani, S.; Boivin, C. M.; Doran, J.; David, M.; Anderson, D.; Christodoulou, C.; Young, A. M.; Hesslewood, S.; Kerr, D. J. *J. Controlled Release* 1999, *57*, 281-290.

[41] Seymour, L. W.; Ferry, D. R.; Kerr, D. J.; Rea, D.; Whitlock, M.; Poyner, R.; Boivin, C.; Hesslewood, S.; Twelves, C.; Blackie, R.; Schatzlein, A.; Jodrell, D.; Bissett, D.; Calvert, H.; Lind, M.; Robbins, A.; Burtles, S.; Duncan, R.; Cassidy, J. *Int. J. Oncol.* 2009, *34*, 1629-1636.

[42] Hemmelmann, M.; Knoth, C.; Schmitt, U.; Allmeroth, M.; Moderegger, D.; Barz, M.; Koynov, K.; Hiemke, C.; Rösch, F.; Zentel, R. *Macromol. Rapid Commun.* 2011, DOI: 10.1002/marc.201000810C.

[43] Workman P.; Twentyman, P.; Balkwill, F.; Balmain, A.; Chaplin, D.; Double, J.; Newell, D.; Raymond, R.; Stables, J.; Stephens, T.; Wallace, J. *Br. J. Cancer* 1998, *77*, 1-10.

[44] Boyer, C.; Bulmus, V.; Davis, T. P.; Ladmiral, V.; Liu, J.; Perrier, S. *Chem. Rev*. 2009, *109*, 5402-5436.

[45] Seymour, L. W.; Miyamoto, Y.; Maeda, H.; Brereton, M.; Strohalm, J.; Ulbrich, K.; Duncan, R. *Eur. J. Cancer* 1995, *31*, 766-770.

[46] Eberhardt, M.; Mruk, R.; Zentel, R.; Theato, P. *Eur. Polym. J.* 2005, *41*, 1569-1575.

[47] Theato, P. *J. Polym. Sci., Part A: Polym. Chem.* 2008, *46*, 6677-6687.

[48] *Polymer Handbook*, 4th ed.; Brandrup, J., Immergut, E. H., Grulke, E. A., Abe, A., Bloch, D. R., Eds.; John Wiley & Sons: New York, 1999.

[49] Perrier, S.; Takolpuckdee, P.; Mars, C. A. *Macromolecules* 2005, *38*, 2033-2036.

[50] Lee, H. B.; Blaufox, M. D. *J. Nucl. Med.* 1985, *26*, 72-76.

[51] Yu, K.; Eisenberg, A. *Macromolecules* 1998, *31*, 3509-3518.

[52] Trappmann, B.; Ludwig, K.; Radowski, M. R.; Shukla, A.; Mohr, A.; Rehage, H.; Böttcher, C.; Haag, R. *J. Am. Chem. Soc.* 2010, *132*, 11119-11124.

[53] Owens Iii, D. E.; Peppas, N. A. *Int. J. Pharm.* 2006, *307*, 93-102.

[54] Ulbrich, K.; Subr, V. *Adv. Drug Delivery Rev.* 2010, *62*, 150-166.

[55] Wilbur, D. S. *Bioconjugate Chem.* 1992, *3*, 433-470.

Supporting Information

Modifying the body distribution of HPMA-based copolymers by molecular weight and aggregate formation

Mareli Allmeroth, Dorothea Moderegger, Barbara Biesalski, Kaloian Koynov, Frank Rösch, Oliver Thews and Rudolf Zentel

Contents

1. Experimental section

I. Synthesis of 4-cyano-4-((thiobenzoyl)sulfanyl)pentanoic acid (CTP)

4-cyano-4-((thiobenzoyl)sulfanyl)pentanoic acid was used as chain transfer agent (CTA) and synthesized according to the literature [1].

II. Synthesis of pentafluorophenyl methacrylate (PFPMA)

Pentafluorophenyl methacrylate was prepared according to reference [2].

III. Synthesis of reactive ester homopolymers

RAFT polymerization of pentafluorophenyl methacrylate with 4-cyano-4-((thiobenzoyl) sulfanyl)pentanoic acid was carried out in a schlenk tube [3, 4]. For this purpose, 4 g of PFPMA were dissolved in 5 mL of absolute dioxane, furthermore CTP and AIBN were added. The molar ratio of CTP/AIBN was chosen 1:8. After three freeze-vacuum-thaw cycles, the mixture was immersed in an oil bath at 65 °C and stirred over night. Afterwards, the polymeric solution was precipitated three times in hexane, centrifuged and dried under vacuum at 40 °C over night. A slightly pink powder was obtained. Yield: 52%. ^{1}H-NMR (300 MHz, $CDCl_3$) δ/ ppm: 1.20-1.75 (br), 2.00-2.75 (br s). ^{19}F-NMR (400 MHz, $CDCl_3$) δ/ ppm: -162.03 (br), -156.92 (br), -152 to -150 (br).

IV. Synthesis of random copolymers

RAFT polymerization of PFPMA with lauryl methacrylate (LMA) by help of CTP was performed in a schlenk tube as well. As an example, 4 g of PFPMA dissolved in 5 mL dioxane, lauryl methacrylate, AIBN and CTP were mixed. The molar ratio of CTP/AIBN was chosen to be 1:8. After three freeze-vacuum-thaw cycles, the mixture was immersed in an oil bath at 65 °C and stirred over night. Afterwards, poly(PFPMA)-*ran*-poly(LMA) was precipitated three times in hexane, centrifuged and dried under vacuum at 40 °C over night. A slightly pink powder was obtained. Yield: 54%. ^{1}H-NMR (300 MHz, $CDCl_3$) δ/ ppm: 0.84 (br t), 1.20-1.75 (br), 2.00-2.75 (br s). ^{19}F-NMR (400 MHz, $CDCl_3$) δ/ ppm: -162.01 (br), -156.95 (br), -152 to -150 (br).

V. Removal of dithioester endgroups

The dithiobenzoate endgroup was removed using the protocol reported by Perrier et al. 2005 [5]. The procedure is described in the supplementary data. Therefore a 25-fold molar excess of AIBN was added to the polymer dissolved in dioxane. After four hours of heating the solution in an oil bath at 70 °C, the polymer was precipitated twice in hexane and collected by centrifugation. The polymer

was dried under vacuum over night, a colorless powder was obtained. Yield: 75%. Removal of the dithioester endgroup could be proven by UV-Vis spectroscopy.

VI. Polymer analogous reaction of homopolymers

Depending on the labeling technique necessary, either for a fluorescent or radioactive marker, two different routes were applied. For subsequent radioactive labeling, the protocol was carried out as follows. As example, 100 mg of the polymeric precursor (M_n = 18000 g/mol) were diluted in 2 mL of absolute dioxane. 5 mg of tyramine, diluted in a DMSO/dioxane mixture, and 10 mg of triethylamine were added. After stirring for four hours at 35 °C, 30 mg of 2-hydroxypropylamine as well as 40 mg of triethylamine were added and the solution was stirred over night. For final removal of reactive ester side groups, further 30 mg of 2-hydroxypropylamine were added the next morning. The solution was precipitated two times in diethyl ether, centrifuged and finally dissolved in a DMSO/water solution for dialysis. After lyophilization a white powder could be obtained. Yield: 79%. ^{1}H-NMR (400 MHz, d. DMSO) δ/ ppm: 0.60-1.40 (br), 1.45-2.20 (br), 2.75-3.10 (br), 3.50-3.80 (br), 4.60-4.80 (br), 6.60-6.70 (br) and 6.85-7.00 (br). For additional fluorescent labeling, the fluorescent marker Oregon Green 488 cadaverine was used. 100 mg of polymeric precursor were diluted in 2 mL of absolute dioxane and 2.75 mg of Oregon Green 488 cadaverine added. Afterwards tyramine and 2-hydroxypropylamine were added, as described by the procedure above.

VII. Polymer analogous reaction of random copolymer

For radioactive labeling of random copolymers the protocol was applied as follows. 100 mg of poly(PFPMA)-*ran*-poly(LMA) copolymer was dissolved in 2 mL of absolute dioxane. As example, for the polymeric system P3*-R (M_n= 17.000 g/mol) 5 mg of tyramine and 10 mg of triethylamine were diluted in a DMSO/dioxane mixture and added to the vessel. After stirring for four hours at 35 °C, 30 mg of 2-hydroxypropylamine as well as 40 mg of triethylamine were added and the solution stirred over night. For final removal of reactive ester side groups further 30 mg of 2-hydroxypropylamine were added the next morning. The solution was precipitated two times in diethyl ether, centrifuged and finally dissolved in a DMSO/water solution for dialysis. After lyophilization a white powder could be obtained. Yield: 51%. ^{1}H-NMR (400 MHz, d. DMSO) δ/ ppm: 0.70-0.90 (br), 0.90-1.40 (br), 1.40-1.90 (br), 2.75-3.10 (br), 3.50-3.80 (br), 4.50-4.75 (br), 6.60-6.75 (br) and 6.85-7.00 (br). For additional fluorescent labeling, 100 mg of polymeric precursor were diluted in 2 mL of absolute dioxane and 2.9 mg of Oregon Green 488 cadaverine were added. Afterwards tyramine and 2-hydroxypropylamine were added, as described by the procedure above.

VIII. Analytical data obtained in isotonic NaCl solution

Isotonic NaCl solution 0.9% was obtained by B. Braun Melsungen AG without any purification. Stock solutions were prepared using 1% of absolute DMSO in isotonic sodium chloride solution.

IX. Critical micelle concentration (cmc) determination by Ring Tensiometry

Cmc determination was accomplished by using the ring tensiometer DCAT 21 of Dataphysics Instruments, Filderstadt. For this purpose, a stock solution of 2 mg polymer/ 20 mL of sodium chloride solution was prepared and stirred for 3 days. By calculation of the SCAT software, version 2.8.1.77, the polymer solution was added dropwise to a known volume of NaCl in a vessel *via* a Hamilton microsyringe. The temperature in the vessel was kept at 37 °C (± 0.1 °C), maintained by a thermostat. The ring was cleaned by heating in a gas flame. Analysis of the obtained data was carried out by using the software mentioned above and additional plotting with OriginPro Version 8.

X. Size determination by Fluorescence Correlation Spectroscopy (FCS)

The hydrodynamic radii of the polymeric systems were determined by Fluorescence Correlation Spectroscopy using a commercial FCS setup (Zeiss, Germany) consisting of the module ConfoCor 2 and an inverted microscope model Axiovert 200 with a Zeiss C-Apochromat 40 ×/1.2 W water immersion objective. The fluorophores were excited with an Argon laser (λ = 488 nm) and the emission was collected after filtering with a LP505 long pass filter. For detection, an avalanche photodiode, enabling single-photon counting, was used. As sample cell, eight-well, polystyrene-chambered cover glass (Laboratory-Tek, Nalge Nunc International) was applied. For sample preparation, stock solutions of 1 mg fluorescently labeled polymer/mL NaCl were applied, diluted to a final concentration of 0.1 mg/mL. The solution was kept at room temperature over night. For reference reason, free Oregon Green 488 cadaverine dye in NaCl-solution was also studied. The calibration of the FCS observation volume was done using a dye with known diffusion coefficient, i.e. Rhodamine6 G. For each solution, 5 measurement cycles with a total duration of 150 seconds were applied. Time dependant fluctuations of the fluorescence intensity $\delta I(t)$ were detected and evaluated by autocorrelation analysis, yielding the diffusion coefficient and hydrodynamic radius of the fluorescent species [6].

XI. Synthesis of [^{18}F]FETos

To an aqueous [^{18}F]fluoride solution (2-8 GBq) 18 mg Kryptofix®2.2.2., potassium carbonate (1 N, 15 µL) and 1 mL acetonitrile were added. The mixture was dried in a stream of nitrogen at 80 °C, the

drying procedure was repeated three times. To the dried residue 13 mg of ethyleneglycol-1,2-ditosylate in 1 mL acetonitrile was added and heated under stirring in a sealed vial at 88 °C for 3 min. Purification of the crude product was accomplished using HPLC (Lichrosphere RP18-EC5, 250×10 mm, acetonitrile/water 50:50, flow rate: 5 mL/min, t_R: 8 min). After diluting the HPLC fraction of 2-[^{18}F]fluoroethyl-1-tosylate with water, the product was loaded on a Sep-Pak C18 cartridge, dried with a nitrogen stream and eluted with 0.8 mL of DMSO [7].

XII. Radiolabeling of polymers using [^{18}F]FETos and purification for ex vivo and in vivo experiments

For radiolabeling, 3 mg of the polymeric precursor were dissolved in 200 µL of dried DMSO. The solution was transferred to a sealed vial and 1 µL of a 5 N sodium hydroxide solution was added. The labeling reaction was started by adding the previously eluted DMSO solution of 2-[^{18}F]fluoroethyl-1-tosylate and the mixture was stirred for 15 min at 120 °C.

For *ex vivo* and *in vivo* experiments, the radiolabeled polymeric systems were freed from low molecular weight byproducts by Sephadex G-25 size exclusion chromatography (HiTrap™ Desalting Column, Sephadex G-25 Superfine, 0.9% NaCl, flow rate: 0.5 mL/min) leading to a pure, ^{18}F-labeled polymer solution ready for subsequent experiments [8].

XIII. Tumor and animal model

AT1 R-3327 prostate carcinoma cells were grown in RPMI medium supplemented with 10% fetal calf serum (FCS) at 37 °C under a humidified 5% CO_2 atmosphere and sub cultivated once per week. For *in vivo* experiments male Copenhagen rats (Charles River Wiga, Sulzfeld, Germany; body weight 180 to 300 g), housed in the animal care facility of the University of Mainz, were used. Animals were allowed access to food and acidified water *ad libitum* before the investigation. Solid carcinomas were heterotopically induced by injection of cells (0.4 mL, approximately 10^4 cells/µL) subcutaneously into the dorsum of the hind foot. Tumors grew as flat, spherical segments and replaced the subcutis and corium completely. Volumes were determined by measuring the three orthogonal diameters (d) of the tumors and using an ellipsoid approximation with the formula: $V = d_1 \times d_2 \times d_3 \times \pi/6$. Tumors were used when they reached a volume of between 1.0 to 2.0 mL approx. 8 to 14 days after tumor cell inoculation.

XIV. Small animal PET studies

For *in vivo* imaging, the radiolabeled polymers were injected into tumor bearing rats. Therefore the animals were anaesthetized with pentobarbital (40 mg/kg, i.p., Narcoren, Merial, Hallbergmoos,

Germany). PET imaging was performed on a µPET Focus 120 small animal PET (Siemens/Concorde, Knoxville, USA). During PET measurements the animals were placed in supine position and breathed room air spontaneously. After a 15 min transmission scan with an external ^{57}Co source, dynamic PET studies were acquired in 2D mode. The radiolabeled polymer was administered as a bolus injection *via* the tail vein with a mean activity of 23.3 ± 1.6 MBq. Afterwards, dynamic PET images were obtained for a total measuring interval of 120 min. Finally, a whole body scan (120-135 min post injection) was performed. For quantitative analysis, the PET listmode data were histogrammed into 20 frames with varying time frames (3-10 min) and reconstructed using OSEM algorithm. µPET image quantification was applied using PMOD software (PMOD Technologies Ltd.).

2. References

[1] E.R. G. Moad, S. H. Thang, Living Radical Polymerization by the RAFT process. Aust. J. Chem. 58 (2005) 379-410.

[2] M. Eberhardt, R. Mruk, R. Zentel, P. Théato, Synthesis of pentafluorophenyl(meth)acrylate polymers: New precursor polymers for the synthesis of multifunctional materials. European Polymer Journal 41(7) (2005) 1569-1575.

[3] P. Theato, Synthesis of well-defined polymeric activated esters. Journal of Polymer Science Part A: Polymer Chemistry 46(20) (2008) 6677-6687.

[4] M. Barz, R. Luxenhofer, R. Zentel, A.V. Kabanov, The uptake of N-(2-hydroxypropyl)-methacrylamide based homo, random and block copolymers by human multi-drug resistant breast adenocarcinoma cells. Biomaterials 30(29) (2009) 5682-5690.

[5] S. Perrier, P. Takolpuckdee, C.A. Mars, Reversible Addition Fragmentation Chain Transfer Polymerization: End Group Modification for Functionalized Polymers and Chain Transfer Agent Recovery. Macromolecules 38(6) (2005) 2033-2036.

[6] R.E. Rigler, E.S., Fluorescence Correlation Spectroscopy. Springer Verlag (New York 2001).

[7] A. Bauman, M. Piel, R. Schirrmacher, F. Rösch, Efficient alkali iodide promoted ^{18}F-fluoroethylations with 2-[^{18}F]fluoroethyl tosylate and 1-bromo-2-[^{18}F]fluoroethane. Tetrahedron Letters 44(51) (2003) 9165-9167.

[8] M.M. Herth, M. Barz, D. Moderegger, M. Allmeroth, M. Jahn, O. Thews, R. Zentel, F. Rösch, Radioactive Labeling of Defined HPMA-Based Polymeric Structures Using [^{18}F]FETos for In Vivo Imaging by Positron Emission Tomography. Biomacromolecules 10(7) (2009) 1697-1703.

This material is available free of charge *via* the Internet at http://pubs.acs.org.

3.3 Structure and size of HPMA-based polymers decide on tumor accumulation but the tumor model makes a difference: A quantitative *in vivo* PET study

Structure and size of HPMA-based polymers decide on tumor accumulation but the tumor model makes a difference: A quantitative *in vivo* PET study

Mareli Allmeroth[*,1], Dorothea Moderegger[*,2], Barbara Biesalski[3], Daniel Gündel[4], Kaloian Koynov[5], Hans-Georg Buchholz[6], Frank Rösch[2], Rudolf Zentel[1] and Oliver Thews[4]

[*] both authors contributed equally

[1] Institute of Organic Chemistry, Johannes Gutenberg University, Duesbergweg 10-14, 55099 Mainz, Germany

[2] Institute of Nuclear Chemistry, Johannes Gutenberg University, Fritz-Strassmann-Weg 2, 55128 Mainz, Germany

[3] Institute of Physiology and Pathophysiology, University Medicine Mainz, Duesbergweg 6, 55128 Mainz, Germany

[4] Institute of Physiology, University Halle, Magdeburger Str. 6, 06097 Halle (Saale), Germany

[5] Max-Planck-Institute for Polymer Research, Ackermannweg 10, 55128 Mainz, Germany

[6] Department of Nuclear Medicine, University Medicine Mainz, Langenbeckstraße 1, 55131 Mainz, Germany

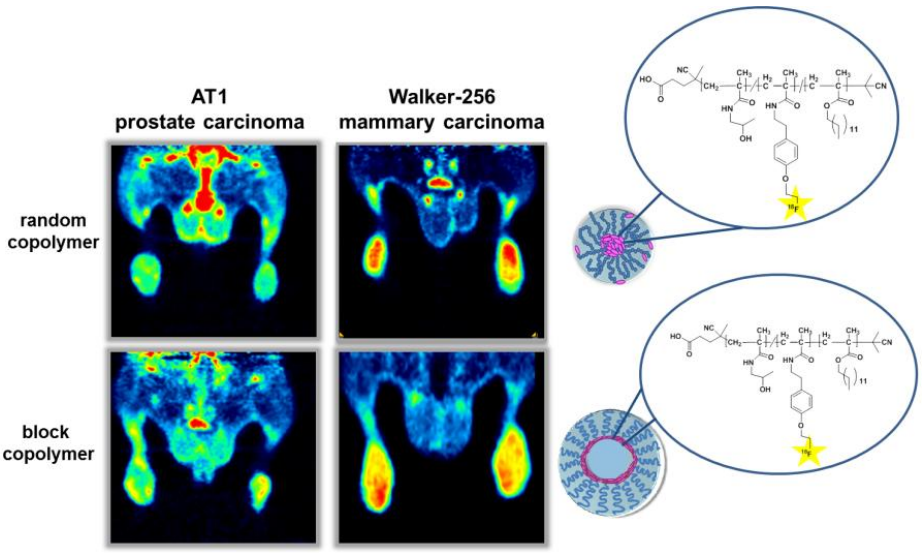

Abstract

Polymeric drug carriers aim to selectively target tumors in combination with protecting normal tissue. In this regard polymer structure and molecular weight are key factors considering organ distribution as well as tumor accumulation of the polymeric drug delivery system. In the present study six different HPMA-based polymer structures (homopolymers, random as well as block copolymers with lauryl methacrylate as hydrophobic group) varying in molecular weight, size and resulting architecture were analyzed in two different tumor models (AT1 prostate carcinoma and Walker 256 mammary carcinoma) *in vivo*. Polymers were labeled with ^{18}F and organ/tumor uptake was followed by *ex vivo* biodistribution as well as *in vivo* µPET imaging. Vascular permeability was measured by dextran extravasation and cell uptake, determined *in vitro* using fluorescence-labeled polymers. Most strikingly, the high molecular weight HPMA-*ran*-LMA copolymer demonstrated highest tumor uptake and blood pool concentration. Obviously the molecular structure (e.g. amphiphilicity) is holding a higher impact on desired *in vivo* properties than polymer size. The results also revealed pronounced differences between the tumor models although vascular permeability was comparable. Accumulation in Walker 256 carcinomas was much higher, presumably due to a better cellular uptake of the polymers in these tumor cells (determined by kinetic cell culture experiments). These investigations clearly indicate that the properties of the individual tumor determine the suitability of polymeric drug carriers. The findings also illustrate the general necessity of a pre-clinical screening to analyze polymer uptake for each individual patient (e.g. by non-invasive imaging) in order to individualize polymer-based chemotherapy.

Keywords: HPMA, fluorine-18 labeling, PET, AT1 Dunning prostate carcinoma R3327, Walker 256 mammary carcinoma, structure-property relationship

Introduction

"Polymer therapeutics" [1] are a promising approach for anticancer treatment. The great benefit of polymer based drug delivery systems consists in a decrease of toxic side effects of the chemotherapeutic agent in healthy tissue, an accumulation in the tumor due to the EPR effect [2] and a longer blood circulation time compared to the pure anticancer drug. In this regard poly-*N*-(2-hydroxypropyl)methacrylamide poly(HPMA) – being non-toxic, non-immunogenic and biocompatible – is holding favorable polymer characteristics for preclinical as well as clinical testing [3-7].

The body distribution of macromolecular therapeutics may not only be affected by specific characteristics of the polymer system such as molecular weight, architecture, lipophilicity or the capability of forming superstructures (resulting in larger diameters). But besides, also biological and physiological properties of the specific tumor may be of high importance. For instance tumor vascularity and perfusion, vascular permeability or metabolic parameters (such as oxygenation, pH or bioenergetic status) may alter the distribution and accumulation of nanotherapeutics [8]. If individual tumors show pronounced differences in their accumulation of specific polymeric structures, the question of a precise pre-therapeutically tailoring of polymer-drug conjugates for each individual patient is arising. Concerning this purpose, non-invasive imaging techniques can be a helpful diagnostic tool providing detailed information of the body distribution as well as tumor accumulation for the individual patient thus enabling to attune polymeric carrier systems for efficient therapy. In this regard, Positron Emission Tomography (PET) constitutes a convenient dynamic imaging technique, allowing a non-invasive visualization of the pharmacokinetics *in vivo,* in real time and with high spatial resolution. Depending on the half-life of the radionuclide applied, the diagnostic time frame can be adjusted from early phase accumulation – using shorter lived isotopes – to long-term imaging over weeks. Until now, studies concerning the *in vivo* behavior of diverse HPMA-based formulations have been almost exclusively carried out using γ-imaging radionuclides e.g. Tc-99m or I-125/131 [9, 10] which have a relatively low spatial resolution. By successful radiolabeling of various HPMA-based polymers with the positron emitters As-72/74 [11] and F-18 [12], we were able to establish PET imaging to assess the *in vivo* capability of potential drug delivery systems. By this labeling approach we were able to demonstrate that the ratio of hydrophilicity/hydrophobicity as well as aggregate formation possessed a major impact on body distribution in the living animal [13].

Generally the influence of molecular structure on the tumor accumulation is a question of high importance. Cabral and coworkers [14] already demonstrated the dependency of the polymer size on tumor uptake in poorly permeable tumor models. But in addition, other molecular characteristics (lipophilicity, superstructures) have to be taken into account as well as tumor properties like vascular permeability or cellular uptake in different tumor lines. The impact of these parameters on polymer accumulation of diverse polymer architectures still remains unclear. Taking these demands into consideration, the aim of the present study was to analyze a broad spectrum of HPMA-based polymer architectures concerning their biological distribution *in vivo* in dependency of the tumor specific model. The polymer structures included homopolymers, random copolymers as well as block copolymers consisting of hydrophilic HPMA and hydrophobic Lauryl Methacrylate (LMA) segments. Both random as well as block copolymers form hydrophilic/hydrophobic superstructures and are interesting as drug delivery vehicles [15-17]. These polymers were tested in two different tumor lines

(AT1 subline of the R-3327 Dunning prostate carcinoma and Walker 256 mammary carcinoma) in order to analyze the impact of tumor specific properties. For this purpose we used radio-labeling with the positron emitting isotope fluorine-18 in order to investigate tumor accumulation as well as whole body distribution by application of µPET imaging and *ex vivo* biodistribution. In particular, the study demonstrates the capability of PET imaging for potential polymeric drug carriers and their use for individual patient therapy.

Results and Discussion

Synthetic route of HPMA-based nanoparticles and their radioactive labeling

In these studies we have synthesized a library of HPMA-based polymeric nanoparticles aiming for deepening knowledge on their structure-property relationships *in vivo*. Starting from the reactive ester precursor pentafluorophenylmethacrylate, we combined reactive ester chemistry with the controlled radical polymerization technique RAFT [18, 19] for polymer preparation. By incorporation of the hydrophobic laurylmethacrylate monomer and subsequent polymeranalogous reaction with 2-hydroxypropylamine [20, 21], nanoparticles with diverse polymer architectures – homopolymers, random as well as block copolymers – are easily realized (Scheme 1). Due to the RAFT concept, these HPMA-based polymer systems can be varied in molecular weight as well as hydrophobic content [13, 15, 12]. The hydrophobically modified polymers form aggregates in water solutions (e.g. buffer). Thus the particle size can be varied between some nm (size of an individual hydrophilic polymer coil depending on the molecular weight) and up to 100 nm for the aggregates. The resulting nanoparticles could be visualized by means of Transmission Electron Microscopy (TEM) [22]. Their molecular structure and the size of the nanoparticles (aggregates) are collected in table 1.

The hydrodynamic radii of the nanosystems were determined by Fluorescence Correlation Spectroscopy (FCS). This method found a minimum of around 1 nm for the low molecular weight homopolymer P1* and showed a slow increase to 3 nm for particle P2* with higher molecular weight. The random copolymers P3* and P4* exhibited a hydrodynamic radius of ~33 nm and 40 nm, thereby displaying the middle-sized nanoparticles in the herein presenting study. The biggest sizes were achieved for the block copolymer structures P5* and P6* with an R_h of around 59 and 113 nm.

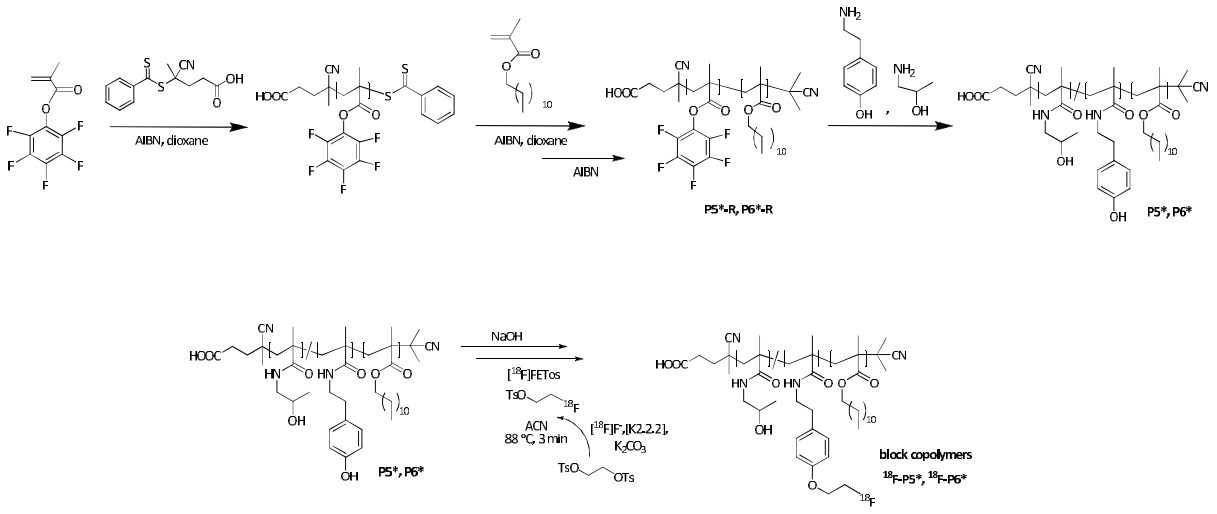

Scheme 1: Reaction scheme of polymeric precursor systems (exemplary block copolymers P5 and P6*), their polymeranalogous conversion and radioactive labeling procedure.*

Table 1: Analytical data of reactive ester homopolymers (P1-R and P2*-R), random copolymers (P3*-R and P4*-R) and block copolymers (P5*-R and P6*-R) as well as the final polymers P1*-P6**

Nomen-clature	Polymeric structure	Monomer ratio	M_n in g/mol	M_w in g/mol	PDI[2]	R_h[5] in nm
P1*-R	Homopolymer	100%[1]	18000[2]	23000[2]	1.29	n.d.
P2*-R	Homopolymer	100%[1]	87000[2]	130000[2]	1.49	n.d.
P3*-R	Random copolymer	80:20%[1]	17000[2]	21000[2]	1.26	n.d.
P4*-R	Random copolymer	80:20%[1]	57000[2]	80000[2]	1.41	n.d.
P5*-R	Block copolymer	60:40%[1]	14000[2]	18000[2]	1.26	n.d.
P6*-R	Block copolymer	60:40%[1]	25000[2]	31000[2]	1.25	n.d.
P1*	Homopolymer	100%[3]	9000[4]	12000[4]	1.29	1.1
P2*	Homopolymer	100%[3]	52000[4]	77000[4]	1.49	3.0
P3*	Random copolymer	82:18[3]	11000[4]	14000[4]	1.26	33.4
P4*	Random copolymer	75:25[3]	39000[4]	55000[4]	1.41	39.9
P5*	Block copolymer	79:21[3]	9000[4]	12000[4]	1.24	58.7
P6*	Block copolymer	75:25[3]	17000[4]	21000[4]	1.24	112.8

[1] Calculated monomer ratio. [2] Determination by GPC in THF as solvent. [3] Monomer ratio determined by ^{1}H-NMR spectroscopy after polymeranalogous reaction with 2-hydroxy-propylamine. [4] Calculated from the molecular weights of the reactive ester polymers P1*-R to P6*-R as determined by GPC in THF as solvent. [5] Hydrodynamic radii determined by Fluorescence Correlation spectroscopy (FCS).

Taking these values into account, the correlation of size, molecular weight and architecture (e.g. amphiphilicity) of the HPMA-based nanoparticles is crucial for understanding their biological uptake in the living organism. Related to former studies [13] which demonstrated a major impact of aggregate formation on the polymer biodistribution pattern for random copolymer particles, the herein presented nanosystems – also including HPMA-LMA block copolymers – were tested *in vivo* with respect to organ distribution and tumor accumulation. For this purpose polymeric systems were labeled with the positron emitting radionuclide [^{18}F]fluorine which exhibits favorable nuclear characteristics ($t_{1/2}$=110 min, high β^+-branching, low beta energy) for high resolution non-invasive PET imaging. Radiolabeling was accomplished in two steps using the prosthetic labeling synthon [^{18}F]FETos, attached to the hydrophilic part of the polymer backbone by covalent linkage to tyramine groups (incorporation efficiency ~4%) (Scheme 1) [12]. Within each polymer architecture, radiolabeling efficiencies were shown to be higher for polymers of lower molecular weight (P1*, P3*, P5*) and highest RCYs were achieved for the homopolymer P1* (RCY = 37 ± 6). This might be due to the better accessibility of the tyramine groups. Following ^{18}F-labeling, biodistribution of the labeled compounds was analyzed by µPET imaging as well as *ex vivo* organ concentration measurements in rats. To investigate the impact of tumor specific tissue and cell properties on the uptake of the varying polymer structures, accumulation was followed in two different tumor lines (subline AT1 of the Dunning prostate carcinoma R3327 and the Walker 256 mammary carcinoma) of the rat.

Organ distribution

Using µPET imaging and *ex vivo* biodistribution analysis allows quantification of the polymer uptake in different organs. Fig. 1A shows the whole body distribution pattern of the different polymers 2 h after i.v. injection. The images clearly indicate pronounced differences with low molecular weight nanoparticles (P1*, P3*, P5*) predominantly found in the kidney whereas high molecular weight polymer particles (P2*, P4*, P6*) were found to a greater extend in liver and spleen. The images also show that the two HPMA-*ran*-LMA copolymers (P3*, P4*) stayed much longer in the blood compartment than the other polymer architectures. In these animals the aorta and the femoral artery are clearly visible as well as the well perfused lung (Suppl. Fig. 1). By administration of the large homopolymer (P2*) the liver is (at least partially) clearly visualized whereas the small homopolymer (P1*) is only seen in the kidney.

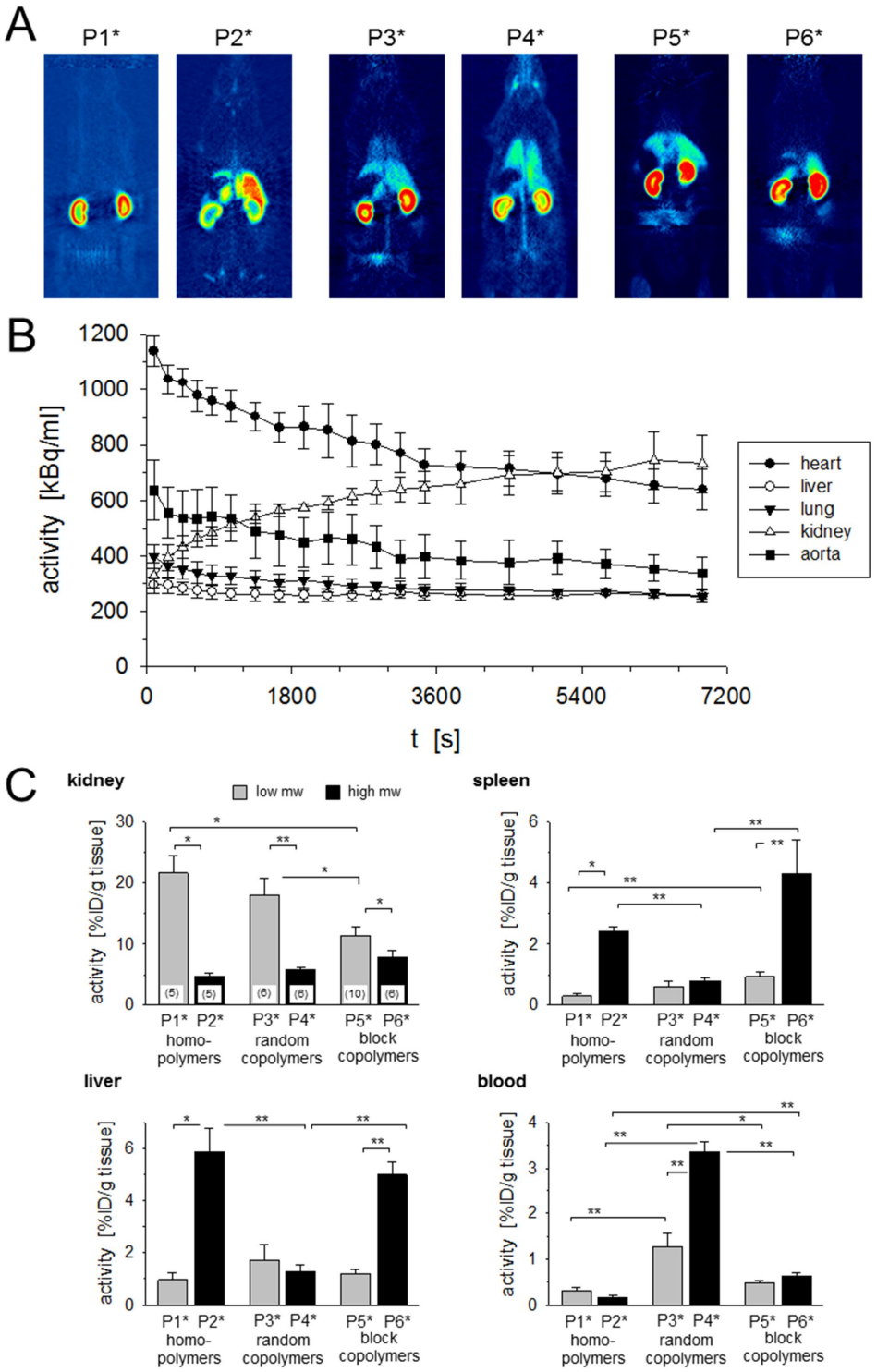

Figure 1: Organ distribution of the polymers (P1 and P2* homopolymers, P3*and P4* random copolymers as well as P5* and P6* block copolymers with low or high molecular weight respectively). (A) Whole body PET images of the distribution of the polymers 2 h after polymer injection. (B) Time activity curves (TAC) for different organs after injection of the random copolymer with high molecular weight (P4*). n=2. (C) Quantification of the polymer uptake in different tissues. Uptake is expressed by the fraction of the injected dose (ID) of the polymer per gram tissue 2 h after i.v. injection. n=5-10, (*) p<0.05, (**)p<0.01.*

Using PET imaging also the time course of uptake into the tissues can be traced. By defining ROIs over different organs the time-activity curve (TAC) displays temporal redistribution. As Fig. 1B demonstrates, the high molecular weight HPMA-*ran*-LMA copolymer (P4*) is continuously excreted by the kidney (as indicated by a continuous increase in activity in this organ) whereas in all other organs the tissue concentration is steadily decreasing.

In order to quantify the organ uptake, biodistribution was measured *ex vivo* 2 h and 4 h after particle injection. The measurements showed pronounced disparities between various organs depending on polymer architecture as well as molecular weight. For the low molecular weight polymers the highest concentrations were found in the kidney (Fig. 1C, Tab. 2, $p<0.001$ ANOVA). Since the molecular weight of these polymeric systems is close to the renal filtration threshold, they can be easily filtrated into primary urine which will lead to the high whole tissue concentration observed. The polymer architecture (homo- *vs*. random copolymers) plays only an insignificant role for renal uptake (or urinary excretion). However, the renal concentration of the low molecular weight block copolymer (P5*) was significantly lower than for both other polymer structures which probably might be the result of their superstructure formation resulting in a much larger molecular diameter (Tab. 1). After 4 h the renal concentration further increased (not statistically significant) for all polymers (Fig. 2) which corresponds well to the TAC curves shown in Fig. 1B.

The high molecular weight homopolymer P2* as well as the block copolymer P6* were taken up most prominently into liver and spleen. The liver concentrations of these polymers were 5-times higher than for all other polymers (Fig. 1C, Tab. 2) indicating that polymer structure is of high importance regarding liver uptake ($p=0.029$ ANOVA). The other polymers showed concentrations on comparable levels. After 4 h the liver concentrations of the random copolymers were markedly, however not statistically significant, lower (Fig. 2) whereas for the block copolymers the concentration remained constant. The organ distribution stays in good accordance to data described by Kissel et al. [9] who investigated an HPMA homopolymer with a molecular weight of 27 kDa – thereby being in between the two here presented homopolymers P1* and P2*. On the other hand the results are partially in contrast to the findings depicted by Lammers et al. [23], where the authors described a much higher accumulation of the HPMA homopolymers in the spleen as compared to the liver. In the present study, liver concentration was 2-3-times higher than in the spleen. The mentioned disparities might be a result of different time points of measurement.

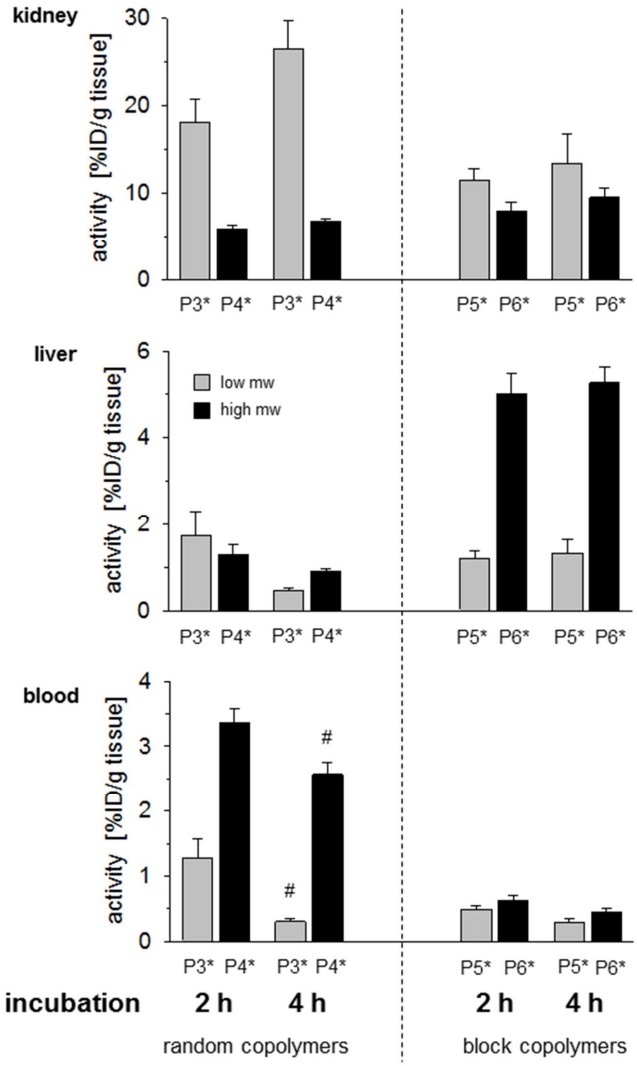

Figure 2: Comparison of the organ distribution of random and block copolymers 2 h and 4 h after injection, respectively. n=3-10, (#) p<0.05 2 h vs. 4 h.

As a result of low renal excretion and low hepatic elimination of the copolymers P3* and P4*, the blood levels of both random copolymers 2 h after injection were significantly higher than those of the homo- and block copolymers. Regarding the high molecular weight polymers P2*, P4* and P6*, the blood concentration of the HPMA-*ran*-LMA copolymer was almost 5-20-times higher (Fig. 1C, $p<0.0001$ ANOVA) and stayed elevated for the whole observation frame of 4 h (Fig. 2). The most probable reason of the prolonged stay of the copolymer in vasculature seems to be the higher lipophilicity of the LMA-containing copolymers [13] and consequential a diminished renal excretion. The blood levels of the homopolymers were markedly lower than described by a previous study [23]. This distinction still remains unclear.

The organ distribution in other tissues was not pronouncedly different among the studied polymer systems or the organ levels directly reflect the disparities in blood compartment (Tab. 2).

Table 2: Polymer uptake in different organs expressed by the fraction of the injected dose (ID) of the polymer per gram tissue 2 h after i.v. injection. n=5-10

	polymer concentration [%ID/g tissue]					
organ	P1*	P2*	P3*	P4*	P5*	P6*
lung	0.23±0.04	0.27±0.04	0.49±0.09	1.33±0.13	0.28±0.05	0.39±0.06
liver	0.96±0.28	5.87±0.9	1.73±0.57	1.3±0.24	1.2±0.18	5.01±0.47
spleen	0.28±0.08	2.41±0.17	0.58±0.18	0.77±0.09	0.94±0.14	4.3±1.1
kidney	24.52±0.94	4.83±0.49	18.06±2.68	5.86±0.4	11.44±1.33	7.95±0.96
muscle	0.09±0.01	0.04±0.01	0.11±0.02	0.16±0.05	0.08±0.03	0.07±0.01
heart	0.12±0.01	0.09±0.01	0.37±0.07	0.72±0.11	0.16±0.02	0.22±0.03
blood	0.33±0.06	0.18±0.03	1.27±0.3	3.36±0.22	0.49±0.05	0.63±0.07
small intestine	0.16±0.02	0.36±0.06	0.29±0.1	0.46±0.11	0.21±0.05	0.23±0.02
testis	0.1±0.01	0.06±0.01	0.15±0.01	0.18±0.02	0.09±0.01	0.1±0.01

Tumor accumulation

The major aim of the presented study was to analyze the uptake of six nanosized polymer architectures in two different tumor models (AT1 prostate carcinoma, Walker 256 mammary carcinoma of the rat) applying PET as a fast and versatile imaging tool. Both tumor cell lines were implanted subcutaneously into the hind foot dorsum and grew with a comparable rate, 7 to 14 days to reach a mean volume of 1.32±0.10 mL. Even though both tumor models show similar growth rate and comparable histology, the uptake of the polymers was fundamentally different.

All polymers accumulate poorly in AT1 tumors with nearly no influence of molecular structure and aggregate size (Fig. 3). Neither polymeric structure (p=0.952 ANOVA) nor molecular weight (p=0.304) had a relevant impact on intratumoral concentrations – although the blood levels were varying noticeably between the different polymer architectures (especially for P3* and P4*, Fig. 1C). The accumulation of the homopolymers was comparable to that described by others [23] who investigated the tumor uptake in the same tumor model, however, at a later time point after polymer injection. Nevertheless they described a better uptake of the large homopolymer as

compared to low molecular weight HPMA-based homopolymers which could not be confirmed in the present study. In principle, AT1 prostate carcinomas do not accumulate any of the polymers very well.

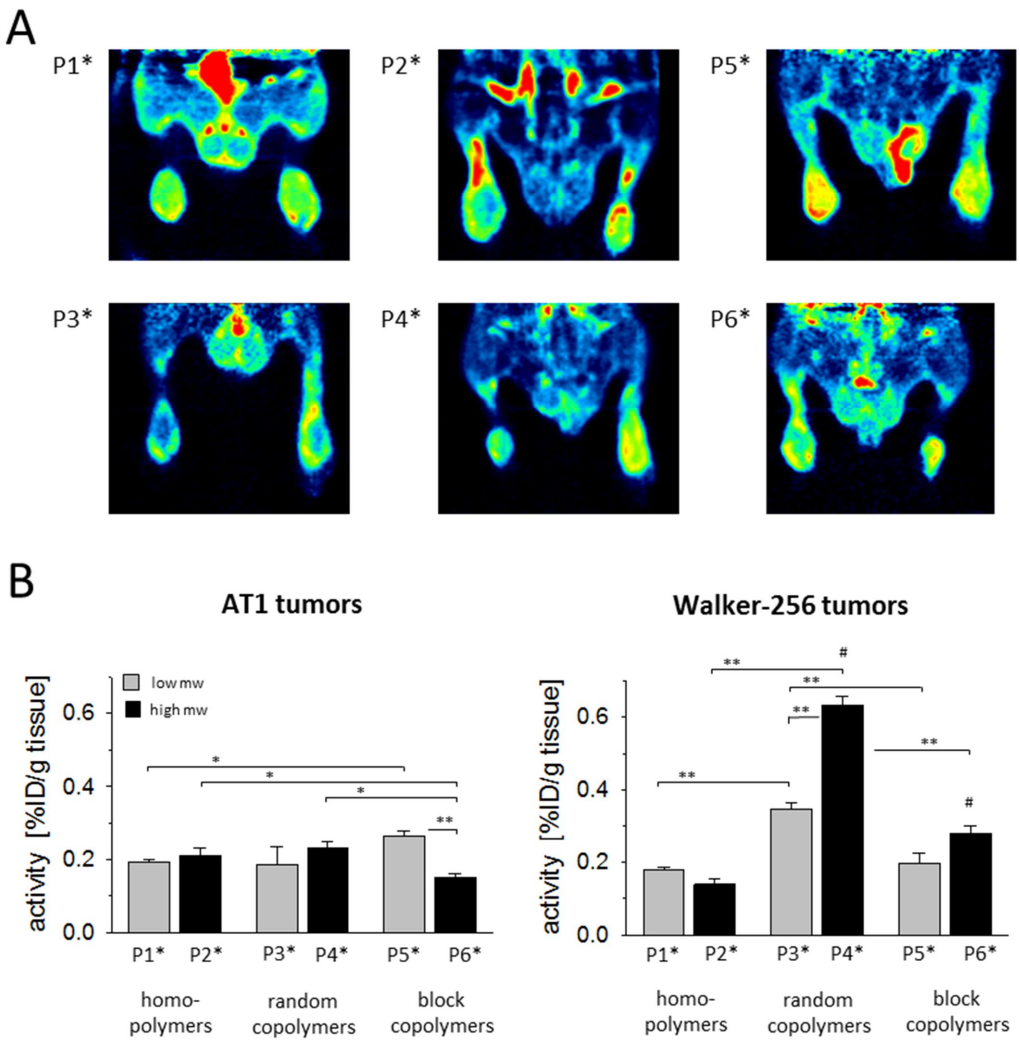

Figure 3: Tumor uptake of the polymers (P1 and P2* homopolymers; P3* and P4* random copolymers; P5* and P6* block copolymers with low or high molecular weight, respectively). (A) Example PET images of polymer accumulation in AT1 prostate carcinomas. (B) Intratumoral polymer concentration in AT1 prostate carcinomas and Walker 256 mammary carcinomas determined by biodistribution measurements 2 h after polymer application. n=5-6; (*) p<0.05, (**) p<0.01; (#) p<0.01 Walker 256 vs. AT1 tumors.*

When analyzing the spatial distribution of the intratumoral uptake in AT1 tumors, PET imaging revealed that the highest concentrations were found in the outer rim of AT1 tumors, a phenomenon seen more or less with all polymers (Fig. 3A).

For more detailed evaluation of the spatial heterogeneity, autoradiograms have been generated and correlated with the histological structure. These microscopic images illustrated that the high concentration in the rim corresponds to the subcutis around the tumor and not to the tumor tissue itself (Fig. 6A). Since the *ex vivo* biodistribution studies were performed in tumor tissue without skin, the values shown in Fig. 3B are not biased by the subcutaneous blood compartment.

In Walker 256 tumors the uptake was highly different, depending on the polymer architecture as well as the molecular weight. Whereas the homo- and the block copolymers were accumulated poorly in the Walker tumors (comparable to AT1 tumors), the uptake of the HPMA-*ran*-LMA copolymers was significantly higher (Fig. 3B). The intratumoral concentration of the large random copolymer (P4*) was 4.6-times higher than for the large homopolymer (P2*) and almost 3-times higher than the HPMA-*ran*-LMA copolymer levels in AT1 tumors (Fig. 3B). Since the random copolymer particles stay much longer in the circulation (blood pool, Fig. 1C) one possible explanation would be the difference of vascularity of AT1 and Walker 256 carcinoma. However, investigation of microvessel density by immunochemistry revealed that there were no profound disparities between both tumor models [24-26]. A marginal indication for the impact of the fraction of blood vessels within the tumor on the polymer uptake might be the fact that in AT1 tumors vascular density increases in larger tumors [27] which slightly correlates with the polymer accumulation (data not shown).

The low molecular weight random copolymer (P3*) also showed a markedly (however not statistically significant $p=0.055$) higher concentration in Walker carcinomas as compared to AT1 tumors. The absolute level of P3*, however, was lower than for P4* (Fig. 3B) which might be the result of a lower blood concentration of P3* (Fig. 1C). Besides others, one possible explanation might be the lower hydrophobicity of the small random copolymer P3* (incorporation efficiency of 18% LMA) compared to its high molecular weight counterpart P4* (25% of LMA-fraction). Obviously the uptake of the random copolymer nanoparticles depends mainly on the tumor entity which was confirmed by ANOVA ($p<0.0001$). The uptake of the block copolymers was also much lower than for the random copolymers (approximately at the same level as for the homopolymers). These data clearly reveal that the intratumoral uptake of polymers is not only a question of molecular size [14] (which is highest for the block polymer particles, Tab. 1) but also strongly dependent on the chemical properties of the polymer architectures (e.g. hydrophobicity/hydrophilicity). However, for a distinct polymeric structure the differences between the tumor lines are tremendous (at least for the random copolymers) indicating that specific tumor cell properties also mainly affect intratumoral accumulation of polymers.

Analysis the time course of polymer uptake in both tumor lines by PET imaging (Fig. 4A) showed that a stable intratumoral concentration was reached 15-20 min after injection (Fig. 4B). The concentrations of the random and block copolymer (P4*, P6*) remained constant even over a longer time span up to 4 h (Fig. 5) although the blood concentration was decreasing over time (Fig. 2). Furthermore, similar results were found in experiments using ^{131}I-labeled random copolymer P4* over a time span of 72 hours. Even tumor enrichment over time – whilst blood pool concentration of the polymer decreased – could be observed (data not shown).

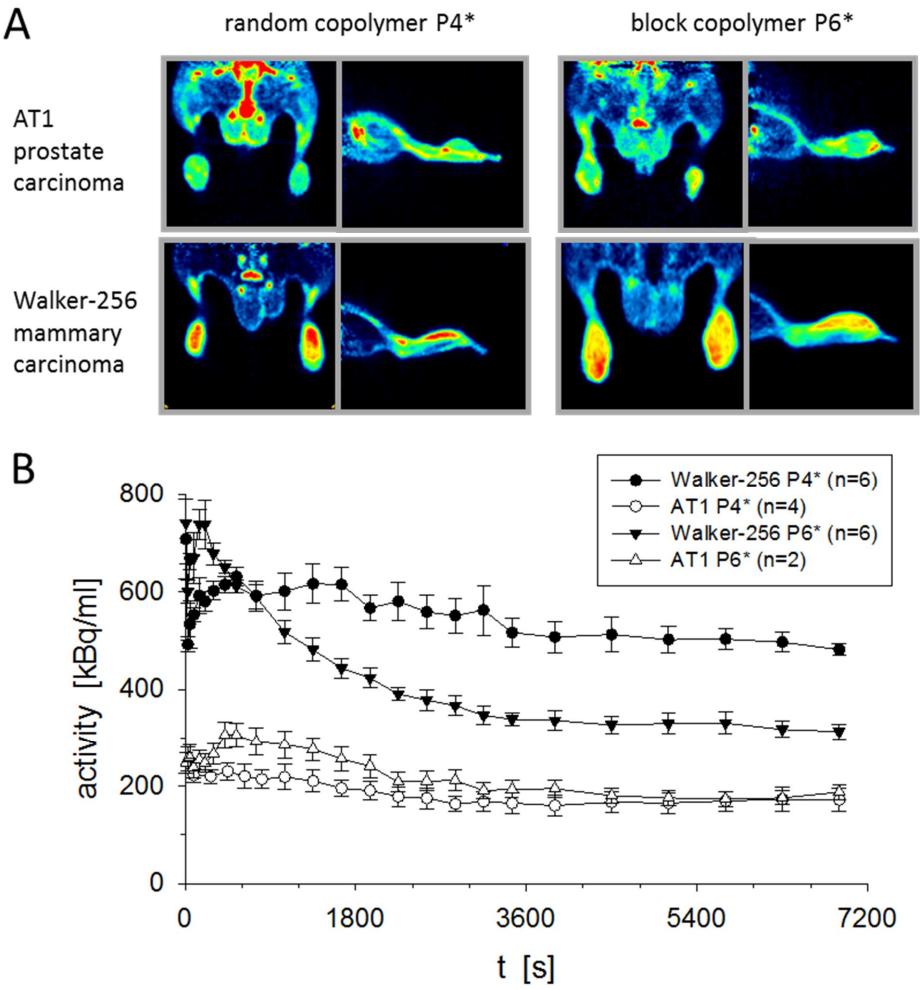

Figure 4: Comparison of polymer uptake in different tumor lines. (A) Example PET images of the accumulation of the large HPMA-ran-LMA and HPMA-b-copolymers in AT1 and Walker 256 carcinomas. (B) Time course of the relative polymer uptake of the large random copolymer (P4) and the large block copolymer (P6*) in Walker 256 and AT1 tumors. Values were normalized to the concentration of the reference tissue (testis).*

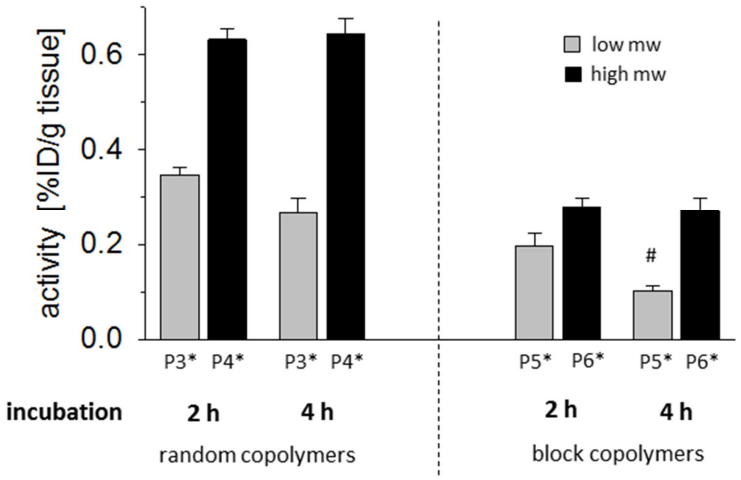

Figure 5: Intratumoral concentration of random and block copolymers in Walker 256 mammary carcinomas 2 and 4 h after injection, respectively. n=4-6, (#) p<0.05 2 h vs. 4 h.

One important aspect resulting from the findings on the HPMA-*ran*-LMA copolymers addresses the cause of the differences between the tumor lines responsible for the diverging uptake. Two tumor specific factors should be taken into account: (1) differences in vascular permeability and (2) differences in cellular uptake of the polymer.

Since former studies of Cabral and coworkers could already demonstrate that vascular permeability affects the tumor uptake of nanosized structures [14], this parameter was also measured in the tumor models used in the present study determining the extravasation of dextrans with different molecular weights (10, 70, 2000 kDa). As shown in Fig. 6B, the vascular permeability for high molecular weight dextrans was slightly (but not statistically significant) different between the two tumor lines. However, although AT1 tumors showed a much lower uptake of the HPMA-*ran*-LMA copolymers compared to Walker 256 tumors, the vascular permeability of these tumors was found to be even higher (Fig. 6B). Studies by other groups analyzing the vascular permeability of these tumor lines also showed that both tumors were moderately permeable for molecules up to a molecular weight of approximately 50-60 kDa but they seem to be more or less impermeable for molecules over 90 kDa [28, 29]. Nonetheless, the results of these studies are difficult to compare with each other due to different techniques used for measuring vascular permeability, whereas the results of the present study (as shown in Fig. 6B) used the same experimental procedure under identical conditions. In the previous studies an equilibrium between blood pool and interstitial space for molecules up to 50-60 kDa was reached at least 60 min post injection [29]. For this reason it seems to be plausible that the low and high molecular weight homo- and block copolymers show comparable

uptake in both tumor lines. The results concerning the HPMA-*ran*-LMA copolymers however are somehow surprising. In contrast to the other polymer structures, these nanoparticles are markedly accumulated in Walker 256 tumors but not in AT1 tumors (although the vascular permeability was lower, Fig. 6B). Beyond that, the high molecular weight random copolymer P4* (M_n=39 kDa) was taken up much stronger than its low molecular weight counterpart P3* (M_n=11 kDa). Therefore other mechanisms besides vascular permeability have to be considered.

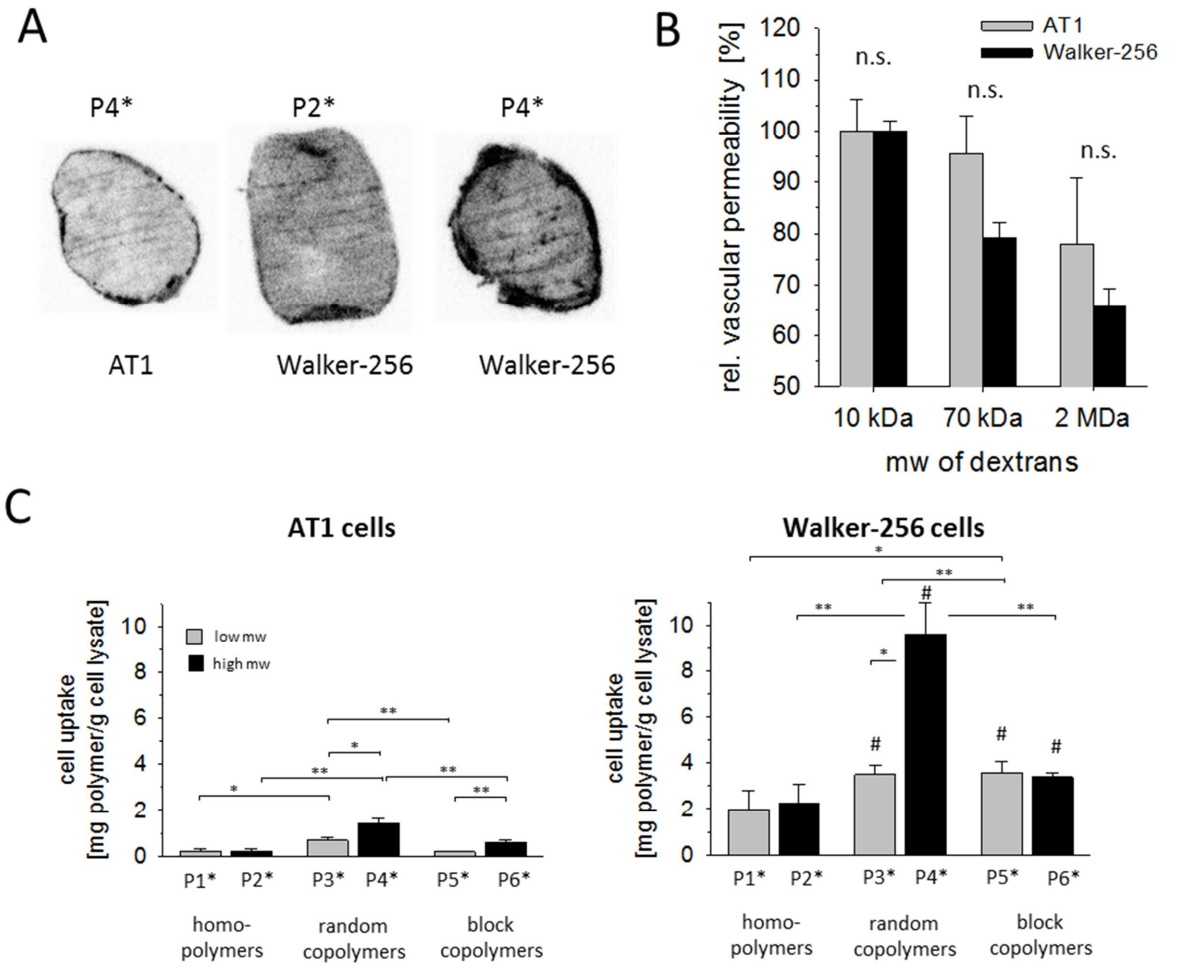

Figure 6: Differences of intratumoral uptake distribution. (A) Autoradiographic images of the polymer distribution within the tumor. (B) Vascular permeability of AT1 and Walker 256 tumors in vivo measured by extravasation of dextrans of different molecular weights (mw). n=2-6. (C) Cellular uptake of the polymers after 2 h incubation at 37°C in AT1 and Walker 256 carcinoma cells in vitro; n=6-12, (*) p<0.05, (**) p<0.01. (#) p<0.01 Walker 256 vs. AT1 cells.

In a further *in vitro* study the cellular uptake of the polymers into AT1 and Walker 256 cells was measured. The cell uptake depended significantly on the tumor cell line (p=0.0001, ANOVA). As shown in Figs. 6C all polymers were taken up in AT1 cells to only a very small extent. However, the

uptake of the HPMA-*ran*-LMA copolymers in Walker 256 cells was approximately 4-6 times higher than in AT1 (Fig. 6C). Obviously, these tumor cells exhibit distinct features leading to a much better cellular uptake which might explain the differences in the *ex vivo* biodistribution experiments. Although differences in the endocytotic processes of both lines might explain these findings, the reason for this differential behavior presently still remains unclear. The cellular uptake of the homopolymers in Walker 256 cells was markedly lower than for the random copolymers. The uptake pattern (Fig. 6C) was therefore similar to the whole tumor tissue results (Fig. 3B) indicating that the combination of *in vivo and in vitro* experiments constitutes a beneficial platform for determining the suitability of polymers as drug carrier systems.

Conclusion

The present study clearly demonstrates that polymer architecture as well as molecular weight and size affect the body distribution of HPMA-based polymers. Using radiolabeling of the polymers with positron emitting isotopes (^{18}F) allows biodistribution analyses as well as non-invasive Positron Emission Tomography (PET) imaging for quantification purposes. Applying these techniques, the results underline the important role of molecular weight concerning renal excretion, whereas polymer structure influences the hepatic uptake as well as elimination and consequential intravascular disposition. In contrast to homo- and block copolymers, HPMA-*ran*-LMA copolymers – exhibiting a higher percentage of hydrophobic segments – remain in the blood compartment for several hours which can be easily followed by PET. When analyzing the tumor uptake of the varying polymer architectures in two different carcinoma lines of the rat, surprisingly, the polymeric nanoparticles demonstrated strongly differing tumor accumulation properties, depending on the respective tumor line. Whereas in AT1 tumors all polymers were accumulated equally to a low extent, Walker 256 tumors remarkably have taken up the HPMA-*ran*-LMA-copolymers approximately 5-times stronger. Since the site of tumor growth, the proliferation rate as well as histological and vascular characteristics were comparable between both tumor lines, other tumor specific properties seem to be responsible for the different polymer accumulation. Cell experiments clearly show that the cellular uptake of the polymers varies markedly between the two cell lines used and could explain (at least partially) the differences seen *in vivo*.

It can be concluded that the variation of structure and size of the herein presented HPMA-based nanoparticles has a dominant influence on a prolonged stay in circulation and on a pronounced uptake of these molecules in the tumor tissue *in vivo*. The results also clearly reveal that the efficacy of a tumor treatment by polymer drug nanocarriers depends strongly on the properties of each individual tumor (depending on the tumor line). The perfect polymer fit has to be chosen for

individual tumors. Concerning the clinical setting, the present studies underline the necessity of a precise polymer characterization in combination with its pre-clinical screening to tailor the polymer carrier system for each individual tumor and patient to be treated. In this regard both radiolabeling as well as imaging of the polymeric architectures using PET is emphasizing a favorable and promising analytical tool for the individualization of polymer-based chemotherapy to the patient's needs, applicable to a variety of nanocarrier systems.

Materials and methods

Materials

All solvents were of analytical grade, as obtained by Sigma Aldrich and Acros Organics. Dioxane was distilled over a sodium/potassium composition. Lauryl methacrylate was distilled to remove the stabilizer and stored at -18 °C. 2,2'-Azo-bis-(isobutyronitrile) (AIBN) was recrystallized from diethyl ether and stored at -18 °C as well.

Methods

Polymer Synthesis

Synthesis of 4-cyano-4-((thiobenzoyl)sulfanyl)pentanoic acid (CTP). 4-cyano-4-((thiobenzoyl)sulfanyl)-pentanoic acid was used as chain transfer agent (CTA) and synthesized according to the literature [19].

Synthesis of pentafluorophenyl methacrylate (PFPMA). Pentafluorophenyl methacrylate was prepared according to reference [21].

Synthesis of reactive ester homopolymers. RAFT polymerization of pentafluorophenyl methacrylate with 4-cyano-4-((thiobenzoyl) sulfanyl)pentanoic acid was carried out in a schlenk tube [13, 15, 20]. For this purpose, 4 g of PFPMA were dissolved in 5 mL of absolute dioxane, furthermore CTP and AIBN were added. The molar ratio of CTP/AIBN was chosen 8:1. After three freeze-vacuum-thaw cycles, the mixture was immersed in an oil bath at 65 °C and stirred overnight. Afterwards, the polymeric solution was precipitated three times in hexane, centrifuged and dried under vacuum at 40 °C overnight. A slightly pink powder was obtained. Yield: 52%. ^{1}H-NMR (300 MHz, $CDCl_3$) δ/ ppm: 1.20-1.75 (br), 2.00-2.75 (br s). ^{19}F-NMR (400 MHz, $CDCl_3$) δ/ ppm: -162.03 (br), -156.92 (br), -152 to -150 (br).

Synthesis of random copolymers. RAFT polymerization of PFPMA with lauryl methacrylate (LMA) by help of CTP was performed in a schlenk tube as well. As an example, 4 g of PFPMA dissolved in 5 mL dioxane, lauryl methacrylate, AIBN and CTP were mixed. The molar ratio of CTP/AIBN was chosen to be 8:1. After three freeze-vacuum-thaw cycles, the mixture was immersed in an oil bath at 65 °C and stirred overnight. Afterwards, poly(PFPMA)-*ran*-poly(LMA) was precipitated three times in hexane, centrifuged and dried under vacuum at 40 °C overnight. A slightly pink powder was obtained. Yield: 54%. ^{1}H-NMR (300 MHz, $CDCl_3$) δ/ ppm: 0.84 (br t), 1.20-1.75 (br), 2.00-2.75 (br s). ^{19}F-NMR (400 MHz, $CDCl_3$) δ/ ppm: -162.01 (br), -156.95 (br), -152 to -150 (br).

Synthesis of block copolymers. The macro-CTA obtained after homopolymerization of PFPMA was dissolved in dioxane, afterwards lauryl methacrylate as well as AIBN were added. As an example, 250 mg of macro initiator were dissolved in 5 mL dioxane, lauryl methacrylate and AIBN (1:8 ratio macro-CTA/AIBN) were mixed. After three freeze-vacuum-thaw cycles, the mixture was immersed in an oil bath at 65 °C and stirred for three days. Afterwards, poly(PFPMA)-*b*-poly(LMA) was precipitated three times in ethanol, centrifuged and dried under vacuum at 40 °C overnight. A slightly pink powder was obtained. Yield: 54%. ^{1}H-NMR (300 MHz, $CDCl_3$) δ/ ppm: 0.84 (br t), 1.20-1.75 (br), 2.00-2.75 (br s). ^{19}F-NMR (400 MHz, $CDCl_3$) δ/ ppm: -162.01 (br), -156.95 (br), -152 to -150 (br).

Removal of dithioester endgroups. The dithiobenzoate endgroup was removed using the protocol reported by Perrier et al. [30]. Therefore a 25-fold molar excess of AIBN was added to the polymer dissolved in dioxane. After four hours of heating the solution in an oil bath at 70 °C, the polymer was precipitated twice in hexane and collected by centrifugation. The polymer was dried under vacuum overnight, a colorless powder was obtained. Yield: 75%. Removal of the dithioester endgroup could be proven by UV-Vis spectroscopy.

Polymer analogous reaction of homopolymers. Depending on the labeling technique necessary, either for a fluorescent or radioactive marker, two different routes were applied. For subsequent radioactive labeling, the protocol was carried out as follows. As example, 100 mg of the polymeric precursor (Mn = 18000 g/mol) were diluted in 2 mL of absolute dioxane. 5 mg of tyramine, diluted in a DMSO/dioxane mixture, and 10 mg of triethylamine were added. After stirring for four hours at 35 °C, 30 mg of 2-hydroxypropylamine as well as 40 mg of triethylamine were added and the solution was stirred overnight. For final removal of reactive ester side groups, further 30 mg of 2-hydroxypropylamine were added the next morning. The solution was precipitated two times in diethyl ether, centrifuged and finally dissolved in a DMSO/water solution for dialysis. After lyophilization a white powder could be obtained. Yield: 79%. ^{1}H-NMR (400 MHz, d. DMSO) δ/ ppm: 0.60-1.40 (br), 1.45-2.20 (br), 2.75-3.10 (br), 3.50-3.80 (br), 4.60-4.80 (br), 6.60-6.70 (br) and 6.85-

7.00 (br). For additional fluorescent labeling, the fluorescent marker Oregon Green 488 cadaverine was used. 100 mg of polymeric precursor were diluted in 2 mL of absolute dioxane and 2.75 mg of Oregon Green 488 cadaverine added. Afterwards tyramine and 2-hydroxypropylamine were added, as described by the procedure above.

Polymer analogous reaction of random copolymer. For radioactive labeling of random copolymers the protocol was applied as follows. 100 mg of poly(PFPMA)-*ran*-poly(LMA) copolymer was dissolved in 2 mL of absolute dioxane. As example, for the polymeric system P3*-R (Mn= 17000 g/mol) 5 mg of tyramine and 10 mg of triethylamine were diluted in a DMSO/dioxane mixture and added to the vessel. After stirring for four hours at 35 °C, 30 mg of 2-hydroxypropylamine as well as 40 mg of triethylamine were added and the solution stirred overnight. For final removal of reactive ester side groups further 30 mg of 2-hydroxypropylamine were added the next morning. The solution was precipitated two times in diethyl ether, centrifuged and finally dissolved in a DMSO/water solution for dialysis. After lyophilization a white powder could be obtained. Yield: 51%. ^{1}H-NMR (400 MHz, d. DMSO) δ/ ppm: 0.70-0.90 (br), 0.90-1.40 (br), 1.40-1.90 (br), 2.75-3.10 (br), 3.50-3.80 (br), 4.50-4.75 (br), 6.60-6.75 (br) and 6.85-7.00 (br). For additional fluorescent labeling, 100 mg of polymeric precursor were diluted in 2 mL of absolute dioxane and 2.9 mg of Oregon Green 488 cadaverine were added. Afterwards tyramine and 2-hydroxypropylamine were added, as described by the procedure above.

Polymeranalogous reaction of block copolymers. For radioactive labeling as well as for fluorescent labeling the above mentioned synthetic route (see polymeranalogous reaction of random copolymers) can be applied.

Characterization

^{1}H-NMR spectra were obtained by a Bruker AC 300 spectrometer at 300 MHz, ^{19}F-NMR analysis was carried out with a Bruker DRX-400 at 400 MHz. All measurements were accomplished at room temperature and spectroscopic data were analyzed using ACDLabs 9.0 1D NMR Manager. The synthesized polymers were dried at 40 °C under vacuum overnight, followed by Gel Permeation Chromatography (GPC). GPC was performed in tetrahydrofuran (THF) as solvent, using following equipment: pump PU 1580, autosampler AS 1555, UV detector UV 1575 and RI detector RI 1530 from Jasco as well as a miniDAWN Tristar light scattering detector from Wyatt. Columns were used from MZ Analysentechnik, 300x8.0 mm: MZ-Gel SDplus 106 Å 5 µm, MZ-Gel SDplus 104 Å 5 µm and MZ-Gel SDplus 102 Å 5 µm. GPC data were evaluated by using the software PSS WinGPC Unity from Polymer Standard Service Mainz. The flow rate was set to 1 mL/min with a temperature of 25 °C.

For synthesis of 2-[^{18}F]fluoroethyl-1-tosylate ([^{18}F]FETos), a Sykam S 1100 pump and a Knauer UV-detector (K-2501) HPLC system were used. Size Exclusion Chromatography (SEC) of ^{18}F-labeled polymers was performed using HiTrap™ Desalting Column, Sephadex G-25 Superfine and a waters pump (1500 series), a Waters UV-detector (2487 λ absorbance detector) and a Berthold LB 509 radiodetector.

Size determination by Fluorescence Correlation Spectroscopy (FCS). The hydrodynamic radii of the polymeric systems were determined by Fluorescence Correlation Spectroscopy using a commercial FCS setup (Zeiss, Germany) consisting of the module ConfoCor 2 and an inverted microscope model Axiovert 200 with a Zeiss C-Apochromat 40 ×/1.2 W water immersion objective. The fluorophores were excited with an Argon laser (λ= 488 nm) and the emission was collected after filtering with a LP505 long pass filter. For detection, an avalanche photodiode, enabling single-photon counting, was used. As sample cell, eight-well, polystyrene-chambered cover glass (Laboratory-Tek, Nalge Nunc International) was applied. For sample preparation, stock solutions of 0.1 mg fluorescently labeled polymer/mL NaCl were applied. The solution was kept at room temperature overnight. For reference reason, free Oregon Green 488 cadaverine dye in NaCl-solution was also studied. The calibration of the FCS observation volume was done using a dye with known diffusion coefficient, i.e. Rhodamine6 G. For each solution, 5 measurement cycles with a total duration of 150 seconds were applied. Time dependant fluctuations of the fluorescence intensity δI(t) were detected and evaluated by autocorrelation analysis, yielding the diffusion coefficient and hydrodynamic radius of the fluorescent species [31].

Radioactive labeling

Synthesis of [^{18}F]FETos. To an aqueous [^{18}F]fluoride solution (2-8 GBq) 18 mg Kryptofix®2.2.2., potassium carbonate (1 N, 15 µL) and 1 mL acetonitrile were added. The mixture was dried in a stream of nitrogen at 80 °C, the drying procedure was repeated three times. To the dried residue 13 mg of ethyleneglycol-1,2-ditosylate in 1 mL acetonitrile was added and heated under stirring in a sealed vial at 88 °C for 3 min. Purification of the crude product was accomplished using HPLC (Lichrosphere RP18-EC5, 250×10 mm, acetonitrile/water 50:50, flow rate: 5 mL/min, t_R: 8 min). After diluting the HPLC fraction of 2-[^{18}F]fluoroethyl-1-tosylate with water, the product was loaded on a Sep-Pak C18 cartridge, dried with a nitrogen stream and eluted with 0.8 mL of DMSO [32].

Radiolabeling of polymers. For radiolabeling, 3 mg of the polymeric precursor were dissolved in 200 µL of dried DMSO. The solution was transferred to a sealed vial and 1 µL of a 5 N sodium hydroxide solution was added. The labeling reaction was started by adding the previously eluted

DMSO solution of 2-[^{18}F]fluoroethyl-1-tosylate and the mixture was stirred for 15 min at 120 °C. For *ex vivo* and *in vivo* experiments, the radiolabeled polymeric systems were freed from low molecular weight byproducts by Sephadex G-25 size exclusion chromatography (HiTrap™ Desalting Column, Sephadex G-25 Superfine, 0.9% NaCl, flow rate: 0.5 mL/min) leading to a pure, ^{18}F-labeled polymer solution ready for subsequent experiments [12, 13].

Tumor and animal models

For animal experiments two rat tumor cell lines were used: (1) Walker 256 mammary carcinoma, (2) subline AT1 of the Dunning prostate carcinoma R3327. Both cell lines were grown in culture in RPMI medium supplemented with 10 mM L-glutamine and 10% fetal calf serum (FCS) at 37 °C under a humidified 5% CO2 atmosphere and sub-cultivated twice per week. For tumor implantation male Sprague-Dawley rats (for Walker 256 tumors) or male Copenhagen rats (for R3327-AT1 tumors) (Charles River Wiga, Sulzfeld, Germany; body weight 150 to 300 g) housed in the animal care facility of the University of Mainz were used in this study. All experiments had previously been approved by the regional animal ethics committee and were conducted in accordance with the German Law for Animal Protection and the UKCCCR Guidelines [33]. Animals were allowed access to food and acidified water ad libitum before the investigation. Solid carcinomas of both cell lines were heterotopically induced by injection of cell suspension of the respective tumor line (0.4 mL approx. 104 cells/µL) subcutaneously into the dorsum of the hind foot. Tumors grew as flat, spherical segments and replaced the subcutis and corium completely. Volumes were determined by measuring the three orthogonal diameters (d) of the tumors and using an ellipsoid approximation with the formula: $V = d1 \times d2 \times d3 \times \pi/6$. Tumors were used when they reached a volume of between 0.5 to 3.0 mL approx. 7 to 14 days after tumor cell inoculation.

Cellular studies and permeability assay

Cellular uptake of polymers. Cellular uptake of homo- and random copolymers into AT1 and Walker 256 cells was measured *in vitro*. Therefore, low and high molecular weight reactive precursor polymers were labeled with the fluorochrome Oregon-Green 488 cadaverine. Uptake experiments were performed using collagen-coated 24-well plates. Collagen A (Biochrom, Berlin, Germany) was diluted with water and pH-adjusted (3.5). Plates were incubated for 30 min and dried. Cells were grown until wells reached ~70% confluence when they were incubated with 500 µL HEPES-buffered Ringer solution (pH=7.4) containing 0.02 mg polymer/mL for 2 h at 37 °C. After washing, the cells were lysed with 250 µL Triton X-MOPS lysis buffer (15 min, room temperature) and mechanically removed from the plate surface. After centrifugation, 100 µL supernatant was pipetted in 96-well

black bottom microplates and analyzed in a microplate-reader (Infinite 200, Tecan, Männedorf, Switzerland) excitation 485 nm, emission 532 nm). Protein content of each sample was determined using Bradford reagent. The polymer uptake was expressed by the content of polymer/per gram cell protein.

Permeability assay. Vascular permeability of the tumor lines was measured by the extravasation of macromolecular dextrans. Therefore FITC- or Texas-Red-labeled dextrans with molecular weights of 10 kDa, 70 kDa or 200 kDa (Invitrogen, Darmstadt, Germany), respectively, were dissolved in saline at a concentration of 12.5 mg/mL. 400 µL of these solutions was injected into the tail vein of tumor bearing animals. After 15 min (10 kDa dextran), 1 h (70 kDa dextran) or 3 h (200 kDa dextran) animals were sacrificed, the tumors were removed, rapidly frozen in liquid nitrogen and cryosections (10 µm) prepared. Using fluorescence microscopy (Keyence, Neu-Isenburg, Germany) at low resolution, images of dextran extravasation were taken from 2 to 3 different regions of each cryosection. Approx. 3 to 4 sections from each tumor were analyzed resulting in 9 to 11 images per tumor. Dextran diffusion (described by the area fraction of the cryosection positive for the fluorochrome) was determined by image analysis software (ImageJ, National Institutes of Health, Bethesda MD, USA). The molecular diameter of the dextrans was determined by Fluorescence Correlation Spectroscopy using Rhodamine6G as calibration dye. Stock solutions of 0.1 mg dextran/mL NaCl were prepared. The diameters of the three dextrans were 1.77±0.1 nm (10 kDa, FITC-labeled), 14.42±1.0 nm (70 kDa, Texas Red-labeled) and 34.99±2.2 nm, respectively.

In vivo µPET imaging and ex vivo biodistribution studies

µPET imaging. For µPET imaging, rats were anaesthetized either with pentobarbital (40 mg/kg, intraperitoneal, Narcoren, Merial, Hallbergmoos, Germany) or with isofluran (2%). Polymers were injected *via* tail vein puncture.

The µPET imaging was performed on a microPET Focus 120 small animal PET (Siemens/Concorde, Knoxville, USA). During PET measurements the animals were placed in supine position and breathed room air spontaneously. Dynamic PET studies were acquired in listmode. The radiolabeled polymers were administered as a bolus injection of 0.4-0.7 mL simultaneously with the start of the PET scan. The mean injected activity of labeled polymers was 23.6±1.3 MBq. The PET listmode data were histogrammed into 25 frames and reconstructed using OSEM2D algorithm. Volumes-of-interests (VOIs) were defined for tumor and reference tissue (testis). The testis was used as a reference since it was in the field of view when imaging the tumors on the feet and because the tissue concentration was relatively constant between all animals on a low level. Time activity curves (TAC) were obtained

with varying time frames (1.5-10 min) for a total measuring interval of 120 min. Ratios of tumor to reference tissue were calculated from integral images between 15' and 120' after polymer injection.

For PET imaging of the time course of body distribution in different internal organs the field of view was located over the trunk from the neck region to the pelvis. TACs were analyzed for VOIs of heart, liver, lung, kidney and aorta.

Biodistribution studies. In order to assess the distribution of the radiolabeled polymers in different organs of the animals, the polymer (concentration of 1 mg in 1 mL sodium chloride solution) was injected i.v. in anaesthetized tumor-bearing rats *via* the tail vein with a mean activity of 11.9 ± 0.7 MBq. After 120 or 240 min, the animals were sacrificed and different organ (kidney, liver, lung, spleen, heart, skeletal muscle, small intestine, testis, blood) and tumor samples were taken. The tissue samples were weighed and minced. Finally, the ^{18}F-activity in the organs was measured in a γ-counter.

In vitro assays

Autoradiography and histological staining. For autoradiography, animals were treated in the same way as in the biodistribution experiments. Immediately after sacrifice (120 or 240 min after polymer injection) tumors were excised and rapidly frozen in liquid nitrogen cooled isopentane. The tissue was then embedded (Tissue-Tek, O.C.T. Compound, Sakura Finetek Europe, Leiden, The Netherlands) and coronar slices (thickness 20 µm) were cut with a cryostat (Slee, Mainz, Germany). The specimens were transferred on coated object holders and dried at room temperature until they were placed on Fuji imaging plates (BAS-SR 2040. 20x40 cm, Fujifilm Europe, Düsseldorf, Germany). After 5 hours of exposure, the phosphor screen was laser scanned in a 50-µm-pixel size mode using an image reader FLA-7000 (Fujifilm). Afterwards autoradiography sections were HE stained (hematoxylin 2 min, rinsed with tap water, eosin 30 s, rinsed) and dehydrated (ethanol) before coverslipped using aquatex mounting medium (Merck, Darmstadt, Germany). HE sections were digitized using digital microscopy (Keyence BZ-8000, Osaka, Japan).

Statistical analysis. Results are expressed as means±SEM. Differences between groups were assessed by the two-tailed Wilcoxon test for paired samples and by multi-factorial ANOVA. The significance level was set at α=5% for all comparisons.

Acknowledgement

The authors would like to thank Nicole Bausbacher and Bengü Yilmaz for their support during animal studies and following interpretation. We also want to thank the Max-Planck Graduate Center (MPGC, M. Allmeroth) as well as the Graduate School Materials Science in Mainz (Excellence Initiative, DFG/GSC 266, D. Moderegger) for financial support. In addition the authors are very thankful for financial support of the DFG (Rösch: RO 985/30-1; Thews: TH 482/4-1, Zentel: ZE 230/21-1) and SAMT Initiative Mainz. Furthermore thanks to Dr. Matthias Barz for fruitful discussion.

Additional information

The authors declare no competing financial interests.

References

[1] Duncan, R. The dawning era of polymer therapeutics. *Nat. Rev. Drug Discov.* 2003, *2*, 347-360.

[2] Matsumura, Y.; Maeda, H. A new concept for macromolecular therapeutics in cancer chemotherapy: Mechanism of tumoritropic accumulation of proteins and the antitumor agent smancs. *Cancer Res.* 1986, *46*, 6387-6392.

[3] Duncan, R. Development of HPMA copolymer-anticancer conjugates: Clinical experience and lessons learnt. *Adv. Drug Deliver. Rev.* 2009, *61*, 1131-1148.

[4] Lammers, T. Improving the efficacy of combined modality anticancer therapy using HPMA copolymer-based nanomedicine formulations. *Adv. Drug Deliver. Rev.* 2010, *62*, 203-230.

[5] Minko, T.; Kopecková, P.; Pozharov, V.; Kopecek, J. HPMA copolymer bound adriamycin overcomes MDR1 gene encoded resistance in a human ovarian carcinoma cell line. *J. Control. Release* 1998, *54*, 223-233.

[6] Nowotnik, D. P.; Cvitkovic, E. ProLindac(TM) (AP5346): A review of the development of an HPMA DACH platinum Polymer Therapeutic. *Adv. Drug Deliver. Rev.* 2009, *61*, 1214-1219.

[7] Ulbrich, K.; Subr, V. Structural and chemical aspects of HPMA copolymers as drug carriers. *Adv. Drug Deliver. Rev.* 2010, *62*, 150-166.

[8] Heuser, L. S.; Miller, F. N. Differential macromolecular leakage from the vasculature of tumors. *Cancer* 1986, *57*, 461-464.

[9] Kissel, M.; Peschke, P.; Subr, V.; Ulbrich, K.; Strunz, A.; Kühnlein, R.; Debus, J.; Friedrich, E. Detection and cellular localisation of the synthetic soluble macromolecular drug carrier pHPMA. *Europ. J. Nucl. Med. Mol. Imaging* 2002, *29*, 1055-1062.

[10] Lu, Z. R. Molecular imaging of HPMA copolymers: Visualizing drug delivery in cell, mouse and man. *Adv. Drug Deliver. Rev.* 2010, *62*, 246-257.

[11] Herth, M. M.; Barz, M.; Jahn, M.; Zentel, R.; Rösch, F. $^{72/74}$As-labeling of HPMA based polymers for long-term in vivo PET imaging. *Bioorg. Med. Chem. Lett.* 2010, *20*, 5454-5458.

[12] Herth, M. M.; Barz, M.; Moderegger, D.; Allmeroth, M.; Jahn, M.; Thews, O.; Zentel, R.; Rösch, F. Radioactive labeling of defined HPMA-based polymeric structures using [^{18}F]FETos for in vivo imaging by positron emission tomography. *Biomacromolecules* 2009, *10*, 1697-1703.

[13] Allmeroth, M.; Moderegger, D.; Biesalski, B.; Koynov, K.; Rösch, F.; Thews, O.; Zentel, R. Modifying the body distribution of HPMA-based copolymers by molecular weight and aggregate formation. *Biomacromolecules* 2011, *12*, 2841-2849.

[14] Cabral, H.; Matsumoto, Y.; Mizuno, K.; Chen, Q.; Murakami, M.; Kimura, M.; Terada, Y.; Kano, M. R.; Miyazono, K.; Uesaka, M.; Nishiyama, N.; Kataoka, K. Accumulation of sub-100 nm polymeric micelles in poorly permeable tumours depends on size. *Nat. Nanotechnol.* 2011, *6*, 815-823.

[15] Barz, M.; Luxenhofer, R.; Zentel, R.; Kabanov, A. V. The uptake of N-(2-hydroxypropyl)-methacrylamide based homo, random and block copolymers by human multi-drug resistant breast adenocarcinoma cells. *Biomaterials* 2009, *30*, 5682-5690.

[16] Kataoka, K.; Harada, A.; Nagasaki, Y. Block copolymer micelles for drug delivery: design, characterization and biological significance. *Adv. Drug Deliver. Rev.* 2001, *47*, 113-131.

[17] Talelli, M.; Rijcken, C. J. F.; van Nostrum, C. F.; Storm, G.; Hennink, W. E. Micelles based on HPMA copolymers. *Adv. Drug Deliver. Rev.* 2010, *62*, 231-239.

[18] Chiefari, J.; Chong, Y. K.; Ercole, F.; Krstina, J.; Jeffery, J.; Le, T. P. T.; Mayadunne, R. T. A.; Meijs, G. F.; Moad, C. L.; Moad, G.; Rizzardo, E.; Thang, S. H. Living free-radical polymerization by reversible addition-fragmentation chain transfer: The RAFT process. *Macromolecules* 1998, *31*, 5559-5562.

[19] Moad, G.; Rizzardo, E.; Thang, S. H. Living radical polymerization by the RAFT process. *Austral. J. Chem.* 2005, *58*, 379-410.

[20] Theato, P. Synthesis of well-defined polymeric activated esters. *J. Polymer Sci. Part A: Polymer Chem.* 2008, *46*, 6677-6687.

[21] Eberhardt, M.; Mruk, R.; Zentel, R.; Théato, P. Synthesis of pentafluorophenyl(meth)acrylate polymers: New precursor polymers for the synthesis of multifunctional materials. *Europ. Polymer J.* 2005, *41*, 1569-1575.

[22] Barz, M.; Tarantola, M.; Fischer, K.; Schmidt, M.; Luxenhofer, R.; Janshoff, A.; Theato, P.; Zentel, R. From defined reactive diblock copolymers to functional HPMA-based self-assembled nanoaggregates. *Biomacromolecules* 2008, *9*, 3114-3118.

[23] Lammers, T.; Kühnlein, R.; Kissel, M.; Subr, V.; Etrych, T.; Pola, R.; Pechar, M.; Ulbrich, K.; Storm, G.; Huber, P.; Peschke, P. Effect of physicochemical modification on the biodistribution and tumor accumulation of HPMA copolymers. *J. Control. Release* 2005, *110*, 103-118.

[24] Häggström, S.; Bergh, A.; Damber, J. E. Vascular endothelial growth factor content in metastasizing and nonmetastasizing dunning prostatic adenocarcinoma. *Prostate* 2000, *45*, 42-50.

[25] Mukherjee, P.; Sotnikov, A. V.; Mangian, H. J.; Zhou, J. R.; Visek, W. J.; Clinton, S. K. Energy Intake and Prostate Tumor Growth, Angiogenesis, and Vascular Endothelial Growth Factor Expression. *J. Nat. Cancer Inst.* 1999, *91*, 512-523.

[26] Wu, H. P.; Feng, G. S.; Liang, H. M.; Zheng, C. S.; Li, X. Vascular endothelial growth factor antisense oligodeoxynucleotides with lipiodol in arterial embolization of liver cancer in rats. *World J. Gastroenterol.* 2004, *6*, 813-818.

[27] Halin, S.; Hammarsten, P.; Wikström, P.; Bergh, A. Androgen-insensitive prostate cancer cells transiently respond to castration treatment when growing in an androgen-dependent prostate environment. *Prostate* 2007, *67*, 370-377.

[28] Gossmann, A.; Okuhata, Y.; Shames, D. M.; Helbich, T. H.; Roberts, T. P. L.; Wendland, M. F.; Huber, S.; Brasch, R. C. Prostate cancer tumor grade differentiation with dynamic contrast-enhanced MR imaging in the rat: comparison of macromolecular and small-molecular contrast media - preliminary experience. *Radiology* 1999, *213*, 265-272.

[29] Su, M. Y.; Mühler, A.; Lao, X.; Nalcioglu, O. Tumor characterization with dynamic contrast-enhanced MRI using MR contrast agents of various molecular weights. *Magn. Reson. Med.* 1998, *39*, 259-269.

[30] Perrier, S.; Takolpuckdee, P.; Mars, C. A. Reversible addition-fragmentation chain transfer polymerization: End group modification for functionalized polymers and chain transfer agent recovery. *Macromolecules* 2005, *38*, 2033-2036.

[31] Rigler, R. *Fluorescence correlation spectroscopy;* Heidelberg, 2001.

[32] Bauman, A.; Piel, M.; Schirrmacher, R.; Rösch, F. Efficient alkali iodide promoted ^{18}F-fluoroethylations with 2-[^{18}F]fluoroethyl tosylate and 1-bromo-2-[^{18}F]fluoroethane. *Tetrahedron Lett.* 2003, *44*, 9165-9167.

[33] Workman, P.; Aboagye, E. O.; Balkwill, F.; Balmain, A.; Bruder, G.; Chaplin, D. J.; Double, J. A.; Everitt, J.; Farningham, D. A.; Glennie, M. J.; Kelland, L. R.; Robinson, V.; Stratford, I. J.; Tozer, G. M.; Watson, S.; Wedge, S. R.; Eccles, S. A. Guidelines for the welfare and use of animals in cancer research. *Br. J. Cancer* 2010, *102*, 1555-1577.

3.3.1 Supplementary results: Influence of hydrophobic LMA incorporation of HPMA-based random copolymers on the behavior *in vivo*

In order to effectively deliver pharmaceutics to the site of disease, an appropriate drug carrier system has to meet distinct requirements. Here, most important beneficial characteristics with respect to improved drug delivery are an enhanced blood circulation time of the polymeric carrier system, an increased retention in the tumor tissue, low non-target site accumulations as well as clearance of the carrier device after drug release – especially for non-biodegradable polymer systems such as HPMA. Regarding these criteria, most promising results were obtained in this study for a HPMA-*ran*-copolymer (further termed $P_{25\%}$*) exhibiting the highest ratio (25%) of randomly incorporated hydrophobic lauryl methacrylate (LMA) side chains within the evaluated HPMA-based polymer systems (cf. sections 3.2 and 3.3). In order to investigate to what extent the observed enhanced blood circulation time, the reduced liver and spleen uptake as well as highest tumor retention (regarding the Walker 256 mammary carcinoma model) of $P_{25\%}$* can be ascribed to the amount of hydrophobic LMA modification, further studies were accomplished to compare the *in vivo* behavior of HPMA-*ran*-copolymers exhibiting lower amounts of incorporated LMA with respect to $P_{25\%}$*. Hence, the polymer systems HPMA-*ran*-copolymer $P_{16\%}$* (LMA ratio of 16%) as well as HPMA-*ran*-copolymer $P_{20\%}$* (20% LMA) were radiolabeled by means of [^{18}F]FETos and evaluated *in vivo* in Walker 256 carcinoma bearing male SD rats. For the purpose of comparison, data obtained for a high M_w HPMA homopolymer $P_{0\%}$* – not exhibiting hydrophobic side chains – as well as HPMA-*ran*-copolymer $P_{25\%}$* are included in this investigation. All studied polymers exhibited molecular weights above the renal threshold [1] and aggregate formation could be observed for the HPMA random copolymers exhibiting laurylmethacrylate as hydrophobic segment using Fluorescence Correlation Spectroscopy [2]. Characteristics of the HPMA-based polymers compared in this study are listed in Table 1.

According to the data, molecular weights of the studied polymers were in the range of M_w = 55-77 kDa (table 1), which is higher than the renal threshold for HPMA-based polymers (~ 45 kDa [1]). Concerning the characteristics in aqueous media, the hydrodynamic radius (R_h) determined for the non-hydrophobically modified homopolymer $P_{0\%}$* was much smaller (R_h = 3.0 nm) – despite its highest molecular weight (M_w = 77 kDa) – compared to the values determined for the random copolymers (R_h = 31-40 nm).

Table 1: Analytical data of homopolymer $P_{0\%}$ as well as copolymers $P_{16\%}$*, $P_{20\%}$* and $P_{25\%}$**

nomenclature	polymer structure	monomer ratio [a]	M_n in g/mol	M_w in g/mol	PDI [b]	R_h in nm [c]
$P_{0\%}$*	homopolymer	100%	52 000	77 000	1.49	3.0
$P_{16\%}$*	random copolymer	84:16	40 000	70 000	1.73	30.9
$P_{20\%}$*	random copolymer	80:20	41 000	65 000	1.59	36.3
$P_{25\%}$*	random copolymer	75:25	39 000	55 000	1.41	39.9

[a] Monomer ratio determined by ^{1}H-NMR spectroscopy after polymeranaolgous reaction with 2-hydroxypropylamine. [b] Determined by GPC in THF as solvent. [c] Hydrodynamic radii determined by Fluorescence Correlation Spectroscopy (FCS).

Interestingly, hydrodynamic radii of the random copolymers were slighly increasing with higher incorporation ratio of hydrophobic laurylmethacrylate. Hence, with gaining hydrophilicity (from $P_{25\%}$* to $P_{16\%}$*) the formed superstructures become more compact in hydrophilic media, which was also observed by Ulbrich et al. [3], wo reported an increase in R_h with decreasing docedyl content for HPMA-based copolymers.

Fluorine-18 labeling by means of [^{18}F]FETos

Radiolabeling of the random copolymers $P_{16\%}$* as well as $P_{20\%}$* by means of [^{18}F]fluoroethylation was accomplished using analog labeling conditions as applied to HPMA homopolymer $P_{0\%}$* and HPMA-*ran*-copolymer $P_{25\%}$* (cf. section 3.2). The respective polymer characteristics as well as radiochemical yields determined using SEC are listed in table 1. Within the four HPMA-based polymer systems, a clear trend was observed for the radiolabeling by means of [^{18}F]FETos. Highest RCYs were obtained for the non-hydrophobically modified homopolymer $P_{0\%}$*, whereas radiolabeling efficiencies decreased with increasing hydrophobicity (i.e. amount of LMA) of the random copolymers. Among the considered polymer systems, the high M_w homopolymer $P_{0\%}$* has the smallest hydrodynamic diameter (R_h = 3.0 ± 0.2 nm) and exhibits a higher surface area-to-volume ratio compared to the HPMA-*ran*-LMA copolymer systems. With a larger surface in proportion of the volume and a decreased compactness due to the random coil formation of the homopolymer $P_{0\%}$*, a higher amount of tyramine groups in relation to the amphiphilic copolymers might be accessible on the surface for the nucleophilic labeling reaction with [^{18}F]FETos resulting in higher RCYs (Table 2). These results show the importance of using versatile labeling strategies in order to introduce the radiolabel into a variety of polymers differing in their physicochemical properties such as hydrophilic-lipophilic balance, surface properties, size and superstructure formation – all possibly influencing the availability of functional groups for attachment of a radiolabel for subsequent *in vivo* studies.

Table 2: Polymer characteristics and radiochemical yields obtained for HPMA-based polymers exhibiting different amounts of LMA

polymeric labeling precursor	LMA ratio in %	M_n in g/mol	M_w in g/mol	RCY in % [a]
HPMA homopolymer $P_{0\%}$*	0	52 000	77 000	24 ± 2
HPMA-*ran*-copolymer $P_{16\%}$*	16	40 000	70 000	16 ± 3
HPMA-*ran*-copolymer $P_{20\%}$*	20	41 000	65 000	12 ± 3
HPMA-*ran*-copolymer $P_{25\%}$* [a]	25	39 000	55 000	9 ± 2

[a] corrected RCYs determined *via* SEC (represented as mean±SEM).

Organ distribution studies

In order to study the influence, the amount of hydrophobic side chains of HPMA-*ran*-LMA copolymers exerts on the pharmacokinetics *in vivo*, biodistribution studies in tumor bearing male SD rats (247 ± 8 g, mean ± SEM, N=26) were carried out and the concentration of the ^{18}F-labeled HPMA-based carrier systems of different amphiphilicity was quantified at 2 h and 4 h post injection in various organs (lung, liver, heart, spleen, kidney) as well as in muscle, blood, small intestine and testis.

Figure 1 shows the uptake of the hydrophilic homopolymer ($P_{0\%}$*) and amphiphilic HPMA copolymers ($P_{16\%}$*, $P_{20\%}$* and $P_{25\%}$*) determined in the liver (Fig. 1A) as well as spleen (Fig. 1B). As clearly seen, the LMA modified copolymers show a distinct lower hepatic and splenic retention both at 2 h and 4 h p.i. Whereas the hydrophilic homopolymer $P_{0\%}$* shows comparatively high levels in these organs (liver: 5.87±0.90, spleen: 2.41±0.17 %ID/g tissue at 2 h), the amphiphilic copolymer with highest hydrophobic modification $P_{25\%}$* exhibited lowest concentrations amongst the studied polymers (liver: 1.30±0.24, spleen: 0.77±0.09 %ID/g tissue at 2 h). These findings indicate, that with increasing hydrophobicity in combination with an increase of size in physiological solution, retention in liver and spleen seems to be reduced. Notably, an incorporation rate of 25% LMA results in a more than fourfold decrease in liver uptake (at 2 h p.i.) and a more than threefold decrease in splenic retention compared to the non-LMA modified homopolymer $P_{0\%}$*. Comparison of the amphiphilic random copolymers exhibiting different amounts of hydrophobic segments, the copolymer $P_{20\%}$* – being in between of the range from 16% LMA to 25% LMA incorporation – shows the highest retention in the liver as well as in the spleen (liver: 3.72±0.39, spleen: 1.07±0.14 %ID/g tissue at 2 h). Furthermore, values determined for $P_{20\%}$* were increasing over the observed time span (4 h: liver: 5.61±0.11 %ID/g tissue, spleen: 1.54±0.08 %ID/g tissue) indicating continuing uptake into these organs of the mononuclear phagocyte system (MPS), which was less pronounced in the case of $P_{16\%}$* and in particular $P_{25\%}$*.

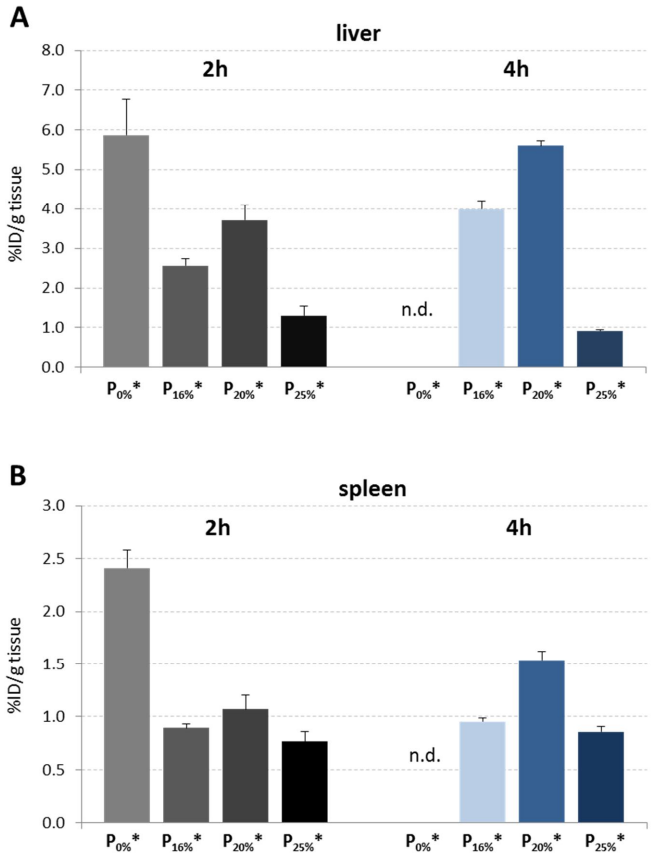

Figure 1: Concentration of HPMA homopolymer $P_{0\%}$ as well as HPMA-ran-LMA copolymers $P_{16\%}$*, $P_{20\%}$* and $P_{25\%}$* in liver (A) and spleen (B) at 2 h and 4 h p.i., expressed as %ID/g (mean±SEM).*

The capillary network of the liver exhibits a fenestrated epithelium, with allows – due to a size of 100-150 nm the fenestrations – almost unrestricted passage of plasma components to the perisinusoidal space, where the hepatocytes are situated. Nanoparticular systems up to about ~20 µm can be taken up by cells of the MPS (Kupffer cells) inside the sinusoid capillaries, which are responsible for phagocytic activity of the liver and represent 80 - 90% of the total body macrophage population [4]. Given that this size limit for phagocatic uptake is much higher compared to the hydrodynamic radii of the polymers (cf. Table 1), the comparable small size differences within the studied polymers (R_h = ~3-40 nm) should not alter the rate of uptake due to presumably unrestricted phagocytosis. However, highest splenic and hepatic uptake was observed for the smallest polymer $P_{0\%}$* (3 nm) whereas minor differences were observed for the random copolymers of lager sizes (30-40 nm). Besides a phagocytic uptake, which might lead to increased liver retention of non-digestible nanoparticles, carrier-mediated transport processes have been characterized in the liver mediating hepatobiliary excretion of cationic compounds such as drugs carrying tertiary or quarternary amines which are protonated in physiological pH [5]. Studies suggest that not only

lipophilicity is a prerequisite for efficient hepatobiliary excretion but rather the balance between hydrophilic and hydrophobic properties play a crucial role [5, 6]. On the basis of the observed results for liver uptake of HPMA-based polymers differing in their hydrophilicity, characteristics such as molecular weight, size, flexibility and/or superstructure formation seem to impair the liver uptake in a considerable way. Here, also endocytic mechanisms might play an important role for the uptake leading to intracellular sequestration especially of more hydrophilic non-biodegradable polymers in lysosomes not being excreted *via* the bile or redistributed into the blood.

Figure 2 compares the values for the distinct polymer systems found in the kidney. For all studied polymers, remaining activity of about 3 - 7 %ID/g was found in the kidney and values gradually increased from 2 h p.i. to 4 h p.i. indicating that all polymeric systems are subjected to renal clearance from the blood stream *via* glomerular filtration.

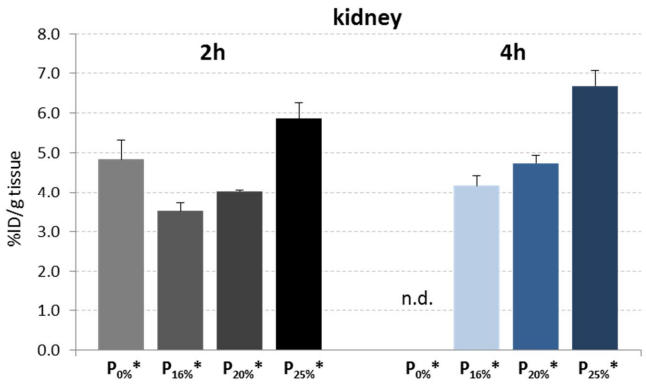

Figure 2: Concentration of HPMA homopolymer $P_{0\%}$ as well as HPMA-ran-LMA copolymers $P_{16\%}$*, $P_{20\%}$* and $P_{25\%}$* in the kidney 2 h and 4 h p.i., expressed as %ID/g (mean±SEM).*

When studying the effect of blood clearance and body distribution of HPMA-based copolymers of different molecular weights, Seymour et al. [7] revealed that HPMA-based polymers of molecular weights less than 45 kDa exhibited rapid urinary excretion and this factor being the major route of elimination from the bloodstream. Within the LMA modified polymer systems of the present study, a clear size dependency was observed. For the random copolymer of lowest molecular weight – $P_{25\%}$* (M_w = 55 kDa) – values obtained in the kidney were highest (5.86 ± 0.40 %ID/g at 2 h and 6.68 ± 0.39 %ID/g at 4 h, respectively), whereas gradually lower renal concentrations were found for the higher molecular weight copolymers $P_{16\%}$* (M_w = 70 kDa) and $P_{20\%}$* (M_w = 55 kDa). Notably, lowest values in the kidney were found for copolymer $P_{16\%}$* (3.51 ± 0.22 %ID/g at 2 h and 4.17 ± 0.25 %ID/g at 4 h, respectively). Hence, these findings stay in good correlation to the results reported by Seymour et al. showing faster blood clearance of polymers with lower molecular weights due to enhanced renal clearance. Furthermore, also molecules exhibiting molecular weights above the renal threshold can

be cleared from the bloodstream *via* glomerular filtration, if the molecular structure is flexible enough to pass the glomerular pores [4, 8]. This might explain the observed renal clearance of the hydrophilic homopolymer $P_{0\%}$*, exhibiting a molecular weight of 77 kDa, which is above the reported renal threshold of 45 kDa [7]. In this regard, renal clearance could be observed for all polymers in the present study, although the amphiphilic copolymers exhibit considerably higher hydrodynamic radii ('compound micelles ' with R_h > 30 nm, table 1) in comparison to the homopolymer (3 nm), which might be due to a high degree in flexibility of the studied polymers.

Concerning the retention of the different polymers in the blood compartment, the obtained results show an opposite trend compared to the accumulation pattern found for hepatic and splenic uptake. Figure 3 depicts the concentrations found in the blood (Fig. 3A) as well as the heart (Fig. 3B) of the hydrophilic homopolymer $P_{0\%}$* and the amphiphilic copolymers $P_{16\%}$*, $P_{20\%}$* and $P_{25\%}$*. Here, pronounced disparities between the different polymer architectures are clearly visible regarding the recovered dose remaining in the blood compartment. For both blood and heart, copolymer $P_{25\%}$* – exhibiting the highest amount of LMA side chains – displayed highest concentrations amongst all polymers. Even 4 h after administration, 2.57 ± 0.18 %ID/g of ^{18}F-$P_{25\%}$* was found in the blood, which translates into more than 40% of $P_{25\%}$* remaining in blood circulation, when assuming a volume of 16 mL for the whole blood volume of the rat [9]. In comparison to $P_{25\%}$*, amphiphilic copolymers of lower LMA incorporation ratio ($P_{16\%}$*, $P_{20\%}$*) show a decreased retention in the blood compartment at both time points investigated. Yet, for the amphiphilic copolymers no linear trend in blood retention as a function of LMA incorporation ratio could be observed (Fig. 3A) with $P_{20\%}$* (1.92 ± 0.07 %ID/g at 2 h and 0.77 ± 0.06 %ID/g at 4 h) showing lower blood concentrations compared to $P_{16\%}$* (2.70 ± 0.17 %ID/g at 2 h and 1.41 ± 0.09 %ID/g at 4 h). These results correlate to the findings observed for hepatic and splenic uptake (Fig. 1) and a higher uptake by organs of the MPS together with renal clearance leads to fast elimination from the blood stream (as seen for $P_{0\%}$*) – or inversely – lower clearance leading to prolonged blood circulation (in case of $P_{25\%}$*). Markedly, for the amphiphilic modified copolymers, at least a 10-fold increase in concentrations was found for the blood compartment in contrast to the hydrophilic homopolymer $P_{0\%}$* at 2 h p.i. (0.18 ± 0.03 %ID/g) underlining the importance of increased size due to aggregate formation ('compound micelles', cf. section 3.2) concerning the longevity of amphiphilic copolymers in the blood compartment.

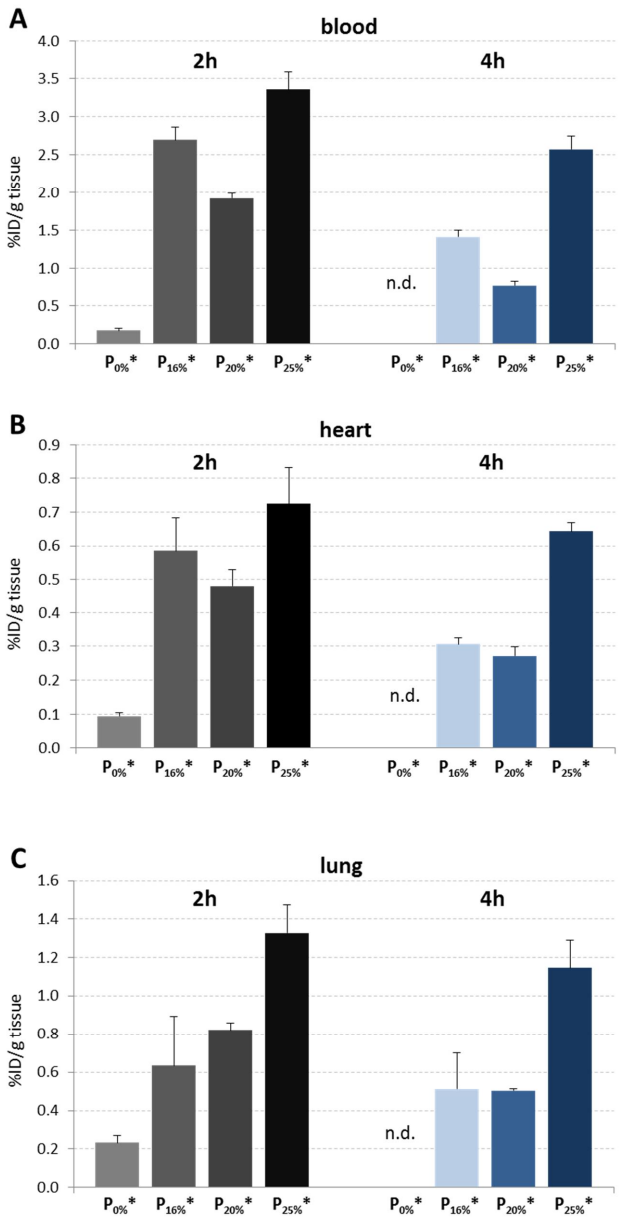

Figure 3: Concentration of HPMA homopolymer $P_{0\%}$ as well as HPMA-ran-LMA copolymers $P_{16\%}$*, $P_{20\%}$* and $P_{25\%}$* in blood (A) and heart (B) and lung (C) at 2 h and 4 h p.i., expressed as %ID/g (mean±SEM).*

Regarding the concentrations found in the heart (Fig. 3B) and lung (Fig. 3C), the uptake patterns in these highly perfused organs reflect the distribution of the copolymers observed in the blood. Throughout higher values were found for the random copolymers in heart and lung. Here, highest values were found for the copolymer $P_{25\%}$* with the highest ratio of hydrophobic modifications, whereas the homopolymer $P_{0\%}$* showed lowest concentrations in the heart and lung (cf. Table 3), which is in consistence with the findings in the blood. Concentrations found for all polymer systems in the small intestine, testes and the muscles were found to be rather constant among each other

and over time as well as comparably low. Entire biodistribution data obtained for the studied organs at 2 h and 4 h are listed in Table 3.

Table 3: Ex vivo organ distribution of HPMA-based polymers exhibiting different amounts of hydrophobic LMA sidechains at 2 h and 4 h post intravenous administration in Walker 256 tumor-bearing rats. Data is represented as %ID/g (mean±SEM)

2 h p.i.	polymer concentration [%ID/g tissue]			
organ	$P_{0\%}$* [a]	$P_{16\%}$* [b]	$P_{20\%}$* [b]	$P_{25\%}$* [c]
lung	0.27±0.04	0.64±0.26	0.82±0.04	1.33±0.13
liver	5.87±0.90	2.56±0.18	3.72±0.39	1.30±0.24
spleen	2.41±0.17	0.90±0.04	1.07±0.14	0.77±0.09
kidney	4.84±0.49	3.51±0.22	4.04±0.03	5.86±0.40
muscle	0.04±0.01	0.09±0.01	0.09±0.01	0.16±0.05
heart	0.09±0.01	0.59±0.10	0.48±0.05	0.72±0.11
blood	0.18±0.03	2.70±0.17	1.92±0.07	3.36±0.22
small intestine	0.36±0.06	0.42±0.06	0.32±0.02	0.46±0.11
testis	0.06±0.01	0.10±0.02	0.11±0.01	0.18±0.02
W 256 tumor	0.14±0.02[c]	0.56±0.10[c]	0.60±0.10[a]	0.63±0.02
4 h p.i.	polymer concentration [%ID/g tissue]			
organ	$P_{0\%}$*	$P_{16\%}$* [b]	$P_{20\%}$* [b]	$P_{25\%}$* [b]
lung	n.d.	0.51±0.19	0.50±0.01	1.01±0.21
liver	n.d.	3.99±0.22	5.61±0.11	0.92±0.04
spleen	n.d.	0.95±0.04	1.54±0.08	0.86±0.05
kidney	n.d.	4.17±0.25	4.74±0.20	6.68±0.39
muscle	n.d.	0.04±0.00	0.05±0.01	0.09±0.00
heart	n.d.	0.31±0.02	0.27±0.03	0.64±0.03
blood	n.d.	1.41±0.09	0.77±0.06	2.57±0.18
small intestine	n.d.	0.34±0.04	0.22±0.02	0.33±0.01
testis	n.d.	0.26±0.02	0.12±0.01	0.16±0.01
W 256 tumor	n.d.	0.49±0.03[c]	0.52±0.12[d]	0.64±0.03[c]

[a] N=5, [b] N=3; [c] N=6; [d] N=2.

The outlined findings illustrate the tremendous influence notably hydrophobic modifications of a carrier system do exert not only in terms of incorporating radioactive labeling probes for subsequent *in vivo* studies, but in particular on the *in vivo* accumulation and biodistribution pattern of the resulting architecturally different polymer based carrier systems.

Tumor accumulation

A major objective of this study was to investigate how amphiphilicity, i.e. the amount of LMA moieties, of HPMA-*ran*-LMA copolymers is influencing the tumor uptake *in vivo*. Based on the encouraging results concerning the uptake of the HPMA-*ran*-copolymer $P_{25\%}$* (P4* in section 3.2) in the Walker 256 mammary carcinoma of the rat, the tumor uptake of random copolymers exhibiting distinct lower amounts of LMA was determined as well and related to values found for the non-modified homopolymer $P_{0\%}$*. As illustrated in Figure 4, a considerably higher tumor uptake was achieved for all of the LMA copolymers at 2 h post injection compared to the homopolymer $P_{0\%}$*. Within the series of HPMA-*ran*-copolymers, highest tumor concentrations were observed for copolymer $P_{25\%}$* (0.63 ± 0.02 %ID/g at 2 h and 0.64 ± 0.03 %ID/g at 4 h). Yet it has to be noted, that the tumors volumes varied in the present study – notably in case of the random copolymers $P_{16\%}$* and $P_{20\%}$*at 2 h (tumor volumes: 1.17±0.95 mL, mean±SD, N=11) possibly leading to deviations in tumor uptake which accounts for the higher SEM values obtained in case of $P_{16\%}$* and $P_{20\%}$*. However, compared to homopolymer $P_{0\%}$* (0.14 ± 0.02 %ID/g at 2 h), the incorporation of 25% LMA moieties – in combination with an increase in size due to superstructure formation – translated into a more than fourfold higher in tumor retention at 2 h after administration of the radiolabeled copolymer $P_{25\%}$*.

In case of $P_{25\%}$*, the considerably higher uptake in the Walker 256 carcinoma could be ascribed to a markedly higher cellular uptake of the random copolymer compared to the homopolymeric system (cf. section 3.2). These *in vitro* studies not only revealed a significant high dependency on the cellular uptake concerning the respective tumor cell line (AT1 prostate carcinoma cells *vs*. Walker 256 mammary carcinoma cells) but also on the polymer architecture (HPMA homopolymers, HPMA-LMA random copolymers and HPMA-LMA block copolymers). Here, among the investigated polymers, $P_{25\%}$* showed higher cellular tumor uptake in both studied tumor cell lines, but in particular, uptake of $P_{25\%}$* into Walker 256 cells compared to AT1 cells was significantly higher *in vitro* as well as *in vivo*.

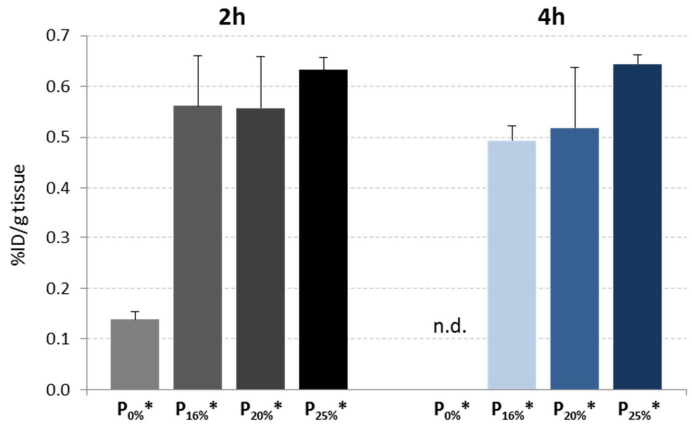

Figure 4: Uptake of HPMA homopolymer $P_{0\%}$ as well as HPMA-ran-LMA copolymers $P_{16\%}$*, $P_{20\%}$* and $P_{25\%}$* in Walker 256 mammary carcinoma at 2 h and 4 h p.i., expressed as %ID/g (mean±SEM).*

Studies by Barz et al. [10] demonstrated the uptake of HPMA-*ran*-LMA copolymers exhibiting 19% and 21% of LMA segments into MDR breast adenocarcinoma cells, although these copolymers were of lower molecular weight (M_w = 20.2 kDa and 39.3 kDa, respectively) compared to $P_{25\%}$*. The higher uptake of the random copolymers at low concentrations into the MDR cells was ascribed to the polymer architecture, consisting of aggregates which display small hydrophilic loops containing some hydrophobic lauryl groups on the outer corona due to the statistic incorporation of LMA. Being more accessible on the outer shell, these LMA moieties might result in a higher cell-membrane affinity explaining the higher uptake observed for these polymer systems [10]. In a study reported by Liu et al. [11], the observed uptake of a HPMA copolymer exhibiting 15.5 wt.% of a hydrophobic tetrapeptide into C4-2 prostate cancer cells revealed that in comparison to polymers modified with charged groups, the hydrophobic group though did not play a dominant role in terms of cellular uptake. Yet, the authors did find that with decreasing molecular weight, the hydrophobically modified polymer was taken up to a higher extent by the cells [11]. Within the range of $P_{16\%}$* to $P_{25\%}$*, the molecular weight of the copolymers decreases from 70 kDa ($P_{16\%}$*) to 55 kDa ($P_{25\%}$*) whilst the tumor uptake is slightly – however not significantly – increasing. Therefore, in accordance to the results of Liu et al., the present study slightly denotes a tendency towards higher tumor uptake with decreasing molecular weight (and hence less dense polymeric superstructures, cf. Table 1) likely due to increased cellular uptake. However, to substantiate these findings, further studies on cellular uptake as well as on tumor uptake *in vivo* need to be accomplished.

Table 3 shows calculated ratios of non-targeted to tumor tissue obtained for the studied HPMA homopolymer ($P_{0\%}$*) as well as *ran*-LMA copolymers ($P_{16\%}$*, $P_{20\%}$*, $P_{25\%}$*). Values < 1 – indicating reduced polymer uptake in healthy tissue – were consistently obtained for all polymers regarding

muscle, small intestine and testis. Furthermore, comparably low ratios for all polymers were found for the uptake in heart (0.6 - 1.1) as well as lung (1.1 - 2.1) signifying concentrations in these tissue being in the range of tumor uptake. Notably, significantly higher ratios with respect to liver, spleen and kidney were observed for the homopolymer $P_{0\%}$* (at 2 h p.i.) in contrast to values obtained for all of the amphiphilic copolymers. Here, the high ratios of $P_{0\%}$* concerning liver and spleen (41.9 and 17.2, respectively) reflect the increased rate of uptake by the organs of the MPS observed for the homopolymer $P_{0\%}$*, being rather unfavorable regarding therapeutic applications for effective cancer treatment.

Table 4: Ratios of non-targeted to tumor tissue calculated for HPMA homopolymer $P_{0\%}$ as well as HPMA-ran-LMA copolymers $P_{16\%}$*, $P_{20\%}$* and $P_{25\%}$* at 2 h and 4 h p.i. (Walker 256 mammary carcinoma)*

2 h p.i.	$P_{0\%}$*	$P_{16\%}$*	$P_{20\%}$*	$P_{25\%}$*
lung / tumor	1.9	1.1	1.4	2.1
liver / tumor	41.9	4.6	6.2	2.1
spleen / tumor	17.2	1.6	1.8	1.2
kidney / tumor	34.6	6.3	6.7	9.3
muscle / tumor	0.3	0.2	0.2	0.3
heart / tumor	0.6	1.1	0.8	1.1
blood / tumor	1.3	4.8	3.2	5.3
small intestine / tumor	2.6	0.8	0.5	0.7
testis / tumor	0.4	0.2	0.2	0.3
4 h p.i.	$P_{0\%}$*	$P_{16\%}$*	$P_{20\%}$*	$P_{25\%}$*
lung / tumor	-	1.0	1.0	1.6
liver / tumor	-	8.1	10.8	1.4
spleen / tumor	-	1.9	3.0	1.3
kidney / tumor	-	8.5	9.1	10.4
muscle / tumor	-	0.1	0.1	0.1
heart / tumor	-	0.6	0.5	1.0
blood / tumor	-	2.9	1.5	4.0
small intestine / tumor	-	0.7	0.4	0.5
testis / tumor	-	0.5	0.2	0.3

With respect to ratios obtained for the homopolymeric architecture, the incorporation of LMA segments apparently leads to improved values for target to non-target tissues. In particular, highest ratios amongst the studied polymers concerning blood/tumor were obtained for the amphiphilic copolymer $P_{25\%}$* exhibiting the highest amount of incorporated LMA segments (blood/tumor: 5.3 at

2 h p.i. and 4.0 at 4 h p.i.). Interestingly, the random hydrophobic modification also seems to result in a markedly decrease in the accumulation of the HPMA-based copolymers in the spleen (Fig. 1B; $P_{0\%}$*: 2.41±0.17 %ID/g *vs*. $P_{25\%}$*: 0.77±0.09 %ID/g at 2 h p.i.). High accumulations in the spleen are often observed for nanoparticles due to a high unspecific uptake by the cells of the mononuclear phagocyte system (MPS) and modifications of the surface chemistry such as PEGylation were shown to effectively minimize MPS related uptake of nanoparticles reflected by lower spleen and liver accumulation of drug delivery systems modified by means of PEG [8, 9].

MicroPET imaging in Walker 256 carcinoma bearing rats

Besides quantitative *ex vivo* biodistribution studies, µPET imaging in Walker 256 bearing rats was accomplished for the random copolymers $P_{16\%}$*, $P_{20\%}$* as well as $P_{25\%}$*. Unfortunately, no small animal PET study of the homopolymer $P_{0\%}$* has been performed using the Walker 256 mammary carcinoma model of the rat. Figure 4 depicts coronar summed µPET images 120-135 min after administration acquired with the ^{18}F-labeled HPMA-*ran*-LMA copolymers. In accordance to the findings in the biodistribution studies (Fig. 1A,B and Table 3), higher liver accumulation is seen for copolymers $P_{16\%}$* and $P_{20\%}$* of lower LMA ratio compared to $P_{25\%}$*. Furthermore, the higher retention of the amphiphilic copolymers in the blood stream is displayed (Fig. 4: aorta (A)), notably in the case of HPMA-*ran*-copolymer $P_{25\%}$*, also exhibiting highest accumulation in the blood as determined *via ex vivo* biodistribution (Fig. 3A). Furthermore, the comparably high concentrations of $P_{25\%}$* found in the lung (Fig. 3C) becomes apparent in the respective µPET image of $P_{25\%}$* underlining the higher retention of this copolymer in the blood considering the lung as being a highly blood supplied organ. In good agreement with the organ distribution findings, renal clearance could be observed for all of the HPMA-*ran*-LMA copolymers, indicated by the appearance of the kidney as well as the bladder(Fig.4: kidney (K) and bladder (B)).

Dynamic µPET imaging of the Walker 256 carcinoma tumors – implanted at the hind food dorsum of the rats – enabled to visualize tumor accumulation of the polymers. Figure 5 shows coronal as well as sagittal µPET summed images of the tumor sections 60-120 min after i.v. administration of the random copolymers $P_{16\%}$*, $P_{20\%}$* and $P_{25\%}$*. The images clearly show tumor uptake for all of the amphiphilic copolymers. However, images of the tumors obtained for $P_{16\%}$* and $P_{20\%}$* reveal a more inhomogeneous distribution of the labeled copolymers within these tumors compared to the tumor section images of $P_{25\%}$*. Due to the higher variation of tumor volumes in the studies performed with $P_{16\%}$* and $P_{20\%}$*, further investigations are needed taking the tumor size as parameter into account, notably considering the findings of Harrington *et al.* who found higher uptakes for ^{111}In-labeled PEGylated liposomes into tumors of smaller size [12, 13].

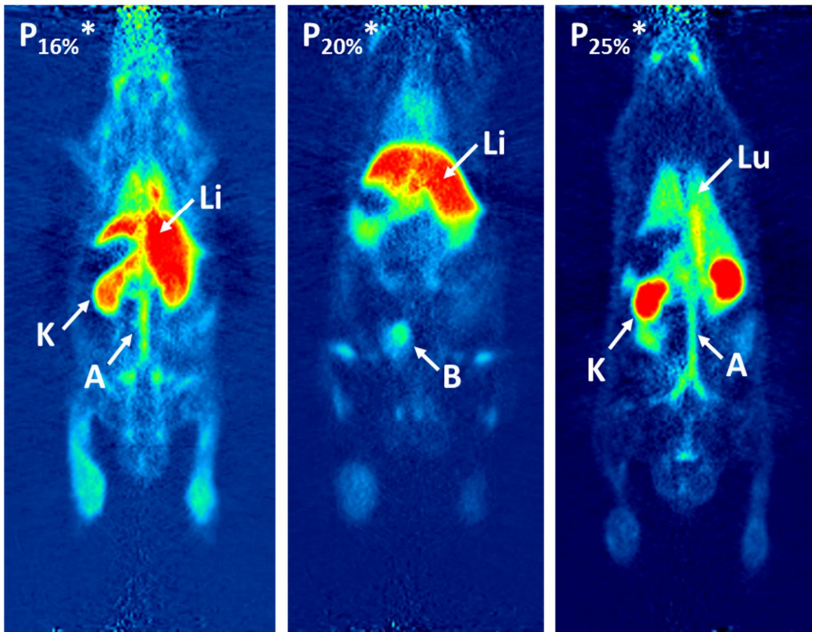

Figure 4: Coronar µPET summed images of HPMA-ran-LMA copolymers $P_{16\%}$, $P_{20\%}$* and $P_{25\%}$* 120-135 min after i.v. injection showing polymer concentration in blood (aorta (A)), liver (Li), kidneys (K) bladder (B) as well as the lung (Lu).*

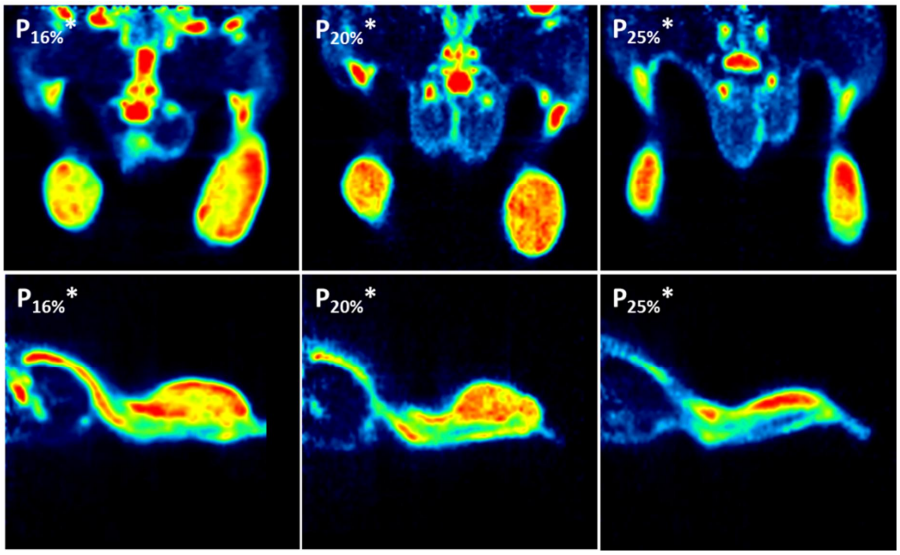

Figure 5: Examples of coronal (top) as well as sagittal (bottom) µPET image sections of Walker 256 tumors 60-120 min after i.v. administration of ^{18}F-labeled random copolymers $P_{16\%}$, $P_{20\%}$* and $P_{25\%}$*.*

The present study revealed that hydrophobic modification by means of a random incorporation of LMA side chains strongly affects the *in vivo* fate of HPMA-based polymers. Compared to the HPMA homopolymer ($P_{0\%}$*), the studied HPMA-*ran*-LMA copolymers showed improved pharmacokinetics

with respect to enhanced blood circulation, lower hepatic and splenic uptake as well as increased tumor accumulation (Walker 256 carcinoma). Although this pharmacokinetic shift is apparent for all of the hydrophobically modified copolymers, the HPMA-*ran*-copolymer $P_{25\%}$* – exhibiting the highest ratio of LMA side chains – showed the most promising *in vivo* performance among the investigated polymers, notably lowest non-target to tumor tissue ratios (Table 4) in combination with highest blood concentration and tumor uptake.

References

[1] Seymour, LW; Miyamoto, Y; Maeda, H; Brereton, M; Strohalm, J; Ulbrich, K; Duncan, R. Influence of molecular weight on passive tumour accumulation of a soluble macromolecular drug carrier. *Eur J Cancer* 1995; 31 (5); 766-770.

[2] Allmeroth, M; Moderegger, D; Biesalski, B; Koynov, K; Rösch, F; Thews, O; Zentel, R. Modifying the Body Distribution of HPMA-Based Copolymers by Molecular Weight and Aggregate Formation. *Biomacromolecules* 2011; 12 (7); 2841-2849.

[3] Chytil, P; Etrych, T; Koňák, Č; Sirova, M; Mrkvan, T; Bouček, J; Říhová, B; Ulbrich, K. New HPMA copolymer-based drug carriers with covalently bound hydrophobic substituents for solid tumour targeting. *J Control Release* 2008; 127 (2); 121-130.

[4] Bertrand, N; Leroux, J. The journey of a drug-carrier in the body: An anatomo-physiological perspective. *J Control Release* 2012; 161 (2); 152-163.

[5] Meijer, DKF; Mol, WEM; Mueller, M; Kurz, G. Carrier-mediated transport in the hepatic distribution and elimination of drugs, with special reference to the category of organic cations. *J Pharmacokinet Biopharm* 1990; 18 (1); 35-70.

[6] Meijer, DK. Current concepts on hepatic transport of drugs. *J Hepatol* 1987; 4 (2); 259-268.

[7] Seymour, LW; Kopeček, J. Effect of molecular weight of *N*-(2-hydroxypropyl)methacrylamide copolymers on body distribution and rate of excretion after subcutaneous, intraperitoneal, and intravenous administration to rats. *J Biomed Mater Res* 1987; 21 (11); 1341-1358.

[8] Rennke, HG; Venkatachalam, MA. Glomerular permeability of macromolecules. Effect of molecular configuration on the fractional clearance of uncharged dextran and neutral horseradish peroxidase in the rat. *J. Clin. Invest* 1979; 63 (4); 713-717.

[9] Lee, HB; Blaufox, MD. Blood volume in the rat. *J Nucl Med* 1985; 26 (1); 72-76.

[10] Barz, M; Luxenhofer, R; Zentel, R; Kabanov, AV. The uptake of *N*-(2-hydroxypropyl)-methacrylamide based homo, random and block copolymers by human multi-drug resistant breast adenocarcinoma cells. *Biomaterials* 2009; 30 (29); 5682-5690.

[11] Liu, J; Bauer, H; Callahan, J; Kopečková, P; Pan, H; Kopeček, J. Endocytic uptake of a large array of HPMA copolymers: Elucidation into the dependence on the physicochemical characteristics. *J Control Release* 2010; 143 (1); 71-79.

[12] Harrington, KJ; Mohammadtaghi, S; Uster, PS; Glass, D; Peters, AM; Vile, RG; Stewart, JS. Effective targeting of solid tumors in patients with locally advanced cancers by radiolabeled pegylated liposomes. *Clin Cancer Res* 2001; 7 (2); 243-254.

[13] Harrington, KJ; Rowlinson-Busza, G; Syrigos, KN; Abra, RM; Uster, PS; Peters, AM; Stewart, JS. Influence of tumour size on uptake of(111)In-DTPA-labelled pegylated liposomes in a human tumour xenograft model. *Br. J. Cancer* 2000; 83 (5); 684-688.

3.4 Comparative study on short and long-term distribution of HPMA-*ran*-LMA copolymers *in vivo* by means of ^{18}F and ^{131}I-labeling revealing tumor retention over time

Comparative study on short and long-term distribution of HPMA-*ran*-LMA copolymers *in vivo* by means of ^{18}F and ^{131}I-labeling revealing tumor retention over time

Dorothea Moderegger[Φ,1], Mareli Allmeroth[Φ,2], Rudolf Zentel[2], Oliver Thews[3] and Frank Rösch[*,1]

[Φ] both authors contributed equally

[1]Institute of Nuclear Chemistry, Johannes Gutenberg University, Fritz-Strassmann-Weg 2, 55128 Mainz, Germany

[2]Institute of Organic Chemistry, Johannes Gutenberg University, Duesbergweg 10-14, 55099 Mainz, Germany

[3]Institute of Physiology, University Halle, Magdeburger Str. 6, 06097 Halle (Saale), Germany

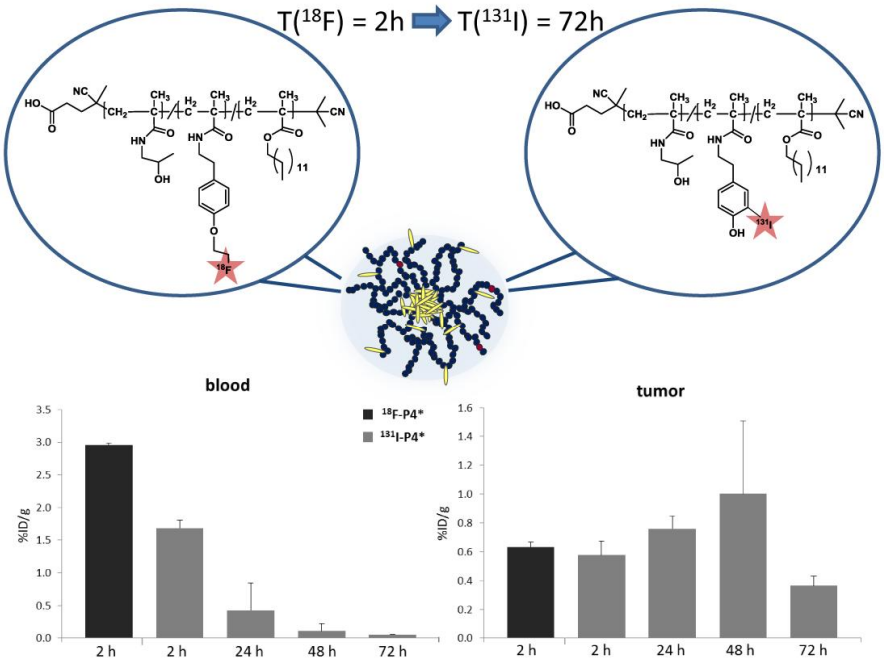

Abstract

With the discovery of the enhanced permeability and retention effect of macromolecules in tumor tissue an increasing need for suitable pre-clinical monitoring of potential nanocarrier systems has emerged. In this regard, both short as well as long term *in vivo* tracking is crucial for understanding structure-property relationships of polymer carrier systems and their resulting pharmacokinetic profile. Based on former studies revealing favorable *in vivo* characteristics for ^{18}F-labeled HPMA-based random copolymers – including prolonged plasma half-life as well as enhanced tumor accumulation over a time span of 4 hours – the presented work focuses on their long term investigation in the living organism. In this respect, four different HPMA-based polymers (homopolymers as well as random copolymers with lauryl methacrylate as hydrophobic segment) were synthesized and subsequent radioactive labeling was accomplished *via* the longer-lived radioisotope iodine-131. *In vivo* results, concentrating on the pharmacokinetics of a high molecular weight HPMA-*ran*-LMA copolymer, were obtained by means of biodistribution studies in the Walker 256 mammary carcinoma model over a time-span of three days. Special emphasis was laid on the time-dependant correlation between blood circulation properties and corresponding tumor accumulation, particularly regarding the EPR effect. Studies revealed that despite a polymer clearance from the blood within 72 hours, there was still an increase in tumor uptake observed over time. This characteristic strongly underlines the “proof-of-principle”, namely the EPR effect, and hence demonstrates the potential of the investigated polymer in terms of efficient anticancer therapy. Furthermore, the findings illustrate the need to combine information of different labeling approaches and *in vivo* evaluation techniques to generate an overall pharmacokinetic picture of potential nanocarriers in the pre-clinical setting.

Keywords: EPR, HPMA, Imaging, Iodine-131, RAFT, Walker 256 mammary carcinoma

Introduction

Polymeric nanocarrier systems are of emerging interest regarding their potential for anticancer therapy. In contrast to the low molecular weight free drug – suffering from short plasma-half lives, high clearance rates and undesirable side effects in healthy tissue – macromolecular based drug delivery vehicles can significantly improve the pharmacokinetic profile of chemotherapeutic agents. Prolonged blood-circulation times, enhanced tumor accumulation due to the EPR effect [1] as well as a decrease of toxic side effects are only some advantages to be named. The EPR effect has been

proposed to lead to a further increase in intratumoral drug concentration over a longer period of time even with a decrease in plasma level.

Regarding clinical implementation, a polymeric drug carrier has to be non-toxic, non-immunogenic, biodegradable or at least biocompatible with appropriate molecular weight to ensure body excretion. Furthermore, narrow molecular weight distributions are needed to guarantee homogeneity of the final conjugates [2, 3]. Among various clinically investigated polymer structures, so far six HPMA anticancer conjugates entered clinical trials – demonstrating the versatility of this multifunctional synthetic polymer in tumor treatment [4-7].

In terms of their therapeutic application area, it is essential that the developed polymer systems are as well-defined as possible [8]. The introduction of controlled radical polymerization techniques like ATRP (Atom Transfer Radical Polymerization) [9] or RAFT (Reversible Addition-Fragmentation Chain Transfer) [10, 11] thus facilitated the access to narrowly-distributed and well-defined polymer structures. Notably, the combination of RAFT with reactive ester chemistry [12-14] is demonstrating an elegant route to diverse polymer architectures [15-17].

Besides the aforementioned high demands on the macromolecular carrier system, especially adequate pre-clinical screening tools are crucial in order to provide an appropriate therapy for the individual patient [18, 19]. In this regard, non-invasive molecular imaging techniques such as Positron Emission Tomography (PET) or Single Photon Emission Computed Tomography (SPECT) constitute helpful diagnostic tools enabling detailed information on the body disposition as well as tumor accumulation of the polymer-drug conjugate in the living organism. In dependency of the incorporated radionuclide, and its particular half-life, the diagnostic time frame can be adjusted from early phase accumulation – by means of shorter-lived isotopes – to long-term imaging over weeks or months.

Former studies in our group already illustrated the successful radiolabeling of various HPMA-based polymers by means of the positron emitters As-72/74 [20] and F-18 [21] thereby establishing µPET imaging for time-efficient screening of potential drug delivery systems. Further investigations on ^{18}F-labeled HPMA-based polymer systems revealed the major impact of molecular weight and aggregate formation on the body distribution in the living animal [22]. The examined polymer structures included homopolymers as well as random copolymers composed of a hydrophilic HPMA and a hydrophobic lauryl methacrylate (LMA) segment. In direct comparison, the high molecular weight random copolymer (M_w = 55 kDa; LMA ratio 25%) exhibited most favorable *in vivo* characteristics – combining prolonged blood circulation times with highest tumor uptake as well as

low liver accumulation and renal excretion properties. However, this specific pharmacokinetic profile was investigated by means of fluorine-18 ($t_{1/2}$ = 110 min) as radioactive marker, enabling a diagnostic time frame of only up to 4 hours. But particularly the observation of enhanced plasma half-life of the random copolymer (after 4 h p.i. ~ 40% of the polymer still remained in the blood pool) was asking for a selective monitoring of this polymer architecture in the long term. In this regard, the enhanced permeability and retention of macromolecules in tumor tissue has to be addressed, not just being a temporary phenomenon of passive targeting to the tumor site but notably allowing a sustained release and accumulation of drugs over weeks and longer [23, 24]. To proof the "EPR effect" for the herein presented HPMA-*ran*-LMA copolymer system, we decided on its radioactive labeling by incorporating the longer-lived γ-emitter iodine-131 ($t_{1/2}$ = 8.1 days). Radioisotopes of iodine are highly suitable for studying the long-term pharmacokinetics of HPMA-based polymer architectures, attributed to their longer half-lives, facile access to radiolabeling procedures as well as direct availability [4, 7, 19, 25]. In addition, the convenience of incorporating iodine-131 at tyramine groups likewise used for ^{18}F-labeling *via* [^{18}F]fluoroethylation enables the direct comparison of short term pharmacokinetics of the applied polymer system (^{131}I- *vs.* O-[^{18}F]fluoroethyl-tyramine labeling). Furthermore, long term distribution of the identical polymer batch by means of I-131 can be accomplished, too.

The aim of the present study focused on radiolabeling of HPMA-based polymers *via* iodine-131 and the consequent long term monitoring of an HPMA-*ran*-LMA copolymer *in vivo*, particularly regarding its blood residence time as well as tumor accumulation / retention properties ("EPR effect") over a time-window of three days. Due to an additional time point in the short-range (2 h), a direct correlation to former studies with ^{18}F-labeled HPMA-based random copolymer can be drawn [22].

Experimental Section

Materials

All solvents were of analytical grade, as obtained by Sigma Aldrich and Acros Organics. Dioxane was distilled over a sodium/potassium composition. Lauryl methacrylate was distilled to remove the stabilizer and stored at -18 °C. 2,2'-Azo-bis-(isobutyronitrile) (AIBN) was recrystallized from diethyl ether and stored at -18 °C as well. Iodine-131 was obtained from GE Healthcare (Braunschweig, Germany).

Polymer synthesis

Synthesis of 4-cyano-4-((thiobenzoyl)sulfanyl)pentanoic acid (CTP)

4-cyano-4-((thio- benzoyl)sulfanyl)pentanoic acid was used as chain transfer agent (CTA) and synthesized according to the literature [11].

Synthesis of pentafluorophenyl methacrylate (PFPMA)

Pentafluorophenyl methacrylate was prepared according to reference [26].

Synthesis of random copolymer

RAFT polymerization of PFPMA with lauryl methacrylate by help of CTP was performed in a schlenk tube [13, 15, 22]. As an example, 4 g of PFPMA dissolved in 5 mL dioxane, lauryl methacrylate, AIBN and CTP were mixed. The molar ratio of CTP/AIBN was chosen to be 8:1. After three freeze-vacuum-thaw cycles, the mixture was immersed in an oil bath at 65 °C and stirred overnight. Afterwards, poly(PFPMA)-*ran*-poly(LMA) was precipitated three times in hexane, centrifuged and dried under vacuum at 40 °C overnight. A slightly pink powder was obtained. Yield: 54%. ^{1}H-NMR (300 MHz, $CDCl_3$) δ/ ppm: 0.84 (br t), 1.20-1.75 (br), 2.00-2.75 (br s). ^{19}F-NMR (400 MHz, $CDCl_3$) δ/ ppm: -162.01 (br), -156.95 (br), -152 to -150 (br).

Removal of dithioester endgroups

The dithiobenzoate endgroup was removed using the protocol reported by Perrier et al. 2005 [27]. Therefore a 25-fold molar excess of AIBN was added to the polymer dissolved in dioxane. After four hours of heating the solution in an oil bath at 70 °C, the polymer was precipitated twice in hexane and collected by centrifugation. The polymer was dried under vacuum over night, a colorless powder was obtained. Yield: 75 %. Removal of the dithioester endgroup could be proven by UV-Vis spectroscopy.

Polymer analogous reaction of random copolymer

For radioactive labeling of random copolymers the protocol was applied as follows. 100 mg of poly(PFPMA)-*ran*-poly(LMA) copolymer was dissolved in 2 mL of absolute dioxane. As example, 5 mg of tyramine and 10 mg of triethylamine were diluted in a DMSO/dioxane mixture and added to the vessel. After stirring for four hours at 35 °C, 30 mg of 2-hydroxypropylamine as well as 40 mg of triethylamine were added and the solution stirred over night. For final removal of reactive ester side groups further 30 mg of 2-hydroxypropylamine were added the next morning. The solution was

precipitated two times in diethyl ether, centrifuged and finally dissolved in a DMSO/water solution for dialysis. After lyophilization a white powder could be obtained. Yield: 51 %. ^{1}H-NMR (400 MHz, d. DMSO) δ/ ppm: 0.70-0.90 (br), 0.90-1.40 (br), 1.40-1.90 (br), 2.75-3.10 (br), 3.50-3.80 (br), 4.50-4.75 (br), 6.60-6.75 (br) and 6.85-7.00 (br).

Radiolabeling

Radiolabeling procedures applied to study ^{131}I-radiolabeling of different HPMA-based polymers are provided as supplementary information. Radioiodination for *in vivo* experiments was performed using the following optimized labeling conditions applying the CAT procedure yielding 49±3 % of ^{131}I-labeled HPMA-*ran*-LMA copolymer P4*: 1 mg P4* in 100 µL of DMSO, 200 µg CAT, 200 µL PBS and 96±16 MBq of [^{131}I]iodide solution.

Polymer Characterization (including experimental setups and FCS measurements) as well as animal experiments are provided as supporting information.

Results and Discussion

To investigate the long-term *in vivo* distribution of HPMA-based polymer structures – with special focus on tumor accumulation characteristics and the EPR (Enhanced Permeability and Retention) effect – two HPMA-based polymer architectures (homopolymers and random copolymers with laurylmethacrylate as hydrophobic group) were synthesized by combining reactive ester chemistry with the RAFT polymerization technique [10, 26, 28]. This approach enables the synthesis of well-defined and narrowly distributed polymer systems and polymeranalogous reaction with primary amines facilitates the incorporation of imaging moieties such as fluorescent dyes or radiolabels. Former studies in our group already demonstrated the tremendous impact of polymer structure (molecular weight, amphiphilicity and superstructure formation) on cellular uptake [15] and in particular on the *in vivo* fate [22]. Since closer investigations revealed favorable *in vivo* characteristics – including prolonged blood-circulation time, low hepatic uptake as well as renal clearance – for a high molecular weight HPMA-*ran*-LMA copolymer over a time span of 4 hours by means of the positron emitter fluorine-18 ($t_{1/2}$=110 min) [22], we decided to selectively examine its long term fate using the γ-emitter iodine-131 ($t_{1/2}$ = 8 d). For a detailed comparison of the radiolabeling process, HPMA homopolymers (P1* and P2*) as well as random copolymers (P3* and P4*) – varying in molecular weight – were investigated. Polymer synthesis and radioactive labeling procedure are depicted in figure 1; polymer characterization in table 1.

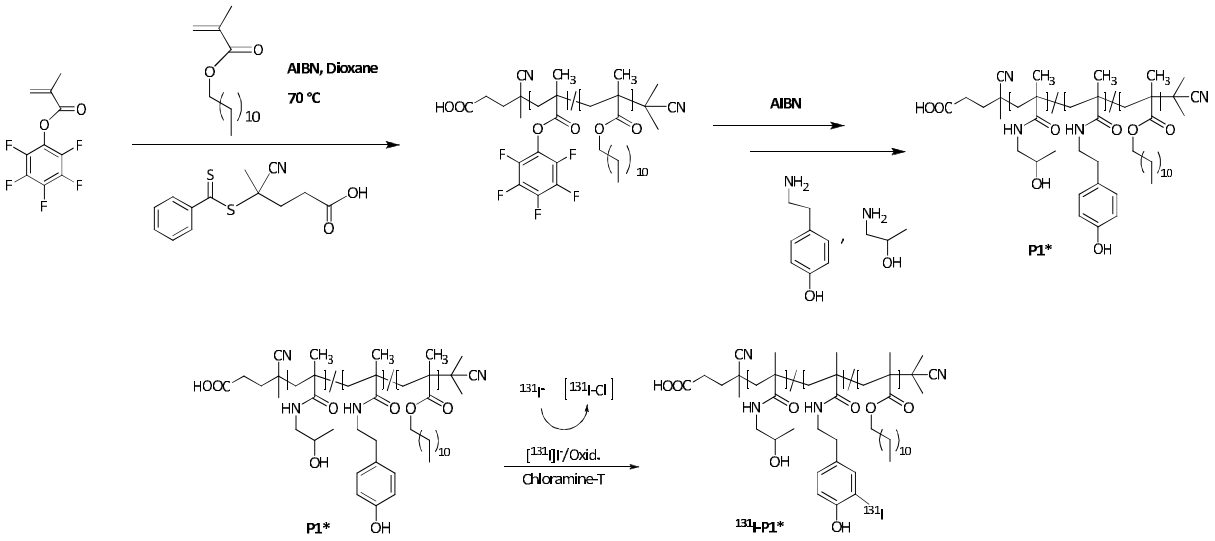

Figure 1: Polymer synthesis via reactive ester approach with subsequent polymeranalogous reaction as well as radioactive labeling procedure by means of Iodine-131.

Table 1: Analytical data of reactive ester precursor polymers (P1-R - P4*-R) as well as final polymeric structures (P1* - P4*)*

Notation	Polymeric structure	Monomer ratio	M_n [g/mol]	M_w [g/mol]	PDI [b)]	R_h [e)] [nm]
P1*-R	Homopolymer	100 %[a)]	18000[b)]	23000[b)]	1.29	n.d.
P2*-R	Homopolymer	100 %[a)]	87000[b)]	130000[b)]	1.49	n.d.
P3*-R	Random copolymer	80:20[a)]	17000[b)]	21000[b)]	1.26	n.d.
P4*-R	Random copolymer	80:20[a)]	57000[b)]	80000[b)]	1.41	n.d.
P1*	Homopolymer	100 %[c)]	9000[d)]	12000[d)]	1.29	1.1
P2*	Homopolymer	1000 %[c)]	52000[d)]	77000[d)]	1.49	3.0
P3*	Random copolymer	82:18[c)]	11000[d)]	14000[d)]	1.26	33.4
P4*	Random copolymer	75:25[c)]	39000[d)]	55000[d)]	1.41	39.9

[a)] Calculated monomer ratio; [b)] Determination by GPC in THF as solvent; [c)] Monomer ratio determined by ^{1}H-NMR spectroscopy after polymeranalogous reaction with 2-hydroxy-propylamine; [d)] Calculated from the molecular weights of the reactive ester polymer P1*-R as determined by GPC in THF as solvent; [e)] Hydrodynamic radii determined by Fluorescence Correlation spectroscopy (FCS)

Former ^{18}F-labeling of HPMA-based polymer systems has been accomplished *via* [^{18}F]fluoroethylation of tyramine groups [21, 22] (~2-4 % incorporation as determined by ^{1}H-NMR) which provide highly activated phenolic rings. Hence, I-131 incorporation can be accomplished by means of electrophilic aromatic substitution; enabling ^{131}I-labeling of the same HPMA-based polymers without prior derivatization of the polymer structure. This approach allows for a direct correlation of structure-property relationships between the ^{18}F- and the ^{131}I-labeled HPMA-*ran*-LMA copolymer *in vivo*.

In order to promote incorporation of ^{131}I *via* direct electrophilic aromatic substitution, reaction conditions were studied to optimize the labeling technique for different HPMA-based architectures. Since direct electrophilic radioiodination requires the generation of an electrophilic radioiodine species by oxidation from [^{131}I]NaI, two different *in situ* oxidants were tested, being commonly applied for radioiodination of proteins: Chloramine-T (N-chloro-4-methylbenzenesulfonamide sodium salt, CAT) and Iodogen™ (1,3,4,6-Tetrachloro-3a,6a-diphenylglycoluril) [29, 30]. Radioactive labeling of polymers was performed in phosphate buffered saline (pH = 7.2) and succeeded within 4 minutes reaction time. Investigations on type and amount of oxidant revealed highest radiochemical yields (RCYs) for CAT regarding I-131 labeling of HPMA homopolymers (P1* M_w = 12 and P2* M_w = 77 kDa respectively); with higher RCY for the high molecular weight homopolymer (see figure S1 supplementary info). Stability of the radiolabel was ensured by means of SEC purification in combination with thin layer chromatography, indicating less than 1% radioiodine detachment from the polymer after 2 days of storage in NaCl at 4 °C. Radioiodination of HPMA-LMA random copolymers (P3* M_w = 11 kDa; P4* M_w = 55 kDa) additionally concentrated on the appropriate choice of reaction solvents since the hydrophobic lauryl methacrylate side chains avoid complete dissolution of the polymers in PBS (solvent dependency see Figure S2 and S3 supplementary info). Concerning the labeling efficiencies, the low molecular weight random copolymer P3* showed highest RCYs (41%, decay corrected) for Iodogen whereas its high molecular weight counterpart P4* exhibited best labeling yields (corrected RCY = 44%) using Chloramine-T.

Due to former short term studies by means of [^{18}F]fluoroethylation, exposing the high molecular weight HPMA-*ran*-LMA copolymer as most suitable candidate for polymer drug delivery [22], we here aimed to investigate its potential as polymeric nanocarrier in more detail and with respect to long term pharmacokinetics. Hence [^{131}I]radioiodination of HPMA-*ran*-LMA copolymer P4* for subsequent *in vivo* evaluation was accomplished using CAT as oxidizing agent as well as DMSO in order to promote ^{131}I-incorporation in sufficient high yields – using 1 mg of polymer precursor in a total synthesis time (including SEC purification) of less than 20 min. Biodistribution studies of ^{131}I-labeled polymer were carried out in Walker 256 tumor bearing rats.

In order to follow the long term biodistribution and tumor accumulation (EPR effect), time points were chosen to be 2 h, 24 h, 48 h and 72 h post injection. Radioiodination efficiencies were determined to be 49±3% (decay corrected) after preparative SEC purification. Figure 2 displays the biodistribution of ^{131}I-P4* in organs of interest (liver, spleen, kidney, lung, heart as well as blood), investigated over up to 72 h in comparison to short term pharmacokinetics observed for ^{18}F-P4*.

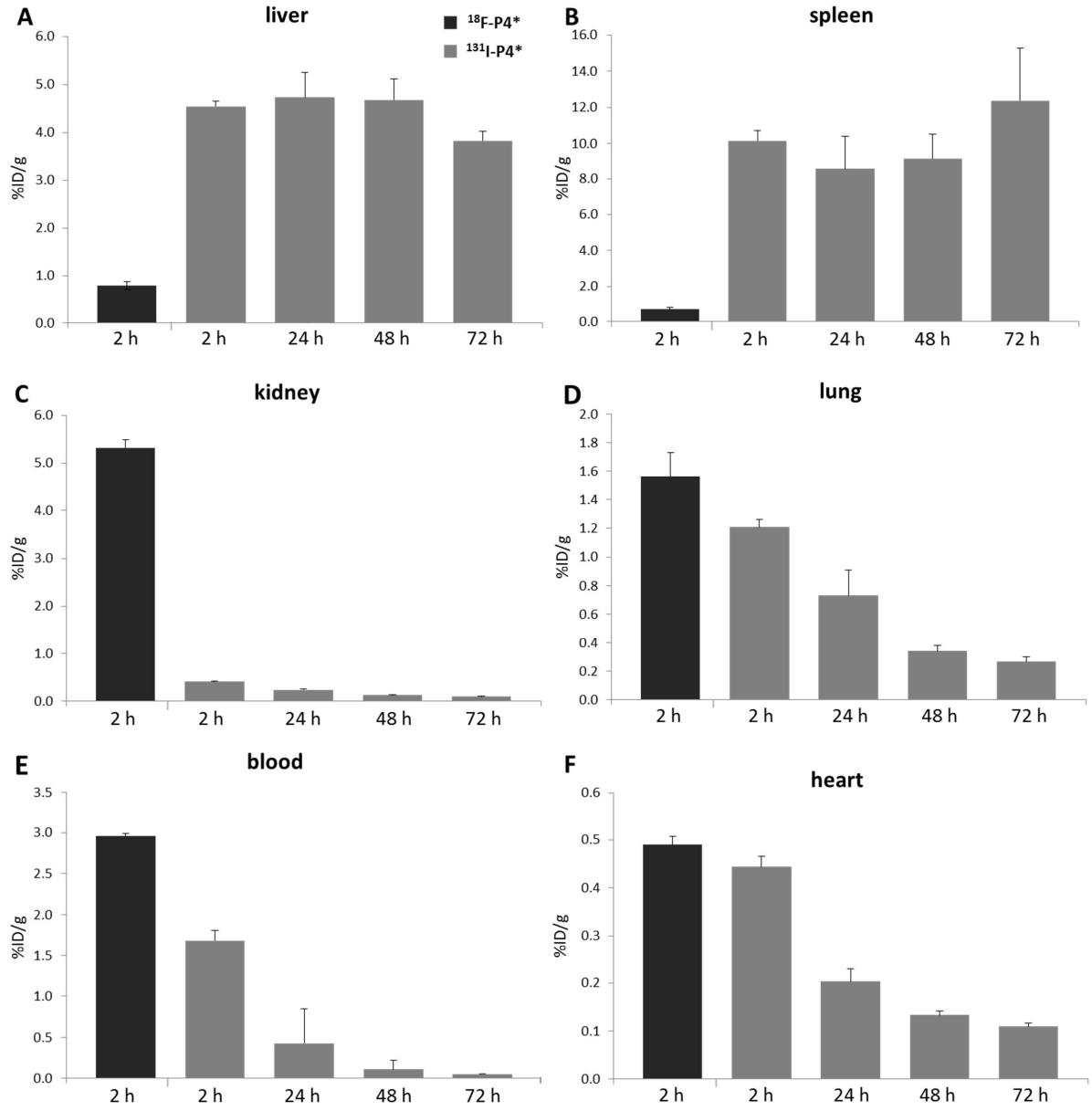

Figure 2: Biodistribution studies of the large HPMA-ran-LMA copolymer P4 in different organs (liver, spleen, kidney, lung, heart and blood) 2 h p.i. using ^{18}F-P4* and for up to 72 h by means of ^{131}I-P4*. Data is expressed as %ID/g tissue (mean±SEM). n=2-3 Almost linear decrease in ^{131}I-P4* level in the kidney (r=-0.934), the lung (r=-0.896) and the heart (r=-0.881).*

Concerning relevant organs of body clearance – i.e. liver, spleen and kidney – striking differences between short term distribution obtained with ^{18}F-P4* and long term disposition measured with the ^{131}I-labeled analog were observed. Hepatic and splenic uptake of ^{131}I-labeled P4* was much higher (over a time span of 72 h) when comparing to the data measured with the ^{18}F-labeled polymer. Even at the same time point (2 h p.i.), the liver concentration of the ^{131}I-labeled compound was 5-times higher compared to ^{18}F-labeling whereas the spleen showed 10-times higher values for ^{131}I-P4* (Figure 2A/B, table S1). This observation may be attributed to an enhanced lipophilicity of the random copolymer system induced by the more hydrophobic iodine radiolabel. Besides, an inverse pattern was observed regarding kidney concentrations of the herein examined high molecular weight random copolymer. Kidney uptake (Figure 2C) of ^{131}I-P4* was strongly reduced, displaying about 14-times lower concentrations compared to ^{18}F-P4*. According to the observed pharmacokinetic shifts in organ uptake between the differently labeled random copolymer P4* it has to be mentioned that the minute amounts of a reporter probe should allow to study pharmacokinetics without effectively altering surface properties or architecture of the carrier system. However *in vivo,* the radiolabel – or its anchoring moiety – might be subjected to degradation (e.g. in the liver) resulting in higher concentrations of lipophilic radiometabolites in the liver or enhanced clearance of hydrophilic metabolites *via* the kidney. Former studies on a [^{18}F]fluoroethylated HPMA homopolymer revealed low initial metabolism rates in the blood, with no further increase for up to 1 h after i.v. administration. Here, no radiometabolites were detected in the urine implying plasma binding of the initially formed ^{18}F-metabolites. Furthermore, no radioactive accumulation in the skeleton due to released [^{18}F]fluoride was observed up to 2 h after polymer administration [22]. Besides, in the present study nearly 1.8-times lower concentrations of ^{131}I-P4* were found in the blood compared to ^{18}F-P4* (1.69±0.12 % ID/g *vs.* 2.60±0.03 % ID/g, respectively) 2 h p.i. which might be ascribed to the observed plasma binding of ^{18}F-radiometabolites leading to an overestimation of initial blood pool concentrations upon ^{18}F-polymer administration. Although the observed disparities in organ distribution are likely attributed to differences in the metabolism of the radiolabels, a potential influence of the radionuclide itself on polymer characteristics and subsequent clearance has to be addressed. Pozzi et al. studied the influence of the radioisotope (^{18}F *vs.* ^{131}I-prosthetic group) on the *in vivo* pharmacokinetics of a model peptide. Notably, the ^{131}I-labeled peptide showed mainly hepatic as well as splenic uptake (likely due to the higher lipophilicity of iodine) whereas the respective ^{18}F-labeled peptide was cleared *via* the renal system [31].

Based on these findings not only the degree of isotope release and its reutilization by plasma binding or organ uptake might account for the discrepancy in organ distribution but also the radionuclide *per se* might impart higher liver and spleenic uptake (as seen for ^{131}I-P4*).

In order to effectively deliver drugs to the target tissue (tumor), a suitable drug carrier system has to meet unique requirements – particularly prolonged retention in the blood pool as well as an EPR mediated accumulation in the tumor tissue is most desired. Regarding these special demands, we wanted to study the potential of the random copolymer P4* in the Walker 256 carcinoma model. Investigation of the polymer concentration in the blood compartment over up to three days (Fig. 2E, blood; Fig. 2F, heart) revealed a continuous clearance of P4*. Major blood clearance was observed within the first 24 h after administration of ^{131}I-P4* with 25% (0.42±0.04 %ID/g) of ^{131}I-P4* remaining in the blood compartment after 1 day. These findings demonstrate even higher blood levels compared to a study of Lammers et al. [32] determining the blood residence time of an iodine-131 labeled HPMA copolymer of 31 kDa. In addition, concentrations at 72 h (0.05±0.01 %ID/g) indicated a total blood clearance of P4* in less than three days. The blood concentration was decreasing almost linearly (r= -0.867). Highly blood supplied organs such as lung (Figure 2D) and heart (Figure 2F) reflect the already investigated course of iodine-131 labeled polymer in the blood.

Besides the aforementioned characteristics of the polymer in the blood pool, the observed trend in tumor accumulation is much more remarkable. Even though we investigated a significant blood clearance of the random copolymer over time, the concentrations found for ^{131}I-P4* gradually increased over a time window of 2 days (Figure 3). Considering that more than 90% of the polymer is being cleared from the blood within this time frame (Figure 2E), the increased retention of P4* in the tumor is directly correlating to the characteristics of EPR-mediated passive tumor accumulation of polymeric nanocarrier systems [1, 24, 33]. Former studies in our group already revealed a significant cellular uptake of the high molecular weight random copolymer P4* in the Walker 256 mammary carcinoma cell line (data not shown) hence assuming that the *in vivo* observed tumor characteristics are related to a combination of increased extravasation of polymer to the tumor tissue (EPR effect) as well as polymer-cell specific interactions at the tumor site. However, highest tumor uptake of ^{131}I-P4* was observed 48 h after administration (1.00±0.51 %ID/g) thus demonstrating the suitability of this HPMA-based copolymer system for anticancer treatment within a time frame of 2 days. The decreasing value found at 72 h after injection (Figure 3) could be the result of differences in tumor growth which might affect the tumor accumulation of the polymer.

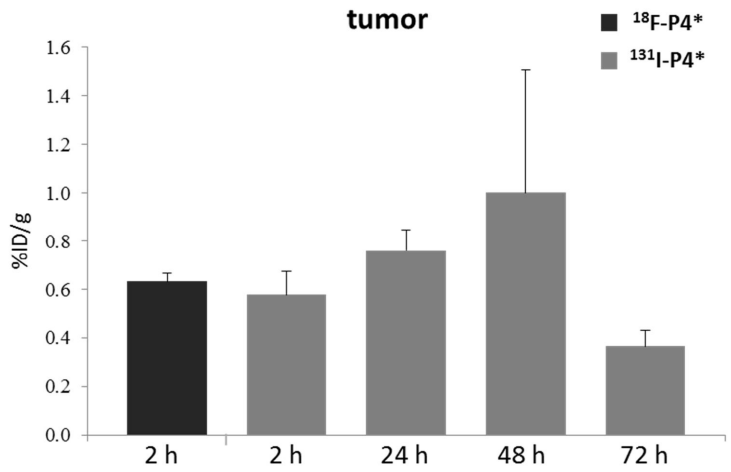

Figure 3: Tumor uptake of the large HPMA-ran-LMA copolymer P4 in the Walker 256 mammary carcinoma model. Distribution was studied 2 h p.i. using ^{18}F-P4* and for up to 72 h by means of ^{131}I-P4*. Data is expressed as %ID/g tissue (mean±SEM).*

Noteworthy, both ^{18}F-P4* and ^{131}I-P4* show similar initial tumor concentrations of about 0.6 % ID/g - despite the observed differences in initial organ and blood pool concentrations. With these findings, both labeling strategies are assumed to be suitable to determine the tumor targeting ability of polymer based drug carrier systems. Although the shorter half-life of ^{18}F (110 min) limits the diagnostic time frame to several hours, [^{18}F]fluoroethylation allows to assess the suitability of drug carriers for efficient tumor treatment profiting from additional PET imaging as valuable short term preclinical tool. However, despite fast and efficient screening of potential polymeric drug delivery vehicles is enabled – with respect to assessing intratumoral distribution – careful interpretation regarding initial organ distribution has to be accomplished. Here application of diverse labeling approaches, not demanding for a prior variation of the polymer structure, are crucial in order to reveal overall pharmacokinetic as well as long term distribution, facilitating the choice of promising drug delivery compounds in the future.

Conclusion

In the present study we could demonstrate the successful introduction of a longer-lived radioisotope into HPMA-*ran*-LMA copolymer structures, enabling their precise tracing in terms of body distribution and especially tumor accumulation over a time span of several days. Radioactive labeling by means of iodine-131 enabled *ex vivo* biodistribution studies of the high molecular weight HPMA-based random copolymer, underlining the significance of tracking the pharmacokinetic profile of polymers in the long run. Based on an observation frame of 3 days, enhanced retention of the

random copolymer P4* in tumor tissue could be proven (at least over 48 hours) – despite its concurrent clearance from the blood pool. These characteristics can be directly correlated to the well-known EPR effect. Furthermore, due to a comparative short term study of ^{18}F-labeled copolymer P4*, the additional labeling approach indicated an accordant tumor uptake pattern for ^{131}I-P4* at the same time point (2 h p.i.). This observation is of major importance since initial organ distribution of the differently labeled high molecular weight HPMA-based random copolymer revealed strong disparities in organ accumulation. In this regard, metabolic studies on the *in vivo* stability of the polymer-bound radiolabels are ongoing. In conclusion, the herein obtained results underline the significance of applying multiple and versatile labeling approaches to determine the potential of polymeric carrier systems for efficient anticancer therapy.

Acknowledgement

The authors would like to thank Barbara Biesalski, Dr. Martin Nowak and Achim Reibel for their support during animal studies. Special thanks go to Danielle Vugts for providing introduction into radioiodination procedures. We also want to thank the Max-Planck Graduate Center (MPGC, M. Allmeroth) as well as the Graduate School Materials Science in Mainz (Excellence Initiative, DFG/GSC 266, D. Moderegger) for financial support. In addition the authors are very thankful for financial support of the DFG (Rösch: RO 985/30-1; Thews: TH 482/4-1, Zentel: ZE 230/21-1) and SAMT Initiative Mainz.

References

[1] Y. Matsumura, H. Maeda, *Cancer Research* 1986, 46, 6387.

[2] R. Duncan, *Nat Rev Drug Discov* 2003, 2, 347.

[3] R. Duncan, *Nat Rev Cancer* 2006, 6, 688.

[4] D. R. F. L. W. Seymour, D. J. Kerr, D. Rea, M. Whitlock, R. Poyner, C. Boivin, S. Hesslewood, C. Twelves, R. Blackie, A. Schatzlein, D. Jodrell, D. Bissett, H. Calvert, M. Lind, A. Robbins, S. Burtles, R. Duncan, J. Cassidy, *Int. J. Oncol.* 2009, 34, 1629.

[5] R. Duncan, *Advanced Drug Delivery Reviews* 2009, 61, 1131.

[6] R. Duncan, M. J. Vicent, *Advanced Drug Delivery Reviews* 2010, 62, 272.

[7] L. W. Seymour, D. R. Ferry, D. Anderson, S. Hesslewood, P. J. Julyan, R. Poyner, J. Doran, A. M. Young, S. Burtles, D. J. Kerr, *Journal of Clinical Oncology* 2002, 20, 1668.

[8] M. Barz, R. Luxenhofer, R. Zentel, M. J. Vicent, *Polymer Chemistry* 2011, 2, 1900.

[9] K. Matyjaszewski, J. Xia, *Chemical Reviews* 2001, 101, 2921.

[10] J. Chiefari, Y. K. Chong, F. Ercole, J. Krstina, J. Jeffery, T. P. T. Le, R. T. A. Mayadunne, G. F. Meijs, C. L. Moad, G. Moad, E. Rizzardo, S. H. Thang, *Macromolecules* 1998, 31, 5559.

[11] E. R. G. Moad, S. H. Thang, *Aust. J. Chem*. 2005, 58, 379.

[12] M. Eberhardt, P. Théato, *Macromolecular Rapid Communications* 2005, 26, 1488.

[13] P. Theato, *Journal of Polymer Science Part A: Polymer Chemistry* 2008, 46, 6677.

[14] M. A. Gauthier, M. I. Gibson, H.-A. Klok, *Angewandte Chemie International Edition* 2009, 48, 48.

[15] M. Barz, R. Luxenhofer, R. Zentel, A. V. Kabanov, *Biomaterials* 2009, 30, 5682.

[16] M. I. Gibson, E. Fröhlich, H.-A. Klok, *Journal of Polymer Science Part A: Polymer Chemistry* 2009, 47, 4332.

[17] C. Boyer, V. Bulmus, T. P. Davis, V. Ladmiral, J. Liu, S. b. Perrier, *Chemical Reviews* 2009, 109, 5402.

[18] T. Lammers, V. Subr, K. Ulbrich, W. E. Hennink, G. Storm, F. Kiessling, *Nano Today* 2010, 5, 197.

[19] T. Lammers, *Advanced Drug Delivery Reviews* 2010, 62, 203.

[20] M. M. Herth, M. Barz, M. Jahn, R. Zentel, F. Rösch, *Bioorganic & Medicinal Chemistry Letters* 2010, 20, 5454.

[21] M. M. Herth, M. Barz, D. Moderegger, M. Allmeroth, M. Jahn, O. Thews, R. Zentel, F. Rösch, *Biomacromolecules* 2009, 10, 1697.

[22] M. Allmeroth, D. Moderegger, B. Biesalski, K. Koynov, F. Rösch, O. Thews, R. Zentel, *Biomacromolecules* 2011 12, 2841.

[23] H. Maeda, G. Y. Bharate, J. Daruwalla, *European Journal of Pharmaceutics and Biopharmaceutics* 2009, 71, 409.

[24] J. Fang, H. Nakamura, H. Maeda, *Advanced Drug Delivery Reviews* 2011, 63, 136.

[25] Z.-R. Lu, *Advanced Drug Delivery Reviews* 2010, 62, 246.

[26] M. Eberhardt, R. Mruk, R. Zentel, P. Théato, *European Polymer Journal* 2005, 41, 1569.

[27] S. b. Perrier, P. Takolpuckdee, C. A. Mars, *Macromolecules* 2005, 38, 2033.

[28] G. R. Moad, E.; Thang, S.H., *Aust. J. Chem.* 2005, 58, 379.

[29] P. R. P. Salacinski, C. McLean, J. E. C. Sykes, V. V. Clement-Jones, P. J. Lowry, *Analytical Biochemistry* 1981, 117, 136.

[30] F. C. Greenwood, W. M. Hunter, *Biochem. J.* 1963, 89, 114.

[31] O. R. Pozzi, E. O. Sajaroff, M. n. M. Edreira, *Applied Radiation and Isotopes* 2006, 64, 668.

[32] T. Lammers, R. Kühnlein, M. Kissel, V. Subr, T. Etrych, R. Pola, M. Pechar, K. Ulbrich, G. Storm, P. Huber, P. Peschke, *Journal of Controlled Release* 2005, 110, 103.

[33] H. Maeda, *Journal of Controlled Release* 2012.

[34] R. E. Rigler, E.S., Springer Verlag New York 2001.

[35] P. Workman, E. O. Aboagye, F. Balkwill, A. Balmain, G. Bruder, D. J. Chaplin, J. A. Double, J. Everitt, D. A. H. Farningham, M. J. Glennie, L. R. Kelland, V. Robinson, I. J. Stratford, G. M. Tozer, S. Watson, S. R. Wedge, S. A. Eccles, *Br J Cancer* 2010, 102, 1555.

Supporting Information

Comparative study on short and long-term distribution of HPMA-*ran*-LMA copolymers *in vivo* by means of ^{18}F and ^{131}I-labeling revealing tumor retention over time

Dorothea Moderegger, Mareli Allmeroth, Rudolf Zentel, Oliver Thews and Frank Rösch

Contents

1. Experimental section

I. Characterization of polymers

^{1}H-NMR spectra were obtained by a Bruker AC 300 spectrometer at 300 MHz, ^{19}F-NMR analysis was carried out with a Bruker DRX-400 at 400 MHz. All measurements were accomplished at room temperature and spectroscopic data were analyzed using ACDLabs 9.0 1D NMR Manager. The synthesized polymers were dried at 40 °C under vacuum overnight, followed by Gel Permeation Chromatography (GPC). GPC was performed in tetrahydrofuran (THF) as solvent, using following equipment: pump PU 1580, autosampler AS 1555, UV detector UV 1575 and RI detector RI 1530 from Jasco as well as a miniDAWN Tristar light scattering detector from Wyatt. Columns were used from MZ Analysentechnik, 300x8.0 mm: MZ-Gel SDplus 106 Å 5 µm, MZ-Gel SDplus 104 Å 5 µm and MZ-Gel SDplus 102 Å 5 µm. GPC data were evaluated by using the software PSS WinGPC Unity from Polymer Standard Service Mainz. The flow rate was set to 1 mL/min with a temperature of 25 °C.

Analytical Size Exclusion Chromatography (SEC) of ^{131}I-labeled polymers was performed using HiTrap™ Desalting Column, Sephadex G-25 Superfine and HPLC system consisting of a waters pump (1500 series), a Waters UV-detector (2487 λ absorbance detector) and a Berthold LB 509 radiodetector. Radiochemical purity was determined using Tec Control chromatography strips (Biodex Medical Systems, Inc., USA). Preparative SEC for removal of free iodine was accomplished using disposable PD-10 Desalting Columns (GE Healthcare) which were preconditioned and eluted with 0.9% (w/v) sodium chloride solution.

II. Synthesis of reactive ester homopolymer

RAFT polymerization of pentafluorophenyl methacrylate with 4-cyano-4-((thiobenzoyl) sulfanyl)pentanoic acid was carried out in a schlenk tube [1-3]. For this purpose, 4 g of PFPMA were dissolved in 5 mL of absolute dioxane, furthermore CTP and AIBN were added. The molar ratio of CTP/AIBN was chosen 8:1. After three freeze-vacuum-thaw cycles, the mixture was immersed in an oil bath at 65 °C and stirred overnight. Afterwards, the polymeric solution was precipitated three times in hexane, centrifuged and dried under vacuum at 40 °C overnight. A slightly pink powder was obtained. Yield: 52 %. ^{1}H-NMR (300 MHz, $CDCl_3$) δ/ ppm: 1.20-1.75 (br), 2.00-2.75 (br s). ^{19}F-NMR (400 MHz, $CDCl_3$) δ/ ppm: -162.03 (br), -156.92 (br), -152 to -150 (br).

III. Synthesis of reactive ester random copolymers

RAFT polymerization of PFPMA with lauryl methacrylate (LMA) by help of CTP was performed in a schlenk tube as well. As an example, 4 g of PFPMA dissolved in 5 mL dioxane, lauryl methacrylate, AIBN and CTP were mixed. The molar ratio of CTP/AIBN was chosen to be 8:1. After three freeze-vacuum-thaw cycles, the mixture was immersed in an oil bath at 65 °C and stirred over night. Afterwards, poly(PFPMA)-*ran*-poly(LMA) was precipitated three times in hexane, centrifuged and dried under vacuum at 40 °C over night. A slightly pink powder was obtained. Yield: 54 %. ^{1}H-NMR (300 MHz, $CDCl_3$) δ/ ppm: 0.84 (br t), 1.20-1.75 (br), 2.00-2.75 (br s). ^{19}F-NMR (400 MHz, $CDCl_3$) δ/ ppm: -162.01 (br), -156.95 (br), -152 to -150 (br).

IV. Polymer analogous reaction of homopolymers

Depending on the labeling technique necessary, either for a fluorescent or radioactive marker, two different routes were applied. For subsequent radioactive labeling, the protocol was carried out as follows. As example, 100 mg of the polymeric precursor (Mn = 18000 g/mol) were diluted in 2 mL of absolute dioxane. 5 mg of tyramine, diluted in a DMSO/dioxane mixture, and 10 mg of triethylamine were added. After stirring for four hours at 35 °C, 30 mg of 2-hydroxypropylamine as well as 40 mg of triethylamine were added and the solution was stirred overnight. For final removal of reactive ester side groups, further 30 mg of 2-hydroxypropylamine were added the next morning. The solution was precipitated two times in diethyl ether, centrifuged and finally dissolved in a DMSO/water solution for dialysis. After lyophilization a white powder could be obtained. Yield: 79%. ^{1}H-NMR (400 MHz, d. DMSO) δ/ ppm: 0.60-1.40 (br), 1.45-2.20 (br), 2.75-3.10 (br), 3.50-3.80 (br), 4.60-4.80 (br), 6.60-6.70 (br) and 6.85-7.00 (br). For additional fluorescent labeling, the fluorescent marker Oregon Green 488 cadaverine was used. 100 mg of polymeric precursor were diluted in 2 mL of absolute dioxane and 2.75 mg of Oregon Green 488 cadaverine added. Afterwards tyramine and 2-hydroxypropylamine were added, as described by the procedure above.

V. Polymer analogous reaction of random copolymers

For radioactive labeling of random copolymers the protocol was applied as follows. 100 mg of poly(PFPMA)-*ran*-poly(LMA) copolymer was dissolved in 2 mL of absolute dioxane. As example, for the polymeric system P3*-R (M_n= 17000 g/mol) 5 mg of tyramine and 10 mg of triethylamine were diluted in a DMSO/dioxane mixture and added to the vessel. After stirring for four hours at 35 °C, 30 mg of 2-hydroxypropylamine as well as 40 mg of triethylamine were added and the solution stirred over night. For final removal of reactive ester side groups further 30 mg of 2-hydroxypropylamine were added the next morning. The solution was precipitated two times in diethyl ether, centrifuged

and finally dissolved in a DMSO/water solution for dialysis. After lyophilization a white powder could be obtained. Yield: 51 %. ^{1}H-NMR (400 MHz, d. DMSO) δ/ ppm: 0.70-0.90 (br), 0.90-1.40 (br), 1.40-1.90 (br), 2.75-3.10 (br), 3.50-3.80 (br), 4.50-4.75 (br), 6.60-6.75 (br) and 6.85-7.00 (br). For additional fluorescent labeling, 100 mg of polymeric precursor were diluted in 2 mL of absolute dioxane and 2.9 mg of Oregon Green 488 cadaverine were added. Afterwards tyramine and 2-hydroxypropylamine were added, as described by the procedure above.

VI. Analytical data obtained in isotonic NaCl solution

Isotonic NaCl solution 0.9% was obtained by B. Braun Melsungen AG without any purification. Stock solutions were prepared using 1% of absolute DMSO in isotonic sodium chloride solution.

VII. Size determination by Fluorescence Correlation Spectroscopy (FCS)

The hydrodynamic radii of the polymeric systems were determined by Fluorescence Correlation Spectroscopy using a commercial FCS setup (Zeiss, Germany) consisting of the module ConfoCor 2 and an inverted microscope model Axiovert 200 with a Zeiss C-Apochromat 40 ×/1.2 W water immersion objective. The fluorophores were excited with an Argon laser (λ= 488 nm) and the emission was collected after filtering with a LP505 long pass filter. For detection, an avalanche photodiode, enabling single-photon counting, was used. As sample cell, eight-well, polystyrene-chambered cover glass (Laboratory-Tek, Nalge Nunc International) was applied. For sample preparation, stock solutions of 1 mg fluorescently labeled polymer/mL NaCl were applied, diluted to a final concentration of 0.1 mg/mL. The solution was kept at room temperature over night. For reference reason, free Oregon Green 488 cadaverine dye in NaCl-solution was also studied. The calibration of the FCS observation volume was done using a dye with known diffusion coefficient, i.e. Rhodamine6 G. For each solution, 5 measurement cycles with a total duration of 150 seconds were applied. Time dependent fluctuations of the fluorescence intensity δI(t) were detected and evaluated by autocorrelation analysis, yielding the diffusion coefficient and hydrodynamic radius of the fluorescent species [4].

VIII. Radiolabeling of polymers

In order to optimize ^{131}I-radiolabeling of HPMA-based polymers, two different *in situ* oxidants were investigated. For radiolabeling using Iodogen™ (1,3,4,6-Tetrachloro-3a,6a-diphenylglycoluril) as oxidizing agent, the reaction vials were coated prior to the radiolabeling with the respective amount of Iodogen™. Consecutively, 50 µL of 0.5 M phosphate buffer (pH = 7.4), 450 µL PBS, 100 µL of the respective polymer as well as 3-10 MBq of ^{131}I (0.05 N NaOH solution) was placed into the coated

vial. At t = 4 min, 100 µL of an aqueous ascorbic acid solution (25 mg/mL, pH=5.0) was added and after 1 min of shaking, the labeling mixture was transferred onto a PD-10 column for subsequent purification using fractionated elution with 0.9% sodium chloride solution.

Radiolabeling procedure using Chloramine-T (N-chloro-4-methylbenzenesulfonamide sodium salt, CAT) was started by placing 3-10 MBq of ^{131}I (0.05 N NaOH solution) in a reaction vial, followed by 50 µL of 0.5 M phosphate buffer (pH = 7.4) and 400-x µL of PBS. After addition of 200-500 µg of the respective polymer in 100 µL of solvent, the radiolabeling reaction was started by adding x µL of a CAT solution (1 mg/mL in 0.9% sodium chloride solution) resulting in a final volume of 550 µL for the radiolabeling mixture. After 4 min, the reaction was quenched and purified according to the Iodogen procedure.

IX. Tumor and animal model

Tumor experiments were performed with the Walker 256 mammary carcinoma of the rat. The named cell line was grown in culture in RPMI medium supplemented with 10 mM L-glutamine and 10% fetal calf serum (FCS) at 37°C under a humidified 5% CO_2 atmosphere and sub-cultivated twice per week. For tumor implantation male Sprague-Dawley rats (Charles River Wiga, Sulzfeld, Germany; body weight 150 to 300 g) housed in the animal care facility of the University of Mainz were used in this study. All experiments had previously been approved by the regional animal ethics committee and were conducted in accordance with the German Law for Animal Protection and the UKCCCR Guidelines [5]. Animals were allowed access to food and acidified water *ad libitum* before the investigation. Solid carcinomas were heterotopically induced by injection of cell suspension of the respective tumor line (0.4 mL approx. 10^4 cells/µl) subcutaneously into the dorsum of the hind foot. Tumors grew as flat, spherical segments and replaced the subcutis and corium completely. Volumes were determined by measuring the three orthogonal diameters (d) of the tumors and using an ellipsoid approximation with the formula: $V = d_1 \times d_2 \times d_3 \times \pi/6$. Tumors were used when they reached a volume of between 0.3 to 2.2 mL approx. 5 to 8 days after tumor cell inoculation. Three days before i.v. injection of ^{131}I-labeled copolymer, potassium iodide (0.1% w/v) was added to animal's drinking water to limit thyroid uptake of any free radioiodide.

X. Biodistribution studies

In order to assess the distribution of the radiolabeled polymers in different organs of the animals, the polymer (concentration of 1 mg in 1 mL sodium chloride solution) was injected i.v. in anaesthetized tumor-bearing rats *via* the tail vein with a mean activity of 9.3 ± 0.2 MBq (for ^{131}I) and 5.2 ± 0.3 MBq (for ^{18}F). After 2, 24, 48 and 72 hours, the animals were sacrificed and different organ (kidney, liver,

lung, spleen, heart, skeletal muscle, small intestine, testis, blood) and tumor samples were taken. The tissue samples were weighed and minced. Finally, the ^{131}I-activity in the organs was measured in a γ-counter.

XI. Statistical analysis

Results are expressed as means±SEM. Differences between groups were assessed by the two-tailed Wilcoxon or Kruskal-Wallis test for unpaired samples. The significance level was set at α=5% for all comparisons. Correlation analysis was performed by calculating the Pearson correlation coefficient.

2. Figures

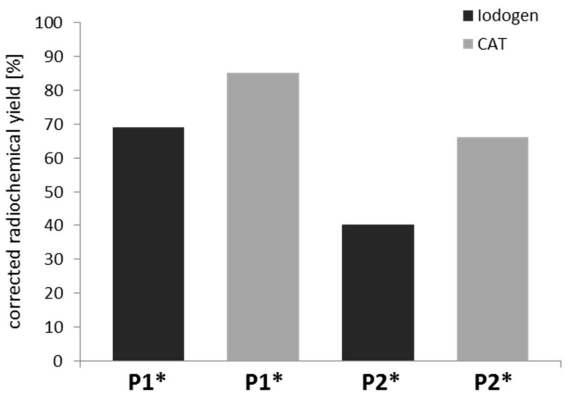

Figure S1: Corrected radiochemical yields for radioiodination of HPMA-based homopolymers P1 and P2* using 25 µg Iodogen™ or 200 µg Chloramine-T as determined using SEC.*

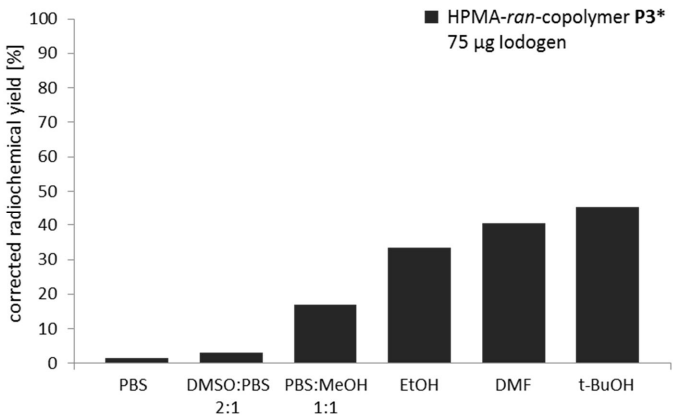

Figure S2: Influence of solvent on the radioiodination of HPMA-ran-LMA copolymer P3 using 75 µg of Iodogen™ as determined using SEC.*

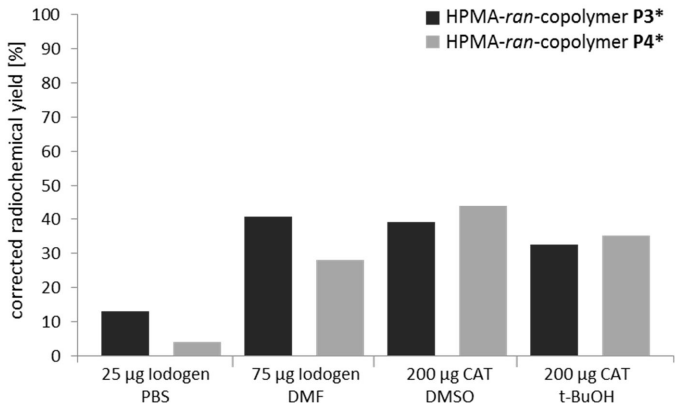

Figure S3: Corrected radiochemical yields of HPMA-ran-LMA copolymers P3 and P4* using Iodogen™ and CAT for I-131 radiolabeling as determined by means of SEC.*

3. Tables

Table 1: Biodistribution data of ^{18}F- and ^{131}I-labeled HPMA-ran-LMA copolymer P4 after i.v. administration in Walker 256 carcinoma bearing rats studied over a time course of up to 3 days. Data is represented as %ID/g tissue (mean±SEM)*

	^{18}F-P4*	^{131}I-P4*			
organ	2 h[a]	2 h[a]	24 h[a]	48 h[a]	72 h[b]
lung	1.56±0.17	1.21±0.05	0.73±0.18	0.34±0.04	0.26±0.04
liver	0.80±0.08	4.55±0.11	4.73±0.51	4.68±0.43	3.83±0.20
spleen	0.74±0.09	10.15±0.55	8.55±1.83	9.11±1.41	12.38±2.90
kidney	5.32±0.17	0.41±0.02	0.24±0.02	0.13±0.02	0.10±0.01
muscle	0.09±0.02	0.09±0.02	0.05±0.01	0.03±0.01	0.04±0.01
heart	0.49±0.02	0.44±0.02	0.20±0.03	0.13±0.01	0.11±0.01
blood	2.96±0.03	1.69±0.12	0.42±0.04	0.11±0.01	0.05±0.01
small intestine	0.26±0.01	0.26±0.01	0.44±0.04	0.37±0.03	0.28±0.04
testis	0.14±0.01	0.14±0.01	0.17±0.02	0.14±0.03	0.13±0.02
W 256 tumor	0.63±0.02	0.58±0.8	0.76±0.09	1.00±0.32	0.37±0.04[c]

[a]N = 3, [b]N = 2, [c]N=4.

4. References

[1] M. Allmeroth, D. Moderegger, B. Biesalski, K. Koynov, F. Rösch, O. Thews, R. Zentel, *Biomacromolecules* 2011, 12, 2841.

[2] M. Barz, R. Luxenhofer, R. Zentel, A. V. Kabanov, *Biomaterials* 2009, 30, 5682.

[3] P. Theato, *Journal of Polymer Science Part A: Polymer Chemistry* 2008, 46, 6677.

[4] R. E. Rigler, E.S., Springer Verlag New York 2001.

[5] P. Workman, E. O. Aboagye, F. Balkwill, A. Balmain, G. Bruder, D. J. Chaplin, J. A. Double, J. Everitt, D. A. H. Farningham, M. J. Glennie, L. R. Kelland, V. Robinson, I. J. Stratford, G. M. Tozer, S. Watson, S. R. Wedge, S. A. Eccles, *Br J Cancer* 2010, 102, 1555.

3.5 PEGylation of HPMA-based block copolymers enhances tumor accumulation *in vivo*: A quantitative study using radiolabeling and Positron Emission Tomography

PEGylation of HPMA-based block copolymers enhances tumor accumulation *in vivo*: A quantitative study using radiolabeling and Positron Emission Tomography

Mareli Allmeroth[1,§], Dorothea Moderegger[1,*], Daniel Gündel[‡], Hans-Georg Buchholz[Φ], Kaloian Koynov[†], Frank Rösch[*], Oliver Thews[‡] and Rudolf Zentel[§]

[1] both authors contributed equally

[§] Institute of Organic Chemistry, Johannes Gutenberg University, Duesbergweg 10-14, 55099 Mainz, Germany

* Institute of Nuclear Chemistry, Johannes Gutenberg University, Fritz-Strassmann-Weg 2, 55128 Mainz, Germany

[‡] Institute of Physiology, University Halle, Magdeburger Str. 6, 06097 Halle (Saale), Germany

[Φ] Department of Nuclear Medicine, University Medicine Mainz, Langenbeckstraße 1, 55131 Mainz, Germany

[†] Max-Planck-Institute for Polymer Research, Ackermannweg 10, 55128 Mainz, Germany

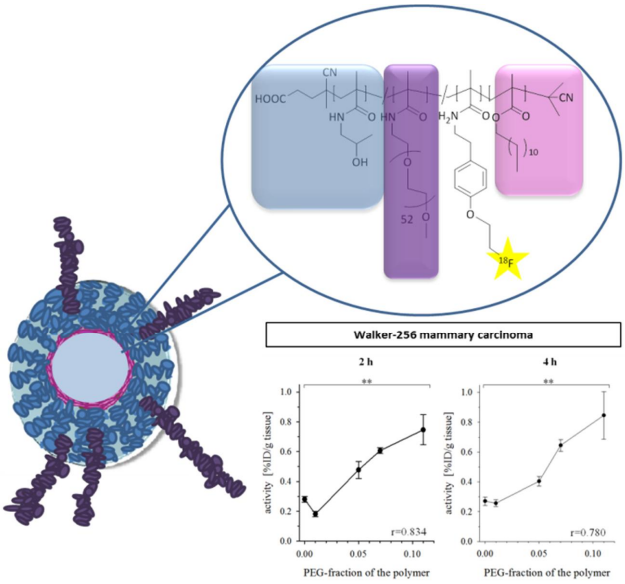

PEGylation of HPMA-*b*-LMA copolymers improves their *in vivo* pharmacokinetics in a linear trend -monitored by PET-

Abstract

Block copolymer micelles are widely established drug delivery systems, particularly in the field of anticancer treatment. Due to their amphiphilic core-shell structure, hydrophobic (chemo) therapeutics can be easily encapsulated. Polymer size as well as surface properties highly determine the *in vivo* potential/performance with PEGylation being the most commonly applied approach to tune pharmacokinetics for efficient drug delivery. In the present study five different HPMA-based block copolymers – with lauryl methacrylate as hydrophobic block – were investigated in the Walker 256 mammary carcinoma *in vivo*. They varied in incorporation ratio of a PEG_{2000} side chain fragment in the hydrophilic block, ranging from block copolymers with 0% PEG to 11% degree of PEGylation. Polymers were labeled with the positron emitter ^{18}F and organ/tumor uptake was quantified by *ex vivo* biodistribution as well as microPET imaging. Tumor cell uptake *in vitro* was studied using fluorescence labeled polymers. Most remarkably, the *in vivo* results revealed a linear trend in tumor accumulation – with lowest tumor uptake of the pure block copolymer to highest enrichment with 11% PEG side chains. Within the studied polymers, the block copolymer of 7% PEGylation exhibited the most favorable organ distribution pattern, showing highest blood-circulation level as well as lowest hepatic and splenic uptake. However, no direct correlation between PEGylation dependent increase in tumor accumulation *in vivo* and the polymer uptake of Walker 256 tumor cells *in vitro* was observed where highest cellular uptake was determined for block copolymers with lowest PEG content (0 and 1%). These findings emphasize the need for reliable (non-invasive) *in vivo* techniques revealing overall polymer distribution and helping to identify drug carrier systems for efficient therapy such as radiolabeling in combination with PET imaging

Keywords: Fluorine-18 labeling, HPMA, PEG, PET, Structure-property relationships, Walker 256 mammary carcinoma

Introduction

Over the last four decades “Polymer therapeutics”, a term describing polymeric drugs, polymer-drug conjugates, polymer-protein conjugates, polymeric micelles as well as polyplexes, have been intensively studied regarding their potential in anticancer treatment [1]. The key benefits of polymer based drug delivery systems compared to the low molecular weight free drug rely on the reduction of usually occurring toxic side effects in healthy tissue, their enhanced accumulation in the tumor due to the EPR effect [2, 3] and an increase in plasma half-life toward the pure chemotherapeutic agent.

Demonstrated by the moderate number of clinically tested polymers, some essential requirements need to be fulfilled by the polymer drug carrier system. Besides being non-toxic, non-immunogenic, biodegradable or respectively biocompatible with an adequate molecular weight to allow body elimination, the carrier system should be narrowly distributed to ensure homogeneity of the final conjugates. In this regard, poly(HPMA) is holding favorable characteristics, already validated by diverse preclinical and clinical studies [4-10].

Nevertheless, major obstacles still have to be overcome. These include the protection of the polymer drug delivery systems versus degrading enzymes or fast uptake by the reticuloendothelial system (RES) resulting in a rapid elimination of the carrier system from the blood stream. Considering these demands, PEG has become firmly established as promising candidate to prolong the pharmacokinetic properties of drugs, with special focus on protein modification as generally described by the term PEGylation [11-16]. The so called "stealth properties" of polyethylene glycol – responsible for low immunogenicity and antigenicity of the coated material – are mainly based on the high hydrophilicity as well as flexibility of the PEG-chains forming a protective layer, thereby e.g. minimizing the identification by opsonin proteins responsible for phagocytic uptake [12, 17, 18]. Regarding their shielding efficacy, optimal molecular weights for polyethylene glycol have been reported to be between 1500 - 5000 g/mol [17, 19]. The above mentioned favorable characteristics of PEG render this polymer valuable for a variety of biomedical applications and particularly in combination with the multifunctional poly(HPMA), polymer drug carrier systems with beneficial synergetic effects can be created.

Previous studies on ^{18}F-radiolabeled HPMA homopolymers and random copolymers revealed that the ratio of hydrophilicity/hydrophobicity as well as aggregate formation possessed a major impact on the body distribution in the living animal [20]. Taking this knowledge into consideration, we subsequently concentrated on the correlation between specific polymer characteristics (e.g. molecular weight, architecture and lipophilicity) and their influence on tumor uptake in two different tumor models. Amphiphilic HPMA-LMA random and block copolymers – both forming superstructures in aqueous media – revealed promising results of tumor accumulation *in vivo* and thus may be attractive candidates for drug delivery [21-23]. Due to the aforementioned results, the question was arising whether the pharmacokinetics of the HPMA-based block copolymers can be improved by incorporation of PEG side chains into the hydrophilic block. To our knowledge, no attempts of combining the favorable characteristics of HPMA and PEG into one polymer chain of a block copolymer have been reported so far.

In contrast to the dynamic nature of random copolymers, amphiphilic block copolymers are characterized by higher stability in hydrophilic media (contributed to their tendency to self-assemble in water driven by a gain of entropy) which is especially advantageous for the entrapment of hydrophobic drugs into the core. Due to their small sizes as well as the formation of a hydrophilic shell providing steric hindrance, prolonged circulation times can be achieved for micellar carriers [24]. With regard to the need of forming well-defined polymers, controlled radical polymerization techniques like ATRP or RAFT [25-28] introduced the facile access to narrowly distributed polymer structures and especially in combination with reactive ester chemistry [21, 29, 30], RAFT offers an elegant route to a variety of polymer architectures and functional groups. Not only imaging moieties (e.g. fluorescent or radioactive markers) and therapeutics can be attached, also the polymer nature of the hydrophilic shell can be easily modified.

The previous results [20] also demonstrated the need for appropriate preclinical screening methodologies to select a suitable therapy for the individual patient [8, 31]. Concerning this purpose, radiolabeling and Positron Emission Tomography (PET) are helpful diagnostic tools providing detailed information on body distribution as well as tumor accumulation in the living organism. Depending on the radionuclide's half-life, the diagnostic time frame can be adjusted from early phase accumulation to long-term imaging over weeks or months. Until now, studies concerning the *in vivo* behavior of diverse HPMA and PEG based nanoparticles have been almost exclusively carried out using either γ-imaging radionuclides like ^{99m}Tc, ^{111}In or $^{125/131}$I [32-36] providing relatively low spatial resolution or by means of the metallic positron emitter ^{64}Cu requiring chelating agents [37-40]. In contrast to these approaches, we demonstrated the successful radiolabeling of various HPMA-based polymers with the positron emitters $^{72/74}$As [41] and ^{18}F [42], thereby establishing PET imaging to assess the *in vivo* capability of potential drug delivery systems.

In this work we have focused on a precise tailoring of HPMA-*b*-LMA copolymers by incorporating different percentages of a linear, amine-functionalized $PEG_{2000\ Da}$ fragment into the hydrophilic block. This approach was aimed to optimize both blood retention time as well as tumor uptake of HPMA-based block copolymers, taking advantage of the so called "stealth properties" of PEG chains $>$ 1500 Dalton towards opsonization processes. In order to correlate the influence of PEG content on the resulting pharmacokinetics *in vivo*, the block copolymers were radiolabeled with the positron emitting nuclide ^{18}F holding ideal nuclear characteristics concerning PET imaging ($t_{1/2}$: 109.7 min, β^+: 635 keV, 96.7%). This enabled to investigate tumor accumulation as well as body distribution in the experimental Walker 256 mammary carcinoma model by means of µPET imaging and *ex vivo*

biodistribution studies. In addition the cellular uptake into tumor cells of PEGylated block copolymers was analyzed.

Materials and methods

Materials

All solvents were of analytical grade, as obtained by Sigma Aldrich and Acros Organics. Dioxane was distilled over a sodium/potassium composition, dichloromethane over calcium hydride. Lauryl methacrylate was distilled to remove the stabilizer and stored at -18 °C. 2,2'-Azo-bis-(isobutyronitrile) (AIBN) was recrystallized from diethyl ether and stored at -18 °C as well.

Experimental setups

Experimental setups can be found in the supplementary information.

Synthesis of the polymers

The polymers $P_{0\%}$ to $P_{11\%}$ were prepared in analogy to reference [20, 21, 42]. The details are added as supplementary information.

Characterization of the polymers

The hydrodynamic radii of the polymeric systems were determined by Fluorescence Correlation Spectroscopy (FCS) using a commercial FCS setup. Thereby aggregate formation of the block copolymers can be proven. The details can be found in the supplementary information.

Radiolabeling and purification for *ex vivo* and *in vivo* experiments

Radiolabeling and subsequent purification of the polymers for *ex vivo* and *in vivo* experiments was accomplished using an ^{18}F-fluoroethylation method modified from Herth et al. [42]. In brief, 3 mg polymer was dried azeotropically three times each with 1 mL of acetonitrile prior to [^{18}F]fluorination. 100 µL of dry DMSO as well as 1 µL of 5 M Cs_2CO_3 solution was added and the labeling reaction was started by adding a dry solution of [^{18}F]FETos in DMSO. Radiolabeling was performed at 120 °C for 18 min. Further details are given in the supporting information.

Animal experiments

Tumor and animal model

For animal experiments the rat tumor cell line Walker 256 mammary carcinoma was used. Experimental details can be found in the supplementary. All experiments had previously been approved by the regional animal ethics committee and were conducted in accordance with the German Law for Animal Protection and the UKCCCR Guidelines [43].

In vivo µPET imaging

For µPET imaging, rats were anaesthetized with pentobarbital (40 mg/kg, intraperitoneal, Narcoren, Merial, Hallbergmoos, Germany). ^{18}F-labeled polymers were injected *via* tail vein puncture. Experimental setup of the microPET is described in the supplementary information.

Biodistribution and cellular uptake studies

Further information on biodistribution as well as cellular studies can be found in the supplementary information.

Statistical analysis

Results are expressed as means ± SEM. Differences between groups were assessed by the two-tailed Wilcoxon or Kruskal-Wallis test for unpaired samples. The significance level was set at α=5% for all comparisons. Correlation analysis was performed by calculating the Pearson correlation coefficient.

Results and discussion

Synthesis and radioactive labeling of HPMA-b-LMA copolymers with varying $PEG_{2000\,Da}$ content

The aim of this study was focused on the impact of PEG_{2000Da} fragments in HPMA-LMA block copolymers and their influence on tumor uptake as well as body distribution of the polymer systems *in vivo*. By combining the controlled radical polymerization technique RAFT (Reversible Addition-Fragmentation Chain Transfer) [27, 28] with reactive ester chemistry [44] we could already demonstrate the facile synthesis of well-defined and narrowly distributed HPMA-based polymer systems – differing in molecular weight as well as incorporation of hydrophobic segments – in former studies [20, 21].

In addition, radioactive labeling using the positron emitter fluorine-18 [42] illustrated successful monitoring of the polymer carrier system in the living organism and further examinations emphasized that particularly polymer architecture as well as molecular weight had a tremendous effect on organ distribution, blood circulation properties and tumor uptake *in vivo* [20]. Taking these results into account, here the focus was laid on the optimization of the *in vivo* characteristics of HPMA-LMA block copolymers, representing the most defined and stable polymer structures. By incorporation of different ratios of PEG_{2000} side chains into the hydrophilic part of the block copolymer structure (0, 1, 5, 7 and 11% respectively) we investigated how hydrodynamic radii, amphiphilicity and aggregate formation as well as spacer linkage is affecting the polymer fate in the living organism. A key aspect of these polymer-dependent features was the correlation to blood pool concentration as well as tumor accumulation. Overall, five different block copolymer structures were synthesized ($P_{0\%}$ to $P_{11\%}$), starting from the same reactive block copolymer precursor system (P*-R). The polymer characteristics are summarized in table 1.

Table 1: Analytical data of reactive ester precursor polymer (P-R) and final polymer structures ($P_{0\%}$ to $P_{11\%}$)*

Nomen clature	Polymer structure	Monomer ratio	PEG_{2000} incorp.[5]	M_n in g/mol	M_w in g/mol	PDI[2]	R_h[6] in nm
P*-R	Block copolymer	60:40%[1]	-	25.000[2]	31000[2]	1.25	n.d.
$P_{0\%}$	Block copolymer	75:25%[3]	0%	17000[4]	21000[4]	1.25	112.8 +/- 5.7
$P_{1\%}$	Block copolymer	75:25%[3]	1%	20000[4]	24000[4]	1.25	55.4 +/- 2.9
$P_{5\%}$	Block copolymer	75:25%[3]	5%	26000[4]	33000[4]	1.25	38.0 +/- 2.1
$P_{7\%}$	Block copolymer	75:25%[3]	7%	30000[4]	38000[4]	1.25	38.1 +/- 2.1
$P_{11\%}$	Block copolymer	75:25%[3]	11%	39000[4]	47000[4]	1.25	53.0 +/- 2.8

[1] Calculated monomer ratio. [2] Determination by GPC in THF as solvent. [3] Monomer ratio determined by ^{1}H-NMR spectroscopy after polymeranalogous reaction with 2-hydroxy-propylamine. [4] Calculated from the molecular weight of the reactive ester polymer P*-R as determined by GPC in THF as solvent. [5] PEG_{2000} incorporation (incorp.) ratio determined by ^{1}H-NMR spectroscopy after polymeranalogous reaction [6] Hydrodynamic radii determined by Fluorescence Correlation Spectroscopy (FCS).

As depicted in table 1, well-defined and narrowly distributed block copolymer systems could be synthesized (PDI = 1.25). The hydrophobic lauryl methacrylate segment was incorporated to an extent of 25%, as determined by gel permeation chromatography and ^{1}H-NMR spectroscopy. Molecular weights (M_n) of the final polymer structures were between 17000 and 39000 g/mol, increasing with higher PEG content. PEG_{2000} segments were linked to the hydrophilic block with efficiencies of 1, 5, 7 and 11% as calculated by ^{1}H-NMR spectroscopy. The pure HPMA-LMA block copolymer $P_{0\%}$ exhibited a hydrodynamic radius of 112.8 nm, thereby representing the highest

aggregate structure investigated in this study. Based on the higher hydrophilicity of polyethylene glycol compared to HPMA, we examined a decrease of R_h values with increasing PEG spacer incorporation, possessing a minimum for $P_{5\%}$ and $P_{7\%}$ (~38 nm). This result stays in good correlation with earlier studies on PEG-coated nanoparticles by Gref at al. [45] assuming that the higher incorporation ratio of PEG imparts lower interfacial tension between the aqueous surrounding and the hydrophobic core. Nevertheless polymer $P_{11\%}$ – exhibiting a linkage efficiency of 11% PEG segments – demonstrated an increase of hydrodynamic radius to 53 nm, probably due to steric hindrance in the polymer chain [46]. A reaction scheme of the polymer synthesis is illustrated in Figure 1.

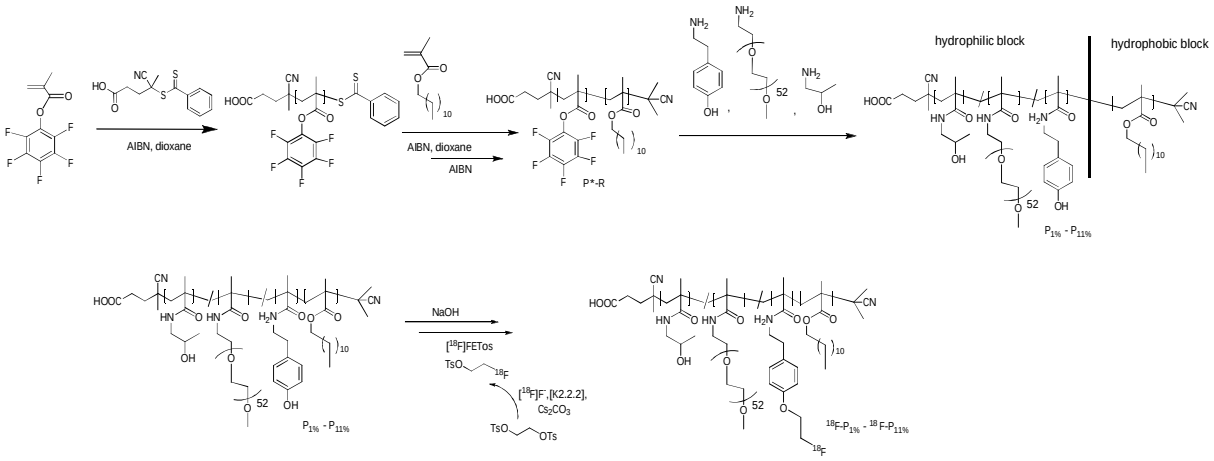

Figure 1: Polymer synthesis as well as radioactive labeling procedure (exemplified for PEG_{2000} modified polymers).

Starting from the reactive ester monomer pentafluorophenyl methacrylate (PFPMA), the macro-CTA was synthesized and further converted to reactive ester block copolymer P*-R. By polymeranalogous reaction of the hydrophilic block, tyramine groups (incorporation of ~ 3%) for radiolabel attachment as well as the amine-functionalized PEG_{2000} fragment and 2-hydroxypropylamine were covalently linked. To perform non-invasive small animal PET imaging as well as for quantification by *ex vivo* biodistribution measurements, the positron emitter fluorine-18 was introduced *via* [^{18}F]fluoroethylation, a method already established for various HPMA-based random and copolymers [20, 42]. In order to promote the incorporation of the fluoroethyl radiolabel, the previously applied radiolabeling conditions [42] were adjusted by using Cs_2CO_3 as base as well as azeotropic drying of the polymer precursors prior to radiolabeling. Nevertheless, radiolabeling efficiencies – as listed in Table 2 – were still comparably low, with highest RCYs achieved for block copolymer $P_{11\%}$ (RCY = 18±2 %).

Table 2: Corrected radiochemical yields for HPMA-based block copolymers $P_{0\%}$ to $P_{11\%}$

Nomenclature	Polymeric structure	PEG_{2000} incorp.[5]	Monomer ratio[3]	M_w in g/mol[4]	RCY in %
^{18}F-$P_{0\%}$	Block copolymer	0%	75:25%	21000[4]	7±0
^{18}F -$P_{1\%}$	Block copolymer	1%	75:25%	24000[4]	11±1
^{18}F -$P_{5\%}$	Block copolymer	5%	75:25%	33000[4]	15±8
^{18}F-$P_{7\%}$	Block copolymer	7%	75:25%	38000[4]	5±1
^{18}F -$P_{11\%}$	Block copolymer	11%	75:25%	47000[4]	18±2

Organ distribution

Regarding the influence of surface chemistry on pharmacokinetics, both PEG length and surface density on block copolymer derived nanoparticles was shown to hold a tremendous impact on clearance from the bloodstream [38, 40, 47].

Quantification of the recovered dose of radiofluorinated block copolymers was accomplished in selected organs (liver, spleen and kidney, heart, blood, lung, muscle, small intestine and testis) 2 h and 4 h after i.v. administration. Biodistribution data of polymers with different degree of PEGylation in the organs is illustrated in Figure 2 and Table 3 (4 h values are depicted in table S1, see supporting information).

As clearly visible, a major dependency of the PEG_{2000} content in the hydrophilic block regarding organ accumulation can be detected. The pure block copolymer $P_{0\%}$ exhibited the highest uptake in the kidney; further increasing over time and hence demonstrating renal clearance (see Fig. 2A). With higher PEG_{2000} percentage a decrease in kidney accumulation could be observed ($r = -0.881$), possessing a minimum for $P_{7\%}$. Apparently the hydrodynamic radii (Tab. 1) of the PEGylated compounds reveal a correlation to their observed kidney uptake. Block copolymers with larger sizes ($P_{0\%}$, $P_{1\%}$ and $P_{11\%}$ with $R_h = 112$, 55 and 53 nm respectively) also showed highest kidney accumulation. A decrease in polymer size resulted in a diminished renal excretion, underlining the high impact of molecular architecture besides size on the clearance of polymer carriers [48]. Furthermore, higher hydrophilicity and PEG surface coverage may gradually lower glomerular filtration, probably attributed to a better shielding efficacy of the highly modified block copolymers toward plasma proteins. In general it has to be noted that all herein presented block copolymers illustrated renal clearance, a major requirement for non-biodegradable nanocarrier systems to circumvent chronic accumulation in the body.

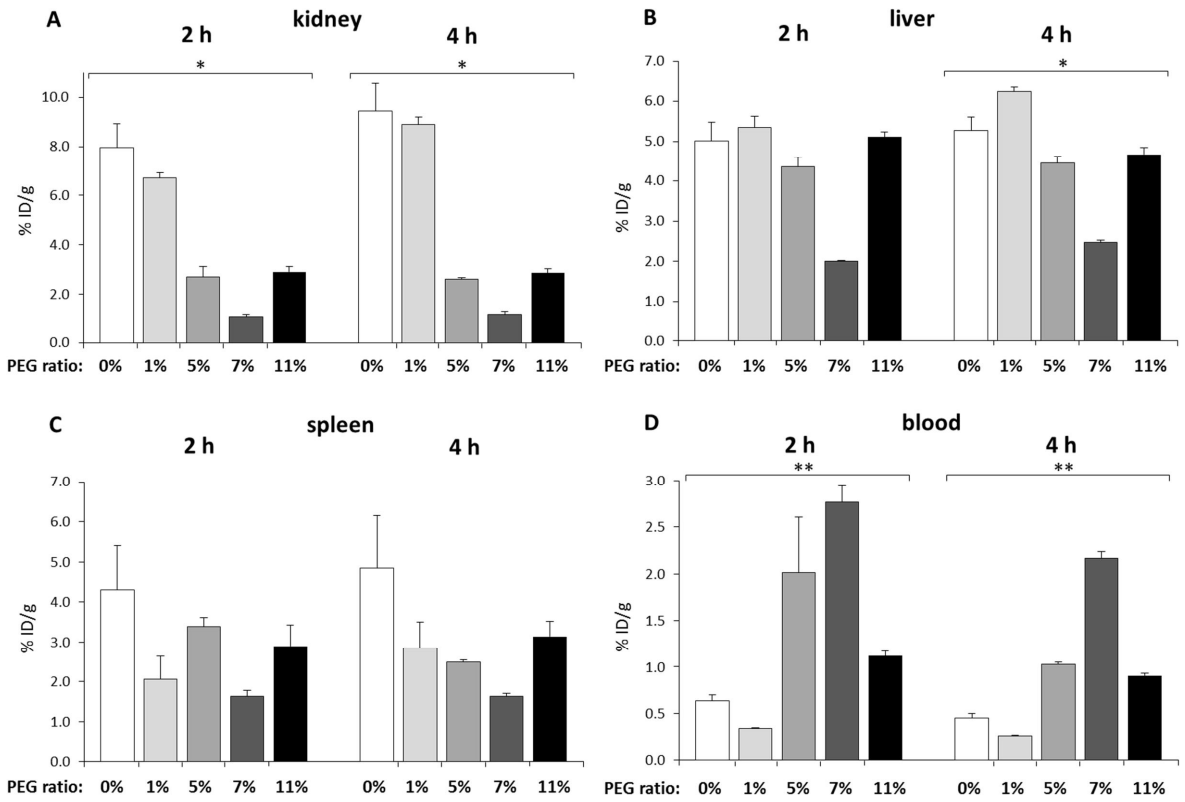

Figure 2: Biodistribution of polymer structures $P_{0\%}$ to $P_{11\%}$, in selected organs (kidney, liver, spleen and blood) 2 and 4 hours p.i. n=2-6, (*) p<0.05, (**) p<0.01.

Table 3: Polymer uptake in different organs expressed by the fraction of the injected dose (ID) of the polymer per gram tissue 2 h after i.v. injection. n=2-6

	polymer concentration [%ID/g tissue]				
organ	0% PEG	1% PEG	5% PEG	7% PEG	11% PEG
lung	0.39±0.06	0.23±0.01	0.74±0.18	1.15±0.01	0.89±0.26
liver	5.01±0.47	5.34±0.29	4.37±0.23	2.01±0.01	5.11±0.13
spleen	4.30±1.10	2.06±0.57	3.39±0.51	1.64±0.15	2.90±0.52
kidney	7.95±0.96	6.72±0.22	2.71±0.41	1.09±0.11	2.91±0.20
muscle	0.07±0.01	0.04±0.01	0.10±0.03	0.05±0.01	0.07±0.01
heart	0.22±0.03	0.11±0.01	0.39±0.08	0.61±0.01	0.31±0.03
blood	0.63±0.07	0.34±0.01	2.01±0.59	2.76±0.18	1.12±0.05
small intestine	0.23±0.02	0.14±0.01	0.22±0.02	0.25±0.05	0.31±0.06
testis	0.10±0.01	0.07±0.01	0.19±0.03	0.19±0.01	0.17±0.01

Interestingly, polymer $P_{7\%}$ which exhibited lowest kidney elimination also showed lowest liver (Fig. 2B; 2.47±0.06 %ID/g tissue) and spleen uptake (Fig. 2C; 1.64±0.07 %ID/g tissue) over a time span of 4 hours, thereby combining favorable characteristics for the application as polymeric nanocarrier

in vivo. However, it has to be noticed that the hepatic or splenic uptake only slightly depends (not statistically significant) on the PEGylation of the polymer. Probably as a result of the differences seen in renal excretion and liver uptake, PEGylation plays an important role for the blood level of the polymers (Fig. 2D, Tab. 3). An augmentation in PEG content resulted in an almost linear increase of polymer concentration in the blood (r=0.878). Only the polymer containing 11% of PEG_{2000} segments showed lower levels. This correlation could either be the result of reduced renal excretion of PEGylated polymers or maybe caused by differences in polymer binding to plasma proteins which should be analyzed in further studies These findings stay in good correlation to investigations of Torchilin et al., showing that a higher percentage of PEG-content led to an improved plasma half-life of "stealth" liposomes in mice [49]. Nevertheless, there seems to be a limit of PEGylation efficacy as demonstrated for decreasing blood values of block copolymer $P_{11\%}$ (0.90±0.02 %ID/g tissue after 4 h). In general, blood levels of all polymers decreased over the prolonged observation time of 4 h (Fig. 2D) indicating the ongoing excretion of the polymers, presumably by the kidney (Fig. 2A). Highly blood supplied organs such as heart and lung directly reflect the blood concentration pattern – exhibiting a minimum level of block copolymer $P_{1\%}$ and highest values for $P_{7\%}$ (see Tab. 3 and Fig./Tab. S1 supporting info). In addition to these findings, polymer accumulation in muscle, small intestine and testis was comparatively low, not demonstrating great differences between the five examined block copolymers varying in PEG_{2000} incorporation efficiencies (cf. Tab. S1 supporting info).

Tumor accumulation

For analysis of the polymer uptake *in vivo* Walker 256 mammary carcinomas were used with a volume of 1.46±0.16 mL. Quantitative biodistribution studies of the tumor tissue were accomplished 2 and 4 h post-injection of the polymer compounds. The dependency of PEGylation on the %ID/g tumor is depicted in Figure 3.

Based on these results, a direct correlation between PEG_{2000} incorporation ratio and tumor uptake can be drawn ($r = 0.834$ and $r = 0.780$, respectively). Even though organ distribution studies (see Figure 2) revealed most favorable characteristics for block copolymer $P_{7\%}$, including highest blood retention and low renal clearance, the tumor data demonstrate a gradual increase in tumor uptake with ascending PEG content. In this regard, the block copolymer with highest PEG level ($P_{11\%}$) also achieved highest tumor uptake – despite lower blood levels compared to $P_{7\%}$. As expected, tumor accumulation is not solely affected by the retention of the polymers in the circulation.

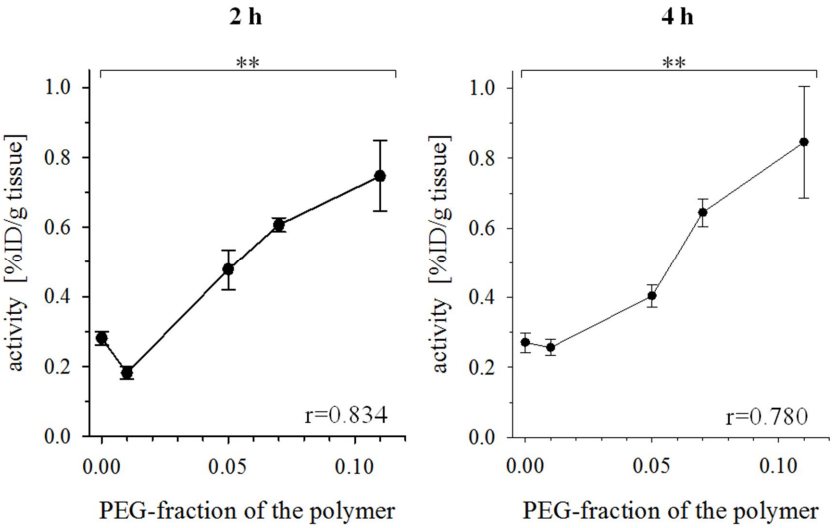

Figure 3: Tumor accumulation of polymers as a function of the incorporated amount of PEG_{2000}. n=4-6, (**) p<0.01.

Analyzing the tumor accumulation of the polymers after 4 hours revealed a similar pattern versus the time point of 120 min. An almost linear correlation between the amount of PEGylation and tumor uptake could be seen. Notably – despite a decrease in blood levels of all polymers after 4 h (Fig. 2) – tumor uptake was even increasing in the tumor tissue. This observation indicated that tumor accumulation is not only the result of a passive redistribution between the blood compartment and the tumor tissue.

MicroPET imaging studies in Walker 256 carcinoma bearing rats

Besides quantification of organ accumulation – clearly demonstrating a correlation of PEGylation on organ distribution and tumor uptake *ex vivo* – both static and dynamic µPET studies were accomplished. Whole-body µPET images (Fig. 4), acquired 2 h post injection, stay in good accordance to the distribution data obtained in major organs (Fig. 2). PET images reveal kidney and bladder accumulation for all block copolymers hence confirming renal clearance. Furthermore, PET studies clearly displayed the disparities regarding blood circulation lifetimes according to different degrees of PEG incorporation. Whereas neither heart nor aorta are displayed in case of $P_{0\%}$ and $P_{1\%}$, PET images of block copolymers exhibiting higher PEG content ($P_{5\%}$, $P_{7\%}$, $P_{11\%}$) explicitly show remaining activity in the blood compartment. This observation is illustrating the enhanced circulation of PEGylated block copolymers in the blood pool which is essential for effective drug delivery (in corresponding with the *ex vivo* biodistribution data, Fig. 2).

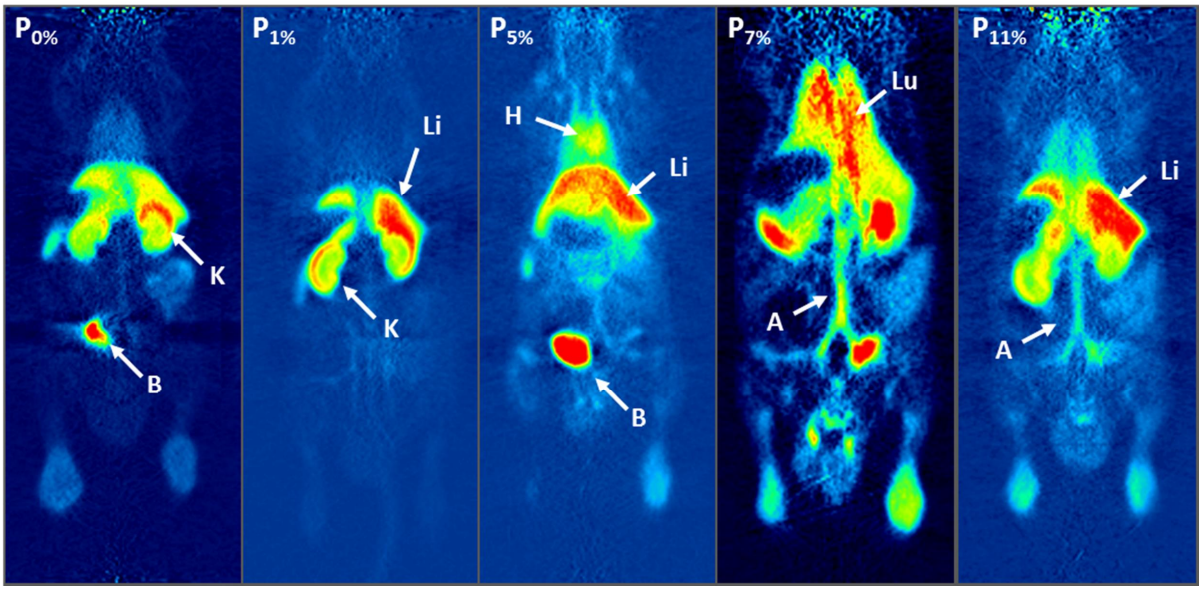

Figure 4: Whole body µPET image sections obtained 120-135 min after administration of ^{18}F-polymers showing renal clearance (kidney (K), bladder (B)), distribution in liver (Li) and lung (Lu) as well as enhanced blood retention (heart (H), aorta (A)) of PEGylated polymers.

Based on the findings regarding enhanced tumor accumulation with increasing PEGylation, the uptake of PEG modified block copolymers in the Walker 256 carcinoma was furthermore studied using dynamic µPET imaging over the course of 2 h after i.v. injection. Coronal slices of summed µPET images through the tumors – implanted at the hind food dorsum – (Fig. 5) clearly display polymer uptake for all ^{18}F-labeled polymers.

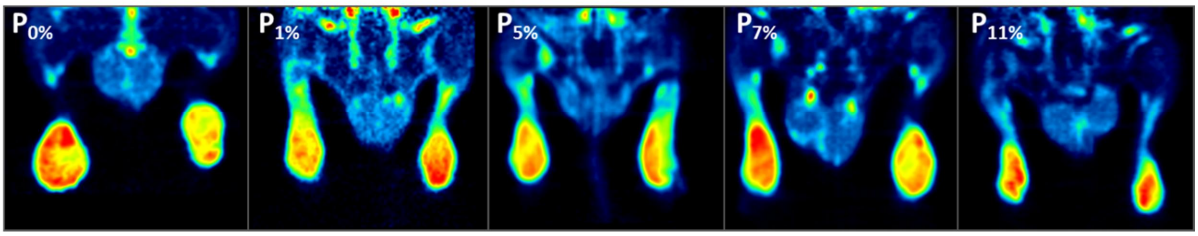

Figure 5: Examples of coronal µPET image sections of Walker 256 tumors 60-120 min after i.v. administration of polymers with varying PEG content illustrating tumor accumulation.

Finally the question arises how the observed disparities in tumor accumulation can be explained. Despite the differences in long term blood concentration of the polymers (seen in the biodistribution experiments, Fig. 2) which may increase the diffusive intratumoral extravasation of the highly PEGylated polymers, the uptake of polymers into the tumor cells might be responsible. Due to this assumption, we additionally investigated the cellular uptake of the presented polymers into Walker 256 cells *in vitro*. Fig. 6 clearly indicates pronounced differences between the block polymers. However, in contrast to the *in vivo* data, the cellular uptake was highest for non- and low PEGylated

polymers ($P_{0\%}$ and $P_{1\%}$) whereas the highly PEGylated compounds showed a distinct lower intracellular accumulation. Another reason for the observed disparities in tumor uptake *in vivo* could be the vascular permeability, since the hydrodynamic radii were markedly different. Polymer structures around an R_h of 50 nm demonstrate most effective tumor enrichment thus staying in good accordance with studies suggesting this radius as suitable limit for nanoparticles regarding cancer therapy [50-52]. Presumably a combination of the increased blood levels together with the reduction of hydrodynamic radius seems to be responsible for the tumor accumulation of the highly PEGylated polymers.

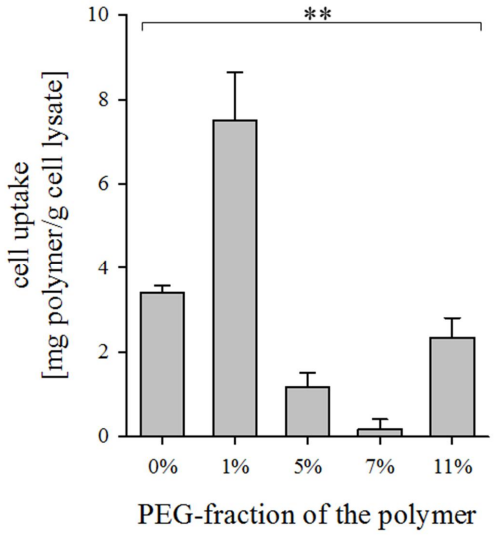

Figure 6: Cellular uptake of the polymers after 2 h incubation at 37°C in Walker 256 carcinoma cells in vitro; n=6, (*) p<0.05.

Conclusion

The present study clearly demonstrates that a controlled modification of HPMA-LMA block copolymers by means of PEGylation has a tremendous impact on their pharmacokinetic profile *in vivo*. Radiolabeling of polymers with positron emitting isotopes such as fluorine-18 in combination with non-invasive Positron Emission Tomography (PET) imaging enables to monitor their biodistribution pattern, particularly regarding tumor accumulation, in a quantitative way. By means of these techniques, we could observe that the degree of PEGylation of block copolymers was responsible for severe disparities in their biodistribution characteristics. Block copolymers with low amounts of PEG_{2000} side chains – exhibiting highest hydrodynamic radii – showed major kidney and RES uptake. Blood retention as well as tumor accumulation was comparatively low. In contrast, higher PEG content caused prolonged blood circulation times of the HPMA-based block copolymers,

even resulting in a linear trend of tumor accumulation with increased PEGylation efficacy. Interestingly, $P_{7\%}$ exhibited most favorable *in vivo* characteristics – including lowest hepatic and splenic uptake as well as highest blood pool concentration 4 h p.i. – but nevertheless $P_{11\%}$ was the block copolymer with highest tumor accumulation in the Walker 256 mammary carcinoma over time. So far, there seems to be a general dependency of polymer size combined with the degree of PEGylation on resulting tumor uptake. This correlation has to be further examined but in general it opens the discussion of selectively induce smaller block copolymer sizes by systematic PEG incorporation to fine-tune them for efficient anticancer therapy. In contrast to the obtained *in vivo* results, an opposite trend could be observed for the *in vitro* studies on this tumor cell line. Notably, in this case highest cellular uptake was determined for non- or low PEGylated compounds. These results clearly indicate that *in vitro* studies cannot be directly transferred to the *in vivo* situation. In particular they underline the importance of (non-invasive) *in vivo* techniques for assessing the intratumoral polymer uptake in order to tailor polymer based (chemo) therapy to the patient needs. Furthermore the herein presented approach emphasizes the versatility of selective PEGylation of amphiphilic block copolymers helping to improve their pharmacokinetic profiles and thus designing potential polymeric drug carrier systems for anticancer treatment.

Acknowledgement

The authors would like to thank Nicole Bausbacher, Barbara Biesalski and Bengü Yilmaz for their support during animal studies and following interpretation. We also want to thank the Max-Planck Graduate Center (MPGC, M. Allmeroth) as well as the Graduate School Materials Science in Mainz (Excellence Initiative, DFG/GSC 266, D. Moderegger) for financial support. In addition the authors are very thankful for financial support of the DFG (Rösch: RO 985/30-1; Thews: TH 482/4-1, Zentel: ZE 230/21-1) and SAMT Initiative Mainz.

References

[1] R. Duncan, The dawning era of polymer therapeutics. *Nat Rev Drug Discov* 2(5) (2003) 347-360.

[2] Y. Matsumura, H. Maeda, A New Concept for Macromolecular Therapeutics in Cancer Chemotherapy: Mechanism of Tumoritropic Accumulation of Proteins and the Antitumor Agent Smancs. *Cancer Research* 46 (12 Part 1) (1986) 6387-6392.

[3] H. Maeda, J. Wu, T. Sawa, Y. Matsumura, K. Hori, Tumor vascular permeability and the EPR effect in macromolecular therapeutics: a review. *Journal of Controlled Release* 65(1-2) (2000) 271-284.

[4] K. Ulbrich, V. Subr, Structural and chemical aspects of HPMA copolymers as drug carriers. *Advanced Drug Delivery Reviews* 62(2) (2010) 150-166.

[5] R. Duncan, L.W. Seymour, K.B. O'Hare, P.A. Flanagan, S. Wedge, I.C. Hume, K. Ulbrich, J. Strohalm, V. Subr, F. Spreafico, M. Grandi, M. Ripamonti, M. Farao, A. Suarato, Preclinical evaluation of polymer-bound doxorubicin. *Journal of Controlled Release* 19(1-3) (1992) 331-346.

[6] M.V. Pimm, A.C. Perkins, J. Strohalm, K. Ulbrich, R. Duncan, Gamma Scintigraphy of the Biodistribution of ^{123}I-Labelled *N*-(2-Hydroxypropyl)methacrylamide Copolymer-Doxorubicin Conjugates in Mice with Transplanted Melanoma and Mammary Carcinoma. *Journal of Drug Targeting* 3(5) (1996) 375-383.

[7] R. Duncan, Development of HPMA copolymer-anticancer conjugates: Clinical experience and lessons learnt. *Advanced Drug Delivery Reviews* 61(13) (2009) 1131-1148.

[8] T. Lammers, V. Subr, K. Ulbrich, W.E. Hennink, G. Storm, F. Kiessling, Polymeric nanomedicines for image-guided drug delivery and tumor-targeted combination therapy. *Nano Today* 5(3) (2010) 197-212.

[9] T. Minko, P. Kopecková, V. Pozharov, J. Kopecek, HPMA copolymer bound adriamycin overcomes MDR1 gene encoded resistance in a human ovarian carcinoma cell line. *Journal of Controlled Release* 54(2) (1998) 223-233.

[10] D.P. Nowotnik, E. Cvitkovic, ProLindac(TM) (AP5346): A review of the development of an HPMA DACH platinum Polymer Therapeutic. *Advanced Drug Delivery Reviews* 61(13) (2009) 1214-1219.

[11] A. Abuchowski, T. van Es, N.C. Palczuk, F.F. Davis, Alteration of immunological properties of bovine serum albumin by covalent attachment of polyethylene glycol. *Journal of Biological Chemistry* 252(11) (1977) 3578-3581.

[12] R. Gref, A. Domb, P. Quellec, T. Blunk, R.H. Müller, J.M. Verbavatz, R. Langer, The controlled intravenous delivery of drugs using PEG-coated sterically stabilized nanospheres. *Advanced Drug Delivery Reviews* 16(2-3) (1995) 215-233.

[13] J.M. Harris, R.B. Chess, Effect of pegylation on pharmaceuticals. *Nat Rev Drug Discov* 2(3) (2003) 214-221.

[14] G. Pasut, F.M. Veronese, Polymer-drug conjugation, recent achievements and general strategies. *Progress in Polymer Science* 32(8-9) (2007) 933-961.

[15] G. Pasut, F.M. Veronese, PEG conjugates in clinical development or use as anticancer agents: An overview. *Advanced Drug Delivery Reviews* 61(13) (2009) 1177-1188.

[16] M.J. Joralemon, S. McRae, T. Emrick, PEGylated polymers for medicine: from conjugation to self-assembled systems. *Chemical Communications* 46(9) (2010) 1377-1393.

[17] M.D. Howard, M. Jay, T.D. Dziubla, X. Lu, PEGylation of Nanocarrier Drug Delivery Systems: State of the Art. *Journal of Biomedical Nanotechnology* 4(2) (2008) 133-148.

[18] A.S. Karakoti, S. Das, S. Thevuthasan, S. Seal, PEGylated Inorganic Nanoparticles. Angewandte Chemie International Edition 50(9) (2011) 1980-1994.

[19] D.E. Owens Iii, N.A. Peppas, Opsonization, biodistribution, and pharmacokinetics of polymeric nanoparticles. *International Journal of Pharmaceutics* 307(1) (2006) 93-102.

[20] M. Allmeroth, D. Moderegger, B. Biesalski, K. Koynov, F. Rösch, O. Thews, R. Zentel, Modifying the Body Distribution of HPMA-Based Copolymers by Molecular Weight and Aggregate Formation. *Biomacromolecules* 12(7) (2011) 2841-2849.

[21] M. Barz, R. Luxenhofer, R. Zentel, A.V. Kabanov, The uptake of *N*-(2-hydroxypropyl)-methacrylamide based homo, random and block copolymers by human multi-drug resistant breast adenocarcinoma cells. *Biomaterials* 30(29) (2009) 5682-5690.

[22] K. Kataoka, A. Harada, Y. Nagasaki, Block copolymer micelles for drug delivery: design, characterization and biological significance. *Advanced Drug Delivery Reviews* 47(1) (2001) 113-131.

[23] M. Talelli, C.J.F. Rijcken, C.F. van Nostrum, G. Storm, W.E. Hennink, Micelles based on HPMA copolymers. *Advanced Drug Delivery Reviews* 62(2) (2010) 231-239.

[24] G. Gaucher, M.-H. Dufresne, V.P. Sant, N. Kang, D. Maysinger, J.-C. Leroux, Block copolymer micelles: preparation, characterization and application in drug delivery. *Journal of Controlled Release* 109(1-3) (2005) 169-188.

[25] K. Matyjaszewski, J. Xia, Atom Transfer Radical Polymerization. *Chemical Reviews* 101(9) (2001) 2921-2990.

[26] C.W. Scales, Y.A. Vasilieva, A.J. Convertine, A.B. Lowe, C.L. McCormick, Direct, Controlled Synthesis of the Nonimmunogenic, Hydrophilic Polymer, Poly(*N*-(2-hydroxypropyl)methacrylamide) via RAFT in Aqueous Media. *Biomacromolecules* 6(4) (2005) 1846-1850.

[27] J. Chiefari, Y.K. Chong, F. Ercole, J. Krstina; J. Jeffery, T.P.T. Le, R.T.A. Mayadunne, G.F. Meijs, C.L. Moad, G. Moad, E. Rizzardo, S.H. Thang, Living Free-Radical Polymerization by Reversible Addition-Fragmentation Chain Transfer: The RAFT Process. *Macromolecules* 31 (1998) 5559-5562.

[28] E.R.G. Moad, S.H. Thang, Living Radical Polymerization by the RAFT process. *Aust. J. Chem*. 58 (2005) 379-410.

[29] M. Eberhardt, R. Mruk, R. Zentel, P. Théato, Synthesis of pentafluorophenyl(meth)acrylate polymers: New precursor polymers for the synthesis of multifunctional materials. *European Polymer Journal* 41(7) (2005) 1569-1575.

[30] M.A. Gauthier, M.I. Gibson, H.-A. Klok, Synthesis of Functional Polymers by Post-Polymerization Modification. *Angewandte Chemie International Edition* 48(1) (2009) 48-58.

[31] T. Lammers, Improving the efficacy of combined modality anticancer therapy using HPMA copolymer-based nanomedicine formulations. *Advanced Drug Delivery Reviews* 62(2) (2010) 203-230.

[32] B. Hoang, H. Lee, R.M. Reilly, C. Allen, Noninvasive Monitoring of the Fate of ^{111}In-Labeled Block Copolymer Micelles by High Resolution and High Sensitivity MicroSPECT/CT Imaging. *Molecular Pharmaceutics* 6(2) (2009) 581-592.

[33] Z.-R. Lu, Molecular imaging of HPMA copolymers: Visualizing drug delivery in cell, mouse and man. *Advanced Drug Delivery Reviews* 62(2) (2010) 246-257.

[34] Y. Zhang, Y. Sun, X. Xu, X. Zhang, H. Zhu, L. Huang, Y. Qi, Y.-M. Shen, Synthesis, Biodistribution, and Microsingle Photon Emission Computed Tomography (SPECT) Imaging Study of Technetium-99m Labeled PEGylated Dendrimer Poly(amidoamine) (PAMAM)-Folic Acid Conjugates. *Journal of Medicinal Chemistry* 53(8) (2010) 3262-3272.

[35] M. Kissel, P. Peschke, V. Subr, K. Ulbrich, A. Strunz, R. Kühnlein, J. Debus, E. Friedrich, Detection and cellular localisation of the synthetic soluble macromolecular drug carrier pHPMA. *European Journal of Nuclear Medicine and Molecular Imaging* 29(8) (2002) 1055-1062.

[36] Z. Yang, S. Zheng, W.J. Harrison, J. Harder, X. Wen, J.G. Gelovani, A. Qiao, C. Li, Long-Circulating Near-Infrared Fluorescence Core-Cross-Linked Polymeric Micelles: Synthesis, Characterization, and Dual Nuclear/Optical Imaging. *Biomacromolecules* 8(11) (2007) 3422-3428.

[37] H. Xie, Z.J. Wang, A. Bao, B. Goins, W.T. Phillips, In vivo PET imaging and biodistribution of radiolabeled gold nanoshells in rats with tumor xenografts. *International Journal of Pharmaceutics* 395(1-2) (2010) 324-330.

[38] G. Sun, A. Hagooly, J. Xu, A.M. Nyström, Z. Li, R. Rossin, D.A. Moore, K.L. Wooley, M.J. Welch, Facile, Efficient Approach to Accomplish Tunable Chemistries and Variable Biodistributions for Shell Cross-Linked Nanoparticles. *Biomacromolecules* 9(7) (2008) 1997-2006.

[39] X. Sun, R. Rossin, J.L. Turner, M.L. Becker, M.J. Joralemon, M.J. Welch, K.L. Wooley, An Assessment of the Effects of Shell Cross-Linked Nanoparticle Size, Core Composition, and Surface PEGylation on in Vivo Biodistribution. *Biomacromolecules* 6(5) (2005) 2541-2554.

[40] K.-i. Fukukawa, R. Rossin, A. Hagooly, E.D. Pressly, J.N. Hunt, B.W. Messmore, K.L. Wooley, M.J. Welch, C.J. Hawker, Synthesis and Characterization of Core-Shell Star Copolymers for In Vivo PET Imaging Applications. *Biomacromolecules* 9(4) (2008) 1329-1339.

[41] M.M. Herth, M. Barz, M. Jahn, R. Zentel, F. Rösch, $^{72/74}$As-labeling of HPMA based polymers for long-term in vivo PET imaging. *Bioorganic & Medicinal Chemistry Letters* 20(18) (2010) 5454-5458.

[42] M.M. Herth, M. Barz, D. Moderegger, M. Allmeroth, M. Jahn, O. Thews, R. Zentel, F. Rösch, Radioactive Labeling of Defined HPMA-Based Polymeric Structures Using [^{18}F]FETos for In Vivo Imaging by Positron Emission Tomography. *Biomacromolecules* 10(7) (2009) 1697-1703.

[43] P. Workman, E.O. Aboagye, F. Balkwill, A. Balmain, G. Bruder, D.J. Chaplin, J.A. Double, J. Everitt, D.A.H. Farningham, M.J. Glennie, L.R. Kelland, V. Robinson, I.J. Stratford, G.M. Tozer, S. Watson, S.R. Wedge, S.A. Eccles, Guidelines for the welfare and use of animals in cancer research. *British Journal of Cancer* 102(11) (2010) 1555-1577.

[44] P. Theato, Synthesis of well-defined polymeric activated esters. *Journal of Polymer Science Part A: Polymer Chemistry* 46(20) (2008) 6677-6687.

[45] R. Gref, M. Lück, P. Quellec, M. Marchand, E. Dellacherie, S. Harnisch, T. Blunk, R.H. Müller, "Stealth" corona-core nanoparticles surface modified by polyethylene glycol (PEG): influences of the corona (PEG chain length and surface density) and of the core composition on phagocytic uptake and plasma protein adsorption. *Colloids and Surfaces B: Biointerfaces* 18 (3-4) (2000) 301-313.

[46] H. Lee, R.G. Larson, Effects of PEGylation on the Size and Internal Structure of Dendrimers: Self-Penetration of Long PEG Chains into the Dendrimer Core. *Macromolecules* 44(7) (2011) 2291-2298.

[47] F. Alexis, E. Pridgen, L.K. Molnar, O.C. Farokhzad, Factors Affecting the Clearance and Biodistribution of Polymeric Nanoparticles. *Molecular Pharmaceutics* 5(4) (2008) 505-515.

[48] M.E. Fox, F.C. Szoka, J.M.J. Fréchet, Soluble Polymer Carriers for the Treatment of Cancer: The Importance of Molecular Architecture. *Accounts of Chemical Research* 42(8) (2009) 1141-1151.

[49] V.P. Torchilin, V.G. Omelyanenko, M.I. Papisov, A.A. Bogdanov Jr, V.S. Trubetskoy, J.N. Herron, C.A. Gentry, Poly(ethylene glycol) on the liposome surface: on the mechanism of polymer-coated liposome longevity. *Biochimica et Biophysica Acta (BBA) - Biomembranes* 1195(1) (1994) 11-20.

[50] M.R. Dreher, W. Liu, C.R. Michelich, M.W. Dewhirst, F. Yuan, A. Chilkoti, Tumor Vascular Permeability, Accumulation, and Penetration of Macromolecular Drug Carriers. *Journal of the National Cancer Institute* 98(5) (2006) 335-344.

[51] J.A. Barreto, W. O'Malley, M. Kubeil, B. Graham, H. Stephan, L. Spiccia, Nanomaterials: Applications in Cancer Imaging and Therapy. *Advanced Materials* 23(12) (2011) H18-H40.

[52] Y.M. H. Cabral, K. Mizuno, Q. Chen, M. Murakami, M. Kimura, Y. Terada, M.R. Kano, K. Miyazono, M. Uesaka, N. Nishiyama & K. Kataoka, Accumulation of sub-100 nm polymeric micelles in poorly permeable tumours depends on size. *Nature Nanotechnology* 6 (2011) 815-823.

Supplementary information

PEGylation of HPMA-based block copolymers enhances tumor accumulation *in vivo*: A quantitative study using radiolabeling and Positron Emission Tomography

Mareli Allmeroth, Dorothea Moderegger, Daniel Gündel, Hans-Georg Buchholz, Kaloian Koynov, Frank Rösch, Oliver Thews and Rudolf Zentel

Contents

1. Experimental Section

I. Experimental setup

^{1}H-NMR spectra were obtained by a Bruker AC 300 spectrometer at 300 MHz, ^{19}F-NMR analysis was carried out with a Bruker DRX-400 at 400 MHz. All measurements were accomplished at room temperature and spectroscopic data were analyzed using ACDLabs 9.0 1D NMR Manager. The synthesized polymers were dried at 40 °C under vacuum over night, followed by Gel Permeation Chromatography (GPC). GPC was performed in tetrahydrofuran (THF) as solvent, using following equipment: pump PU 1580, autosampler AS 1555, UV detector UV 1575 and RI detector RI 1530 from Jasco as well as a miniDAWN Tristar light scattering detector from Wyatt. Columns were used from MZ Analysentechnik, 300x8.0 mm: MZ-Gel SDplus 10^{6} Å 5 µm, MZ-Gel SDplus 10^{4} Å 5 µm and MZ-Gel SDplus 10^{2} Å 5 µm. GPC data were evaluated by using the software PSS WinGPC Unity from Polymer Standard Service Mainz. The flow rate was set to 1 mL/min with a temperature of 25 °C.

Synthesis of 2-[^{18}F]fluoroethyl-1-tosylate ([^{18}F]FETos), was performed using a homemade automated synthesis module including a Knauer K-501 pump, a Knauer K-2501 UV-detector (Herbert Knauer GmbH, Berlin, Germany) and a radiodetector connected in series. HPLC purification was accomplished using a LiChrospher RP-18 EC 5µ (250 x 10 mm) (50:50 water-acetonitrile at 5 mL/min). ^{18}F-labeled polymers were isolated using a chromatographic system consisting of a waters pump (1500 series), a Waters UV-detector (2487 λ absorbance detector), a Berthold LB 509 radio detector and a HiTrap™ Desalting Column, Sephadex G-25 Superfine.

Recovered radioactive doses were determined using a Perkin Elmer 2470 Wizard^{2} γ-counter.

II. Synthesis of 4-cyano-4-((thiobenzoyl)sulfanyl)pentanoic acid (CTP)

4-cyano-4-((thiobenzoyl)sulfanyl)pentanoic acid was used as chain transfer agent (CTA) and synthesized according to the literature [1].

III. Synthesis of pentafluorophenyl methacrylate (PFPMA)

Pentafluorophenyl methacrylate was prepared according to reference [2].

IV. Synthesis of reactive ester homopolymers (macro-CTA)

RAFT polymerization of pentafluorophenyl methacrylate with 4-cyano-4-((thiobenzoyl) sulfanyl)pentanoic acid was carried out in a schlenk tube [3, 4]. For this purpose, 4 g of PFPMA were dissolved in 5 mL of absolute dioxane, furthermore CTP and AIBN were added. The molar ratio of

CTP/AIBN was chosen 1:8. After three freeze-vacuum-thaw cycles, the mixture was immersed in an oil bath at 65 °C and stirred over night. Afterwards, the polymeric solution was precipitated three times in hexane, centrifuged and dried under vacuum at 40 °C over night. A slightly pink powder was obtained. Yield: 52%. ^{1}H-NMR (300 MHz, $CDCl_3$) δ/ ppm: 1.20-1.75 (br), 2.00-2.75 (br s). ^{19}F-NMR (400 MHz, $CDCl_3$) δ/ ppm: -162.03 (br), -156.92 (br), -152 to -150 (br).

V. Synthesis of reactive ester block copolymers

The macro-CTA obtained after homopolymerization of PFPMA was dissolved in dioxane, afterwards lauryl methacrylate as well as AIBN were added. As an example, 250 mg of macro initiator were dissolved in 5 mL dioxane, lauryl methacrylate and AIBN (1:8 ratio macro-CTA/AIBN) were mixed. After three freeze-vacuum-thaw cycles, the mixture was immersed in an oil bath at 65 °C and stirred for three days. Afterwards, poly(PFPMA)-*b*-poly(LMA) was precipitated three times in ethanol, centrifuged and dried under vacuum at 40 °C over night. A slightly pink powder was obtained. Yield: 54%. ^{1}H-NMR (300 MHz, $CDCl_3$) δ/ ppm: 0.84 (br t), 1.20-1.75 (br), 2.00-2.75 (br s). ^{19}F-NMR (400 MHz, $CDCl_3$) δ/ ppm: -162.01 (br), -156.95 (br), -152 to -150 (br).

VI. Removal of dithioester endgroups

The dithiobenzoate endgroup was removed using the protocol reported by Perrier et al. 2005 [5]. Therefore a 25-fold molar excess of AIBN was added to the polymer dissolved in dioxane. After four hours of heating the solution in an oil bath at 70 °C, the polymer was precipitated twice in hexane and collected by centrifugation. The polymer was dried under vacuum over night, a colorless powder was obtained. Yield: 75%. Removal of the dithioester endgroup could be proven by UV-Vis spectroscopy.

VII. Synthesis of amine functionalized PEG_{2000} fragment

To synthesize the PEG_{2000}-amine fragment, a modified two step synthesis was accomplished [6]. For the first step as example, 50 g of mPEG2k (n = 0.025 mol) were dissolved in 250 mL of toluene. The PEG solution in toluene was azeotropically dried by distilling off 125 mL of solvent. Afterwards the solution was cooled to room temperature and 100 mL of anhydrous dichloromethane were added. Subsequent, the solution was cooled to 0-5 °C and 3.66 mL (n= 0.0362 mol) of triethylamine as well as 3.72 mL of methanesulfonyl chloride (n= 0.032 mol) were dropwise added *via* a rubber septa. The mixture was stirred for 2 hours at ca. 4 °C and then stirred at room temperature over night under argon gas. The next morning the mixture was concentrated on a rotary evaporator and filtered through a coarse glass frit (glass frit should be heated up to prevent solidifying). Precipitation of the

product was carried out with approx. 500 mL of a mixture (30:70 v/v) of cold isopropyl alcohol and diethyl ether. The product was collected and dried under vacuum over night to give 34.61 g (67% yield) of a white powder. ^{1}H-NMR (300 MHz, $CDCl_3$) δ/ ppm: 3.05 (s), 3.34 (t), 3.61 (br t), 4.35 (t). For the second step, a 1-L, round-bottom flask equipped with a magnetic stirrer as well as a nitrogen inlet bubbler was charged with 3 g of mPEG 2 kDa mesylate (n= 0.0015 mol) and 900 mL of ammonium hydroxide aqueous solution (30% v/v). To this solution 90 mg of ammonium chloride was added. The solution was warmed carefully to dissolve all of the PEG mesylate. The solution was stirred at room temperature for 5 days while venting excess gases through a bubbler to prevent pressure buildup. After completion of the reaction, 80 g of sodium chloride were added and the mixture was 4 times extracted with 200 mL of dichloromethane. The combined organic extracts were dried over sodium sulfate for 1 h, filtered and evaporated (not completely). Precipitation was carried out by addition of 900 mL of cold diethyl ether, filtered and dried under vacuum over night. Yield: 2.14 g (67%) of a white powder. ^{1}H-NMR (300 MHz, $CDCl_3$) δ/ ppm: 2.92 (t), 3.35 (t), 3.61 (br t), 3.85 (t).

VIII. Polymer analogous reaction of block copolymers

For radioactive labeling of block copolymers the protocol was applied as follows. 100 mg of poly(PFPMA)-*b*-poly(LMA) copolymer was dissolved in 2 mL of absolute dioxane. Exemplary for $P_{7\%}$ (M_n = 25.000 g/mol), 5.4 mg of tyramine and 4 mg of triethylamine were diluted in a DMSO/dioxane mixture and added to the vessel. After stirring for 10 hours at 45 °C, 160 mg of amine-functionalized PEG_{2k} in 500 µL DMSO as well as 8 mg of triethylamine were added and the solution stirred for 1 ½ days. Thereafter, 21 mg of 2-hydroxypropylamine and 28 mg of Et_3N were added and the solution further stirred for 48 hours. For final removal of reactive ester side groups 20 mg of 2-hydroxypropylamine were additionally added the next morning. The solution was precipitated two times in diethyl ether, centrifuged and finally dissolved in a DMSO/water solution for dialysis. After lyophilization a white, crystalline powder could be obtained. Yield: 51%. ^{1}H-NMR (400 MHz, d. DMSO) δ/ ppm: 0.70-0.90 (br), 0.90-1.40 (br), 1.40-1.90 (br), 2.75-3.10 (br), 3.20-3.25 (s), 3.45-3.55 (br), 3.65-3.85 (br), 4.50-4.75 (br), 6.60-6.75 (br) and 6.85-7.00 (br). For additional fluorescent labeling, 100 mg of polymeric precursor were diluted in 2 mL of absolute dioxane and 2.9 mg of Oregon Green 488 cadaverine were added. Afterwards tyramine, $PEG\text{-}amine_{2kDa}$ and 2-hydroxypropylamine were added, as described by the procedure above.

IX. Size determination by Fluorescence Correlation Spectroscopy (FCS)

The hydrodynamic radii of the polymeric systems were determined by Fluorescence Correlation Spectroscopy using a commercial FCS setup (Zeiss, Germany) consisting of the module ConfoCor 2 and an inverted microscope model Axiovert 200 with a Zeiss C-Apochromat 40 ×/1.2 W water immersion objective. The fluorophores were excited with an Argon laser (λ = 488 nm) and the emission was collected after filtering with a LP505 long pass filter. For detection, an avalanche photodiode, enabling single-photon counting, was used. As sample cell, eight-well, polystyrene-chambered cover glass (Laboratory-Tek, Nalge Nunc International) was applied. For sample preparation, stock solutions of 0.1 mg fluorescently labeled polymer/mL NaCl were applied. The solution was kept at room temperature over night. For reference reason, free Oregon Green 488 cadaverine dye in NaCl-solution was also studied. The calibration of the FCS observation volume was done using a dye with known diffusion coefficient, i.e. Alexa Fluor 488. For each solution, 5 measurement cycles with a total duration of 150 seconds were applied. Time dependant fluctuations of the fluorescence intensity $\delta I(t)$ were detected and evaluated by autocorrelation analysis, yielding the diffusion coefficient and hydrodynamic radius of the fluorescent species [7].

X. Radiolabeling of polymers and purification for ex vivo and in vivo experiments

Radiolabeling of the polymers was accomplished by means of [^{18}F]fluoroethylation using a two-step synthesis procedure modified from [8]. In a first step, the labeling synthon [^{18}F]fluoroethyl tosylate ([^{18}F]FETos) was synthesized using a homemade automated synthesis module. The modular synthesis started with collecting the aqueous [^{18}F]F^- solution (800-6000 MBq) on a SepPak-QMA cartridge (Waters, USA). [^{18}F]F^- was eluted from the cartridge with 15 µL 1M K_2CO_3 solution, 18 mg Kryptofix 2.2.2 (Merck) in 1 mL acetonitrile and residual water was removed by azeotropic drying. To the dried K^+/[^{18}F]F^-/Kryptofix 2.2.2/carbonate complex, 14 mg of 1,2-ethylene ditosylate in 1mL of MeCN were added, and the mixture was heated at 87 °C for 3 min. Purification of the crude product was accomplished using semipreparative HPLC (Lichrospher RP18-EC5, 250 × 10 mm, MeCN/H_2O 1:1 (v/v), flow rate: 5 mL/min, R_t: 8 min). The HPLC fraction of [^{18}F]FETos was diluted with 50 mL of H_2O and collected on a SPE cartridge (Strata X, Phenomenex, USA). After drying in a stream of He, the purified labeling synthon was eluted from the cartridge with 0.9 mL of DMSO yielding [^{18}F]FETos in about 60% decay-corrected RCY after a total synthesis time of 50 min. In order to promote the second step the radioactive labeling procedure, 3 mg of the polymeric labeling precursor were dried azeotropically using acetonitrile (3 x 1 mL) and solved subsequently in 200 µL of dried DMSO. 1 µL of a 5M Cs_2CO_3 solution was added and the clear solution was heated for 1 min at 120 °C. The radiolabeling reaction was started by adding 0.8 mL of [^{18}F]FETos in DMSO to the clear polymer solution and the mixture

was heated for 18 min at 120 °C. After cooling to RT, purification of the ^{18}F-labeled polymer was accomplished using Size Exclusion Chromatography (HiTrap™ Desalting Column, Sephadex G-25 Superfine, 0.9% NaCl solution, flow rate: 0.5 mL/min) leading to a pure, ^{18}F-labeled polymer solution ready for subsequent *ex vivo* and *in vivo* experiments.

XI. Tumor and animal model

Cells lines were grown in culture in RPMI medium supplemented with 10 mM L-glutamine and 10% fetal calf serum (FCS) at 37°C under a humidified 5% CO_2 atmosphere and sub-cultivated twice per week. For tumor implantation male Sprague-Dawley rats (Charles River Wiga, Sulzfeld, Germany; body weight 195 to 315 g) housed in the animal care facility of the University of Mainz were used in this study. Animals were allowed access to food and acidified water ad libitum before the investigations. Solid carcinomas were heterotopically induced by injection of cell suspension (0.4 mL approx. 10^4 cells/µL) subcutaneously into the dorsum of the hind foot. Tumors grew as flat, spherical segments and replaced the subcutis and corium completely. Volumes were determined by measuring the three orthogonal diameters (d) of the tumors and using an ellipsoid approximation with the formula: $V = d_1 \times d_2 \times d_3 \times \pi/6$. Tumors were used when they reached a volume of between 0.5 to 3.0 mL approx. 7 to 14 days after tumor cell inoculation.

XII. In vivo µPET imaging

The µPET imaging was performed on a microPET Focus 120 small animal PET (Siemens/Concorde, Knoxville, USA). Animals were placed supine and breathed room air spontaneously. Dynamic PET studies were acquired in listmode. The radiolabeled polymers were administered as a bolus injection of 0.4-0.7 mL simultaneously with the start of the PET scan. The mean injected activity of labeled polymers was 21.7±2.2 MBq. The PET listmode data were histogrammed into 25 frames and reconstructed using OSEM2D algorithm. Volumes-of-interests (VOIs) were defined for tumor and reference tissue (testis). The testis was used as a reference since it was in the field of view when imaging the tumors on the feet and because the tissue concentration was relatively constant between all animals on a low level. Time activity curves (TAC) were obtained with varying time frames (1.5-10 min) for a total measuring interval of 120 min. Ratios of tumor to reference tissue were calculated from integral images between 15' and 120' after polymer injection.

XIII. Biodistribution and cellular uptake studies

In order to assess the distribution of the radiolabeled polymers in different organs of the animals, the polymer (concentration of 1 mg in 1 mL sodium chloride solution) was injected i.v. in anaesthetized

tumor-bearing rats *via* the tail vein with a mean activity of 11.1 ± 0.4 MBq. After 120 or 240 min, the animals were sacrificed and different organ (kidney, liver, lung, spleen, heart, skeletal muscle, small intestine, testis, blood) and tumor samples were taken. The tissue samples were weighed and minced. Finally, the ^{18}F-activity in the organs was measured in a γ-counter.

Cellular uptake of pure and PEGylated block copolymers into Walker 256 cells was measured *in vitro*. Therefore, the polymeric precursors were labeled with the fluorochrome Oregon-Green 488 cadaverine (see VIII: polymeranalogous reaction of block copolymers). Uptake experiments were performed using collagen-coated 24-well plates. Collagen A (Biochrom, Berlin, Germany) was diluted with water and pH-adjusted (3.5). Plates were incubated for 30 min and dried. Cells were grown until wells reached ~70% confluence when they were incubated with 500 µl HEPES-buffered Ringer solution (pH=7.4) containing 0.02 mg polymer/mL for 2 h at 37°C. After washing, the cells were lysed with 250 µl Triton X-MOPS lysis buffer (15 min, room temperature) and mechanically removed from the plate surface. After centrifugation, 100 µl supernatant was pipetted in 96-well black bottom microplates and analyzed in a microplate-reader (Infinite 200, Tecan, Männedorf, Switzerland; excitation 485 nm, emission 532 nm). Protein content of each sample was determined using Bradford reagent. The polymer uptake was expressed by the content of polymer/per gram cell protein.

2. Tables and Figures

Table S1: Organ distribution 4 hours post injection. Polymer uptake in different organs expressed by the fraction of the injected dose (ID) of the polymer per gram tissue. n=2-3.

4 h p.i.	polymer concentration [%ID/g tissue]				
Organ	$P_{0\%}$	$P_{1\%}$	$P_{5\%}$	$P_{7\%}$	$P_{11\%}$
lung	0.35±0.04	0.21±0.03	0.61±0.08	0.74±0.24	0.62±0.04
liver	5.27±0.35	6.24±0.11	4.45±0.17	2.47±0.06	4.68±0.17
spleen	4.84±1.30	2.84±0.66	2.48±0.06	1.64±0.07	3.14±0.38
kidney	9.45±1.12	8.89±0.29	2.61±0.06	1.20±0.12	2.86±0.18
muscle	0.05±0.01	0.05±0.01	0.07±0.01	0.05±0.01	0.07±0.01
heart	0.15±0.01	0.09±0.01	0.33±0.01	0.52±0.05	0.29±0.01
blood	0.45±0.05	0.26±0.01	1.03±0.02	2.16±0.07	0.90±0.02
small intestine	0.32±0.05	0.15±0.02	0.26±0.01	0.32±0.02	0.29±0.03
testis	0.09±0.01	0.07±0.01	0.17±0.01	0.26±0.02	0.20±0.01

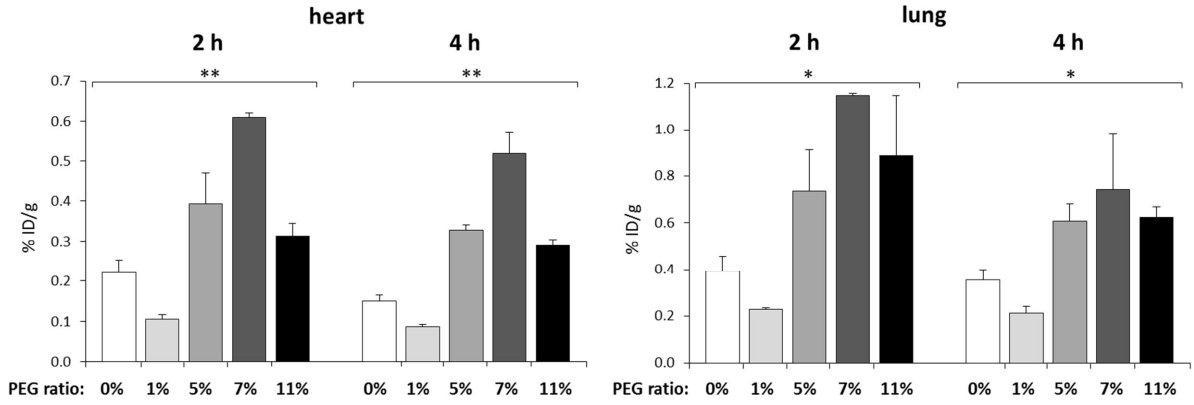

Figure S1: Biodistribution of polymer structures $P_{0\%}$ to $P_{11\%}$, in heart and lung 2 and 4 hours p.i. Uptake is expressed by the fraction of the injected dose (ID) of the polymer per gram tissue. n=2-6, (*) p<0.05, (**) p<0.01.

2. References

[1] E.R. G. Moad, S. H. Thang, Living Radical Polymerization by the RAFT process. *Australian Journal of Chemistry* 58 (2005) 379-410.

[2] M. Eberhardt, R. Mruk, R. Zentel, P. Théato, Synthesis of pentafluorophenyl(meth)acrylate polymers: New precursor polymers for the synthesis of multifunctional materials. *European Polymer Journal* 41(7) (2005) 1569-1575.

[3] P. Theato, Synthesis of well-defined polymeric activated esters. *Journal of Polymer Science Part A: Polymer Chemistry* 46(20) (2008) 6677-6687.

[4] M. Barz, R. Luxenhofer, R. Zentel, A.V. Kabanov, The uptake of N-(2-hydroxypropyl)-methacrylamide based homo, random and block copolymers by human multi-drug resistant breast adenocarcinoma cells. *Biomaterials* 30(29) (2009) 5682-5690.

[5] S.b. Perrier, P. Takolpuckdee, C.A. Mars, Reversible Addition-Fragmentation Chain Transfer Polymerization: End Group Modification for Functionalized Polymers and Chain Transfer Agent Recovery. *Macromolecules* 38(6) (2005) 2033-2036.

[6] Hoffmann-La ROCHE AG, K. Conde-Knape, W. Danho, G. Ehrlich, N. Fotouhi, D.C. Fry, W. Khan, A. Konkar, C.M. Rondinone, J. Swistok, R.A. Taub, J.W. Tilley, NEUROPEPTIDE-2 RECEPTOR-AGONISTS Patent WO/2007/065808 (2007).

[7] R.E. Rigler, E.S., Fluorescence Correlation Spectroscopy. Springer Verlag (New York 2001).

[8] M.M. Herth, M. Barz, D. Moderegger, M. Allmeroth, M. Jahn, O. Thews, R. Zentel, F. Rösch, Radioactive Labeling of Defined HPMA-Based Polymeric Structures Using [^{18}F]FETos for In Vivo Imaging by Positron Emission Tomography. *Biomacromolecules* 10(7) (2009) 1697-1703.

3.6 Fluorine-18 labeling approach for HPMA-based polymers *via* click chemistry

Fluorine-18 labeling approach for HPMA-based polymers *via* click chemistry

Dorothea Moderegger[1], Mareli Allmeroth[2], H. Schieferstein[1], Hans-Georg Buchholz[3], Oliver Thews[4], Rudolf Zentel[2] and Frank Rösch[1]

[1] Institute of Nuclear Chemistry, Johannes Gutenberg University, Fritz-Strassmann-Weg 2, 55128 Mainz, Germany

[2] Institute of Organic Chemistry, Johannes Gutenberg University, Duesbergweg 10-14, 55099 Mainz, Germany

[3] Department of Nuclear Medicine, University Medicine Mainz, Langbenbeckstraße 1, 55131 Mainz, Germany

[4] Institute of Physiology, University Halle, Magdeburger Str. 6, 06097 Halle (Saale) Germany

Abstract

Copolymers of *N*-(2-hydroxypropyl)methacrylamide (HPMA) are promising polymeric drug nanocarrier systems for medical applications especially in the field of anticancer treatment. In terms of efficient drug delivery to the tumor site, the carrier system needs to be carefully designed. To guide design optimization of polymeric drug delivery vehicles toward clinical applications, sufficient knowledge about the *in vivo* behavior is required. Here, positron emission tomography (PET) is a highly valuable molecular imaging technique to assess the pharmacological profile of radiolabeled polymer based drug delivery systems non-invasively *in vivo*. In the present study, a versatile fluorine-18 labeling strategy based on the Cu(I)-catalyzed cycloaddition between alkynes and azides (click reaction) has been translated to a HPMA-based copolymer (P1*, M_w=12 kDa) using the prosthetic labeling synthon [^{18}F]F-PEG$_3$-N$_3$. Preparation of [^{18}F]F-PEG$_3$-N$_3$ was accomplished using automated synthesis and subsequent ^{18}F-labeling of P1* *via* the click reaction was studied to accomplish radiolabeled ^{18}F-P1* in high yields in a total synthesis time of less than 100 min. Although ^{18}F-P1* showed excellent stability *in vitro*, a preliminary small animal study revealed partial metabolic degradation of the ^{18}F-label *in vivo*. A µPET study carried out in a tumor-bearing rat (AT1 prostate carcinoma) showed anticipated renal elimination of the hydrophilic polymer as well as marginal elevated radioactivity levels in AT1 tumors, studied by means of dynamic and static µPET imaging. Regarding the significance of non-invasive *in vivo* imaging tools for preclinical screening of potential drug carrier systems, the successful implementation of an ^{18}F-click labeling approach for HPMA-based polymers presented herein might constitute a promising versatile labeling strategy. This technique is needed in order to use PET imaging of various carrier architectures for guiding their design toward efficient polymer based tumor treatment.

Introduction

Since macromolecular drug delivery systems first appeared in the 1970s, nanomedicine has become a growing field of science concentrating on the development of nano-sized tools for diagnosis, prevention and treatment of diseases [1]. Amongst the array of nanomedical devices, “polymer therapeutics” – comprising polymeric drugs, polymer-drug conjugates, polymer-protein conjugates, polymeric micelles, and polyplexes – have emerged as promising drug delivery vehicles [2-6]. Using macromolecular drug delivery, the pharmacokinetic profile of systemically applied (chemo)therapeutics can be significantly improved. Notably, enhanced blood-circulation, higher target site accumulation due to the EPR effect [7] as well as a decrease in non-target toxicity are key

advantages of polymer based drug delivery resulting in an impovement of the therapeutic index of low molecular weight drugs.

Beside poly(ethylene glycol) (PEG) [8], polyglutamic-acid [9] and polysaccharide derivatives [10], six anticancer conjugates based on the biocompatible backbone *N*-(2-hydroxypropyl)methacrylamide (HPMA) have entered clinical trials so far, underlining the potential of developing HPMA-based drug delivery systems for effective cancer treatment [11-13].

Nevertheless, extensive knowledge about the biodistribution and pharmacokinetics is needed to improve and tailor drug carrier systems to meet the requirements of a particular medical application. Here, non-invasive molecular imaging techniques such as magnetic resonance (MR) imaging, single photon emission computed tomography (SPECT) or positron emission tomography (PET) are particularly suitable to follow circulation time and organ accumulation of potential drug delivery systems. In contrast to MRI, notably PET offers the possibility to study pharmacokinetics of macromolecular therapeutics in real time and high resolution by using only nanomolar amounts of a positron emitting radiolabel. The major challenge for using PET to guide the development of new generation polymer therapeutics, is the development of versatile radiolabeling strategies to incorporate a positron emitter into architecturally diverse polymeric carrier systems. Labeling approaches applied to HPMA-based polymers so far using longer-lived positron emitters, e. g. ^{64}Cu ($t_{1/2}(^{64}Cu)$=12.7 h) [14] or $^{72/74}$As ($t_{1/2}(^{72}As)$=26 h, $t_{1/2}(^{74}As)$=17.8 d) [15] which offer the possibility for long-term PET imaging [16, 17]. Yet, ^{64}Cu requires voluminous chelating agents to be introduced into a polymeric carrier in order to promote radiolabeling, possibly altering the overall polymer architecture and pharmacokinetics [18, 19]. Nonetheless, the growing number of new and diverse polymeric systems developed for potential drug delivery applications asks for less time-consuming and efficient *in vivo* screening methodologies. Here, PET imaging based on shorter-lived isotopes allows insight into initial pharmacokinetis thereby already hinting at the suitability of the respective polymer architecture in terms of efficient drug delivery.

Because of its excellent physical and nuclear characteristics – providing visualization of high spatial resolution – the short-lived positron emitter fluorine-18 ($t_{1/2}$=110 min) is considered to be the ideal radioisotope for PET. Recently, we have developed PET-based HPMA copolymers for short-term *in vivo* visualization, using a prosthetic group labeling approach by means of 2-[^{18}F]fluoroethyl-1-tosylate ([^{18}F]FETos) [20]. Translating ^{18}F-fluoroethylation into diverse precisely characterized homo as well as amphiphilic HPMA copolymers enabled their systematic evaluation *in vivo* by means of *ex vivo* biodistribution as well as small animal PET studies [21]. By determination of short-term *in vivo* pharmacokinetics, structure property relationships could be studied thereby underlining the benefit

of using ^{18}F-radiolabeling to assess the potential of distinct biocompatible polymers as potential drug carriers. However, in order to accomplish PET imaging, further versatile fluorine-18 labeling strategies need to be established in order to make PET studies accessible to polymeric systems with a large variety of architectures. Especially the introduction of ^{18}F to functionally complex molecules has been proven to be difficult and many labeling approaches require harsh conditions or long synthesis times with poor overall yields. In this context, click chemistry – a concept which was first introduced in 2001 by Sharpless and coworkers [22] – ideally complies with the requirements of fluorine-18 labeling *via* prosthetic groups [23]. In this regard, the Cu(I)-catalyzed cycloaddition between alkynes and azides, forming regioselectively 1,4-disubstituted 1,2,3-triazoles, has demonstrated to be very efficient requiring only mild reaction conditions, being highly selective and providing high yields. Furthermore, the formed triazole structures were shown to be very stable under physiological conditions [24], meeting the requirements for *in vivo* applications. Hence, this reaction has found numerous applications not only in the preparation and functionalization of polymeric drug delivery systems [25] but has also been employed for prosthetic ^{18}F-labeling of peptides [26, 27] and nanoparticles [28, 29] for *in vivo* PET imaging. Therefore, establishing ^{18}F-labeling of HPMA-based systems by means of click chemistry might constitute a further versatile and mild approach in order to introduce fluorine-18 into diverse polymer architectures for subsequent non-invasive PET imaging.

In this work we report the automated synthesis of the ^{18}F-labeling synthon 1-azido-2-(2-(2-[^{18}F]fluoroethoxy)ethoxy)ethane ([^{18}F]F-PEG$_3$-N$_3$) and its suitability for site-specific ^{18}F-labeling of potential HPMA-based drug carrier systems by means of Cu(I)-catalyzed azide-alkyne cycloaddition. Radiolabeling *via* click chemistry was studied using the HPMA-*ran*-alkyne copolymer P1* which was synthesized using the controlled radical polymerization technique RAFT (Reversible Addition Fragmentation Chain Transfer) in combination with reactive ester chemistry [30, 31] providing narrowly-distributed and well-defined polymer structures favorable for applications as potential drug delivery system. Based on the efficiency and versatility of the click reaction, the implementation of an ^{18}F-click labeling strategy might provide a very promising alternative in order to introduce fluorine-18 into a variety of HPMA-based drug delivery systems in oder to profit from fast and efficient non-invasive PET imaging as preclinical screening tool.

Materials and Methods

Materials

All reagents were purchased from Sigma-Aldrich and used without further purification unless otherwise stated. Water was purified and de-ionized (18 MΩcm) using a Milli-Q water filtration system. Aqueous [^{18}F]-fluoride ([^{18}F]F^-) solution was purchased from ZAG Zyklotron AG (Eggenstein-Leopoldshafen, Germany).

^{1}H-NMR spectra were obtained by a Bruker AC 300 spectrometer at 300 MHz at room temperature and spectroscopic data were analyzed using MestReC Lite 4.7.0.0.

Radio-TLCs (thin layer chromatography) were performed using Merck TLC Plate Silica Gel 60 F254 and were analyzed with an Instant Imager (Canberra Packard). Automated synthesis of 1-azido-2-(2-(2-[^{18}F]fluoroethoxy)ethoxy)ethane ([^{18}F]F-PEG$_3$-N$_3$) was performed on a self-constructed automated synthesis module. The system included a Peltier reactor module, equipped with a magnetic stirrer and a temperature and radioactivity sensor. Solvents were evaporated using a stream of helium regulated by a flow controller module. Semi-preparative high-performance liquid chromatography (HPLC) purification was performed using a Knauer K-501 pump, a Knauer K-2501 UV-detector (Herbert Knauer GmbH, Germany) and a radiodetector (Novo, Germany) connected in series. For HPLC purification a Phenomenex Luna 10 µ Prep C18(2) 250 x 10 mm column (50/50 water - acetonitrile at 5 mL/min) was used. As Solid Phase Extraction (SPE) colums Waters Sep-Pak Light Accell Plus QMA cartridges and Oasis HLB Plus cartridges were employed. Size Exclusion Chromatography (SEC) of the ^{18}F-labeled polymer P1* was performed using a HiTrap™ Desalting Column, Sephadex G-25 Superfine as well as a Waters pump (1500 series), a Waters UV-detector (2487 λ absorbance detector) and a Berthold LB 509 radiodetector. Radioactivitiy of the ^{18}F-labeled synthon, SPE cartridges and the ^{18}F-labeled polymer were measured in a digital ionization chamber (ISOMED 2000, MED GmbH, Germany).

Synthesis of HPMA-*ran*-alkyne polymer P1*

Synthesis of reactive precursor polymer *via* RAFT technique was achieved according to the literature [32], leading to PFPMA (pentafluorophenylmethacrylate)-homopolymers. The alkyne moiety was introduced *via* postpolymerization modification as already described for comparable polymer structures [21].

Preparation of 2-(2-(2-azidoethoxy)ethoxy)ethyl 4-methylbenzenesulfonate (3)

The ^{18}F-labeling precursor was synthesized by using a modified method reported by Meunier *et al.* [33] starting with triethylene glycol. In brief, a solution of triethylene glycol (1) (3.0 g, 20.0 mmol) in 10 mL dichloromethane was slowly added to a solution of p-toluenesulfonyl chloride (8.4 g, 44.0 mmol, 50 mL CH_2Cl_2) at 0 °C (ice bath). Triethylamine (5.1 g, 50.0 mmol) was added slowly and the resulting mixture was stirred at room temperature for 2 h and then refluxed overnight. The resulting mixture was cooled to room temperature, evaporated *in vacuo* and the resulting residue was dissolved in 10 mL dichloromethane. The solution was washed with water and brine and concentrated *in vacuo*. The crude product was purified by column chromatography using ethyl acetate:hexane (1:1) to afford 3.7 g (8.1 mmol, 40%) of 2 as a white solid. ^{1}H-NMR (300 MHz, $CDCl_3$) δ (in ppm) = 2.44 (s, 6H, CH3), 3.52 (s, 4H), 3.65 (t, 4H), 4.14 (t, 4H), 7.34 (d, 4H), 7.79 (d, 4H).

In a second step, 70.8 mg (1.1 mmol) sodium azide were added to a solution of 1.0 g (2.2 mmol) of 2 in ethanol (25 mL). The reaction was stirred under reflux overnight, cooled to room temperature and evaporated *in vacuo*. The residue was dissolved in dichlormethane and washed with water and brine. The combined organic phases were dried over Na_2SO_4, concentrated and the crude product was purified using column chromatography using a gradient of 1:5 to 1:1 (v:v) ethyl acetate/hexanes to afford 287.3 mg (0.9 mmol, 40%) of 3 as a colorless oil. ^{1}H-NMR (300 MHz, $CDCl_3$) δ (in ppm) = 2.41 (s, 3H), 3.33 (t, 2H), 3.68-3.56 (m, 8H), 4.12 (t, 2H), 7.32 (d, 2H), 7.75 (d, 2H).

Radiochemistry

Non-automated synthesis of [^{18}F]F-PEG$_3$-N$_3$

For automated production of the clickable labeling synthon 4 the reaction temperature and the amount of precursor for the radiofluorination reaction was optimized in acetonitrile. In order to provide dry [^{18}F]fluoride for the nucleophilic radiolabeling procedure, the aqueous [^{18}F]fluoride solution was passed through a QMA cartridge, eluted with a solution of 15 µmol K_2CO_3 and 40 µmol Kryptofix 222 in 1 mL acetonitrile and dried azeotropically under helium flow and reduced pressure at 80 °C. In a typical reaction, 10-30 µmol of tosyl azide precursor 3 were dissolved in 700 µL of dry acetonitrile, heated under stirring in a sealed vial at 80 °C - 100 °C and the labeling reaction was started by adding 300 µL of a solution of the dried Kryptofix 222/[^{18}F]fluoride complex in acetonitrile. The reaction mixture was kept at the considered temperature for 20 minutes and for kinetic measurements, samples were taken from the solution at 1, 2, 5, 10, 15 and 20 min. Samples were quenched with water and the radiochemical yield (RCY) was determined by radio-TLC

(n-hexane/ethyl acetate 1:1, R_f = 0.75). The ^{18}F-labeled synthon was purified using HPLC (Luna 10µ Prep C18(2) 250 x 10 mm, acetonitrile/water 50:50 (v/v), flow rate: 5 mL/min, R_f: 4.5 min).

Automated synthesis of [^{18}F]F-PEG$_3$-N$_3$

The modular system employed for the radiosynthesis of [^{18}F]F-PEG$_3$-N$_3$ is configured as depicted in Figure 1. Before start of synthesis, the modular system was equipped as follows: Vessel A was filled with 15 µmol K_2CO_3, 40 µmol Kryptofix 222 in 1 mL acetonitrile, vessel B was charged with 20 µmol of tosylate precursor in 1 mL acetonitrile and vessel C was loaded with 1 mL of acetonitrile/water 1:1. Preconditioned SPE columns (QMA: 15 mL 1M K_2CO_3 followed by 15 mL water; HLB: 15 mL methanol followed by 15 mL water) were inserted and container D – collecting the HPLC fraction of [^{18}F]F-PEG$_3$-N$_3$ – was filled with 100 mL of water. After connecting the sealed vial with the delivered no-carrier added aqueous [^{18}F]F$^-$ solution (500-2600 MBq), the synthesis was started. Subsequently, [^{18}F]fluoride was trapped on the QMA cartridge, eluted with the solution of vessel A into the reactor and dried azeotropically under helium flow and reduced pressure at 80 °C. After cooling to 40 °C, the solution of vessel B – containing labeling precursor 3 – was added and nucleophilic [^{18}F]fluorination reaction was performed at 90 °C for 10 min. The reaction mixture was cooled to 40 °C, solution of vessel C was added, and the mixed solution in the reactor was transferred *via* a syringe to a 2 mL sample loop of an injector valve for subsequent HPLC purification. The peak corresponding to [^{18}F]F-PEG$_3$-N$_3$ (R_f = 4.5 min) was collected under stirring into vessel D. Subsequently, the diluted HPLC fraction was passed through a HLB cartridge and dried under a stream of helium.

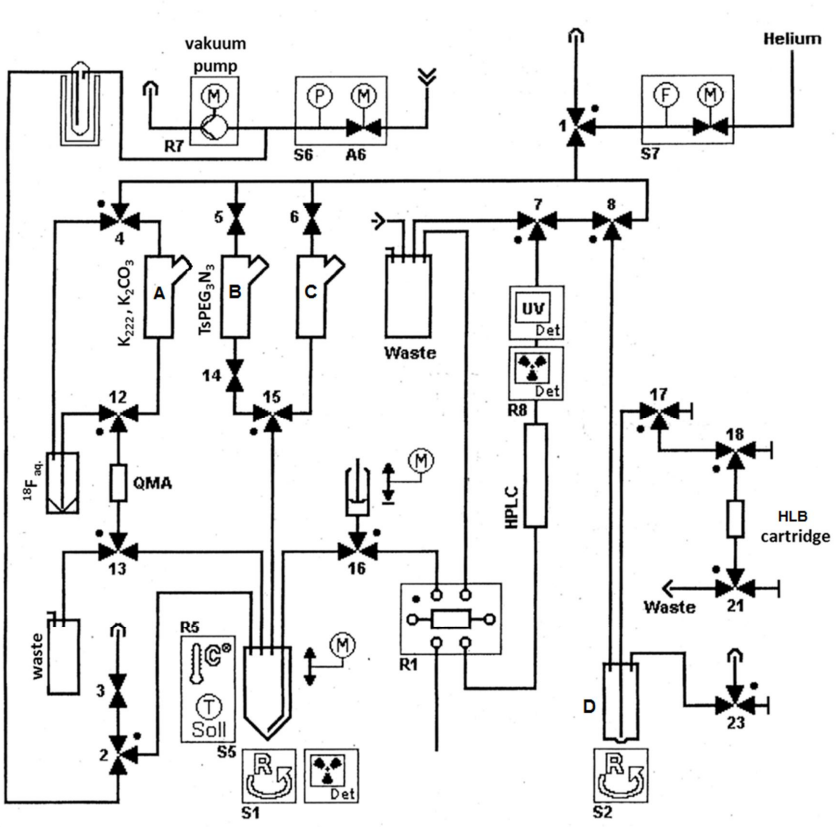

Figure 1: Process panel of the modular system for automated radiosynthesis of [^{18}F]F-PEG$_3$-N$_3$.

^{18}F-labeling of the polymer using [^{18}F]F-PEG$_3$-N$_3$

For optimization of radiofluorination of the HPMA-based polymer *via* click reaction, [^{18}F]F-PEG$_3$-N$_3$ was eluted off the HLB cartridge using methanol or acetonitrile depending on the final solution mixture of the click reaction (cf. Table 2). Each labeling reaction was accomplished using 3.0 mg of polymer P1* in a final reaction volume of 1 mL. The polymer was presolved in 200 µL methanol in a sealed vial and Cu(I) – either as solid CuI or as aqueous Cu_2SO_4 solution – was added. Designated amounts of sodium L-ascorbate solution, *N*,*N*-diisopropylethylamine and 2,6-lutidine were added sequentially (cf. Table 2). The labeling reaction was started by adding [^{18}F]F-PEG$_3$-N$_3$ (14.0 - 470.0 MBq) and the resulting mixture was heated at 40 °C for 20 min. RCYs were determined using SEC (HiTrap Desalting Column, Sephadex G-25 Superfine, 0.9 % NaCl, flow rate: 0.5 mL/min).

For the animal study, optimized click labeling conditions were used as followed: 3 mg polymer, 10 µmol CuI, 100 µmol sodium L-ascorbate, 0.3 mmol 2,6-lutidine in 1 mL of water:acetonitrile:methanol 4:4:2 (v/v). Purification using Sephadex G-25 size exclusion chromatography as described above yielded ^{18}F-P1* in 55% RCY after a total synthesis time of about 95 min as pure, ^{18}F-labeled polymer solution for subsequent *in vivo* studies.

In vitro metabolic stability

To analyze the serum stability of ^{18}F-labeled polymer P1*, 150 µL of purified ^{18}F-P1* were incubated with 400 µL fetal calf serum (FCS) at 37 °C. After 60 and 120 minutes of incubation, 75 µL of the mixture were taken, mixed with 50 µL of acetonitrile and centrifuged. Subsequently, the supernatant was analyzed using size exclusion chromatography as described above.

Initial *in vivo* µPET study of ^{18}F-labeled HPMA polymer P1*

The study was performed using the subline AT1 of the Dunning prostate carcinoma R3327 of the rat. The solid tumors were induced by subcutaneous injection of a cell suspension into the dorsum of the hind food and reached a volume of 1.5 mL when the experiment was performed. A male Copenhagen rat (230 g) housed in the animal care facility of the University of Mainz was investigated. The experiment had previously been approved by the regional animal ethics committee and was conducted in accordance with the German Law for Animal Protection and the UKCCCR Guidelines [34]. Positron emission tomography scans were performed with a Siemens/Concorde Microsystems µPET Focus 120 small animal PET scanner. For µPET imaging, the rat was anaesthetized using pentobarbital, (40 mg/kg, intraperitoneal, Narcoren, Merial, Hallbergmoos, Germany) placed in supine position for PET measurements and breathed room air spontaneously. Dynamic PET measurement was acquired in 2D mode after bolus injection of 29.0 MBq (0.6 mL) of ^{18}F-labeled polymer P1* in 0.6 mL 0.9% NaCl solution *via* tail vein puncture. Time activity curves (TAC) were obtained with varying time frames (1.5-10 min) for a total measuring interval of 120 min. The PET listmode data were histogrammed into 20 frames and reconstructed using OSEM algorithm. Volumes-of-interests (VOIs) were defined for tumor and reference tissue (testis). Testis was used as reference since they showed a relatively constant tissue concentration and lay in the field of view when imaging the tumors on the feet and because the tissue concentration was relatively constant. Uptake ratios of tumor to reference tissue were calculated from integral images between 15’ and 120’ after radiopolymer injection.

Analysis of blood and urine samples

For metabolic studies, blood and urine samples were taken after the µPET measurement and analyzed by means of SEC. The collected probes were spun in a centrifuge at 2000 g for 1 min at 20 °C, and the supernatants were taken and analyzed *via* SEC (system and conditions as described above).

Results and Discussion

In order to use PET studies to guide the way to new generation nanomedicines, versatile fluorine-18 labeling strategies need to be established transferable to a large variety of macromolecular architectures. The favorable characteristics of the copper-catalyzed azide-alkyne cycloaddition were shown to be ideally suitable for prosthetic ^{18}F-labeling when first applied to peptides [35] but also for the ^{18}F-labeling of cross-linked iron oxide nanoparticles as reported by Devaraj *et al.* and Nahrendorf *et al.* [28, 29].

To assess the suitability of fluorine-18 labeling *via* a click chemistry approach for HPMA-based carrier systems, a random HPMA-*ran*-alkyne copolymer (P1*) was synthesized using a combination of RAFT polymerization and reactive ester approach [36] (Scheme 1). Functionalization of the reactive ester homopolymer P1*-R by polymeranalogous reaction [31] with the primary amines 2-hydroxypropylamine and 2-(2-(prop-2-ynyloxy)ethoxy)ethanamine yielded the HPMA-based copolymer P1* of narrow polydispersity. For introduction of a fluorine-18 label, 3% of the primary amine exhibiting a terminal alkyne was incorporated into the polymer in order to enable subsequent ^{18}F-radiolabeling *via* click chemistry. Values for molecular weight and size distribution (PDI) of P1* are listed in Table 1.

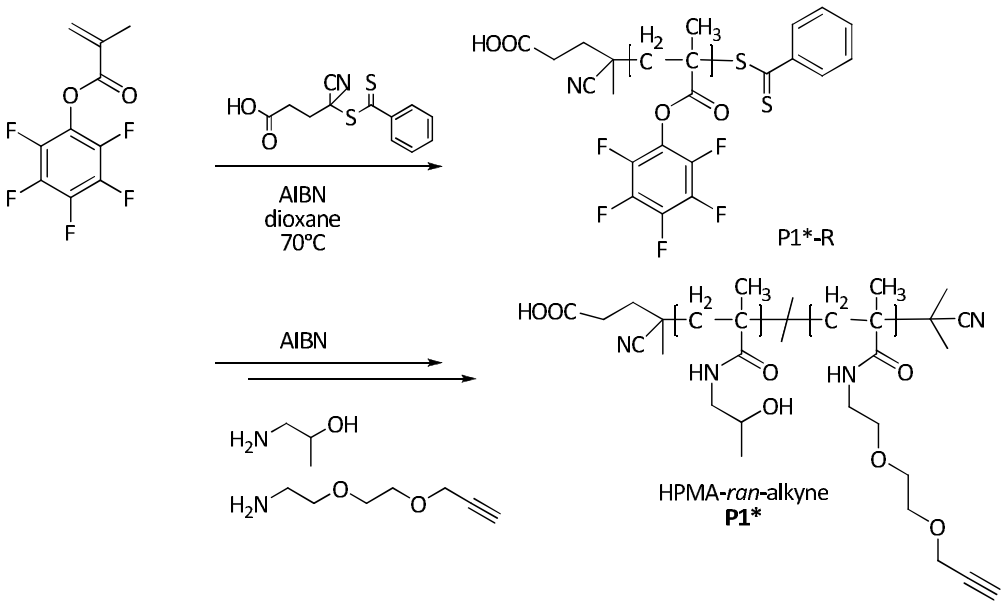

Scheme 1: Synthesis of HPMA-based polymer P1 for fluorine-18 labeling approach via click chemistry using RAFT polymerization technique and reactive ester approach*

*Table 1: Analytical data of alkyne functionalized HPMA polymer P1**

nomenclature	polymeric structure	monomer ratio [a]	M_n in g/mol [b]	M_w in g/mol [b]	PDI
P1*	random copolymer	97:3	9000	12000	1.29

[a] Monomer ratio determined by ^{1}H-NMR spectroscopy after polymer-analogous reaction with 2-hydroxypropylamine. [b] Calculated from the molecular weights of the reactive ester polymers as determined by GPC in THF as solvent.

For fluorine-18 labeling of HPMA-based polymers, a two-step labeling procedure using the prosthetic labeling group [^{18}F]F-PEG$_3$-N$_3$ was chosen in order to incorporate the PET nuclide into HPMA-based polymer architectures both site-specifically and under mild labeling conditions. To establish the prosthetic ^{18}F-labeling *via* click chemistry, the tosylate precursor 3 for synthesis of the prosthetic labeling group was prepared starting from triethylene glycol 1 (Figure 2) and labeling conditions for efficient automatisation of the preparation of [^{18}F]F-PEG$_3$-N$_3$ were investigated at first.

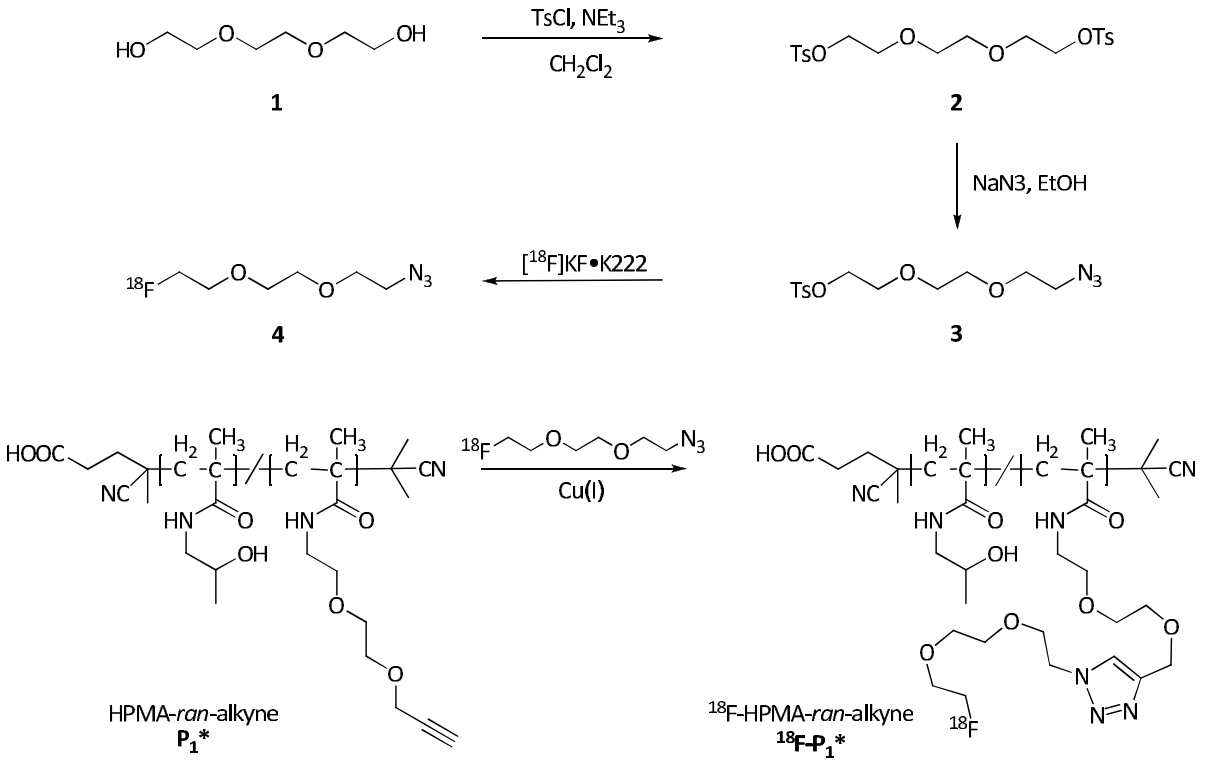

Figure 2: Synthesis of the ^{18}F-labeled prosthetic group [^{18}F]F-PEG$_3$-N$_3$ (4) and conjugation via Cu(I) catalyzed cycloaddition to HPMA model polymer P1.*

As shown in Figure 3, evaluation of the nucleophilic radiofluorination reaction of the tosylate precursor 3 in acetonitrile showed 80% RCY after 10 min at 90 °C using 20 µmol of the tosylate precursor (15 µmol K_2CO_3 and 40 µmol Kryptofix 222) as analyzed by radio-TLC. Transferring the labeling conditions to a remotely controlled synthesis of [^{18}F]F-PEG$_3$-N$_3$ resulted in 68 ± 3 % RCY before and 52 ± 5 % RCY after HPLC purification and SPE-fixation (n = 6). In total, >99% radiochemical

purity in an overall synthesis time of 55 min could be achieved thus leading to comparable results as reported by Nahrendorf *et al.* [29, supporting information] using automated synthesis.

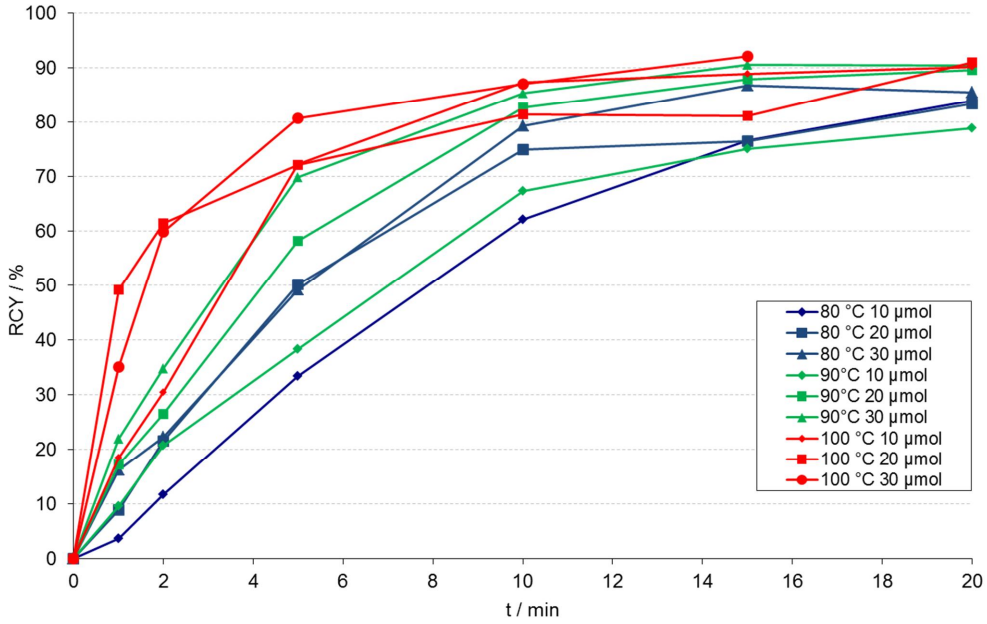

Figure 3: Kinetics of the radiofluorination reaction using the tosylate precursor at different temperatures and amounts of precursor (15 µmol K_2CO_3, 40 µmol Kryptofix 222, 1 mL acetonitrile).

To optimize the click reaction for the ^{18}F-labeling of HPMA polymer P1*, two different sources for the catalytic Cu(I) species were studied. In a first set of reactions (entry 1-3, Table 2) the Cu(II) salt Cu_2SO_4 was used, which provides the Cu(I) species *in situ* when a reducing agent e.g. sodium L-ascorbate is added. RCYs, determined by means of SEC after 20 min at 40 °C, were highest when 20 µmol Cu_2SO_4, 60 µmol sodium L-ascorbate and 0.3 mmol of 2,6-lutidine as base were used. Interestingly, although the addition of a nitrogen base is only essential when using a direct Cu(I) catalyst source in pure organic solvents to provide deprotonation, best results were achieved in case of Cu_2SO_4 when the nitrogen base 2,6-lutidine was added. Overall, higher radiochemical yields were achieved when using the Cu(I) salt CuI, which directly generates the catalytic Cu(I) species for the cycloaddition (entry 5-9, Table 2). Although all reactions were accomplished in a water containing solvent mixture, nitrogen base 2,6-lutidine was added to the reaction mixture to facilitate deprotonation, which already turned out to be beneficial in the first set of reactions using Cu_2SO_4. In general, higher RCYs were obtained using higher amounts of CuI, leading to an increase of more than 50% of labeled ^{18}F-P1* when using 100 µmol (entry 4, Table 2) instead of 10 µmol (entry 6, Table 2) of CuI. Best results were obtained when the reducing agent sodium L-ascorbate in up to 10-fold excess was added to the reaction. By

preventing oxidation of the Cu(I) species by atmospheric oxygen, the addition of sodium L-ascorbate yielded more than 70% of ^{18}F-labeled polymer even when using a low amount of CuI (entry 5, Table 2), which is in accordance to results reported by Marik and Sutcliffe-Gouldon [35] being the first who applied click chemistry for ^{18}F-labeling of unprotected peptides.

Table 2: Corrected radiochemical yields of ^{18}F-HPMA-ran-alkyne at various conditions using 3 mg of polymer precursor after 20 min at 40 °C

entry	solvent	Cu(I) source	sodium L-ascorbate	base	RCYs (%)
1	800 µL MeOH 200 µL H_2O	20 µmol Cu_2SO_4	60 µmol		36
2	600 µL MeOH 300 µL H_2O	20 µmol Cu_2SO_4	60 µmol	0.3 mmol DIPEA	26
3	800 µL MeOH 200 µL H_2O	20 µmol Cu_2SO_4	60 µmol	0.3 mmol 2,6-lutidine	42
4	200 µL MeOH 400 µL MeCN 400 µL H_2O	10 µmol CuI		0.3 mmol 2,6-lutidine	30
5	600 µL MeOH 200 µL MeCN 200 µL H_2O	10 µmol CuI	100 µmol	0.3 mmol 2,6-lutidine	73
6	200 µL MeOH 400 µL MeCN 400 µL H_2O	100 µmol CuI		0.3 mmol 2,6-lutidine	67
7	200 µL MeOH 400 µL MeCN 400 µL H_2O	10 µmol CuI	100 µmol	0.3 mmol 2,6-lutidine	79
8	200 µL MeOH 400 µL MeCN 400 µL H_2O	50 µmol CuI	100 µmol	0.3 mmol 2,6-lutidine	72
9	200 µL MeOH 400 µL MeCN 400 µL H_2O	100 µmol CuI	100 µmol	0.3 mmol 2,6-lutidine	98

In the cited study, moderate to excellent RCYs (54-99%) – depending on the peptide – were achieved by applying 130 µmol of sodium L-ascorbate, 13 µmol CuI and 0.14 mmol of *N*,*N*-Diisopropylethylamine as base. However, in case of ^{18}F-labeling of the HPMA-based copolymer P1*, almost quantitative results were achieved when using a very high amount of CuI (100 µmol) in the presence of sodium L-ascorbate and 2,6-lutidine (entry 9, Table 2). In a study by Devaraj *et al*. the alkyne-derivative of the labeling synthon [^{18}F]F-PEG$_3$-N$_3$ was used for ^{18}F-radiolabeling of azide-functionalized iron oxide nanoparticles (CLIO). Here, only 0.4 µmol of copper catalyst in combination with 10-fold excess of sodium L-ascorbate were needed in order to achieve RCYs of 58% for ^{18}F-CLIO [28]. Yet, Cu(II)SO$_4$ in combination with the Cu(I)-chelating ligand bathophenanthrolinedisulfonic acid disodium salt was used as catalyst system and unfortunately, no RCYs were provided for the inversed radiolabeling using [^{18}F]F-PEG$_3$-N$_3$ and the alkyne functionalized CLIO nanoparticle [29].

Compared to our previous results using the prosthetic group [^{18}F]FETos for radiofluorination of HPMA-based polymers [21], the applied Cu(I) catalyzed click reaction succeeded with higher radiochemical yields under very mild conditions. [^{18}F]fluoroethylation of a HPMA-based homopolymer of equal molecular weight (but having 3% of tyramine groups incorporated for attachment of the radiolabel instead of 3% alkyne groups in case of the polymer P1* used herein) yielded only 37±6 % of the ^{18}F-fluorethylated HPMA polymer using quite harsh conditions for the conjugation reaction [21].

To estimate the metabolic stability before *in vivo* experiments, serum stability was studied *in vitro* for up to 120 minutes. Size exclusion elugrams after 1 and 2 hours incubation of purified ^{18}F-P1* in fetal calf serum (FCS) did not show any low molecular weight radioactive contaminants indicating a stable fluorine-18 radiolabel for up to 2 hours (Figure 4).

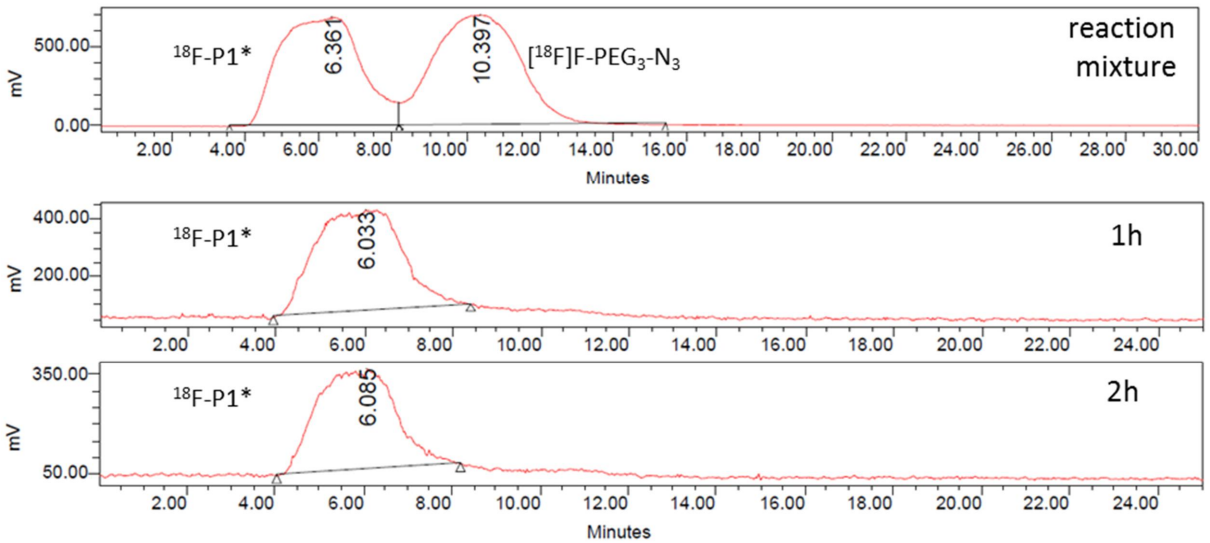

Figure 4: Radioanalytical Sephadex G-25 chromatography of ^{18}F-labeled HPMA polymer ^{18}F-P1 before purification and after 1 h and 2 h incubation of purified ^{18}F-P1* in FCS showing excellent serum stability of radiofluorinated HPMA polymer for up to 2 h.*

Based on these excellent results, the suitability of the click labeling approach for *in vivo* imaging of HPMA-based polymers was studied by means of initial µPET measurements to follow the *in vivo* behavior of the HPMA-based polymer P1*. Although no residual copper could be detected in the purified polymer solution after SEC workup, radiolabeling of P1* was performed using the lowest possible amount of CuI (10 µmol, cf. entry 5, Table 2) for *in vivo* studies yielding pure, radiolabeled polymer ^{18}F-P1* in sufficient high RCYs after preparative SEC in 0.9% NaCl solution for *in vivo* experiments.

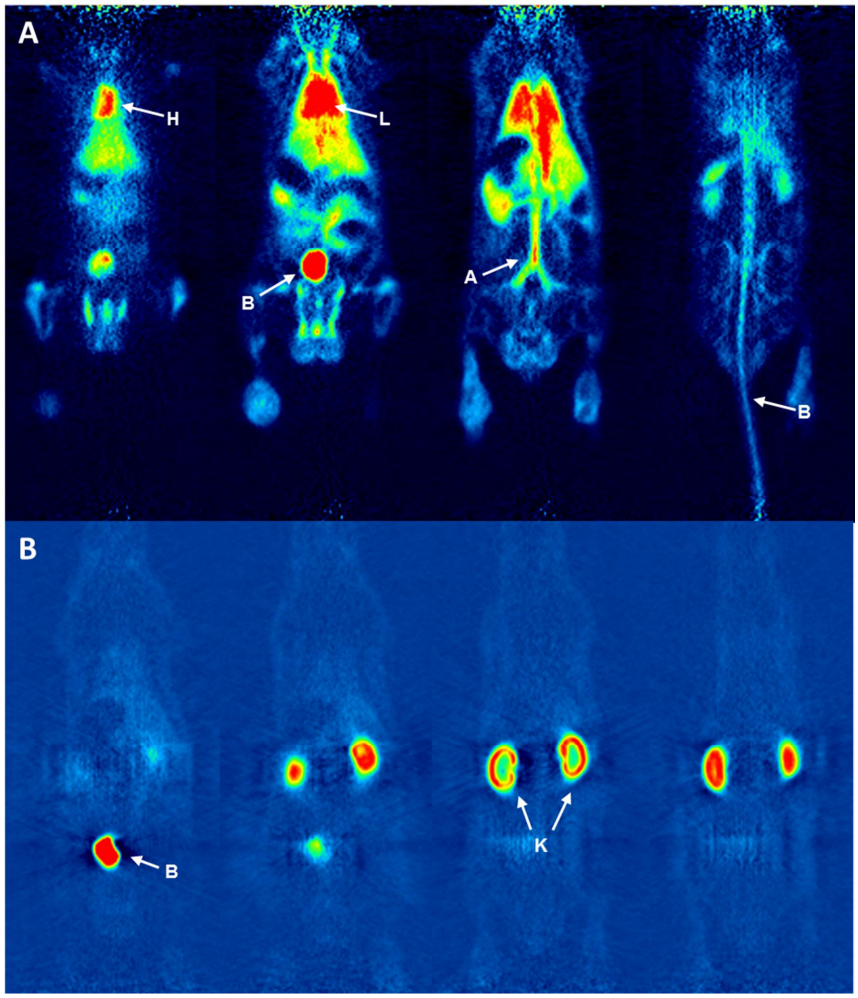

Figure 5: Comparison of coronar µPET summed images in different depths 120-135 min after i.v. injection of low molecular weight HPMA homopolmers. A: ^{18}F-click labeled homopolymer ^{18}F-P1 (M_w=12 kDa) showing activities in heart (H), lung(L) and kidney(K) B: [^{18}F]FETos labeled HPMA homopolymer of M_w=13 kDa showing predominantly renal clearance (K: kidney, B: bladder).*

Following our previous experiments using low M_w HPMA homopolymers – but a radiofluorination approach using [^{18}F]FETos as prosthetic group labeling approach [20, 21] – an initial *in vivo* µPET study was performed using the AT1 Dunning prostate carcinoma tumor model of the rat. Figure 5A shows the recorded whole body µPET image of ^{18}F-P1* in different depths of the rat (coronal slices). As expected for a hydrophilic low molecular weight HPMA homopolymer below the renal threshold for HPMA-based polymer systems (M_w<45 kDa [37]), strong accumulation of the radiolabeled polymer in kidney and bladder was observed. These findings stay in good accordance to the renal clearance identified as predominant excretion pathway of the [^{18}F]FETos labeled homopolymer of comparable size (M_w=12 kDa, cf. Figure 5B).

Nevertheless, in contrast to the results obtained for the low molecular weight fluoroethylated HPMA homopolymers, the new ^{18}F-labeled HPMA polymer ^{18}F-P1* presented herein, exhibited distinct differences in the distribution pattern. Beside renal clearance, remaining radioactivity in heart and aorta as well as in the lung was observed (Figure 5A). Metabolic studies analyzing blood and urine probes taken after µPET measurements revealed radioactive metabolites of low molecular weight being present in both blood plasma and urine of about 25% and 16%, respectively (Figure 6). Furthermore, a slight radioactivity accumulation in the skeleton of the rat is visible in the whole body scan (Figure 5A) which indicates that some of the ^{18}F-label detached from the polymer, leading to formation of free [^{18}F]fluoride which accumulates in bones or is cleared *via* the kidneys. In addition, [^{18}F]fluoride also displays in highly vascularized tissues such as heart and lung [38].

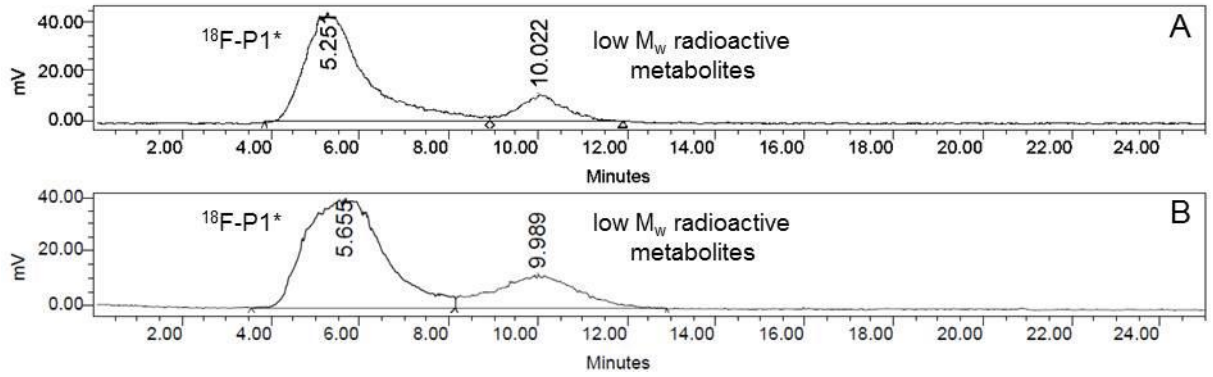

Figure 6: Metabolic study of blood and urine. Radioanalytical SEC elugrams of blood plasma (A) and urine (B) probes taken 135 min after tail vein injection of ^{18}F-labeled HPMA polymer ^{18}F-P1 showing low molecular weight radioactive metabolites.*

These results found for the homopolymer P1* – labeled *via* a click approach – stay in contrast to former findings on the biodistribution of low molecular weight HPMA polymers (M_w=32 kDa [20] as well as M_w=12 kDa [21]) obtained using an [^{18}F]FETos radiolabeling approach. In these studies, no accumulation in the skeleton and only renal clearance of these polymers – exhibiting M_w below the renal threshold for glomerular filtration – could be observed. (cf. Figure 5B). Studies on low molecular weight endothelin receptor radioligands revealed an inverse stability concerning a ^{18}F-fluorethylated receptor ligand [39] compared to a fluorinated derivative using a polyethylene glycol click approach of a longer PEG chain length as reported herein [40]. *In vitro*, their PEGylated derivative showed no polar metabolites whereas the fluoroethylated ligand underwent rapid defluoroethylation *in vitro* and *in vivo*. Considering, that these results are based on the metabolism of a rather small molecule compared to the HPMA-based polymer P1*, a possible explanation might be the difference in accessibility of the two radiolabels on the macromolecular architecture. When using the click approach, the ^{18}F-radiolabel is attached at the end of a longer and more hydrophilic

PEG chain compared to the more hydrophobic fluoroethyl radiolabel ([^{18}F]FETos approach). Being more displayed on the surface of the polymer coil and thereby more accessible for metabolic degradation, this characteristic might explain the reduced stability of the [^{18}F]F-PEG$_3$-N$_3$ radiolabel observed despite the high metabolic stability of the triazole junction reported so far [41]. Possibly, metabolic degradation at the PEG moiety rather than the triazole junction and subsequent release of free [^{18}F]fluoride might account for the observed findings which remains to be investigated in further detail in future studies.

Summed µPET images of AT1 tumors (Figure 7) as well as dynamic µPET imaging performed within 0-120 min post i.v. injection of ^{18}F-P1* (Figure 8) did not show any significant tumor accumulation of the polymer after administration. In fact, relative polymer uptake followed for up to 2 h during dynamic µPET acquisition reveals continuous decrease of activity in AT1 tumor tissue almost reaching radioactivity levels of non-targeted reference tissue (Figure 8). In comparison, dynamic µPET imaging of low M_w homopolymers labeled *via* [^{18}F]FETos showed slightly higher accumulation into AT1 tumors (^{18}F-P1*: ~130%, [^{18}F]fluorethylated homopolymer: ~190%; relative activity compared to reference tissue testes).

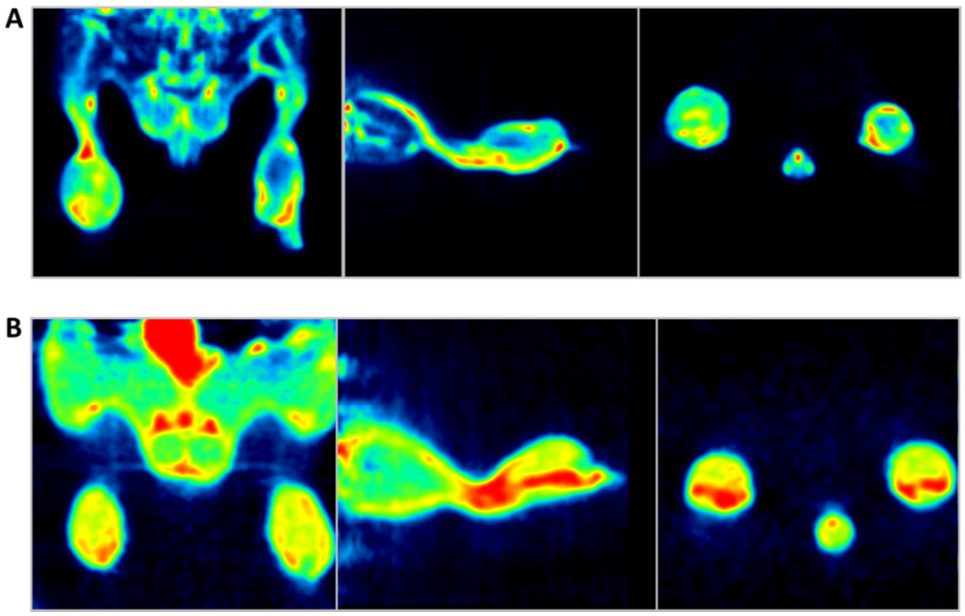

Figure 7: µPET images of AT1 tumors. Coronal, sagittal and axial section plane (from left to right) of AT1 tumors implanted on the hind food dorsum of the rat 60-120 min after i.v. injection of ^{18}F-P1(A) as well as [^{18}F]fluoroethylated HPMA homopolymer (B).*

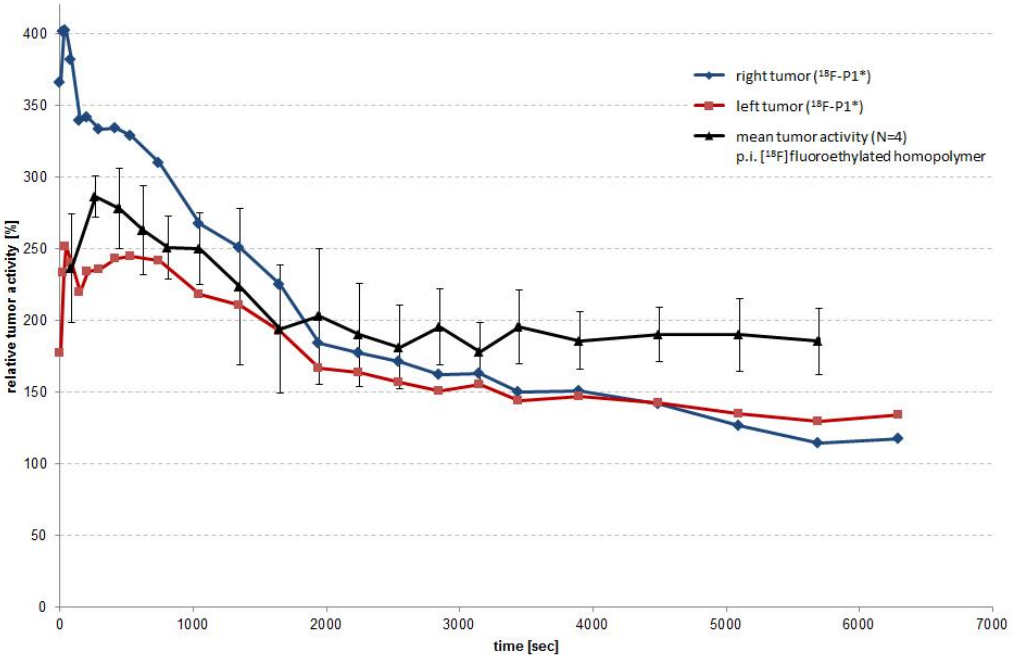

Figure 8: Time activity curves of the relative polymer uptake of ^{18}F-HPMA-ran-alkyne (^{18}F-P1) in AT1 tumors compared to mean polymer uptake into AT1 tumors of low M_w HPMA homopolymers labeled via [^{18}F]fluoroethylation (N=4, mean±SD). Values are normalized to the concentration levels of the reference tissue (testes).*

Further evaluation in our groups on the tumor accumulation of architecturally different HPMA-based polymers revealed, that not only polymer architecture and molecular weight played a significant role regarding tumor uptake (higher uptake of amphiphilic HPMA random laurylmethacrylate copolymers compared to hydrophilic homopolymeric systems) but furthermore, significant differences in polymer uptake depending on the tumor model could be identified. Notably, higher intratumoral concentrations *in vivo* in combination with higher cellular uptake *in vitro* were observed for the Walker 256 mammary carcinoma in comparison to the AT1 prostate carcinoma of the rat. Referring to these studies, closer investigation of the sagittal µPET tumor image slice (Figure 7A) shows only significant activities after administration of ^{18}F-P1* in the outer rim of the AT1 tumor. This stays in good correlation to previous investigations of [^{18}F]fluoroethylated homopolymers (Figure 7B), also revealing higher ^{18}F-polymer concentrations in the outer rim of AT1 tumors (further analyzed using autoradiography of tissue slices) which could be allocated to the subcutis around the tumor by correlation with the histological structure. Hence, the present findings based on an ^{18}F-click chemistry labeling approach were in good agreement with previous findings and further studies following this proof-of-principle are needed in order to assess the potential of this promising approach regarding *in vivo* evaluation by means of non-invasive PET imaging of architecturally diverse HPMA-based polymers for effective anticancer drug delivery.

Conclusions

In the present study, we reported the successful implementation of a click labeling approach in order to introduce fluorine-18 into potential drug carrier systems for fast and efficient preclinical screening by means of non-invasive positron emission tomography. Fluorine-18 labeling of the HPMA-based polymer P1* *via* click chemistry was accomplished in high yields in less than 100 min using a two-step procedure *via* the prosthetic labeling group [^{18}F]F-PEG$_3$-N$_3$ which was prepared using automated synthesis. Despite excellent stability of this labeling moiety *in vitro*, a preliminary small animal µPET study revealed partial metabolism of the ^{18}F-click label, which remains to be evaluated in more detail in future studies. Being time-efficient, mild as well as providing high yields, this click reaction based ^{18}F-labeling approach constitutes a further versatile alternative to introduce fluorine-18 into potential drug carrier systems required in order to use PET imaging for preclinical *in vivo* screening to identify appropriate carrier architectures and to guide design optimization.

Acknowledgements

We would like to thank Nicole Bausbacher, Barbara Biesalski and Bengü Yilmaz for their support during animal studies and following interpretation. We also want to thank the Max-Planck Graduate Center (MPGC, M. Allmeroth) as well as the Graduate School Materials Science in Mainz (Excellence Initiative, DFG/GSC 266, D. Moderegger) for financial support. In addition, we are very thankful for financial support of the DFG (Rösch: RO985/30-1; Thews: TH482/4-1, Zentel: ZE 230/21-1) and the SAMT research cluster Mainz.

References

[1] Duncan, R; Gaspar, R. Nanomedicine(s) under the Microscope. *Mol Pharm* 2011; 8 (6); 2101-2141.

[2] Dhal, PK; Polomoscanik, SC; Avila, LZ; Holmes-Farley, SR; Miller, RJ. Functional polymers as therapeutic agents: Concept to market place. *Advanced Drug Delivery Reviews* 2009; 61 (13); 1121-1130.

[3] Matsumura, Y; Kataoka, K. Preclinical and clinical studies of anticancer agent-incorporating polymer micelles. *Cancer Science* 2009; 100 (4); 572-579.

[4] Duncan, R. The dawning era of polymer therapeutics. *Nat Rev Drug Discov* 2003; 2 (5); 347-360.

[5] Duncan, R. Polymer conjugates as anticancer nanomedicines. *Nat Rev Cancer* 2006; 6 (9); 688-701.

[6] Haag, R; Kratz, F. Polymer Therapeutics: Concepts and Applications. *Angew Chem Int Ed* 2006; 45 (8); 1198-1215.

[7] Matsumura, Y; Maeda, H. A New Concept for Macromolecular Therapeutics in Cancer Chemotherapy: Mechanism of Tumoritropic Accumulation of Proteins and the Antitumor Agent Smancs. *Cancer Res* 1986; 46 (12 Part 1); 6387-6392.

[8] Greenwald, RB; Choe, YH; McGuire, J; Conover, CD. Effective drug delivery by PEGylated drug conjugates. *Adv Drug Deliver Rev* 2003; 55 (2); 217-250.

[9] Li, C; Yu, D; Newman, RA; Cabral, F; Stephens, LC; Hunter, N; Milas, L; Wallace, S. Complete Regression of Well-established Tumors Using a Novel Water-soluble Poly(L-Glutamic Acid)-Paclitaxel Conjugate. *Cancer Res* 1998; 58 (11); 2404-2409.

[10] Hreczuk-Hirst, D; Chicco, D; German, L; Duncan, R. Dextrins as potential carriers for drug targeting: tailored rates of dextrin degradation by introduction of pendant groups. *Int J Pharm* 2001; 230 (1-2); 57-66.

[11] Seymour, LW; Ferry, DR; Kerr, DJ; Rea, D; Whitlock, M; Poyner, R; Boivin, CM; Hesslewood, S; Twelves, C; Blackie, R; Schatzlein, A; Duncan, J; Bissett, D; Calvert, H; Lind, M; Robbins, A; Burtles, S; Duncan, R; Cassidy, J. Phase II studies of polymer-doxorubicin (PK1, FCE28068) in the treatment of breast, lung and colorectal cancer. *Int J Oncol* 2009; 34 (6).

[12] Duncan, R; Vicent, MJ. Do HPMA copolymer conjugates have a future as clinically useful nanomedicines? A critical overview of current status and future opportunities. *Adv Drug Deliver Rev* 2010; 62 (2); 272-282.

[13] Vasey, PA; Kaye, SB; Morrison, R; Twelves, C; Wilson, P; Duncan, R; Thomson, AH; Murray, LS; Hilditch, TE; Murray, T; Burtles, S; Fraier, D; Frigerio, E; Cassidy, J. Phase I Clinical and Pharmacokinetic Study of PK1 [*N*-(2-Hydroxypropyl)methacrylamide Copolymer Doxorubicin]: First Member of a New Class of Chemotherapeutic Agents–Drug-Polymer Conjugates. *Clin Cancer Res* 1999; 5 (1); 83-94.

[14] Kozempel, J; Hruby, M; Novakova, M; Kucka, J; Leseticky, L; Lebeda, O. Novel polymer vectors of ^{64}Cu. *Radiochim Acta* 2009; 97 (12); 747-752.

[15] Herth, MM; Barz, M; Jahn, M; Zentel, R; Rösch, F. $^{72/74}$As-labeling of HPMA based polymers for long-term in vivo PET imaging. *Bioorg Med Chem Lett* 2010; 20 (18); 5454-5458.

[16] Hamoudeh, M; Kamleh, MA; Diab, R; Fessi, H. Radionuclides delivery systems for nuclear imaging and radiotherapy of cancer. *Adv Drug Deliver Rev* 2008; 60 (12); 1329-1346.

[17] Liu, Y; Welch, MJ. Nanoparticles Labeled with Positron Emitting Nuclides: Advantages, Methods, and Applications. *Bioconjug Chem* 2012; 120206095602009.

[18] Fani, M; Del Pozzo, L; Abiraj, K; Mansi, R; Tamma, ML; Cescato, R; Waser, B; Weber, WA; Reubi, JC; Maecke, HR. PET of somatostatin receptor-positive tumors using ^{64}Cu- and ^{68}Ga-somatostatin antagonists: the chelate makes the difference. *J. Nucl. Med* 2011; 52 (7); 1110-1118.

[19] Kobayashi, H; Wu, C; Kim, MK; Paik, CH; Carrasquillo, JA; Brechbiel, MW. Evaluation of the in vivo biodistribution of indium-111 and yttrium-88 labeled dendrimer-1B4M-DTPA and its conjugation with anti-Tac monoclonal antibody. *Bioconjug Chem*; 10 (1); 103-111.

[20] Herth, MM; Barz, M; Moderegger, D; Allmeroth, M; Jahn, M; Thews, O; Zentel, R; Rösch, F. Radioactive Labeling of Defined HPMA-Based Polymeric Structures Using [^{18}F]FETos for In Vivo Imaging by Positron Emission Tomography. *Biomacromolecules* 2009; 10 (7); 1697-1703.

[21] Allmeroth, M; Moderegger, D; Biesalski, B; Koynov, K; Rösch, F; Thews, O; Zentel, R. Modifying the Body Distribution of HPMA-Based Copolymers by Molecular Weight and Aggregate Formation. *Biomacromolecules* 2011; 12 (7); 2841-2849.

[22] Kolb, HC; Finn, MG; Sharpless, BK. Click Chemistry: Diverse Chemical Function from a Few Good Reactions. *Angew Chem Int Ed* 2001; 40 (11); 2004-2021.

[23] Ross, TL. The Click Chemistry Approach Applied to Fluorine-18. *CRP* 2010; 3 (3); 202-223.

[24] Kolb, HC; Sharpless, BK. The growing impact of click chemistry on drug discovery. *Drug Discov Today* 2003; 8 (24); 1128-1137.

[25] Lallana, E; Sousa-Herves, A; Fernandez-Trillo, F; Riguera, R; Fernandez-Megia, E. Click Chemistry for Drug Delivery Nanosystems. *Pharm Res* 2012; 29 (1); 1-34.

[26] Li, Z; Wu, Z; Chen, K; Chin, FT; Chen, X. Click Chemistry for ^{18}F-Labeling of RGD Peptides and microPET Imaging of Tumor Integrin Expression. *Bioconjug Chem* 2007; 18; 1987-1994.

[27] Ramenda, T; Bergmann, R; Wüst, F. Synthesis of ^{18}F-labeled Neurotensin(8-13) via Copper-Mediated 1,3-Dipolar [3+2]Cycloaddition Reaction. *Lett Drug Des Discov* 2007; 4 (4); 279-285.

[28] Devaraj, NK; Keliher, EJ; Thurber, GM; Nahrendorf, M; Weissleder, R. ^{18}F Labeled Nanoparticles for *in Vivo* PET-CT Imaging. *Bioconjug Chem* 2009; 20 (2); 397-401.

[29] Nahrendorf, M; Keliher, EJ; Marinelli, B; Waterman, P; Feruglio, PF; Fexon, L; Pivovarov, M; Swirski, FK; Pittet, MJ; Vinegoni, C; Weissleder, R. Hybrid PET-optical imaging using targeted probes. *Proc Natl Acad Sci U.S.A* 2010; 107 (17); 7910-7915.

[30] Eberhardt, M; Theato, P. Synthesis of pentafluorophenyl(meth)acrylate polymers: New precursor polymers for the synthesis of multifunctional materials. *Eur Polym J* 2005; 41 (7); 1569-1575.

[31] Barz, M; Tarantola, M; Fischer, K; Schmidt, M; Luxenhofer, R; Janshoff, A; Theato, P; Zentel, R. From Defined Reactive Diblock Copolymers to Functional HPMA-Based Self-Assembled Nanoaggregates. *Biomacromolecules* 2008; 9 (11); 3114-3118.

[32] Barz, M; Luxenhofer, R; Zentel, R; Kabanov, AV. The uptake of *N*-(2-hydroxypropyl)-methacrylamide based homo, random and block copolymers by human multi-drug resistant breast adenocarcinoma cells. *Biomaterials* 2009; 30 (29); 5682-5690.

[33] Meunier, SJ; Wu, Q; Wang, S; Roy, R. Synthesis of hyperbranched glycodendrimers incorporating α-thiosialosides based on a gallic acid core. *Can J Chem* 1997; 75 (11); 1472-1482.

[34] Workman, P; Aboagye, EO; Balkwill, F; Balmain, A; Bruder, G; Chaplin, DJ; Double, JA; Everitt, J; Farningham, DAH; Glennie, MJ; Kelland, LR; Robinson, V; Stratford, IJ; Tozer, GM; Watson, S; Wedge, SR; Eccles, SA. Guidelines for the welfare and use of animals in cancer research. *Br. J. Cancer* 2010; 102 (11); 1555-1577.

[35] Marik, J; Sutcliffe-Goulden, JL. Click for PET: rapid preparation of [^{18}F]fluoropeptides using Cu^{I} catalyzed 1,3-dipolar cycloaddition. *Tetrahedron Lett* 2006; 47 (37); 6681-6684.

[36] Moad, G; Rizzardo, E; Thang, SH. Radical addition-fragmentation chemistry in polymer synthesis. *Polymer* 2008; 49 (5); 1079-1131.

[37] Seymour, LW; Miyamoto, Y; Maeda, H; Brereton, M; Strohalm, J; Ulbrich, K; Duncan, R. Influence of molecular weight on passive tumour accumulation of a soluble macromolecular drug carrier. *Eur J Cancer* 1995; 31 (5); 766-770.

[38] Knaus, RM; Dost, FN; Johnson, DE; Wang, CH. Fluoride distribution in rats during and after continuous infusion of $Na^{18}F$. *YTAAP* 1976; 38 (2); 335-343.

[39] Höltke, C; Law, MP; Wagner, S; Kopka, K; Faust, A; Breyholz, H; Schober, O; Bremer, C; Riemann, B; Schäfers, M. PET-compatible endothelin receptor radioligands: Synthesis and first in vitro and in vivo studies. *Bioorganic & Medicinal Chemistry* 2009; 17 (20); 7197-7208.

[40] Michel, K; Büther, K; Law, MP; Wagner, S; Schober, O; Hermann, S; Schäfers, M; Riemann, B; Höltke, C; Kopka, K. Development and Evaluation of Endothelin-A Receptor (Radio)Ligands for Positron Emission Tomography. *J Med Chem* 2011; 54 (4); 939-948.

[41] Breinbauer, R; Köhn, M. Azide-Alkyne Coupling: A Powerful Reaction for Bioconjugate Chemistry. *ChemBioChem* 2003; 4 (11); 1147-1149.

4 Summary, conclusions and future perspectives

Macromolecular drug delivery systems are being developed to improve the therapeutic effect of (chemo)therapeutic drugs by enhancing their availability and concentration at the target site in combination with a reduction of non-target toxicity. Based on the inherent tendency to passively accumulate in tumor tissue due to the EPR effect and the ability to combine various functionalities (e.g. drugs, targeting vectors, imaging probes) within one macromolecule, polymer based drug delivery systems have taken great interest in pharmaceutical and medical research.

In this respect, poly-*N*-(2-hydroxypropyl)methacrylamide (pHPMA) is a promising polymeric backbone to be used as macromolecular drug delivery system not at least owing to its high biocompatibility and feasible multifunctionality. In terms of using HPMA-based polymers for efficient tumor treatment, a suitable carrier system for chemotherapeutic drugs has to meet distinct requirements for medical applications.

First of all, the carrier system itself should be well defined and characterized in terms of physico-chemical parameters and furthermore allow for functionalization in order to achieve a high drug payload. Moreover, preferable pharmacokinetics for efficient drug delivery are only characterized by a sufficient longevity of the polymer conjugate in circulation in combination with a high and selective accumulation in the tumor tissue. Therefore, distinct parameters of the polymeric drug carrier such as hydrophilic-lipophilic balance, molecular weight, surface chemistry, hydrodynamic diameter or formation of superstructures in physiological media need to be considered as they determine the properties of the drug delivery system *in vivo* [1, 2].

Nevertheless, those physico-chemical parameters by far do not predict the ‘real’ behavior in a living biological system. Hence, appropriate *in vivo* imaging techniques such as PET are remarkably valuable and crucial in order to quantitate pharmacokinetics and biodistribution to guide design optimization, but also to deepen the comprehension of dynamic processes *in vivo*. Here, radiolabeling with the short-lived positron emitter fluorine-18 enables to follow initial organ distribution and tumor uptake of polymer architectures without altering the overall structure. Similarly, labeling of the same polymers with longer-lived iodine isotopes provides insight into long-term pharmacokinetics *ex vivo*. This allows estimating the suitability of distinct polymer architectures with respect to the above mentioned preferable attributes which drug delivery systems should ideally exhibit for effective (tumor) treatment.

However, labeling of diverse HPMA-based polymer architectures with these two radiohalogen isotopes asks for sophisticated synthetic (radio)chemistry. In this respect, the present thesis concentrated on using versatile strategies for introducing the positron emitter fluorine-18 as well as the β^--emitter iodine-131 into HPMA-based polymeric systems (cf. Fig. 1). With the labeling techniques developed, a second focus of this work was set on studying relationships between polymeric architectures and their biological behavior. The rational was to correlate amphiphilicity, surface properties, size as well as overall polymer architecture with organ distribution and tumor accumulation in the animal model of the rat in order to assess suitable characteristics for HPMA-based drug delivery systems. In the following, the findings will be highlighted in more detail.

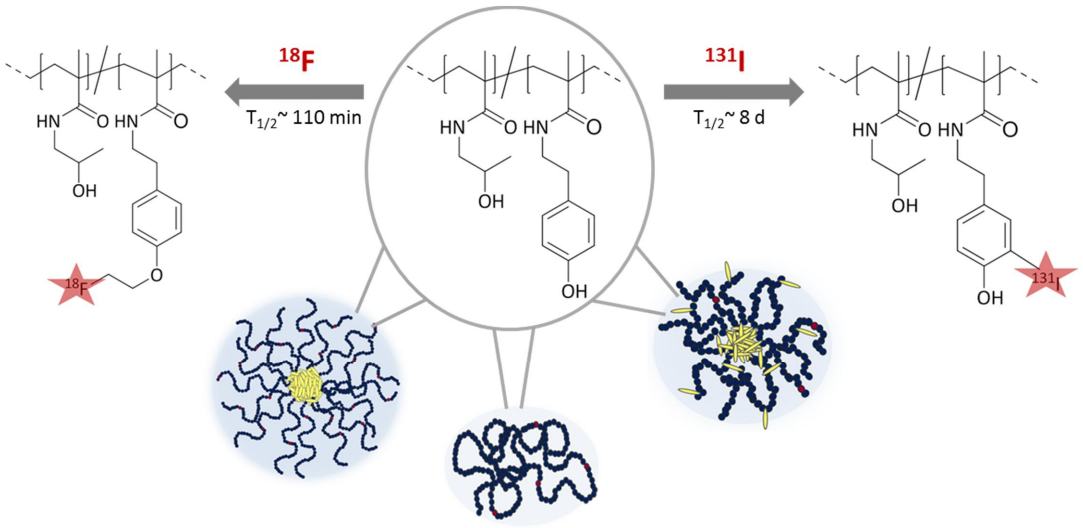

Figure 1: Illustration of ^{18}F- and ^{131}I-labeling of diverse HPMA-based polymer architectures for short and long-term in vivo and *ex vivo evaluations.*

4.1 Labeling chemistry

Using an indirect labeling approach *via* a small prosthetic group allows for a regio-selective introduction of ^{18}F applying less harsh reaction conditions compared to direct radiofluorination. Section 3.1 covers the transfer of the [^{18}F]fluoroethylation labeling reaction to defined HPMA-based polymers which were synthesized *via* RAFT polymerization of reactive ester methacrylates and subsequent transformation into HPMA-based polymers by means of polymer analogous reaction using primary amines. On the basis of three distinct HPMA-based homopolymers (with M_w of about 13, 32 and 70 kDa) as well as one block copolymer system (M_w = ~16 kDa), it was shown that incorporation of about 4% of tyramine moieties within the HPMA polymer backbone enabled to selectively introduce ^{18}F *via* a [^{18}F]fluoroethyl moiety (Fig. 2).

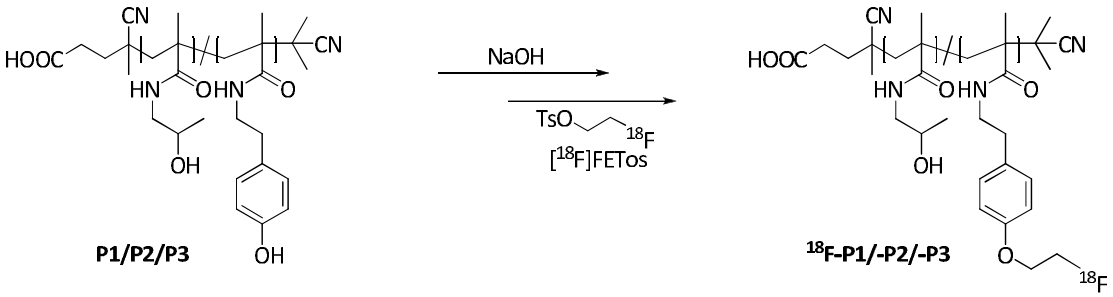

Figure 2: Fluorine-18 labeling via [^{18}F]FETos of HPMA-based polymers.

Optimization of the labeling conditions for [^{18}F]fluoroethylation resulted in throughout high radiochemical yields (> 50%) for the studied polymers after 10 min reaction time at 120 °C as determined by analytical radio TLC and SEC. Still, with decreasing M_w of the homopolymers and hence increasing surface-to-volume ratio, higher radiolabeling efficiencies were obtained. The successful ^{18}F-labeling enabled preliminary *in vivo* studies of the homopolymer P2 in healthy rats proofing renal clearance as anticipated for this hydrophilic polymer with a M_w below the renal threshold for glomerular filtration (~45 kDa [3]). A metabolism study of the fluorine-18 labeled homopolymer P2 demonstrated sufficient high *in vivo* stability hence underlining the appropriateness of using [^{18}F]fluoroethylation for *in vivo* PET imaging and biological evaluation of HPMA-based polymers.

The findings included in this work so far underline the potential of using [^{18}F]fluoroethylation in combination with PET as pre-clinical tool to identify suitable polymeric drug carrier architectures for medical applications. However, a main rationale in macromolecular drug delivery research relies on the enhanced permeability and retention observed for macromolecules in tumor tissue (EPR effect), allowing for passive accumulation and sustained drug release over weeks [4, 5]. In this respect, radiolabeling using longer-lived isotopes such as I-131 ($t_{1/2}$ = 8 d) is needed to complement the initial biodistribution and tumor uptake (evaluated by means of ^{18}F-labeling) in order to study long-term fate and particularly EPR-mediated tumor retention of HPMA-based polymers [6]. By using electrophilic aromatic substitution, iodine-131 can be incorporated into HPMA-based systems at the same functional aromatic group (tyramine) used for ^{18}F-radiolabeling *via* [^{18}F]FETos. Hence, direct ^{131}I-labeling at tyramine moieties constitutes an elegant labeling approach not demanding for structural modifications of the HPMA-based polymers investigated so far (cf. Figure 1). In order to accomplish long-term studies, ^{131}I-labeling of HPMA-based homo- as well as random LMA copolymers was studied with respect to type and amount of *in situ* oxidant needed to promote the electrophilic iodine species, showing higher yields by applying Chloramine-T compared to Iodogen (covered in

section 3.4). Optimization regarding the solvent applied for pre-dissolving of the amphiphilic copolymers finally resulted in 49±3% RCY by using Chloramine-T and DMSO in case of ^{131}I-P4*.

Fluorine-18 labeling allows for early quantitation of pharmacokinetics using organ distribution studies as well as PET imaging, thereby time-efficiently guiding design optimization of potential nanomedicines. However, the variety of potential drug delivery architectures asks for versatile labeling strategies transferable to chemically diverse and complex carrier systems in order to benefit from non-invasive PET imaging. In this regard, "click chemistry" – i.e. the Cu(I)-catalyzed cycloaddition between alkynes and azides – has shown to be highly suitable and efficient in terms of introducing labeling moieties into a wide range of molecules [7, 8]. Chapter 3.6 covers the application of a click labeling approach in order to introduce fluorine-18 into HPMA-based polymers *via* the azide functionalized labeling synthon [^{18}F]F-PEG$_3$-N$_3$. Subsequent to optimization of synthon preparation including automated synthesis, the alkyne functionalized HPMA polymer P1* was used in order to study radiolabeling using the respective click labeling synthon. In contrast to the [^{18}F]fluoroethylation approach demanding elevated temperatures, radiolabeling of P1* using click chemistry succeeded in very high yields at low temperatures which underlines the benefit of this approach to accomplish ^{18}F-labeling of complex polymer architectures exhibiting sensitive functional groups e. g. peptide-based targeting vectors (cf. Fig. 3). Despite a high serum stability *in vitro*, a proof-of-principle µPET study of ^{18}F-P1* revealed that the ^{18}F-click label was subjected to minor metabolic degradation *in vivo*, which remains to be investigated in more detail in further studies.

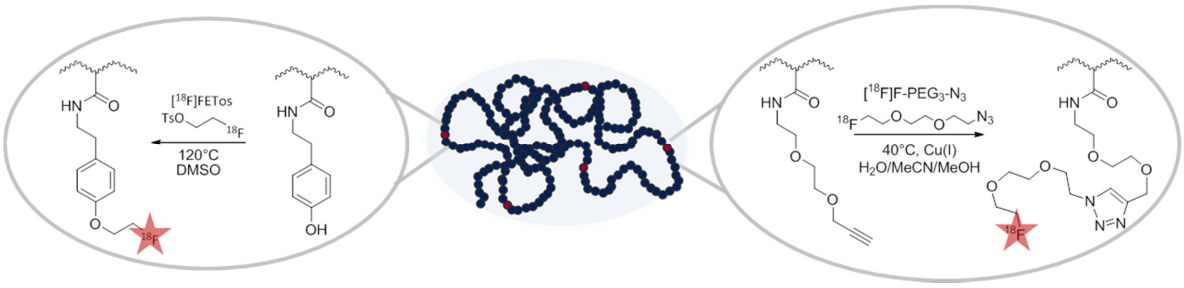

Figure 3: Schematic illustration of the two different prosthetic labeling approaches for ^{18}F-labeling of polymers using [^{18}F]FETos or [^{18}F]F-PEG$_3$-N$_3$.

4.2 Evaluation of HPMA-based polymer architectures

The promising findings of the proof-of-principle studies highly encourage to investigate more thoroughly whether fluorine-18 labeling by means of [^{18}F]FETos is suited to assess the potential of distinct HPMA-based polymer architectures for use as effective drug delivery systems *in vivo*. The comparably short half-life of fluorine-18 ($t_{1/2}$ = 110 min) might appear rather inappropriate to study the long-term fate of these non-biodegradable polymers or to follow passive tumor accumulation – over several days – based on the EPR effect. However, *in vivo* µPET imaging of the initial distribution of a particular polymer system using fluorine-18 labeling might provide sufficient information e.g. on fast clearance, non-target accumulation and initial tumor disposition in an efficient way in order to select favorable qualities of a carrier system that warrant further inquiries. As covered in section 3.2, this was subsequently successfully applied to [^{18}F]fluoroethylation of another set of well-defined and precisely characterized HPMA-based polymers of distinct characteristics. The polymers differed both in architecture (HPMA homopolymers *vs*. random copolymers exhibiting LMA as hydrophobic group) and in M_w, which was chosen to be below and above the renal threshold for each polymer architecture (Table 1, P1*-P4*).

Table 1: Characteristics of HPMA-based homopolymers, random LMA copolymers as well as LMA block copolymers P1-P6**

nomenclature	polymeric structure	LMA ratio	M_w in g/mol	PDI	R_h in nm
Poly(HPMA)-*ran*-tyramine homopolymer (P1*)	homopolymer	0%	12 000	1.29	1.1
Poly(HPMA)-*ran*-tyramine homopolymer (P2*)	homopolymer	0%	77 000	1.49	3.0
Poly(HPMA)-*ran*-LMA copolymer (P3*)	random copolymer	18%	14 000	1.26	33.4
Poly(HPMA)-*ran*-LMA copolymer (P4*)	random copolymer	25%	55 000	1.41	39.9
Poly(HPMA)-*b*-LMA copolymer (P5*)	block copolymer	21%	12 000	1.24	58.7
Poly(HPMA)-*b*-LMA copolymer (P6*)	block copolymer	25%	21 000	1.24	112.8

Whereas in isotonic solution, formation of individual coils was found for both homopolymeric systems, larger aggregates above a critical micelle concentration were found for the random copolymers with hydrodynamic radii (R_h) of about 30-40 nm. These disparities based on different M_w and polymer architectures became apparent *in vivo* and were reflected by considerable changes in blood clearance and biodistribution within the polymer systems at 2 h after administration. All polymers were shown to be subjected to renal clearance, yet this was significantly more pronounced for the low M_w polymers (P1*, P3*) within this study. Comparison of the distribution of

corresponding polymers of approximately same sizes but with varying architectures (P1* *vs.* P3* and P2* *vs.* P4*) revealed much lower liver accumulation for the high M_w homopolymer P2* compared to its amphiphilic counterpart, copolymer P4*. Besides the reduction in liver uptake, both of the hydrophobically modified copolymers showed an increased retention in the blood compartment which was most pronounced for the high M_w copolymer P4* for which a more than 17-fold higher concentration was found in the blood compared to the high M_w homopolymer P2* (3.8 ± 0.5 %ID/g *vs.* 0.2 ± 0.1 %ID/g, respectively). Using µPET imaging, the promising characteristics of HPMA-*ran*-LMA copolymer P4* regarding drug carrier applications became apparent and reduced liver uptake as well as increased retention in the blood compartment were clearly imaged non-invasively *in vivo* (Fig. 4).

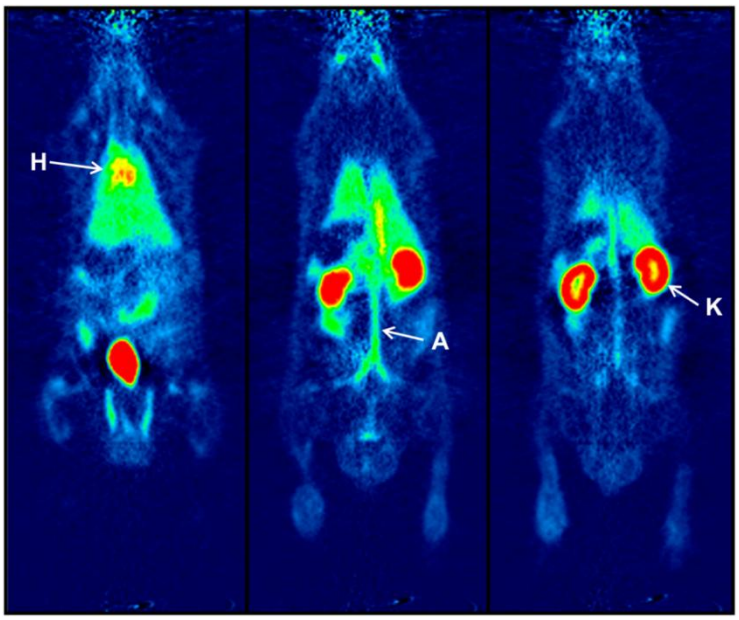

Figure 4: Representative coronar µPET images of HPMA-ran-LMA copolymer ^{18}F-P4 (55 kDa) 2 h after i.v. injection. The images show accumulation in kidneys (K) and bladder as well as remaining activity in the blood (heart (H); aorta (A)) [9].*

To further investigate whether ^{18}F-labeling and µPET imaging is valuable in order to evaluate the potential of distinct HPMA-based polymers for anticancer treatment applications, the *in vivo* evaluations so far were carried out in tumor bearing Copenhagen rats, using the Dunning AT1 prostate carcinoma model of the rat. Before, promising accumulation for a M_w = 65 kDa HPMA-based polymer at 168 h p.i. have been reported for this prostate tumor model by Lammers et al. using ^{131}I-labeling [6]. However, in our studies, non of the respective polymers P1*-P4* was markedly accumulated within the first 2 h studied, and despite the differences in blood clearance, only a marginally higher accumulation in the AT1 tumor model compared to the reference tissue (testis)

was observed for all polymers. Considering the vast heterogeneity of tumor tissue, these different findings encouraged to extend the biological evaluations taking into account further aspects such as a) time-dependent accumulation, b) different tumor models, c) tumor specific parameters such as cellular uptake and vascular permeability and not least d) studying more defined and less dynamic polymer architectures such as amphiphilic blockcopolymer micelles [10].

In this regard, distinct homo- and random LMA copolymers (P1*-P4*) together with two LMA blockcopolymers (P5*, P6*, cf. Table 1) were evaluated *in vivo* by means of [^{18}F]fluoroethylation taking another tumor model into account, the Walker 256 mammary carcinoma of the rat. These studies (discussed in section 3.3) focused on gaining deeper knowledge about structure-property relationships *in vivo* on the basis of six different HPMA-based polymer systems – differing in M_w, hydrodynamic radius, superstructure formation and amphiphilicity – regarding organ distribution over a time period of 4 h as well as specific macromolecule-tumor interactions. Comparison of the organ distribution revealed pronounced differences depending on molecular weight and polymer architecture. Whereas the high molecular weight homopolymer P2* and the block copolymer P6* were taken up markedly into liver and spleen, the random copolymers P3* and P4* – exhibiting a higher amount of hydrophobic sidechains – showed lower renal excretion as well as decreased hepatic uptake. As a result, amongst the six polymer systems studied over up to 4 h p.i., highest blood levels were found for the HPMA-*ran*-LMA copolymers P3* and P4* being almost 20-fold higher in comparison. These findings show the importance of a careful design of a carrier system as high M_w in combination with superstructure formation such as polymeric micelles might result in high liver and spleen uptake (as seen for P6*) whereas rather undefined and more flexible structures of small sizes such as random coil forming homopolymers might be subjected to a fast renal clearance (as seen for P1*) both leading to a loss in circulation of the carrier system needed for effective tumor treatment.

Studies on tumor accumulation revealed striking differences both depending on polymer characteristics (M_w *vs.* polymer architecture) and tumor cell line (AT1 *vs.* Walker 256 carcinoma). Although both tumors exhibited comparable tumor characteristics regarding histology, vascularisation, tumor growth and proliferation rate, strong differences in tumor accumulation within the studied polymers and tumor models were observed. Whereas all polymers were accumulated rather equally in AT1 tumors – but only to a low extent – Walker 256 tumors showed significant differences in tumor uptake depending on both M_w and polymer architecture. Here, homo- and block copolymers showed tumor concentrations comparable to the AT1 tumor model,

whereas significantly higher uptake in the Walker 256 model was found for random copolymers P3* (~2-times higher) as well as P4* (3-times higher) compared to the uptake seen in AT1 tumors (Fig. 5).

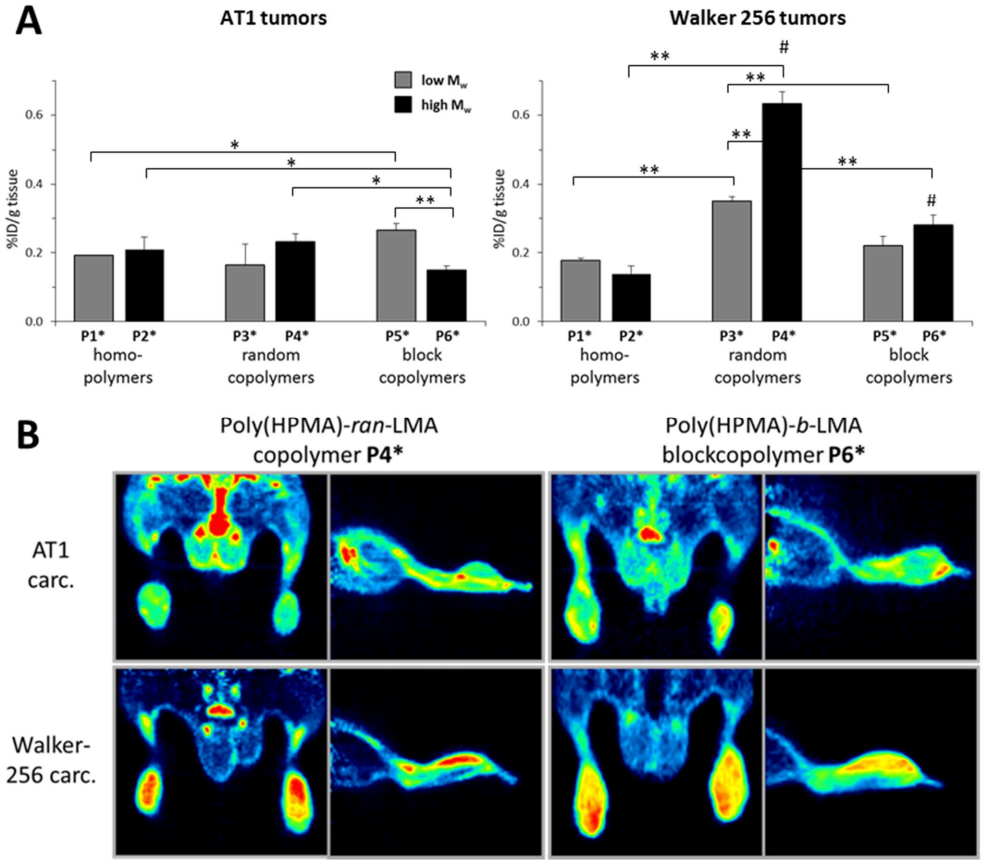

Figure 5: Comparison of intratumoral concentration 2 h p.i. of P1-P6* (A) and representative summed PET images of copolymers P4* and P6* (B) in AT1 prostate carcinomas and Walker 256 mammary carcinomas. n=5-6; (*) p<0.05, (**) p<0.01; (#) p<0.01 Walker 256 vs. AT1 tumors.*

These differences in tumor accumulation, being enormous regarding a distinct polymer structure, indicate that intratumoral uptake is not only highly dependent on the physico-chemical properties e.g. hydrophobic-hydrophilic balance of a polymeric system but is also dependent on tumor cell specific properties. *In vitro* studies on the cellular uptake using fluorescent labeled P1*-P6* revealed a 4-6 fold higher uptake of all polymers into Walker 256 compared to AT1 carcinoma cells. Considering the comparable vascular permeability determined for both carcinoma models, these results suggest, that the higher accumulation in the Walker 256 tumor observed *in vivo* might be based on differences in cellular uptake, i.e. in the endocytotic processes of both cell lines.

Owing to the observed pharmacokinetic profile as well as tumor cell uptake of copolymer P4*, the question arose whether the relatively high ratio (25%) of randomly incorporated laurylmethacrylate

(LMA) side chains is relevant in order to promote beneficial *in vivo* performance for effective drug delivery. Therefore, a comparative study (discussed in 3.3.1) was performed, including the HPMA-*ran*-LMA copolymers $P_{16\%}$* (16% LMA) and $P_{20\%}$* (20% LMA) revealing improved pharmacokinetics for all hydrophobically modified polymers with respect to prolonged plasma half-life, lower liver and spleen uptake as well as higher tumor uptake (Walker 256 carcinoma) compared to the hydrophilic homopolymer $P_{0\%}$* (P2*, Table 1). Yet, amongst the investigated series of polymers, copolymer P4* ($P_{25\%}$*) of highest LMA ratio showed the most promising *in vivo* characteristics regarding drug delivery applications, particularly highest tumor and blood concentrations.

These findings – determined by means of fluorine-18 labeling and subsequent systematic short-term *in vivo* evaluation – encourage to further develop amphiphilic LMA copolymers for drug delivery applications. However, insight into the long-term fate of these carrier systems is needed, especially with respect to prolonged blood retention and passive tumor accumulation based on the EPR effect. Following the optimization of ^{131}I-labeling of amphiphilic HPMA copolymers, a proof-of-principle study could be accomplished with the HPMA-*ran*-LMA copolymer P4* – so far showing most promising short-term *in vivo* characteristics – and organ distribution as well as tumor uptake (Walker 256 carcinoma) was investigated over up to 3 days (section 3.4). In this study, disparities in the organ distribution pattern of the ^{131}I-labeled P4* compared to ^{18}F-fluoroethylated P4* at 2 h p.i. were observed, notably with higher hepatic and splenic uptake of the radioiodinated copolymer possibly due to increased lipophilicity of ^{131}I-P4* or distinct metabolisms of the radiolabels and/or their anchoring moieties, which remains to be elucidated in more detail. Most strikingly, despite an observed total blood clearance of less than 3 days, enhanced tumor uptake of ^{131}I-P4* over 48 h could be proven, indicating EPR-mediated retention of the copolymer at the tumor site and encouraging the development of HPMA-LMA copolymers for sustained drug delivery applications.

Major drawbacks towards translating polymer based drug delivery systems into the clinics have often been related to unfavorable pharmacokinetics such as fast clearance and/or high non-target tissue uptake but also to poor homogeneity of polymer conjugates which are inherently polydisperse and dynamic structures [11]. In this respect, block copolymer micelles hold promising characteristics regarding drug delivery applications owing amongst others to their defined amphiphilic core-shell structure enabling incorporation of hydrophobic drugs and to their higher stability in aqueous media [10]. However, the HPMA-LMA block copolymers (P5*, P6*; section 3.3) evaluated so far did not outreach the favorable *in vivo* characteristics observed for the HPMA-LMA random copolymers. Based on the known and widely exploited effects that PEGylation exerts in terms of prolonging pharmacokinetic properties of drugs ('stealth properties') [12, 13], further studies (section 3.5)

concentrated on whether distinct incorporation of PEG segments (M_w = 2000 Da) into the hydrophilic block improves the pharmacokinetics of HPMA-LMA block copolymer micelles, notably regarding blood retention and tumor uptake. In this investigation, five HPMA-*b*-LMA block copolymers – ranging from 0% PEG to 11% PEG incorporation (cf. Table 2) – were radiolabeled by means of [^{18}F]fluoroethylation and subsequent *in vivo* evaluation revealed a tremendous impact of polymer architecture in relation to PEG_{2000} incorporation ratio regarding *in vivo* pharmacokinetics.

Table 2: Characteristics of HPMA-*b*-LMA copolymers $P_{0\%}$ - $P_{11\%}$ exhibiting different amounts of PEG_{2000} sidechains

nomenclature	polymeric structure	LMA ratio	PEG_{2000} ratio	M_w in g/mol	PDI	R_h in nm
Poly(HPMA)-*b*-LMA copolymer ($P_{0\%}$)	block copolymer	25%	0%	21 000	1.25	112.8
Poly(HPMA)-PEG_{2000}-*b*-LMA copolymer ($P_{1\%}$)	block copolymer	25%	1%	24 000	1.25	55.4
Poly(HPMA)-PEG_{2000}-*b*-LMA copolymer ($P_{5\%}$)	block copolymer	25%	5%	33 000	1.25	38.0
Poly(HPMA)-PEG_{2000}-*b*-LMA copolymer ($P_{7\%}$)	block copolymer	25%	7%	38 000	1.25	38.1
Poly(HPMA)-PEG_{2000}-*b*-LMA copolymer ($P_{11\%}$)	block copolymer	25%	11%	47 000	1.25	53.0

Whereas block copolymers of low PEG content and higher hydrodynamic radii (R_h) showed increased kidney as well as splenic and hepatic uptake, higher PEG_{2000} ratios (yielding smaller polymer architectures) resulted in prolonged blood retention and lower concentrations in spleen and liver.

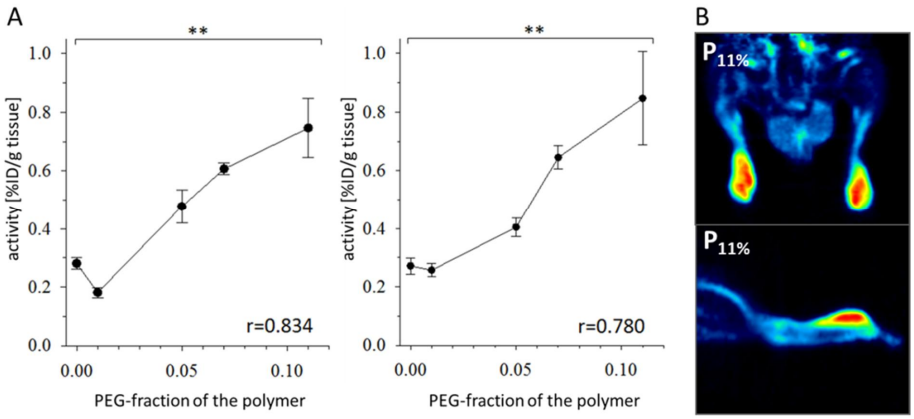

Figure 6: A: Tumor accumulation of HPMA-LMA block copolymers as a function of PEG_{2000} ratio. B: representative coronal (top) and sagittal (bottom) µPET image sections of Walker 256 tumors 60-120 min p.i. of ^{18}F-$P_{11\%}$ showing tumor accumulation.

Most strikingly, a linear trend of tumor accumulation was observed with increasing PEGylation ratio resulting in highest tumor uptake (Walker 256 carcinoma) observed for block copolymer $P_{11\%}$

(Figure 6). Although the increased uptake observed *in vivo* could not be related to a higher tumor cell uptake *in vitro,* these findings underline both the importance of a precise tailoring (regarding size and surface properties) of polymeric drug carriers as well as using non-invasive *in vivo* techniques such as PET in order to develop polymer based delivery systems for efficient (chemo)therapy to the patient needs.

4.3 Outlook

Based on the findings included in this work – realized by using different radiolabeling approaches and subsequent *in vivo* evaluation of potential drug carriers – several aspects remain to be elucidated. The recognized profit of using non-invasive imaging techniques for pre-clinical assessment needs versatile labeling strategies to be developed that can be attuned in terms of drug carrier system and medical time frame. However, despite the promising approaches presented herein ([^{18}F]fluoroethylation, ^{18}F-click labeling as well as ^{131}I-labeling), further studies regarding the differences observed in organ distribution (^{131}I-labeling approach) as well as metabolism of the radiolabel/attachment moiety need to addressed and studied in more detail. Using a similar anchoring moiety of the carrier system (tyramine) for the attachment of different radiolabels (*via* ^{18}F-fluoroethylation or electrophilic radioiodination) is an elegant approach not demanding for structural changes at the carrier site. Applied with regard to long term distribution, the proof-of-principle study showed tumor retention of ^{131}I-P4* and further studies including the HPMA homo and *ran*-LMA copolymers as well as the block copolymer systems (HPMA-*b*-LMA and HPMA-PEG$_{2000}$-*b*-LMA) are crucial to relate structural properties to pharmacokinetics and tumor uptake in the long run. Furthermore, radioiodination using the positron emitting isotope I-124 ($t_{1/2}$=4.2 d) instead of I-131 might complement these studies using non-invasive PET imaging permitting repeated investigations of the same animals and hence different tumor growth stages.

Radiolabeling using metallic radionuclides (e.g. ^{68}Ga, ^{44}Sc, ^{99m}Tc,) further constitutes a valuable approach in terms of benefiting from image guided drug development and drug delivery. Besides the ease of availability (elution from in-house radionuclide generators), the chelator based labeling procedure – needed in order to incorporate metallic radionuclides into target molecules – allows for both imaging and therapy by replacing the chelated diagnostic radionuclide by therapeutic radiometals (^{177}Lu, ^{90}Y). Together with the multifunctionality polymers provide, polymer based drug delivery systems comprising (chemo)therapeutics, imaging probes and/or radiotherapeutic nuclides ('nanotheranostics') can be designed [14, 15]. Still, this labeling approach requires bulky chelating moieties to be attached to the carrier system that might alter surface properties (i.e. surface charge)

as well as overall architecture of the carrier system, which has to be considered in terms of its use to guide design optimization of potential drug delivery systems [16, 17].

During the past decades, huge efforts have been made to develop efficient drug delivery devices in order to improve current (chemo)therapeutic treatments. In this respect, a main part of this work focused on studying different polymer architectures aiming to identify structure-property characteristics favorable for medical applications. On the basis of these studies, further progress towards polymer based drug delivery should comprise the introduction of functionalities such as (chemo)therapeutic drugs or targeting ligands to the carrier system. Notably, the introduction of tumor targeting vectors – e.g. monoclonal antibodies, peptide hormones, oligosaccharides or oligopeptides – into the carrier systems evolves as highly interesting aspect to be investigated in further studies. For example, in the case of the evaluated PEGylated block copolymer micelles, *in vitro* data revealed low cellular uptake for polymers of higher PEG_{2000} incorporation ratio, whereas *in vivo*, a promising pharmacokinetic profile was observed for these carrier systems. Hence, incorporation of ligands, which target receptors that are overexpressed in tumors and mediate endocytosis might further increase tumor retention due to higher intracellular disposition. Here, folic acid has emerged as promising targeting vector and was shown to improve tumor retention and tumor cell uptake of various nanoparticles [18, 19] including HPMA-based polymers [20].

Considering these ideas, radiolabeling in combination with molecular imaging techniques such as PET constitutes a valuable non-invasive tool to advance the development towards efficient nanomedicines by identifying suitable candidates at an early stage in development and by helping to guide design optimization. Further progress towards hybrid systems comprising targeting ligands, drugs and imaging moieties provides essential knowledge on the nanotheranostics pharmacokinetics, delivery of the drug to the target site and off-target deposition. Not at least, non-invasive imaging allows pre-screening of patients approaching personalized medicine. In the end, all these efforts aim to overcome the drawbacks of state-of-the-art anticancer treatments in order to improve the quality of life of future patients.

References

[1] Fox, ME; Szoka, FC; Fréchet, JMJ. Soluble Polymer Carriers for the Treatment of Cancer: The Importance of Molecular Architecture. *Acc Chem Res* 2009; 42 (8); 1141-1151.

[2] Barreto, JA; O'Malley, W; Kubeil, M; Graham, B; Stephan, H; Spiccia, L. Nanomaterials: Applications in Cancer Imaging and Therapy. *Adv Mater* 2011; 23 (12); H18.

[3] Seymour, LW; Kopeček, J. Effect of molecular weight of *N*-(2-hydroxypropyl)methacrylamide copolymers on body distribution and rate of excretion after subcutaneous, intraperitoneal, and intravenous administration to rats. *J Biomed Mater Res* 1987; 21 (11); 1341-1358.

[4] Matsumura, Y; Maeda, H. A New Concept for Macromolecular Therapeutics in Cancer Chemotherapy: Mechanism of Tumoritropic Accumulation of Proteins and the Antitumor Agent Smancs. *Cancer Res* 1986; 46 (12 Part 1); 6387-6392.

[5] Maeda, H. Tumor-Selective Delivery of Macromolecular Drugs via the EPR Effect: Background and Future Prospects. *Bioconjug Chem* 2010; 21 (5); 797-802.

[6] Lammers, T; Kühnlein, R; Kissel, M; Šubr, V; Etrych, T; Pola, R; Pechar, M; Ulbrich, K; Storm, G; Huber, P; Peschke, P. Effect of physicochemical modification on the biodistribution and tumor accumulation of HPMA copolymers. *J Control Release* 2005; 110 (1); 103-118.

[7] Ross, TL. The Click Chemistry Approach Applied to Fluorine-18. *CRP* 2010; 3 (3); 202-223.

[8] Lallana, E; Sousa-Herves, A; Fernandez-Trillo, F; Riguera, R; Fernandez-Megia, E. Click Chemistry for Drug Delivery Nanosystems. *Pharm Res* 2012; 29 (1); 1-34.

[9] Allmeroth, M; Moderegger, D; Biesalski, B; Koynov, K; Rösch, F; Thews, O; Zentel, R. Modifying the Body Distribution of HPMA-Based Copolymers by Molecular Weight and Aggregate Formation. *Biomacromolecules* 2011; 12 (7); 2841-2849.

[10] Gaucher, G; Dufresne, M; Sant, VP; Kang, N; Maysinger, D; Leroux, J. Block copolymer micelles: preparation, characterization and application in drug delivery. *J Control Release* 2005; 109 (1-3); 169-188.

[11] Vicent, MJ; Dieudonné, L; Carbajo, RJ; Pineda-Lucena, A. Polymer conjugates as therapeutics: future trends, challenges and opportunities. *Expert Opin Drug Deliv* 2008; 5 (5); 593-614.

[12] Pasut, G; Veronese, FM. PEG conjugates in clinical development or use as anticancer agents: An overview. *Adv Drug Deliver Rev* 2009; 61 (13); 1177-1188.

[13] Joralemon, MJ; McRae, S; Emrick, T. PEGylated polymers for medicine: from conjugation to self-assembled systems. *Chem. Commun* 2010; 46 (9); 1377.

[14] Lammers, T; Kiessling, F; Hennink, WE; Storm, G. Nanotheranostics and Image-Guided Drug Delivery: Current Concepts and Future Directions. *Mol Pharm* 2010; 7 (6); 1899-1912.

[15] Ting, G; Chang, C; Wang, H; Lee, T. Nanotargeted Radionuclides for Cancer Nuclear Imaging and Internal Radiotherapy. *J Biomed Biotechnol* 2010; 2010; 1-18.

[16] Kobayashi, H; Wu, C; Kim, MK; Paik, CH; Carrasquillo, JA; Brechbiel, MW. Evaluation of the in vivo biodistribution of indium-111 and yttrium-88 labeled dendrimer-1B4M-DTPA and its conjugation with anti-Tac monoclonal antibody. *Bioconjug Chem*; 10 (1); 103-111.

[17] Fani, M; Del Pozzo, L; Abiraj, K; Mansi, R; Tamma, ML; Cescato, R; Waser, B; Weber, WA; Reubi, JC; Maecke, HR. PET of somatostatin receptor-positive tumors using ^{64}Cu- and ^{68}Ga-somatostatin antagonists: the chelate makes the difference. *J. Nucl. Med* 2011; 52 (7); 1110-1118.

[18] Lu, Y; Low, PS. Folate-mediated delivery of macromolecular anticancer therapeutic agents. *Adv. Drug Deliv. Rev* 2002; 54 (5); 675-693.

[19] Xia, W; Low, PS. Folate-Targeted Therapies for Cancer. *J. Med. Chem* 2010; 53 (19); 6811-6824.

[20] Barz, M; Canal, F; Koynov, K; Zentel, R; Vicent, MJ. Synthesis and in vitro evaluation of defined HPMA folate conjugates: influence of aggregation on folate receptor (FR) mediated cellular uptake. *Biomacromolecules* 2010; 11 (9); 2274-2282.

5 Appendices

5.1 Abbreviations

AIBN	azobisisobutyronitrile	MRI	magnetic resonance imaging
ATRP	Atom Transfer Radical Polymerization	MRS	magnetic resonance spectroscopy
CAT	chloramine-T	M_w	weight average molecular weight
$CDCl_3$	deuterated clochloroforme	NaCl	sodium chloride
CLIO	cross-linked iron oxide nanoparticle	n. d.	not determined
CMC	critical micelle concentration	NMP	Nitroxide-Mediated Radical Polymerization
CPM	counts per minute	NMR	Nuclear Magnetic Resonance
CT	computed tomography	OSEM	Ordered Subset Expectation Maximization
d	day	PAMAM	poly(amido amine)
d	dublett (NMR)	PBS	phosphate buffered saline
DMF	dimethylformamide	PDI	polydispersity index
DMSO	dimethyl sulfoxide	PEG	polyethylene glycol
DNPs	diamond nanoparticles	PET	positron emission tomography
EPR	enhance permeation and retention	PFPMA	pentafluorophenyl methacrylate
FCS	fetal calf serum	PG	polyglutamic acid
[^{18}F]FETos	2-[^{18}F]fluoroethyl-1-tosylate	PM	polymerization
[^{18}F]FDG	2-deoxy-2-[^{18}F]fluoro-D-glucose	ppm	parts per million (NMR)
^{18}F-SFB	*N*-succinimidyl 4-[^{18}F]-fluorobenzoate	q	quartett (NMR)
g	gram	RAFT	Reversible Addition-Fragmentation chain Transfer
GBq	gigabequerel	*ran*	random
GPC	gel permeation chromatography	RCY	radiochemical yield
h	hour	RES	reticuloendothelial system
HPLC	high pressure liquid chromatography	R_h	hydrodynamic radius
HSA	human serum albumin	s	singulett (NMR)
Hz	Hertz	sec	second
ID	injected dose	SEC	size exclusion chromatography
kBq	kilobequerel	SEM	Standard Error of the Mean
kDa	kilo Dalton	SD	Sprague Dawley
L	liter	S_NAr	nucleophilic aromatic substitution
LMA	lauryl methacrylate	SPECT	single photon emission computed tomography
m	multiplett (NMR)	SUV	standard uptake value
M	molar	t-BuOH	tert-Butanol
MBq	megabequerel	THF	tetrahydrofuran
MeCN	acetonitrile	TLC	thin layer chromatography
MeOH	methanol	VOI	Volume of Interest
min	minute	W 256	Walker 256 mammary carcinoma of the rat
M_n	number average molecular weight	µPET	small animal PET
MPS	mononuclear phagocyte system		

5.2 List of Publications

M. Herth, M. Barz, D. Moderegger, M. Allmeroth, M. Jahn, O. Thews, R. Zentel, F. Rösch: *Radioactive labeling of defined HPMA-based polymeric structures using [^{18}F]FETos for in vivo imaging by Positron Emission Tomography (PET).* Biomacromolecules (2009); 10 (7); 1697-1703 (doi: 10.1021/bm8014736).

M. Allmeroth, D. Moderegger, B. Biesalski, K. Koynov, F. Rösch, O. Thews, R. Zentel: *Modifying the Body Distribution of HPMA-Based Copolymers by Molecular Weight and Aggregate Formation.* Biomacromolecules (2011); 12 (7); 2841-2849 (doi: 10.1021/bm2005774).

M. Hemmelmann, C. Knoth, U. Schmitt, M. Allmeroth, D. Moderegger, M. Barz, K. Koynov, C. Hiemke, F. Rösch, R. Zentel: *HPMA Based Amphiphilic Copolymers Mediate Central Nervous Effects of Domperidone.* Macromol Rapid Commun 2011; 32 (9-10); 712-717 (doi: 10.1002/marc.201000810).

M. Allmeroth, Dorothea Moderegger, B. Biesalski, D. Gündel, K. Koynov, H.-G. Buchholz, F. Rösch, R. Zentel, O. Thews: *Structure and size of HPMA-based polymers decide on tumor accumulation but the tumor model makes a difference: A quantitative in vivo PET study*, Angewandte Chemie, in preparation.

M. Allmeroth, D. Moderegger, R. Zentel, O. Thews, F. Rösch: *Comparative study on short and long-term distribution of HPMA-ran-LMA copolymers in vivo by means of ^{18}F and ^{131}I-labeling revealing tumor retention over time*, Macromolecular Rapid Communication, in preparation.

M. Allmeroth, D. Moderegger, D. Gündel, H.-G. Buchholz, K. Koynov, F. Rösch, O. Thews, R. Zentel: *PEGylation of HPMA-based block copolymers enhances tumor accumulation in vivo: A quantitative study using radiolabeling and Positron Emission Tomography*, Journal of Controlled Release, in preparation.

D. Moderegger, M. Allmeroth, H. Schieferstein, H.-G. Buchholz, O. Thews, R. Zentel, F. Rösch: *Fluorine-18 labeling approach for HPMA-based polymers via click chemistry,* in preparation.

M. Allmeroth, D. Moderegger, D. Huesmann, K. Koynov, H.-G. Buchholz, F. Rösch, O. Thews, R. Zentel: *Monitoring of non-linear PEG based copolymers by means of Positron Emission Tomography in vivo: The influence of molecular weight on their pharmacokinetic profile,* in preparation.

6 Acknowledgment

"No one who achieves success does so without acknowledging the help of others. The wise and confident acknowledge this help with gratitude."

Alfred North Whitehead (1861-1947)